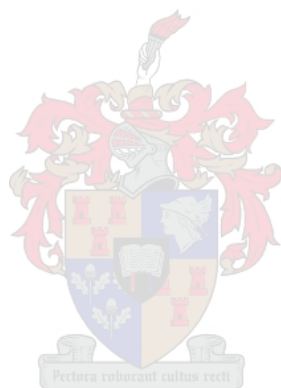# The development of *N*-functionalized 4-azapodophyllotoxins as novel anticancer agents

By Marthinus Gerhardus Botes

Dissertation presented for the degree of Doctor of Philosophy in the Faculty of Science at Stellenbosch University

Supervisor: Professor Willem A. L. van Otterlo

Co-supervisor: Dr Margaret A. D. Blackie

December 2020

Declaration

By submitting this dissertation electronically, I declare that the entirety of the work contained therein is my own, original work, that I am the sole author thereof (save to the extent explicitly otherwise stated), that reproduction and publication thereof by Stellenbosch University will not infringe any third party rights and that I have not previously in its entirety or in part submitted it for obtaining any qualification.

December 2020

Abstract

As malignant carcinomas are one of the world's leading causes of death in terms of non-communicable diseases, there is a strong need for the development of highly specific antiproliferative agents. Cancer is also an ever-increasing concern in Africa, so the there is also a need to develop anticancer agents that are easily accessible through short synthetic strategies.

To this end, we have synthesized a small library of more than 30 novel *N*-functionalized 4-azapodophyllotoxin analogues and analysed these compounds for their antiproliferative activity. The compounds were synthesized in overall yields of 35-57% for the 4*N*-aryl derivatives and 18-35% for the 4*N*-triazolo derivatives. Multicomponent reactions (MCRs) were employed as the main method for the synthesis of the desired scaffolds, after optimizing the procedure to afford the desired compounds from *N*-functionalized naphthylamines. The *N*-propargyl analogues were further derivatised through "click" chemistry with a range of different azides. The antiproliferative activity of these compounds were determined against an oesophageal cancer cell line, WHCO1. Two of the 4*N*-triazolo analogues exhibited inhibitory activities comparable to the known anticancer agent cisplatin ($IC_{50} = 9.2$ μM).

These were 11-(4-hydroxy-3,5-dimethoxyphenyl)-4-((1-((2*R*,3*R*,4*S*,5*S*,6*R*)-3,4,5-trihydroxy-6-(hydroxymethyl)tetrahydro-2*H*-pyran-2-yl)-1*H*-1,2,3-triazol-4-yl)methyl)-4,11-dihydrobenzo[*g*]furo[3,4-*b*]quinolin-1(3*H*)-one (**231**, $IC_{50} = 8.8$ μM) and 4-((1-((2*R*,3*R*,4*S*,5*S*,6*R*)-3,4,5-trihydroxy-6-(hydroxymethyl)tetrahydro-2*H*-pyran-2-yl)-1*H*-1,2,3-triazol-4-yl)methyl)-11-(3,4,5-trimethoxyphenyl)-4,11-dihydrobenzo[*g*]furo[3,4-*b*]quinolin-1(3*H*)-one (**232**, $IC_{50} = 8.3$ μM). The 4*N*-aryl analogues also showed good inhibitory activity, with IC_{50} values ranging between 11-35 μM, with 4-(4-fluorobenzyl)-11-(4-hydroxy-3,5-dimethoxyphenyl)-4,11-dihydrobenzo[*g*]furo[3,4-*b*]quinolin-1(3*H*)-one (**181**, $IC_{50} = 11.7$ μM) and 4-benzyl-11-(3,4,5-trimethoxyphenyl)-4,11-dihydrobenzo[*g*]furo[3,4-*b*]quinolin-1(3*H*)-one (**185**, $IC_{50} = 12.9$ μM) the most potent of these compounds. The 4*N*-propargyl 4-azapodophyllotoxin analogues were also evaluated for their antiproliferative activity, however, the analogues containing the podophyllotoxin and etoposide-derived pendent rings, **174** and **176**, respectively) were found to be inactive. The analogues with the modified E-rings were, interestingly, fairly potent inhibitors, as 11-(3,5-dibromo-4-hydroxyphenyl)-4-(prop-2-yn-1-yl)-4,11-dihydrobenzo[*g*]furo[3,4-*b*]quinolin-1(3*H*)-one (**177**, $IC_{50} = 2.7$ μM) and 11-(5-bromo-2-hydroxyphenyl)-4-(prop-2-yn-1-yl)-4,11-dihydrobenzo[*g*]furo[3,4-*b*]quinolin-1(3*H*)-one (**178**, $IC_{50} = 23.3$ μM) were active against the WHCO1 cell line.

We have also undertaken *in silico* molecular modelling studies through the use of the Schrödinger Maestro suite, so as to supplement our biological evaluation data and in so doing gain more understanding into the potential active sites that these molecules target. These molecular modelling studies did confirm literature observations that noted the importance of the 4′-hydroxyl group on the pendent E-ring of this class of compounds. This was observed in the favourable docking scores of active compounds such as **177**, **181** and **231** against the active site of topoisomerase II.

As these compounds strongly mimic etoposide, the molecular modelling studies on the topoisomerase II crystal structure (PDB ID: 3QX3) also gave insight as to why the 4*N*-triazolo-glycoside 4-azapodophyllotoxins fared better in the antiproliferative studies than the 4*N*-aryl analogues, as π-π interactions between the triazole ring and the adenosine group on the DNA fragment could be observed. The glycoside groups were stabilized in the solvent exposed region of the active pocket.

New insights have thus been gained into the structure-activity relationships of these compounds through the combination of biological evaluation and *in silico* molecular modelling.

Acknowledgements

Academic Acknowledgements

Firstly, I wish to thank my supervisor, Professor Willem van Otterlo for the opportunity to pursue my postgraduate studies in Organic Chemistry, by affording me the chance to do a PhD after the completion of my MSc in Chemistry. Also, I wish to thank my co-supervisor, Dr. Margaret Blackie for her input and support.

I would also like to thank Professor Ivan Green for his mentorship and guidance over the past 8 years, having been an invaluable teacher in the finer methods in synthetic chemistry. Also to Dr Catherine Kaschula, who performed the biological evaluation of our novel compounds that helped me to complete this thesis.

I would also like to thank Dr Bernard Dippenaar for performing the electrostatic potential calculations.

A thank you also goes out to the Group of Medicinal and Organic Chemistry.

To, the technical staff of the De Beers building, without whom we would not have been able to perform our research. Raymond, Debbie and Maxwell, you have been the support structure we would not have been able to function without. And to Mary, you are still missed by all of us that have called the De Beers building our research home.

To Elsa and Jaco for all their assistance with our NMR spectroscopy and Marietjie Stander and her colleagues at the Mass Spectrometry Unit.

Personal Acknowledgements

The biggest thank you goes to my parents and siblings, for keeping me sane and always being there to support me. I would not have been able to do this without you.

My friends that have been incredible motivators over my years at Stellenbosch University.

Acknowledgements for Funding

I wish to thank the NRF for the funding for this project.

Table of Contents

List of Figures

List of Schemes

List of Tables

List of Abbreviations

1. Introduction

NCI	National Cancer Insitute
NCD	Non-communicable Disease
WHO	World Health Organization
USA	United States of America
HBV	Hepatitis B Virus
HCV	Hepatitis C Virus
HIV	Human Immunodeficiency Virus
IARC	International Agency for Research on Cancer
CRC	Colorectal cancer
GDP	Gross Domestic Product

2. Natural Products in Chemistry

NMR	Nuclear Magnetic Resonance
DOS	Diversity-Oriented Synthesis
DTS	Diverted Total Synthesis
MCR	Multicomponent Reaction
MCC	Multiple-Component Condensation
3-CR	Three Component Reaction
4-CR	Four Component Reaction
U-3CR	Ugi Three Component Reaction
U-4CR	Ugi Four Component Reaction
P-3CR	Passerini Three Component Reaction
MW	Microwave
Bmim	1-Butyl-3-methylimidazolium
Tf	Triflate

HPFQ	4-(2-Hydroxyethyl)-10-phenyl-3,4,6,7,8,10-hexahydro-1*H*-cyclopenta[*g*]furo[3,4-*b*]quinoline-1-one
THF	Tetrahydrofuran
SAR	Structure Activity Relationship
FMO	Frontier Molecular Orbital
BSA	Bovine serum albumin
FRET	Fluorescent Resonance Energy Transfer
DNA	Deoxyribose Nucleic Acid
HSA	Human serum albumin
MTA	Microtubule Targeting Agent

3.   *N*-Functionalized arylamines

DMF	*N,N*-dimethyl formamide
TLC	Thin layer chromatography
DIPEA	Diisopropyl ethylamine

4.   Multicomponent Reactions

m/z	Mass to charge ratio
MWI	Microwave irradiation
BCP	Bond Critical Point

5.   Azides

DMAP	*N,N*-dimethylpyridin-4-amine
DMSO	Dimethylsulfoxide

6.   Click Chemistry

DFT	Density Functional Theory

7.   Biological Evaluation

MT	Microtubule
PDB	Protein Database
LID	Ligand Interaction Diagram

VAL	Valine
MET	Methionine
LEU	Leucine
ALA	Alanine
CYS	Cysteine
THR	Threonine
GLN	Glutamine
ASP	Aspartate
LYS	Lysine
SER	Serine

1.1 Introduction

1.1.1 Cancer

The National Cancer Institute (NCI) defines cancer as uncontrolled, abnormal cellular division which can invade surrounding tissues, as well as spread to different parts of the body.[1] Throughout this dissertation, cancer will be used as an umbrella term to describe diseases which hold to the NCI definition of uncontrolled and abnormal cell growth, unless specified to refer to individual cell lines.

Cancer is a non-communicable disease (NCD), thus a disease of long duration that can be attributed to physiological, environmental, genetic and lifestyle factors (or a combination of these factors) – as defined by the World Health Organization (WHO).[2] Globally, cancer is estimated to be the leading cause of death.[3]

To gain a better understanding of cancer in a broader context, statistics from the United States of America (USA) will first be considered, before the available data from Africa will be addressed. This is to highlight certain challenges faced from an African perspective, however, it should be noted that reliable and comprehensive data is more difficult to obtain for Africa than for a developed nation such as the USA.[4] Parkin and co-workers remark on the difficulty of reliable statistics in the report, *Cancer in Africa*, as data for mortality is even more difficult to ascertain than incidence, as most African countries do not have mandated structures to gather the necessary data.[4]

1.1.2 Cancer Statistics in the United States of America

Cancer, a highly prevalent non-communicable disease, has been reported to be the second leading cause of death in the United Stated of America.[5] A study in 2005 by Danaei *et al.* looked at mortality rates of various cancers from 1990 to 2001 and found that there was a 17% decline in the age group 30-69 years, but an increase of 0.4% in individuals over 70 years of age.[6] A similar trend is observed in the work published by Jemal and co-workers between 2004 and 2017.[5,7–10] These studies considered, amongst other trends, incidence and mortality for four distinct time periods, 1996-2000[10], 2002-2006[9], 2008-2012[7] and 2010-2014.[5] The trend for the non-hispanic white and black populations in the United States is shown below in Graph 1.

Mortality Rates for Non-Hispanic White and Black Populations
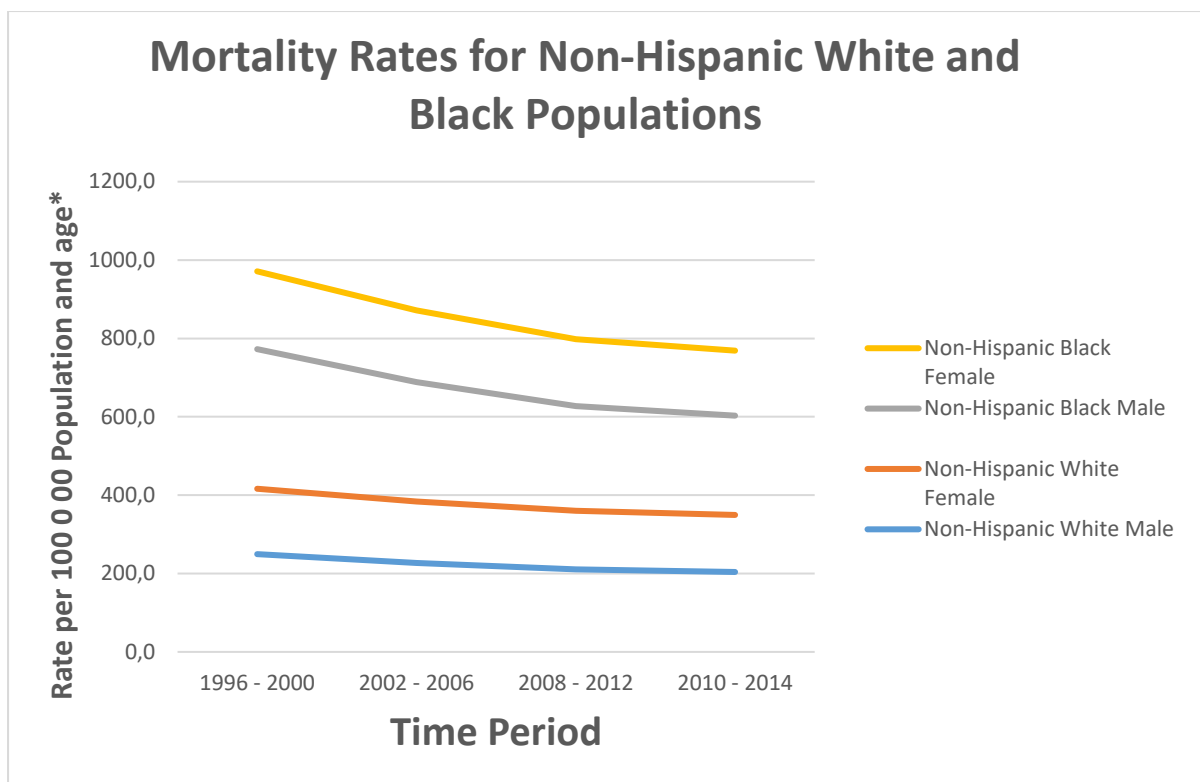
Graph 1: Mortality Rates for cancer under Non-Hispanic White and Black Populations. *Rate given per 100 000 people and normalized to the 2000 National US Census Data. Data compiled from the studies by Jemal and co-workers.[5,7–10]

This trend for the decline in mortality amongst these two races holds for four of the five major races considered in the studies.

Table 1: Mortality Rates for All Cancers per Race. *Rate given per 100 000 people and normalized to the 2000 National US Census Data. Data compiled from the studies by Jemal and co-workers.[5,7–10]

		1996 - 2000	2002 - 2006	2008 - 2012	2010 - 2014
Non-Hispanic White	Male	249.5	226.7	210.6	204.0
	Female	166.9	157.3	149.2	145.5
Non-Hispanic Black	Male	356.2	304.2	267.7	253.4
	Female	198.6	183.7	170.4	165.9
Asian/Pacific Islander	Male	154.8	135.4	128.4	122.7
	Female	102.0	95.1	91.2	88.8
Native American/ Native Alaskan	Male	172.3	183.3	186.7	183.6
	Female	115.8	140.1	133.9	129.1
Hispanic	Male	176.7	154.8	148.0	142.5
	Female	112.4	103.9	99.4	97.7

The only race group for which there was an increase over the four time periods was the group of Native American and Alaskan populations. This can be seen in Table 1, which shows the data collected by Jemal and co-workers.[5,7–10]

All data considered, a note can be made of a higher rate of mortality for men compared to women, as well as a faster general decline in mortality over the observed period for the male population. Many factors are cited for the disparity between the rates of mortality for men and women. As the authors noted, the historical differences in tobacco use can be viewed as an indication as to why lung cancer mortality rates for men are higher than in the female population. Regular tobacco use of women occurred much later than in the male population and never rose to such high levels, as understanding of the dangers of smoking became better understood in the early 80's.[5]

When individual cancers are considered, the same declining trend does not hold as strongly. The data for colon and rectal, lung and bronchus, and liver cancers for the five race groups are given below in Table 2, followed by graphic representations of the data sets. The three types of cancers and their trends will be briefly discussed in terms of different observable trends between the different race groups.

1.1.3 Colon and Rectal Cancers

The data presented by Jemal and co-workers on the mortality due to colon and rectal cancers for the different race groups, show a general downwards trend, as can be seen in Graph 2. This trend holds for all but the Native American and Alaskan demographic, where the mortality has remained fairly constant for the male population. However, a slight increase in the mortality in terms of the female population can be observed over the period between 1996 and 2014 (as seen in Graph 3).

It can be noted that the non-Hispanic black population shows the greatest decrease in mortality due to colon and rectal cancers, with both the male and female population showing significant reduction in death (data for the male population shown in Graph 2 and the female population in Graph 3). The mortality rate for the black population is, however, still much higher than that of the other demographics. Similarly, although not as great a decrease, a decrease can also be observed for the non-Hispanic white, Asian and Pacific Islander and Hispanic populations.

Table 2: Mortality Rates for Race Groups for Specific Cancers (Male and Female). *Rate given per 100 000 people and normalized to the 2000 National US Census Data. Data compiled from the studies by Jemal and co-workers.[5,7–10]

Race (Male)	Cancer	1996 - 2000	2002 - 2006	2008 - 2012	2010 - 2014
Non-Hispanic White	Colon & Rectum	25.3	21.4	18.2	17.3
	Lung & Bronchus	78,1	69.9	62.2	58.3
	Liver	6.0	6.8	7.6	8.0
Non-Hispanic Black	Colon & Rectum	34.6	31.4	27.6	25.9
	Lung & Bronchus	107.0	90.1	74.9	69.8
	Liver	9.3	10.8	12.8	13.3
Asian/Pacific Islander	Colon & Rectum	15.8	13.8	13.0	12.4
	Lung & Bronchus	40.9	36.9	34.0	31.7
	Liver	16.1	15.0	14.5	14.3
Native American/ Native Alaskan	Colon & Rectum	18.5	20.0	18.8	19.5
	Lung & Bronchus	52.9	48.0	49.1	46.2
	Liver	7.6	10.3	13.9	14.9
Hispanic	Colon & Rectum	18.4	16.1	15.6	15.0
	Lung & Bronchus	40.7	33.9	29.5	27.3
	Liver	10.5	11.3	12.9	13.1

Race (Female)	Cancer	1996 - 2000	2002 - 2006	2008 - 2012	2010 - 2014
Non-Hispanic White	Colon & Rectum	17.5	14.9	12.9	12.3
	Lung & Bronchus	41.5	41.9	41.4	39.8
	Liver	2.7	2.9	3.1	4.6
Non-Hispanic Black	Colon & Rectum	24.6	21.6	18.2	16.9
	Lung & Bronchus	40.0	40.0	36.7	35.5
	Liver	3.7	3.9	4.4	4.6
Asian/Pacific Islander	Colon & Rectum	11.0	10.0	9.4	8.8
	Lung & Bronchus	19.1	18.2	18.2	18.0
	Liver	6.7	6.6	6.1	6.1
Native American/ Native Alaskan	Colon & Rectum	12.1	13.7	15.6	14.0
	Lung & Bronchus	26.2	33.5	32.1	30.8
	Liver	4.3	6.5	6.3	6.8
Hispanic	Colon & Rectum	11.4	10.7	9.6	9.2
	Lung & Bronchus	15.1	14.4	13.7	13.4
	Liver	5.0	5.1	5.6	5.8

4

Mortality Rates for Males - Colon and Rectal Cancers
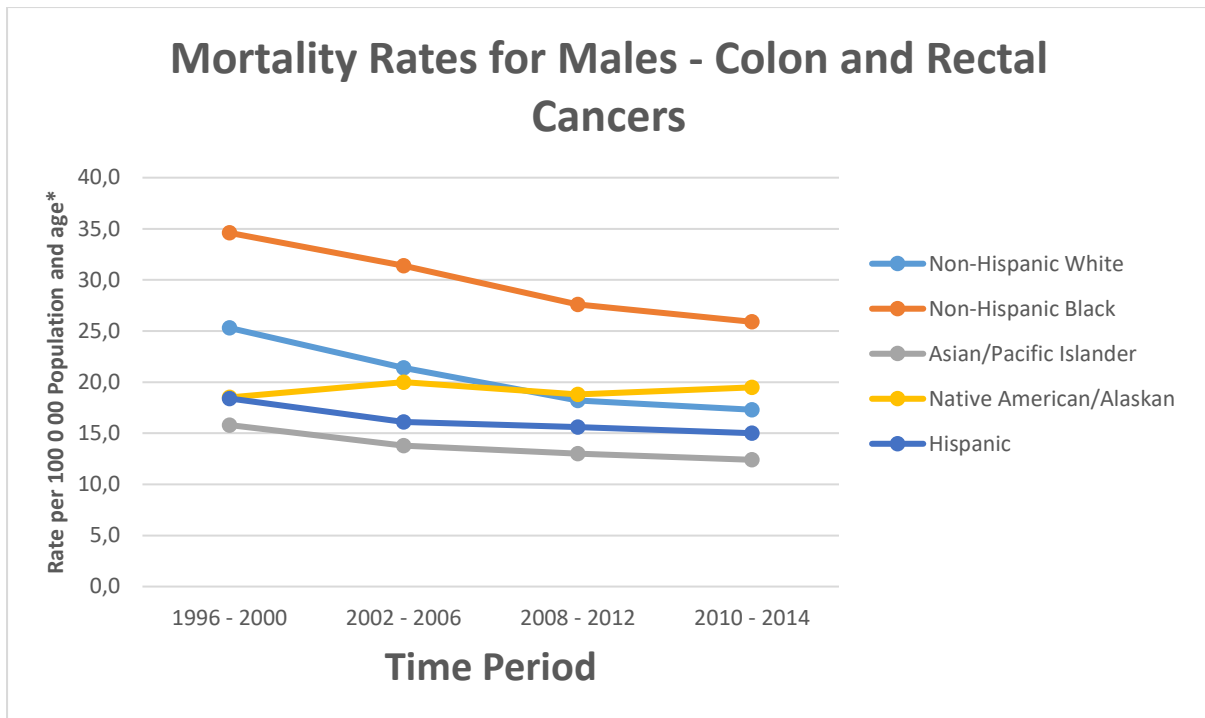
Graph 2: Mortality rates and colon and rectal cancers for the male population. Data compiled from the studies by Jemal and co-workers.[5,7–10]

Mortality Rates for Females - Colon and Rectal Cancers
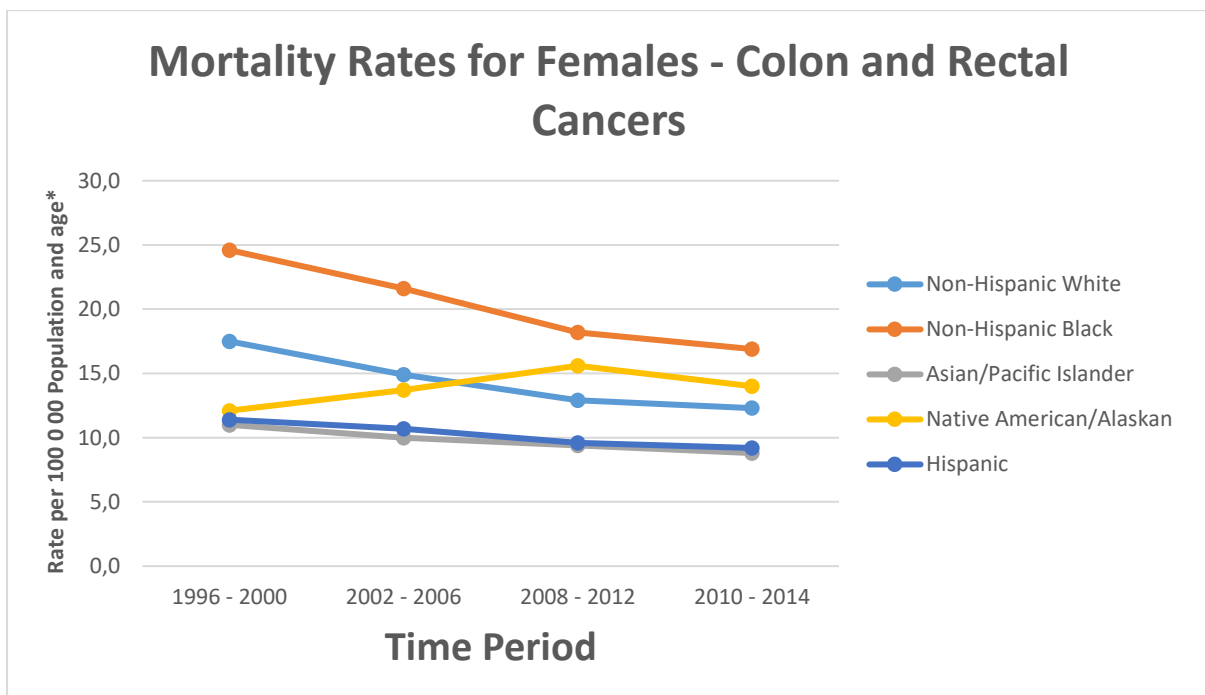
Graph 3: Mortality rates and colon and rectal cancers for the female population. Data compiled from the studies by Jemal and co-workers.[5,7–10]

Colorectal cancers are amongst the leading causes of death under the umbrella term "cancer" in the United States of America, as well as one of the most prevalent under both men and

women.[11] Lifestyle is commonly cited as the most prevalent cause, as the effect of diet on the intestinal flora is posited to play a major role in the proliferation of malignant neoplastic cells within the intestinal tract.[12] The decrease in fiber intake is, controversially, cited as the most likely cause of the increase in colorectal adenomas, as most western diets have decreased fiber intake with an increase in refined carbohydrates, which also leads to other complications such as insulin resistance and hyperinsulinemia.[13,14]

1.1.4 Lung Cancers

Lung cancers show the same general declining trend under the male population; however, it should be noted that the mortality rate is much higher than for that of colorectal cancers. The demographic with the lowest incidence of lung cancers, the US Hispanic male population, still shows a mortality rate per 100 000 people comparable to that of the highest incidence of colorectal cancers (Graph 2 and 3).

A great decrease in mortality can be seen under the non-Hispanic black and white male populations and slight decreases under the Hispanic, Asian and Pacific Islander males (Graph 4). Again, it can be noted that the mortality under the Native American and Alaskan male population remains relatively constant over observed time period. However, under the female population, an increase in mortality is observed (Graph 5). This can be attributed to observations made by Jemal and co-workers that smoking was only taken up by the female population at a later time than the male population and rates of quitting were much lower, as the female population kept smoking until later in life. This would lead to an observation of increased mortality in the observed time period that would mimic a similar peak under male smokers.

The other four demographics show fairly constant rates of mortality over the time period between 1996 and 2014. When the mortality rate of lung cancers is considered for most of the observed populations, it can be noted that mortality remains fairly constant for all but two of the demographics, Non-Hispanic white and black males (Graph 4). These two demographics do show a significant decline in incidence between 1996 and 2014. The trend can be rationalised by considering a report in 1996 that linked good nutrition to a decreased likelihood of cancer cell proliferation.[15] As the Non-Hispanic black and white male populations showed the greatest rate of mortality due to lung and bronchial cancers, a more significant decrease was also noticed over the observed time (Graph 4).

Many reasons can be attributed to the general decline in lung cancer prevalence and mortality for the male population. As early as 1938, the link between bronchial carcinomas and exposure to metals and mining dust had been made[16,17] and in the 80 years since, the

improvement in mine health and safety as well as increased automation (as well as a decrease in mining jobs) has led to lower incidences and resulting cancer-related mortality in the miner population. Another principal reason is the increase in public awareness of the health risks associated with smoking tobacco products.
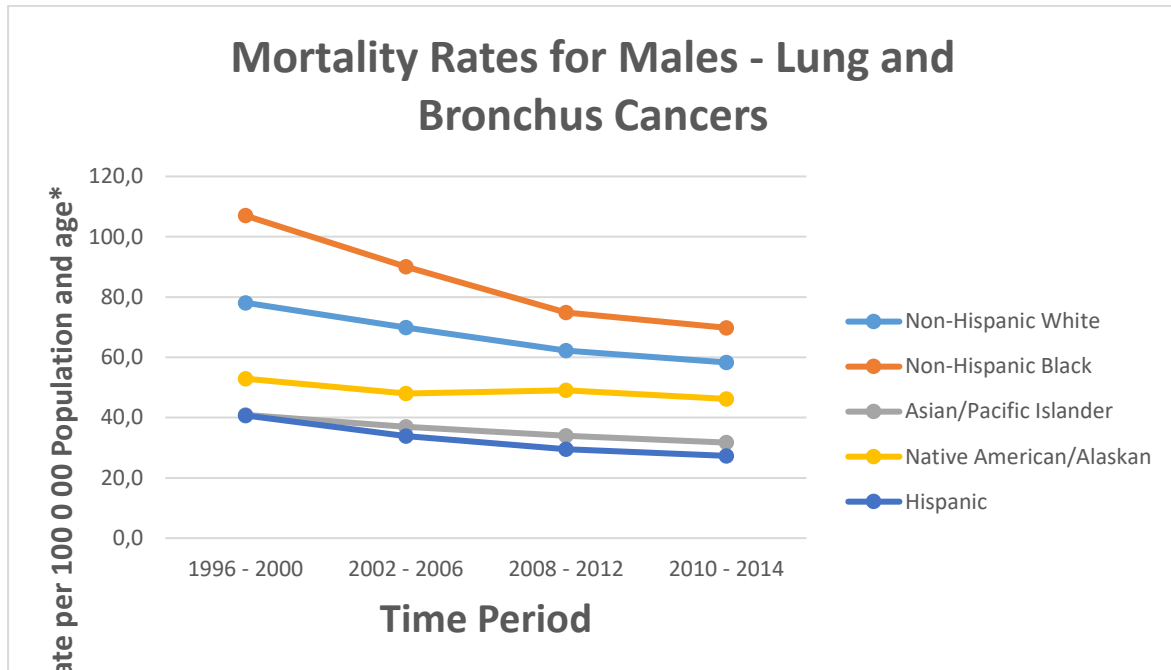
Graph 4: Mortality rates for lung and bronchus cancers for the male population. Data compiled from the studies by Jemal and co-workers.[5,7–10]

Graph 5: Mortality rates for lung and bronchus cancers for the female population. Data compiled from the studies by Jemal and co-workers.[5,7–10]

7
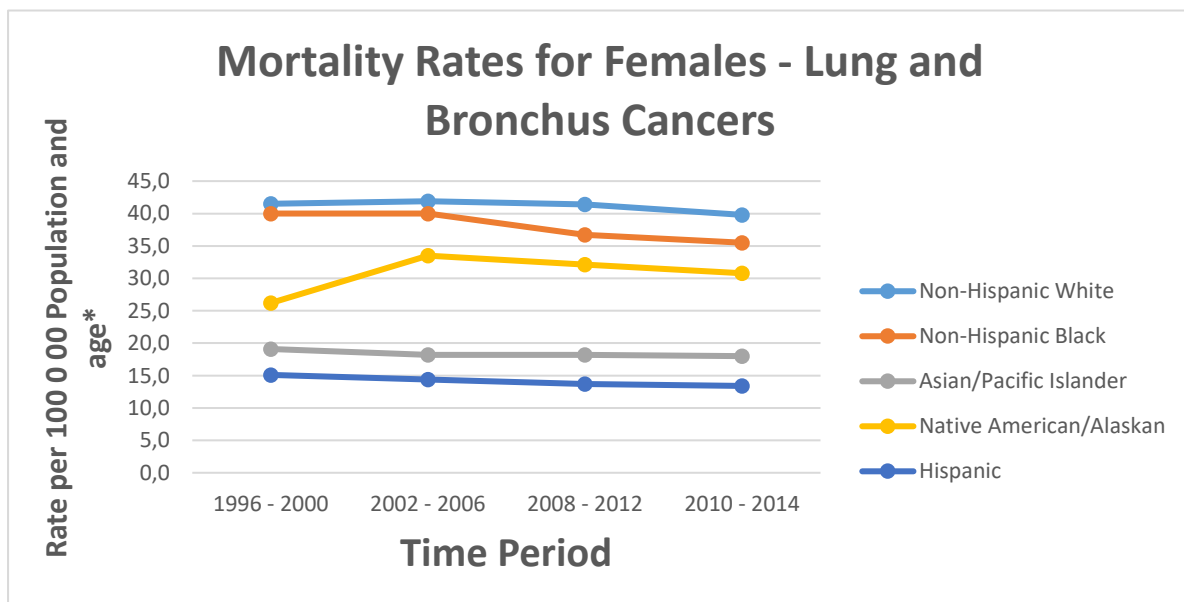
1.1.5 Liver Cancers

Whereas colorectal cancers (Graphs 2 and 3) show a general declining trend and lung cancers show a constant rate of mortality (Graphs 4 and 5), the same is not observed for liver cancers (Shown below in Graphs 6 and 7).

Only one of the four demographics for males, the Asian and Pacific Islander group, show a declining trend (Graph 6). The other four demographics show increases in liver cancer mortality, with an almost 50% increase in incidence observed for the Native American and Alaskan male demographic.

The same trends can be observed for the female population as well, with increasing mortality rate observed for all demographics except the Asian and Pacific Islander population (Graph 7).
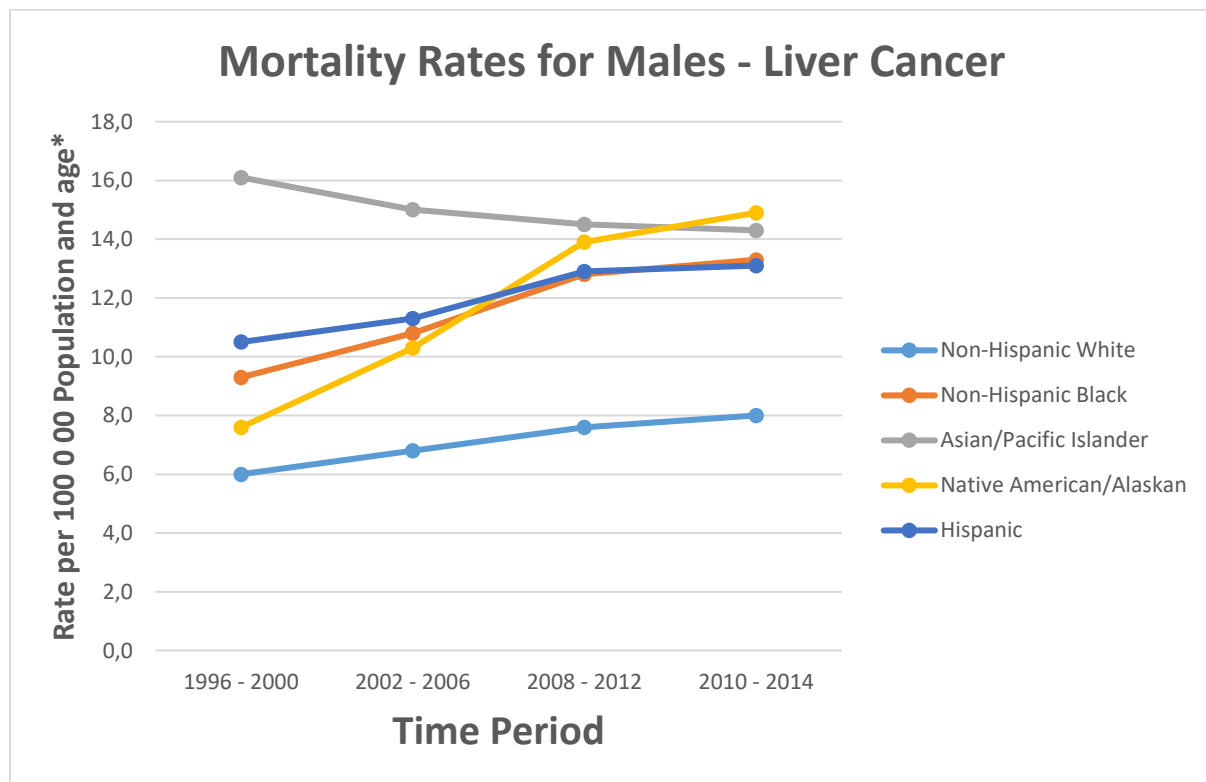
Graph 4: Mortality rates for liver cancer for the male population. Data compiled from the studies by Jemal and co-workers.[5,7–10]
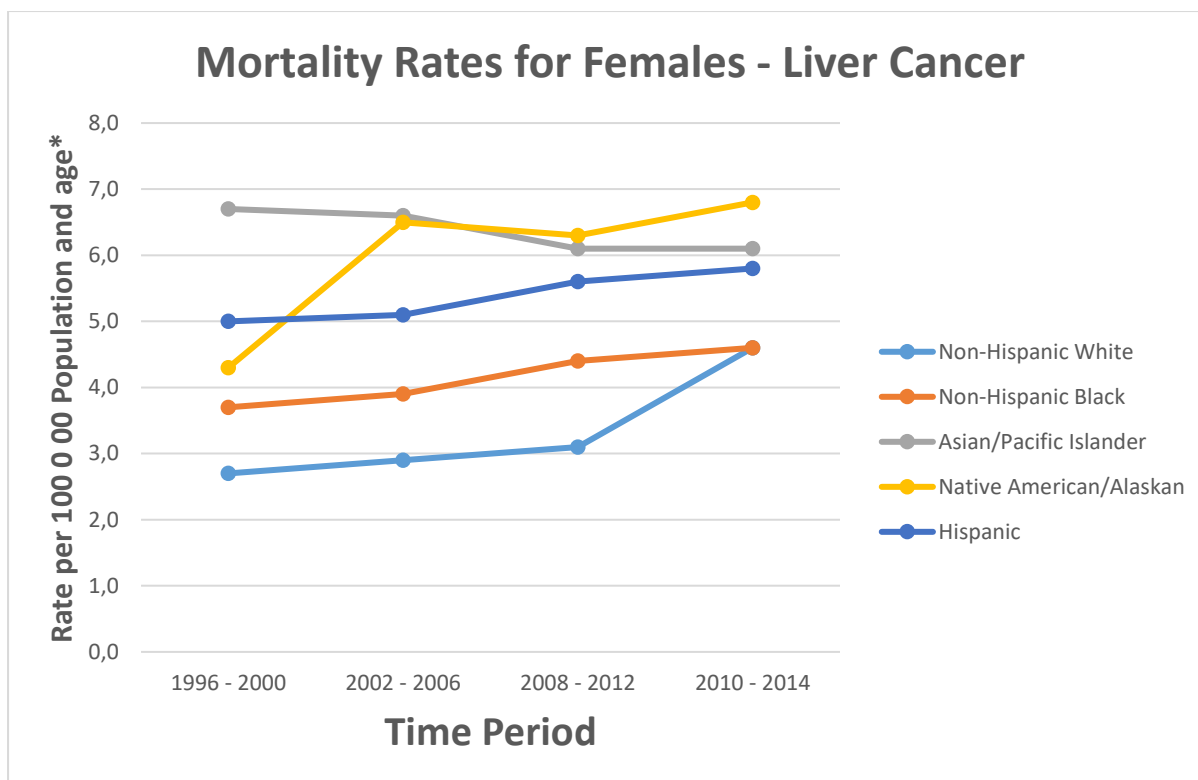
Mortality Rates for Females - Liver Cancer

Graph 5: Mortality rates for lung and bronchus cancers for the female population. Data compiled from the studies by Jemal and co-workers.[5,7–10]

The mortality and increase in mortality due to liver cancer can be noted in the data collected between 1996 and 2014 (compiled data from Jemal and co-workers shown in Table 2 and compiled graphic representations shown in Graphs 6 and 7). Hepatic cancers have generally been attributed to viral infections, such as the Hepatitis B (HBV) and C viruses (HCV), leading to compromised hepatic health.[18] In combination with HBV and HCV, the abuse of alcohol can also be a strong contributing factor in hepatic carcinogenesis – especially in the case of individuals that have developed liver cirrhosis - and is estimated to be a contributing factor in 45% of liver cancer cases.[18,19]

Due to the contribution of alcohol abuse to the development of hepatic neoplasms, liver cancer can therefore also be seen as another lifestyle-associated cancer.

The cancer statistics of the United States is always a good starting point when considering the progression and history of cancer, as reliable data have been collected for several decades. African nations have, however, started focusing on the incidence and prevalence over the last decade and much more reliable data are available. This will be discussed in the next section.

1.2 Cancer in Africa

Statistical data has been noted to be much more difficult to obtain in many African nations than in developed nations. This can be attributed to the socio-economic factors faced on the African continent, such as much larger portions of the population residing in rural areas, less accessible healthcare due to poverty and distance from these facilities, and other concurrent health problems such as tuberculosis, malaria and human immunodeficiency virus (HIV).[3]

In the last two decades, there have been more concerted efforts to address these challenges and gain a more comprehensive idea of the effect, incidence and mortality rate in African nations due to cancer.[4] This initiative included adding more centres for cancer registries throughout the nations in Africa that can collate the reports of cancer incidence and mortality.

Based on data reported in the International Agency for Research on Cancer (IARC) Globocan 2012 study, Parkin and co-workers found that there was an approximately 847 000 new cases of cancer reported yearly in Africa, accounting for 6% of total reported new cases worldwide. The same study found that Africa also accounted for approximately 591 000 cancer-related deaths (7.2% of the global total) in the same year, with close to 75% of these reports from sub-Saharan African nations.[3]

The IARC has predicted that the annual number of new diagnoses of cancer within Africa could rise to one million by the current year (2020). This is especially problematic as cancer survival rates on the continent are only about half that of developed nations, as a recent overview by Stefan reported in the case of breast cancer.[20] This study found that the 5-year survival rate of women diagnosed in the European Union is at 82%, whereas survival rates in Africa range between 12 and 46% (Gambia and Uganda, respectively).[20]

The different cancer treatment methods, such as surgical oncology, radiotherapy and chemotherapy, also need to be investigated in terms of their accessibility within the different world regions. For the purposes of this dissertation, however, only the availability of chemotherapy will be discussed.

1.2.1 Cancer statistics in Africa

The reliability and consistency for data on cancer incidence and mortality rates in Africa have not always been readily available due to various circumstances, principle amongst which is the limited formal cancer registry systems in sub-Saharan African nations. As noted by May and Anandasabapathy, only 23 of 47 countries have such systems in place.[21] This has been improved over the past twenty years as more studies have focused on the prevalence of non-communicable diseases. These studies have highlighted trends for certain cancers that have

generally been more prevalent in high-income, developed countries than in middle- and low-income countries. Amongst these, alarming trends for colorectal cancers (CRCs) have been noted for sub-Saharan African countries.[21–23] In East Africa, CRC incidence rates at one hospital was recorded to have increased by over 300% in two decades of observation. This increase in incidence correlated with other studies done across sub-Saharan Africa.[21]

Problematic as the data are, it must be considered that these diagnoses were generally symptomatic and that the patients had already developed a late-stage onset of the malignancies. Therefore, the increase in incidence from 2,9 to 9,6 cases per 100 000 people per year could potentially have been greater if more advanced diagnostic techniques had been available.[21]

Another observation made when the data were interpreted was that in the population, 20% of diagnoses were made on patients under 40 years of age, in comparison to 3 to 7% in higher-income countries.[21]

South Africa, considered a lower middle-income country based on GDP per capita, has a CRC incidence rate that resembles that of upper middle- and higher-income countries, at an incidence rate between 6 and 8% of patients.[23]

Studies, such as one by Jemal and co-workers, have shown that although cancer incidence rates amongst African nations are generally lower than in more developed nations, greater upward trends can be observed for cancers such as lung, stomach and colorectal cancers.[24]

1.2.2 Chemotherapy in Africa

The World Health Organisation lists 22 chemotherapeutic agents that are deemed essential for treatment of malignant neoplasms in both adults and children. The main challenge that is evident in this list is that none of these 22 agents form part of the core list of chemotherapeutic agents that are deemed essential in the treatment of malignant carcinomas (with less reliance on specialized training and equipment), but that they are merely on the complementary list as these treatments require specialized facilities (and, therefore, specialists that can administer them), higher costs associated with these treatments and a low cost-effectiveness in comparison with medicines on the core list.[21,25]

Considering the socio-economic challenges faced by Africa (as mentioned earlier), these three challenges become even more difficult to overcome, as specialized facilities are generally situated in metropolitan areas and therefore less accessible to poorer, less urbanized, afflicted individuals.

Another major problem in recent years, has been the critical shortages of these chemotherapeutic agents in developed countries, which in turn has a roll-over effect on developing nations. The governments of developing nations frankly do not have the financial strength to compete for these limited resources against developed nations, which of course deepens the already critical shortage faced by developing nations. When this is coupled with data on the availability of these drugs and the associated cost in comparison with the international market price, the problem is clearly one that needs to be addressed through more innovative and critical research. It has been reported that essential medicine prices can range from 2.7 to 6.1 times higher than the international reference prices, in the public and private sectors, respectively. The availability is also only reported to be at 44.3% in state-run facilities and only at 55.3% in private health care facilities.[25]

There is also an associated problem in the treatment of the pain commonly experienced during cancer treatment, in the form of opioid painkillers. The reported amount used in Africa for pain treatment in the period between 2007 and 2009 was only enough to treat an approximate 120 000 patients. This accounts for only about a third of patients that require pain treatment, and when it is considered that South African patients received 71% of the treatment, it is clear how under-supplied Africa as a whole is.[20]

Stefan also reported on how severe the financial impact can be on patients in African nations, with private drug treatments costing the equivalent of between one and seven months of salary.[20]

1.2.3 Possible strategies for treatment

As our focus is on the development of novel antiproliferative agents, we will discuss possible ways in which the shortage and cost associated with chemotherapeutic drugs can be addressed in terms of Africa.

In order to attain a more comprehensive idea of the problem, it should be realized that the supply and cost are two of the most important challenges faced in cancer treatment, after the challenges mentioned about diagnoses. The shortage in the global supply of anti-neoplastic agents (and by extension, the supply in Africa) can be attributed to the widespread incidence of cancer.[3] As the estimated leading cause of death by non-communicable diseases, meeting the demand for treatment worldwide lies in solving the problem of the effective production of currently approved chemotherapeutic agents.

These compounds generally have high costs and low yields associated with their production, along with generating chemical waste as an environmental concern. [26,27] The investment into research initiatives as an expense must also be noted as another hurdle for many developing

nations. As mentioned earlier, global shortages generally leave poorer or developing nations less able to financially compete for the limited supply of necessary medicinal agents.

It is, therefore, necessary to address this problem by generating more intellectual capital on home soil and develop new medicinal compounds that are more easily synthesized. This will lessen the financial burden on African nations and begin to curb the growing health problems, in terms of both communicable and non-communicable diseases. One of the possible solutions in addressing the treatment of cancer in Africa lies in the synthesis of novel antiproliferative agents. This will be discussed in the next section, with focus on the importance of natural products and pharmacophores.

1.3 Conclusion

As the development of African countries continue and flourish due to international investments and technological advances, the rise of non-communicable diseases will continue as well. It is therefore imperative that developing nations pursue strategies for advancing their medical sciences, including the development of pharmaceutical treatments, so as to combat the inevitable rise. This study looked at the development of novel topoisomerase II inhibitors in short and efficient synthetic strategies to this end. The next chapter will consider the inspiration of natural products in drug design and then focus on podophyllotoxin analogues as compounds of interest.

2.1 Natural products in Chemistry and drug design

There has long been a symbiotic relationship between synthetic chemistry and natural product discovery, as natural product discovery drove the need for more innovative ways of solving synthetic challenges. Natural products also provided insight into biological activities and pathways, with these structures seen as evolutionarily privileged structures.[28,29]

The birth of organic chemistry is attributed to the synthesis of urea by Wöhler in 1828 and has grown from there to landmark syntheses, such as strychnine (**1**, Figure 1) by Woodward and the prostaglandins (**2** and **3**, Figure 1) by Corey.[30–32] The rapid evolution of the field since its birth can be attributed to significant advances in analytical methods, with spectroscopic methods such as nuclear magnetic resonance (NMR) spectroscopy playing an instrumental role in advancements in the field of synthetic organic chemistry. This led to concepts such as atom- and redox-economy in synthetic strategies, to provide more efficient methods of producing complex structures. Modern analytical techniques have also led to the advancement of asymmetric catalysis and synthesis, also increasing the efficiency of synthetic procedures.[28]

Strychnine
1

Prostaglandin E$_2$
2
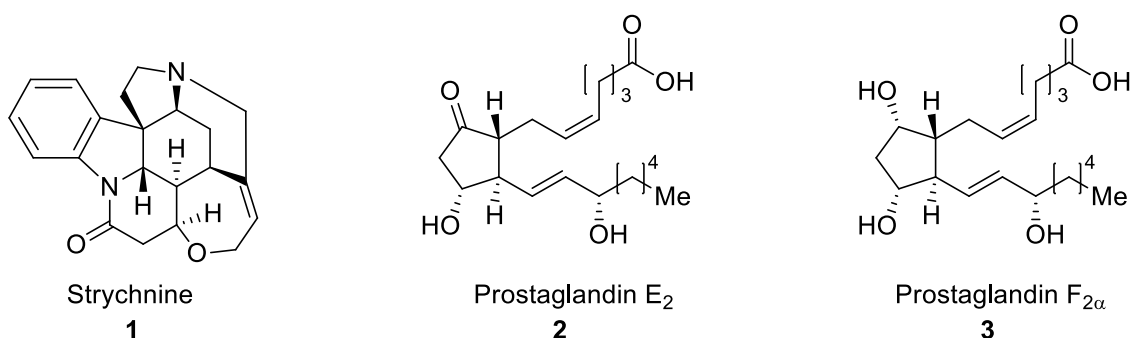
Prostaglandin F$_{2\alpha}$
3

Figure 1: Strychnine and Prostaglandins E$_2$ and F$_{2\alpha}$.[30–32]

Many research groups focused their efforts on synthesizing a singular natural target, but another area also developed where the focus was on generating compounds with more diverse chemical structures, termed diversity-oriented synthesis (DOS).[33] The goal of the DOS approach focuses on the efficient syntheses (generally less than five-steps) of compounds that can probe the chemical space of active sites in drug design. The approach also allows for the attachment of delivery vehicles and warheads, which greatly improves the possible medicinal applicability of the approach.

The DOS approach was, at first, viewed as an orthogonal research area to that of the more classical target-focused approach, but this view has started to change since the start of the 21st century. The combination of the two different approaches has led to Danishefsky coining

the term diverted total synthesis (DTS).[28,34] This approach would use a natural lead as inspiration and only maintain certain functional groups or chemical markers in three-dimensional space, with, as aim of this approach, a late-stage intermediate well-suited for variation.

A good example of the DTS approach can be seen in the work by Danishefsky and co-workers, where a commercially available compound (**4**) afforded migrastatin (**5**) in ten steps (Scheme 1).[34]
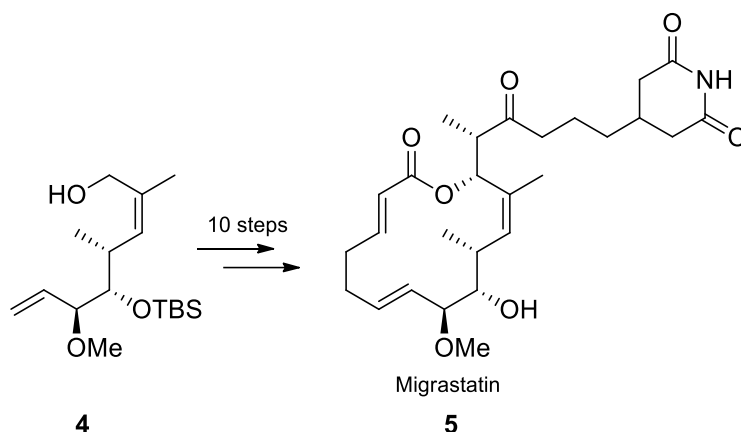
Scheme 1: Migrastatin.[34]

It was found that the macrocyclic lactone core was susceptible to many naturally occurring esterases found in biological systems, so a series of different macrocyclic cores were synthesized, as shown in Figure 2.
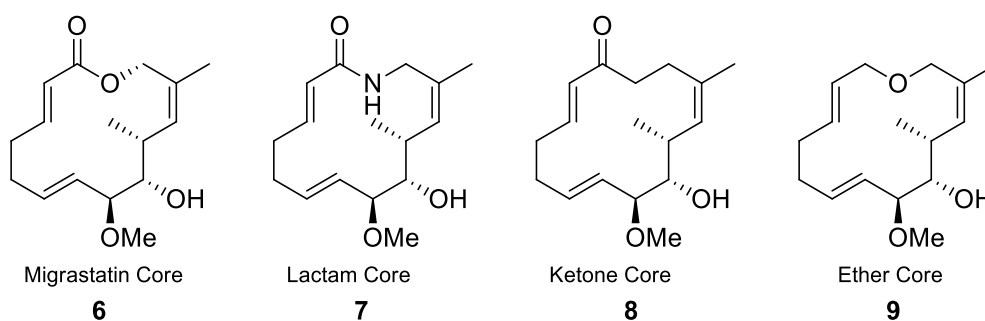
Figure 2: The Migrastatin core and different derived core structures.[34]

This included a lactam (**7**), ketone (**8**) and ether core (**9**). These cores showed increased stability, and as a subsequent study by Yang and co-workers showed, a biotinylated analogue (**10**) of the migrastatin ketone core (**8**) maintained comparable activity against 4T1 breast cancer cell migration (shown in Figure 3).[35]
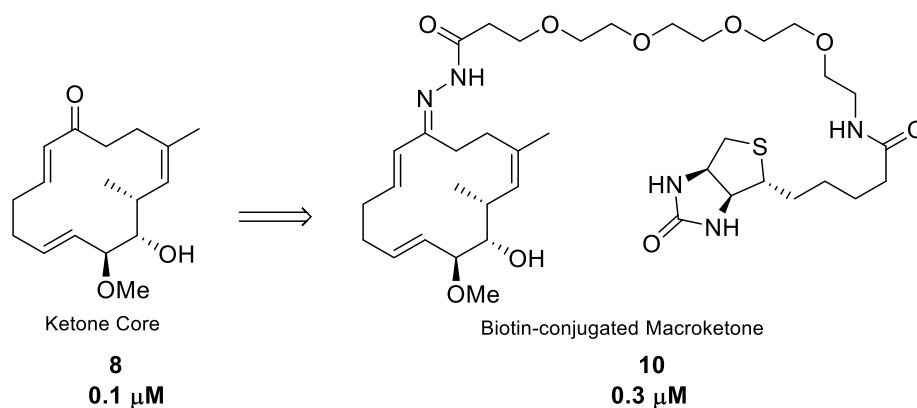
Figure 3: Activities of the ketone core and biotinylated macroketone, as done by Yang and co-workers.[35]

Burke and Schreiber also showed another example of this approach where one intermediate can be transformed into widely varied products through the addition of different reagents (shown in Scheme 2).[33]
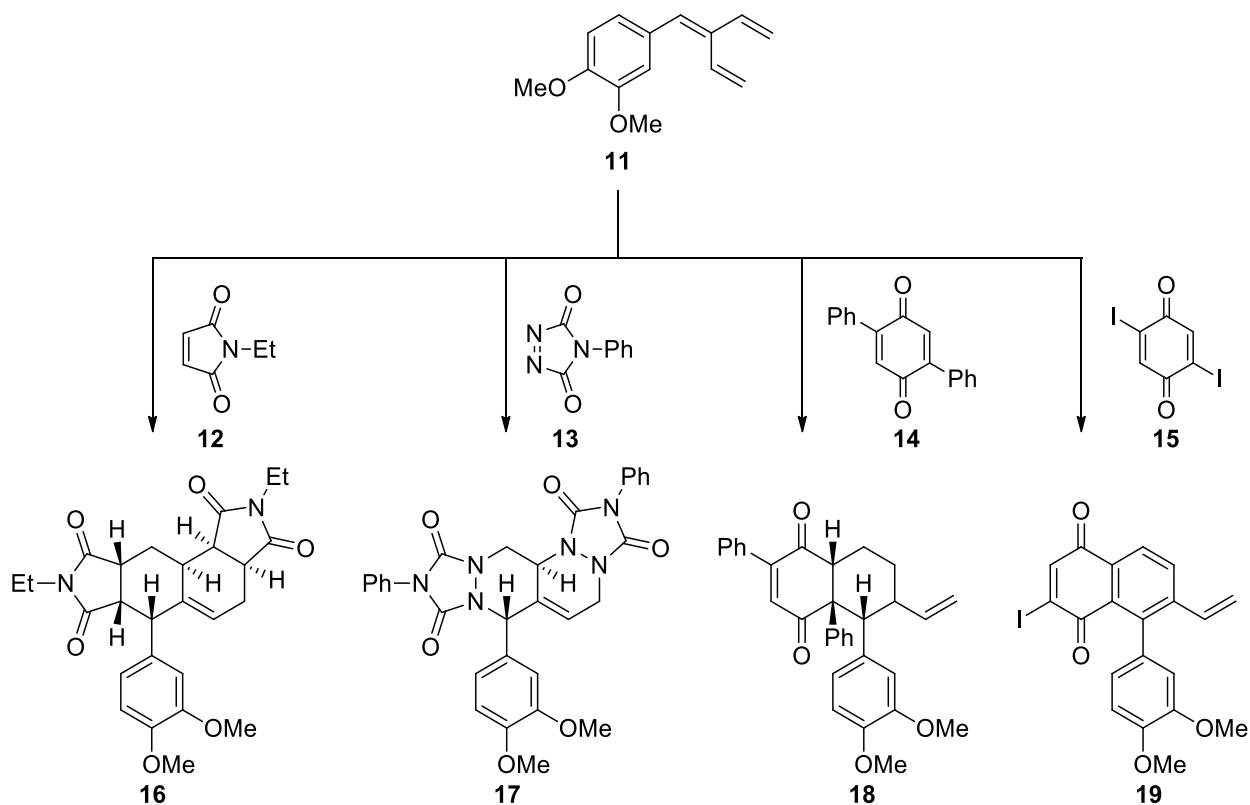
Scheme 2: Work by Burke and Schreiber that shows the diverted total synthesis approach.[33]

The diverted approach employed the use of various electrophiles to produce widely varied substrates inspired by quinones as pharmacophores. The *bis*-addition of compounds **12** and **13** to triene **11** through cycloaddition reactions delivered polycyclic compounds **16** and **17**.

The synthesis of products **18** and **19** was also achieved through the *mono*-addition of quinones **14** and **15** to triene **11**.Another example of the DTS approach, although not explicitly stated to be such, is in the work on natural scaffolds such as the makaluvamines (representative examples **20-23** are shown in Figure 4).
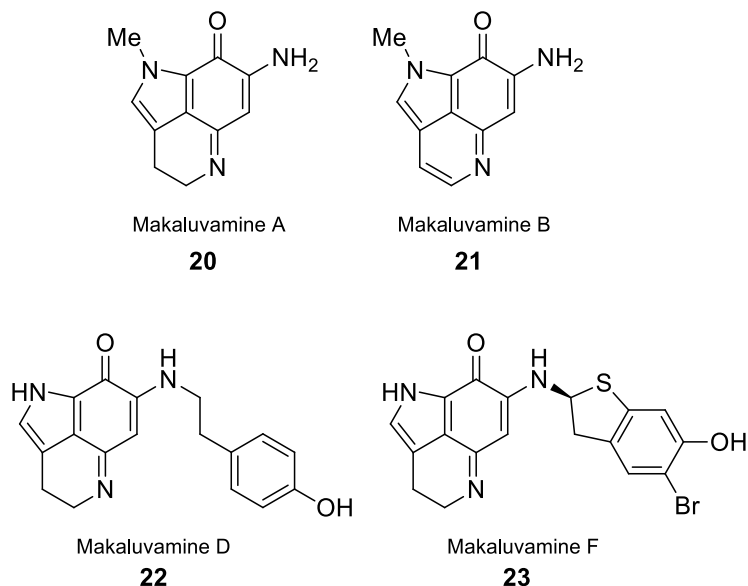
Figure 4: Selected natural makaluvamines.[36,37]
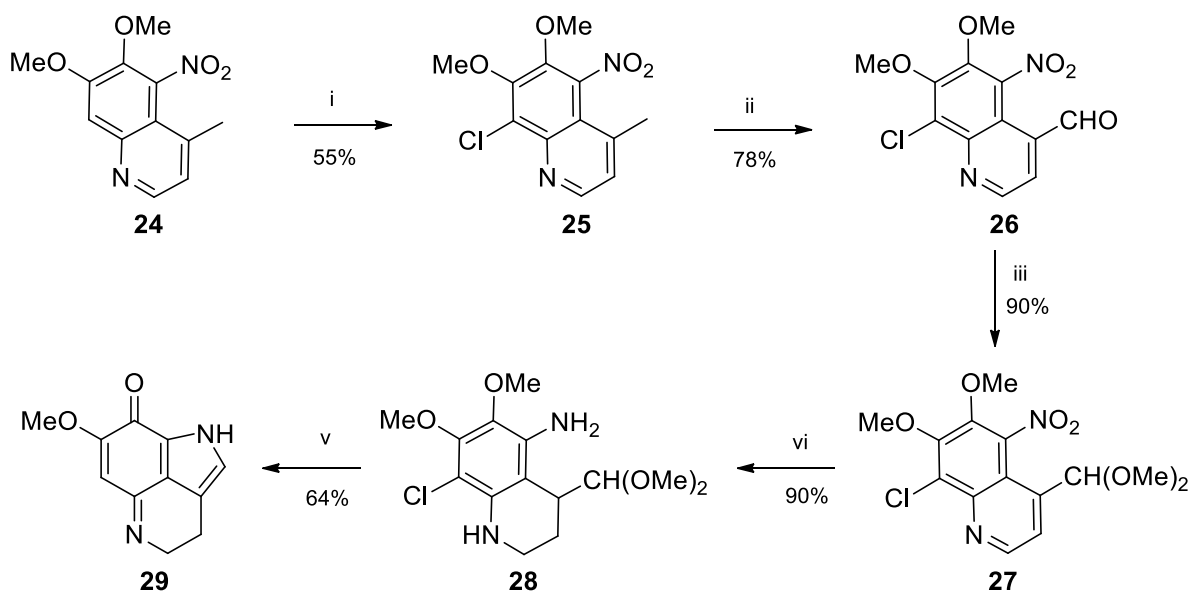
Scheme 3: Synthesis of makaluvamines by Joule and co-workers.[38] Reagents and conditions: i) NCS, DMF, 60 °C ii) I$_2$, t-BuI, FeCl$_2$, TFA, DMSO, 80 °C iii) MeOH, HCl, reflux iv) NaBH$_4$, NiCl$_2$, MeOH, 0 °C v) aq. 1N HCl, THF, 40 °C.

The syntheses of makaluvamines (a synthetic procedure by Joule and co-workers is shown in Scheme 3) are especially well-suited to the DTS approach, as the pyrroloiminoquinone core structure of makaluvamines can be varied through a substitution of the methoxy-group on compound **29**.[38] The substitution of the methoxy-group on compound **29** with the appropriate amines could, thereby, deliver makaluvamines D and F (compounds **22** and **23**, Figure 4), as well as novel analogues when the amines are varied. A study on this DTS approach using makaluvamines has been done previously in our group.[39]

2.2 Multicomponent reactions and the DTS approach

One of the most powerful techniques in utilising the DTS approach, is through the use of multicomponent reactions (MCRs). Armstrong and co-workers remarked on the value of this strategy and referred to it as multiple-component condensation (MCC) reactions.[40] From here on in the text, only the term MCR will be used, which will include Armstrong and co-workers' MCC reactions. The general accepted definition for a MCR is the incorporation of three or more compounds into the general backbone of a product in a one-pot reaction. Whether the incorporation into the final product is through sequential addition or a concerted mechanism, is of lesser importance in the classification. In addition, these reactions are also atom economic and are generally wide in scope as the reaction would rely on the different functional groups, thus the substituents can be varied to generate greater libraries of compounds.[40–42]

The first MCR was discovered as far back as 1838 by Laurent and Gerhardt, but the first publication specifically identifying MCRs only appeared in 1850 and was known as the Strecker reaction.[41,43] Laurent and Gerhardt isolated a product with poor solubility from a reaction of bitter almond oil (of which the main component is benzaldehyde (**30**) along with some hydrocyanic acid) and ammonia to give the aminobenzyl cyanide (**31**), which condensed with the excess benzaldehyde to give the resulting Schiff base (**32**, Scheme 4).[43]
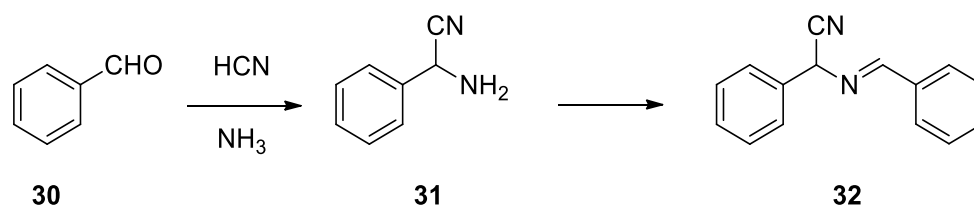
Scheme 4: Synthesis by Laurent and Gerhardt, the first recognized MCR.[43]

In this synthesis, the three components in the reaction mixture were all incorporated into the final product. This led to what is now known as the Strecker reaction, the condensation of an aldehyde, hydrocyanic acid and ammonia. Over the next six decades more MCRs were reported utilizing different substrates, although all of these were still variations of the Strecker

reaction. This included aldehydes, substituted amines and another nucleophile. Scheme 5 shows generalized reaction schemes of the Biginelli, Doebner and Hantzsch MCRs.
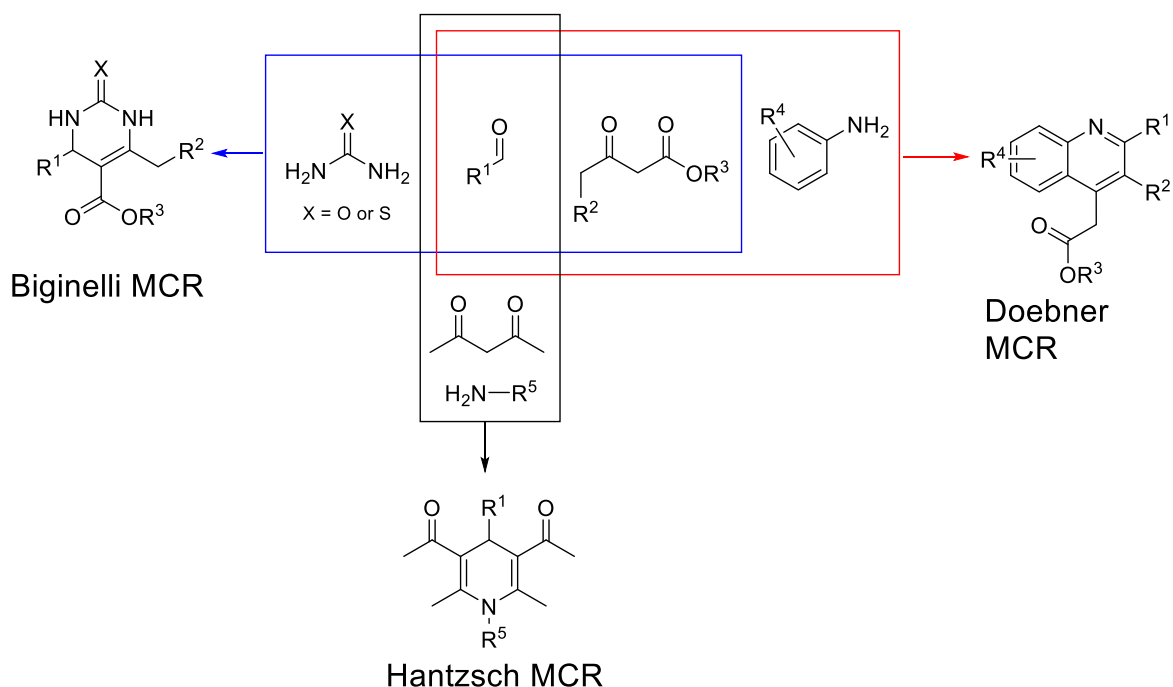
Scheme 5: Three examples of different MCRs.[44]

These three MCRs all include a substituted amine (urea in the Biginelli MCR, arylamines in the Doebner MCR and monosubstituted amines in the Hantzsch MCR) and an aldehyde. The other nucleophile in these examples is a 1,3-diketone species.[44]
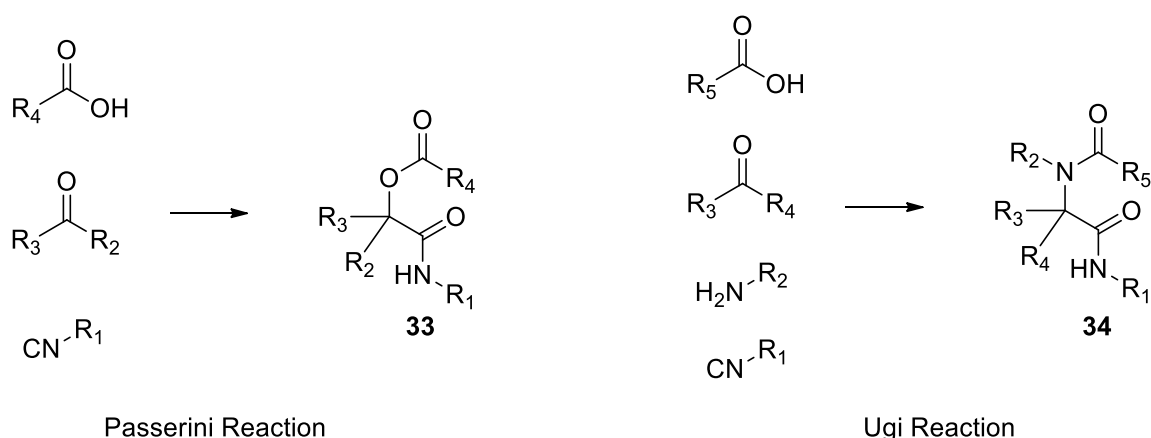
Scheme 6: Generalized schemes for the Passerini and Ugi MCRs.

Other variations in the MCR approach involved the use of isocyanides, carboxylic acids and aldehydes as part of a three component MCR (3-CR), as was reported by (and named after) Mario Passerini, to generate α-alkoxyamides (**33**, Scheme 6), and the use of the abovementioned compounds along with a monosubstituted amine as a four component MCR

19

(4-CR), as was reported by (and named after) Ivar Ugi, to generate *bis*-amides (**34**, Scheme 6).[40,41]

The vast array of new compounds available through the single step strategy of a MCR highlighted the value of these reactions. Armstrong and co-workers noted that a 3-CR strategy utilizing 20 structurally different inputs can theoretically generate a library of 8000 compounds and utilizing a 4-CR strategy with 20 structurally different inputs can generate up to 160 000 compounds.[40] This efficient method of exploring chemical space of potential medicinally viable pharmacophores offers a great way of understanding the efficacy of certain bioisosteres over others.[34,45]

Ugi 4-component reaction:
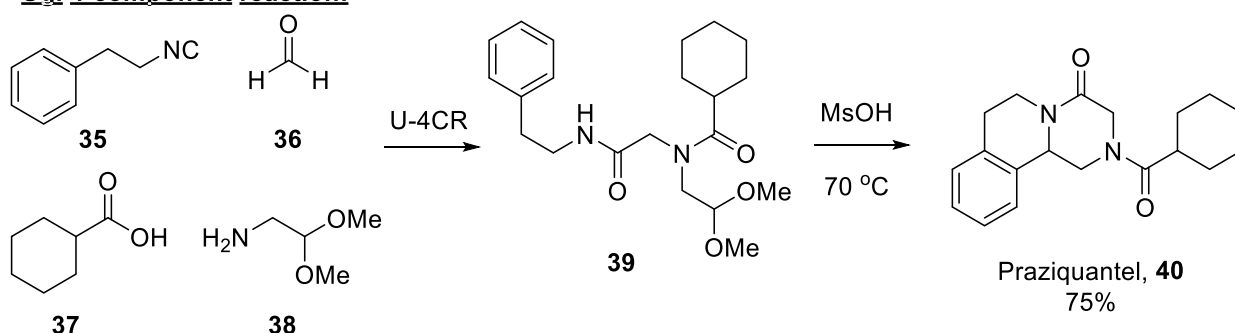
Ugi 3-component reaction:
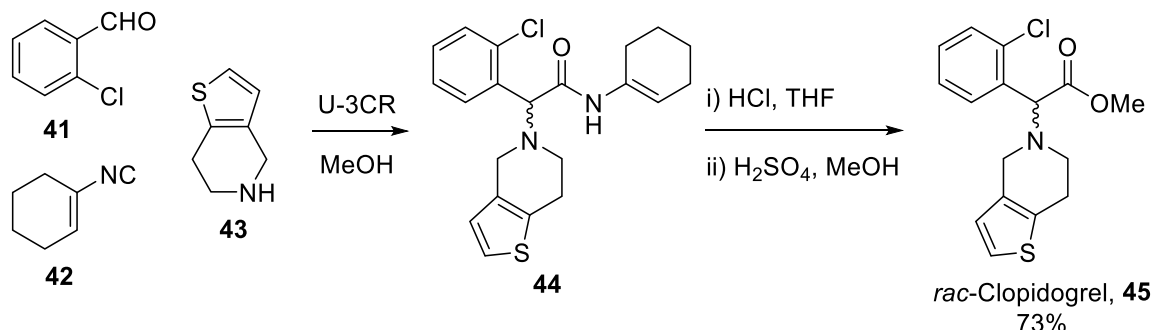
Passerini 3-component reaction:
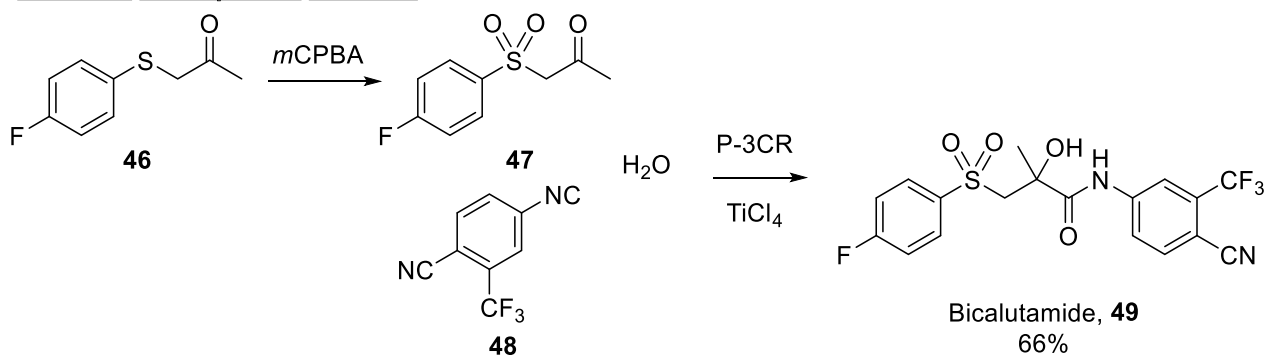
Scheme 7: Syntheses of three medicinal compounds utilizing a MCR as a key step. Ugi 4-component reaction in the synthesis of praziquantel, Ugi 3-component reaction in the

synthesis of clopidogrel, and Passerini 3-component reaction in the synthesis of bicalutamide.[42]

Scheme 7 shows the syntheses of three medicinal compounds that utilize a MCR as a key step. In the representative examples, the final compounds were synthesized in no more than 3 steps from commercially available or readily accessible starting materials (**35-38**, **41-43**, **46** and **48**) with overall yields between 66% and 75%.The syntheses of praziquantel (**40**) and clopidogrel (**45**) involved three (U-3CR) and four (U-4CR) component Ugi MCRs, respectively, as the principle step. The synthesis of bicalutamide (**49**) employed a three component Passerini MCR (P-3CR) as the principle step (by using water instead of a carboxylic acid and TiCl$_4$ as a catalyst).[42]

This dissertation will focus primarily on a modified version of the Hantzsch dihydropyridine synthesis, which incorporates an aldehyde, 1,3-diketone and amine into a dihydropyridine scaffold (Scheme 8).
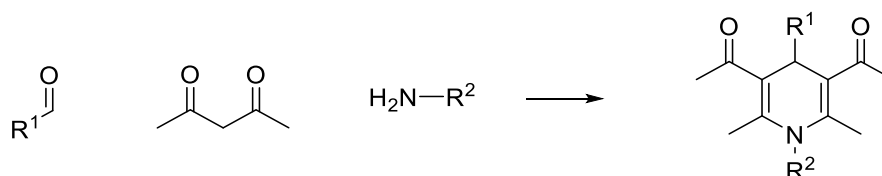
Scheme 8: Generalized scheme of the Hantzsch dihydropyridine MCR.

The next section is the review published by our group on advances in MCR chemistry on 4-azadidehyropodophyllotoxin as potential anticancer agents. The review was published in the journal, *Chemistry of Heterocyclic Compounds*:

Synthesis of 4-azapodophyllotoxins with anticancer activity by multicomponent reactions (Review)

M.G. Botes, **S.C. Pelly**, **M.A.L. Blackie**, **A. Kornienko**, **W.A.L. van Otterlo**, *Chemistry of Heterocyclic Compounds,* Vol. 50, No. 2, **2014**.

The section includes the review (adapted and formatted so as to form part of this dissertation), followed by an expanded section that covers publications of interest in the field after the publication of the review.

2.2.1 *Synthesis of 4-azapodophyllotoxins with anticancer activity by multicomponent reactions (Review)*

In the last 13 years, considerable advances have been made in the development of 4-azapodophyllotoxins as anticancer agents. The current review covers this research with an emphasis on the synthesis of less stereochemically complex podophyllotoxin analogues by efficient. The review includes a short introduction to the area of 4-azapodophyllotoxins prepared by multicomponent reactions, after which the debate concerning the precise mechanisms of such reactions is highlighted. This is followed by a description of the 4-azapodophyllotoxin libraries and a discussion of their documented anticancer activities. The review concludes with an analysis of the proposed mode of action and future directions in this fascinating area of research.

In 2011, Alegria and Malhotra published a general review on the syntheses and applications of azapodophyllotoxins, providing a broad overview of the area.[46] However, because the multicomponent reaction (MCR) approach appears to be the most promising and direct method of generating 4-azapodophyllotoxins with single-digit nanomolar activities, it was felt that a focused discussion specifically emphasizing the synthesis of such analogues by way of the MCRs, would be helpful to the scientific community. In addition, the current review includes recent mechanistic investigations that could be useful in a further development of this approach to expand its scope and permit access to new azapodophyllotoxins. Finally, the antiproliferative activity of some of the more potent analogues that have been synthesized since 2011 will be discussed as well. It should be noted that the development of the MCR-based approach to access new 4-azapodophyllotoxins in this area of research parallels the recognition of these powerful MCR strategies in medicinal chemistry as a whole.[42]

A significant proportion of the cancer drugs currently on the market are either natural products or are based on a natural product lead compound.[47] This is due to the intrinsic bio-relevance of natural molecules and this insight has led to widespread screening of natural compounds to identify new structural leads.[48] A study by Newman and Cragg revealed that 49% of the compounds used for the treatment of cancer between 1981 and 2010 were either natural products, derived from a natural product by semisynthesis, or were based on a natural pharmacophore and made by total synthesis.[47]

Podophyllotoxin (**50**) (Figure 5) is a naturally-occurring cyclolignan that has been studied extensively in the last few decades as one such anticancer lead, owing to its disruption of cell mitosis through the destabilization of microtubules.[49] Podophyllotoxin was isolated from podophyllin – a resin produced following the alcohol extraction of members of the genus

Podophyllum.[48,49] The pharmacological value of the podophyllotoxins has been known for centuries. These compounds were used as cathartic and anthelmintic agents in ancient times and podophyllotoxin-related lignans were used as topical treatments of the type I herpes simplex virus and measles.[50] The antiviral efficacy of podophyllotoxin (**50**) has also been demonstrated through its successful use for the treatment of venereal and perianal warts.[48–51] Among its diverse pharmacological properties the antitumour activities have generated the most interest. It has been an effective agent in the treatment of various oncological conditions, such as Wilms' tumours, genital tumours, non-Hodgkin lymphomas, and lung cancer.[48] Podophyllotoxin (**50**) and structurally related compounds, deoxypodophyllotoxin (**51a**) (Figure 5), α- and β-peltatins (**52**), (**53**), picropodophyllotoxin (**54**), amongst others, all inhibit cell proliferation through the destabilization of microtubules during the metaphase of the mitotic cycle. Notwithstanding highly potent antiproliferative action and the inhibition of tumour cell growth, podophyllotoxin failed clinical trials due to severe gastrointestinal side-effects.[47–49] Fortunately, its failure in this clinical context, led to the development of semisynthetic derivatives that have found widespread use as late stage cancer treatments in the clinic.
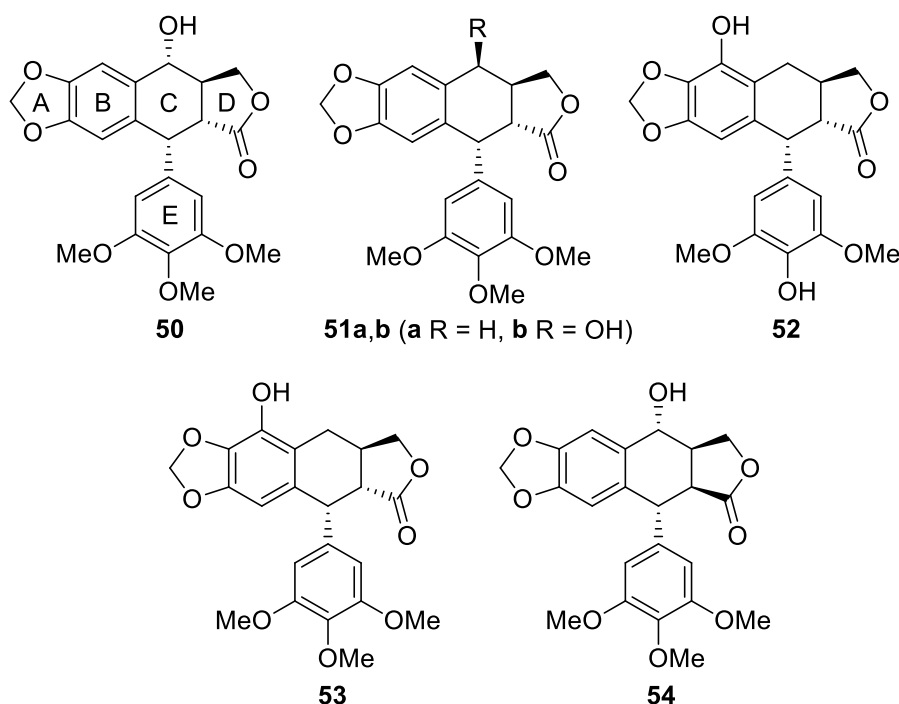
Figure 5: Podophyllotoxin and related cyclolignans.[49]

Among the latter, there are two glycoside-substituted epimers, etoposide (**55a**) and teniposide (**55b**), and the water-soluble prodrug, Etopophos (**55c**) (Figure 6). It is interesting to note that these derivatives operate through a different mechanism of action compared to that of the parent compound. Whereas podophyllotoxin destabilizes the assembly of microtubules (by binding to the colchicine site in tubulin and therefore referred to as a tubulin poison), the

23

semisynthetic derivatives **55a–c** inhibit tumour growth by stabilizing a cleavable complex with DNA and topoisomerase II (referred to as a topoisomerase poison).[48] These mechanisms of inhibition will be discussed in more depth in Section 8.1, *Biological Evaluation and Results*, in the context of the antiproliferative activity of the compounds synthesized in this study.

Although effective, these drugs are still only available through semisynthetic methods, as total syntheses of the podophyllotoxin scaffold are still long and inefficient due to the presence of the four contiguous stereocenters on the C-ring. For example, Norman and co-workers synthesized an analogue of podophyllotoxin with a phenyl E-ring in 19 steps.[52] The most recent formal synthesis of podophyllotoxin (**50**) was reported by Ishikawa and co-workers in 2013, to produce podophyllotoxin (**50**) in 10 steps,[53] opening up the possibility to reengineer the natural compound with other groups in the A-, B- and E-rings.[54] (For another formal synthesis of podophyllotoxin (**50**), see the synthesis by Zhang and co-workers.[55]) This structural complexity, and the associated tedious synthetic approaches, has led to investigations into the necessity of the chiral centres for the biological activity and these efforts led to the discovery of the so-called 4-azapodophyllotoxins (**56a**) and (**57**) (Figure 6).

55a: R^1 = Me, R^2 = H; **b:** R^1 = thiophen-2-yl, R^2 = H; **c:** R^1 = Me, R^2 = PO$_3^-$
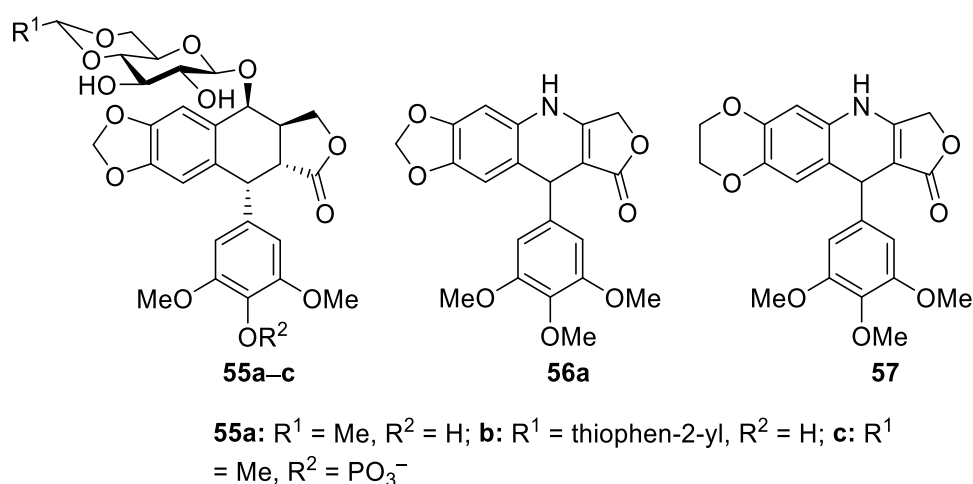
Figure 6: Semisynthetic podophyllotoxin derivatives, **55a-c**, and 4-azapodophyllotoxins **56** and **57**.

In 2000, Takeya and co-workers reported the synthesis of two 4-azapodophyllotoxin analogues **56a** and **57** (Scheme 9, Figure 2) that had an activity of more than twice that of the naturally occurring cyclolignan **50**, even as racemic mixtures. In addition, a number of other synthesized compounds from this group had activities comparable to podophyllotoxin (**50**).[56] A substantial advantage of these compounds was that they were prepared in only three steps and in high yields.[56,57] Even though these analogues were still as toxic as podophyllotoxin, the relative ease with which they could be synthesized provided an opportunity to explore different ring systems by changes in the A, B and E rings of the podophyllotoxin scaffold (See Figure 5

24

for the ring labelling of podophyllotoxins). The variation of the AB-ring system was restricted by the anilines that could be used in this method.[58] The first step in the synthesis involved the reaction of aniline **58a** with tetronic acid (**59**) leading to anilolactone **60**, followed by a condensation with an appropriate aldehyde **61** in trifluoroacetic acid and with the addition of *p*-chloranil to afford the intermediate quinoline **62**. This limited the scope of this method to non-*N*-substituted anilines and required reduction with a weak reducing agent, such as sodium cyanoborohydride, to form the intended product **56a**.[56,57]

Takeya and co-workers
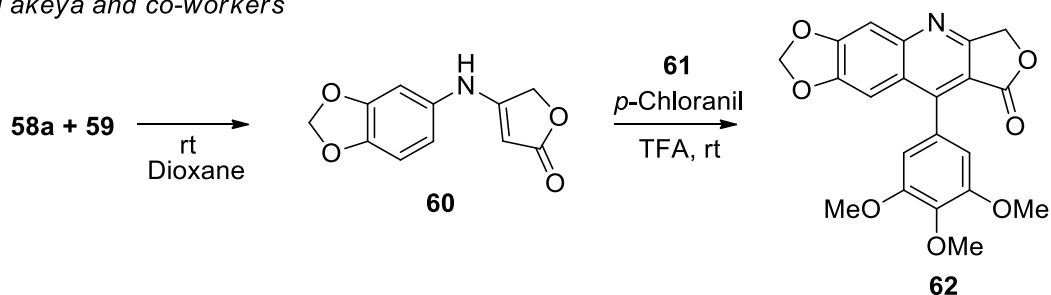
Giorgi-Renault and co-workers
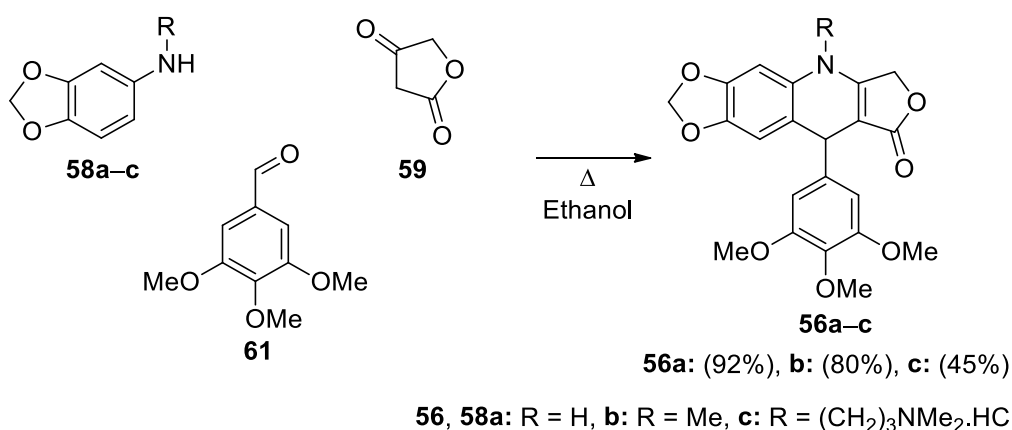
Scheme 9: A comparison of MCR [58] and step-wise synthesis [56,57] of 4-azapodophyllotoxins.

A much more straightforward synthesis of these analogues was then reported by Giorgi-Renault and co-workers in 2002, who described a one-pot MCR for the synthesis of 4-aza-2,3-didehydropodophyllotoxin analogues **56a–c** in good to excellent yields (Scheme 9).[58] Also the reaction conditions were very simple: the corresponding aniline **58a–c**, benzaldehyde **61** and tetronic acid (**59**) were stirred at reflux in ethanol as solvent. The MCR introduced by Giorgi-Renault and co-workers relies on the innate nucleophilicity and electrophilicity of tetronic acid (**10**) to first form a Knoevenagel adduct between the benzaldehyde and tetronic acid, which then undergoes nucleophilic attack by the aniline **58a–c** to form the 4-aza-2,3-didehydropodophyllotoxin scaffold **56a-c** (see the debate concerning the exact mechanism later in this review). This means that, without the quinoline intermediate involved, *N*-substituted

anilines can be used and the position 4 is open for further derivatization.[58] The only limitation was that, for the success of the MCR, the aniline **58a** had to have an electron-donating group in the *meta*-position.

Since this first report of a MCR being used to generate the 4-azapodophyllotoxin scaffold, there has been a veritable explosion in the field of synthetic podophyllotoxin analogues and an exploration of a wide variety of different substituents in the A, B, and E-rings of the scaffold.[29,46,66–75,58,76–81,59–65] Both of the above approaches have been utilized by Semenova and co-workers who have prepared various polyalkoxy analogues using similar protocols and employing allylpolyalkoxybenzenes, isolated from parsley oil, that were subsequently converted into the corresponding benzaldehydes **63** (Scheme 10).[59] These aldehydes were then utilized in the MCR strategy, resulting in a set of 4-azapodophyllotoxins with significant variation in E-ring substitution, as well as the modification of the A- and B-rings (representative examples are shown in Scheme 10 – for more examples, see the work by Semenova *et al.*[59]). Interestingly, the methylenedioxy moiety in the AB-ring system appears to be of no critical importance for anti-cancer activity, since the 6-methoxy derivative **56d** (Scheme 10), also showed potent antiproliferative action.[59,60]
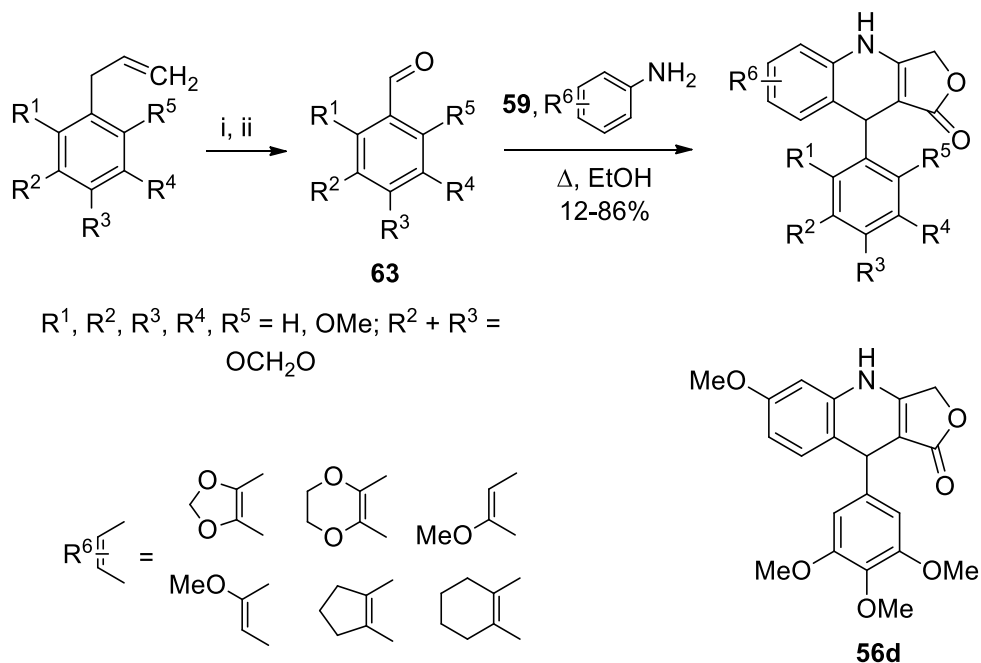
Scheme 10: Synthesis of polyalkoxy 4-azapodophyllotoxins by Semenova and co-workers.[59] i) Powdered KOH, (n-Bu)$_4$N$^+$Br$^-$, 100°C, 40 min; ii) O$_3$, CHCl$_3$–MeOH–Py, 80:20:3 (v/v), –15°C, 1–2 h.

Although this review focuses on the anti-cancer activity of synthetic 4-azapododophyllotoxins, it is interesting to note that, similar to the natural podophyllotoxin **1**, these scaffolds do have other applications as well. Cyclolignan analogues generated by MCR have also been studied for their insecticidal properties. For example, a 2009 study by Frackenpohl and co-workers described an investigation of the activity of a library of MCR products against the mustard beetle (*Phaedon cochleariae*), and the fall armyworm (*Spodoptera frugiperda*).[61] Murlykina and co-workers also synthesized 4-azapodophyllotoxins as part of their study of generating these structures via MCRs.[62]

Mechanistic Investigations

In their initial report, Giorgi-Renault and co-workers proposed a mechanism for the MCR resulting in the compound **56a** containing a dihydropyridine scaffold.[58] As previously mentioned, the first step proposed was the condensation of a substituted benzaldehyde **61** with tetronic acid (**59**) to form the Knoevenagel adduct **64** (Scheme 11), followed by a nucleophilic attack of the aniline **58a** on the ketone functionality of the adduct **64** to form the proposed intermediate **65**. Through the loss of a water molecule, the product **56a** is then formed.
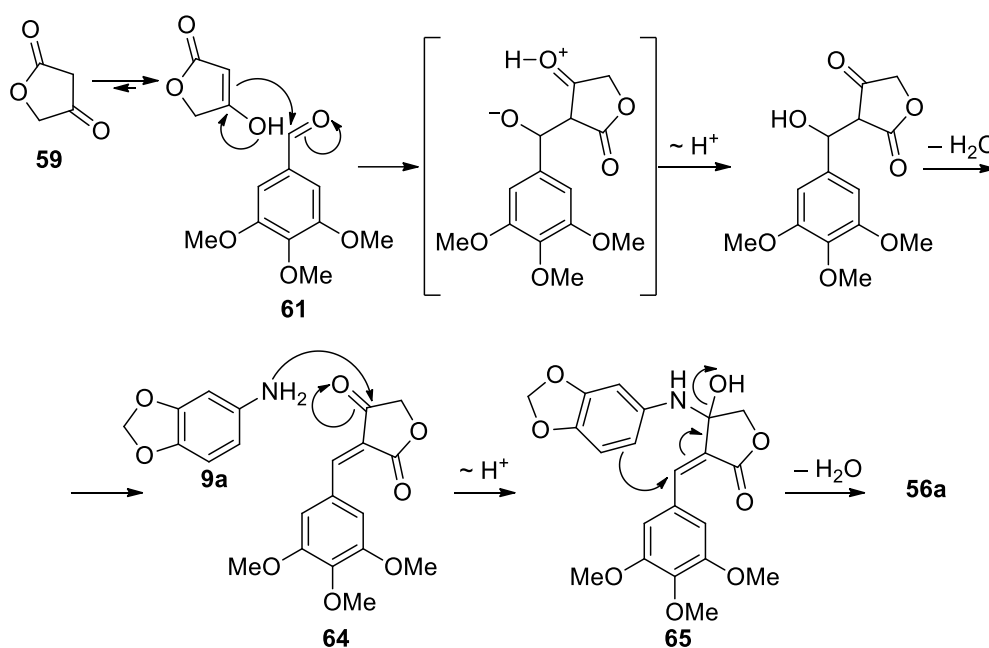
Scheme 11: Mechanism suggested by Giorgi-Renault and co-workers.[58]

This proposed sequence was investigated by doing first a two-step reaction, i. e. by only adding the aniline **58** after formation of the Knoevenagel adduct **64**. Using this two-step process, the 4-azapodophyllotoxin analogue **56a** was readily obtained in 85% yield. Following the success of this approach, the authors added all three components in one-pot, which gave

27

compound **56a** in a yield of 92%. It is interesting to observe that even *N*-substituted anilines were tolerated; for example, the MCR, when using *N*-methylaniline, gave a yield of 80%.

Another group, Tu and co-workers, proposed an alternative mechanism in which aniline first reacts with aromatic aldehyde. The resulting imine **66** then reacts with tetronic acid (**59**) to form the Knoevenagel adduct which, in turn, eliminates aniline (Scheme 12).[63] Aniline then adds to the elimination product **67**, and the amino group attacks the ketone functionality in compound **68**. After a proton transfer, a cyclic intermediate is formed. The loss of water then leads to the formation of a 4-azapodophyllotoxin derivative.

The mechanism discussed above differs from that proposed by Giorgi-Renault and co-workers in how the aniline reacts with the Knoevenagel adduct. Instead of a nucleophilic attack by the lone pair of the nitrogen of the aniline, a Hantzsch-type addition of the aniline to the Knoevenagel adduct is suggested.[64,82] This mechanism is again discussed in the later work of Tu and co-workers, where the nucleophilic attack occurs by way of the *ortho*-carbon atom of the aniline ring.[65,66,74] It should be noted that this mechanism has also been proposed by the group of Shi and co-workers.[68]
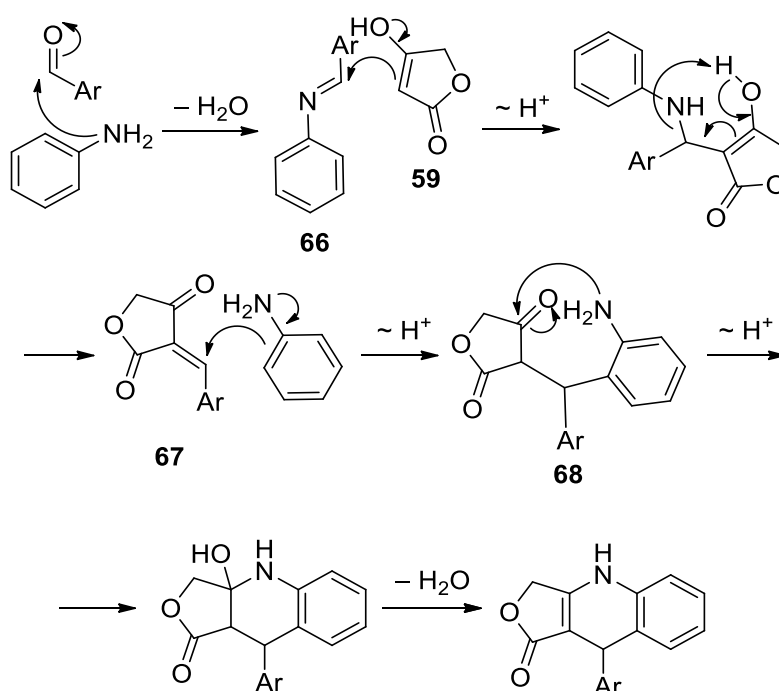
Scheme 12: Mechanism proposed by Tu and co-workers[63,65–67] and Shi and co-workers.[68]

Of interest, is that Shi and co-workers have employed a modified MCR by using a catalyst such as L-proline to afford products in greater yields and with less limitation on the substrates.[68] With L-proline acting as catalyst, the mechanism proposed involves the enamine **69** formation through the reaction of tetronic acid (**59**) with L-proline (Scheme 13). Compound

69 is then reacts with aldehyde to generate intermediate **70** which through the loss of water, forms the iminium Knoevenagel adduct **71**. Using catalyst loadings of 10 mol % L-proline, Tu and co-workers[66] showed that the requirement of the presence of an electron-donor in the *meta*-position of the aniline, initially identified by Giorgi-Renault and co-workers[58], no longer applied. For example, the use of 4-methylaniline in this modified MCR gave a 4-azapodophyllotoxin analog with 93% yield.
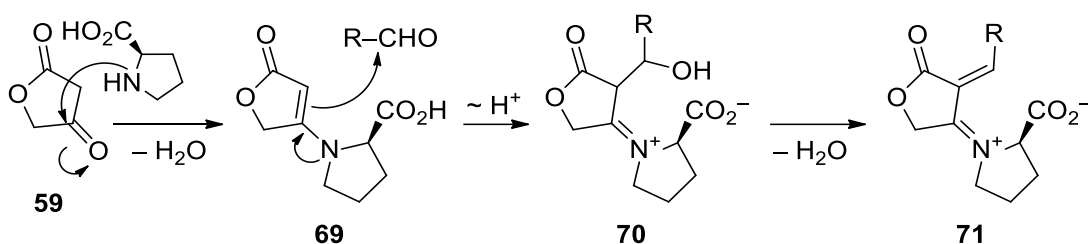
Scheme 13: Iminium Knoevenagel adduct formation as suggested by Tu and co-workers.[74]

With the successful application of L-proline as catalyst, a more recent study by Shi and co-workers then explored the use of five other organocatalysts (Figure 7), along with L-proline, for use in similar MCRs to synthesize compound **72** (Figure 7).[68] None of these additions, however, proved to be as efficient as L-proline.
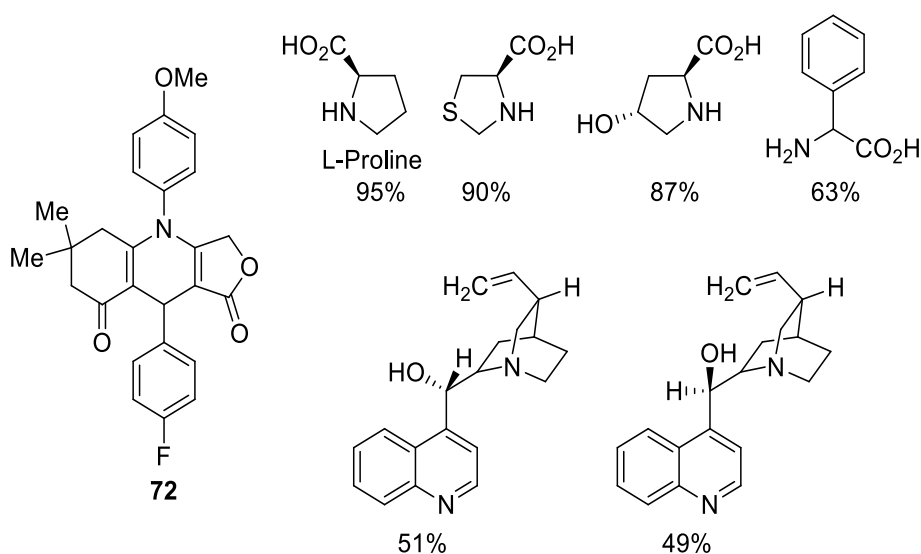
Figure 7: Organocatalysts used in MCRs by Shi and co-workers in the synthesis of compound **72**.[83]

However, these mechanisms were still just conjecture and the research groups focused more on the activity of the compounds produced, than on investigations into the reaction mechanism. Therefore, after a report by Bayer CropScience[61], in which the high yields for MCRs reported by Giorgi-Renault and co-workers[58] were not achieved, Roche and co-workers

investigated the mechanism of the MCR by performing step-wise reactions between the different components.[70] In this work, three reaction sequences were carried out, all in 2-pentanol at 120°C. The study began with the investigation of the reaction of tetronic acid (**59**) and 3,4,5-trimethoxybenzaldehyde **61**, to form the (Reaction 1, Scheme 14). However, no Knoevenagel adduct **64** formed after an hour. This was followed by using the same reaction order as originally published by Takeya and co-workers.[56,57] This involved the reaction of aniline **73** and tetronic acid (**59**) to form anilolactone **74**, followed by reaction of this product with the benzaldehyde **61** (Reaction 2, Scheme 14). Rather than using trifluoroacetic acid and *p*-chloranil in this reaction as per Takeya and co-workers,[56,57] the reaction conditions were kept the same as for a one-pot MCR. Roche and co-workers observed a full conversion to anilolactone **74** after just 5 minutes. However, the addition of a suitable benzaldehyde **61** in the second step produced no expected product and only returned the unreacted anilolactone **74**.[70] Lastly, these researchers reacted the aniline **73** with the benzaldehyde **61** (Reaction 3, Scheme 14). The full conversion to imine **76** occured within 5 minutes, and with the subsequent addition of tetronic acid (**59**), the 4-azapodophyllotoxin analog **75** was produced in 31% yield. Based on the third set of reaction conditions, the aniline **73** was thus deemed to serve a dual purpose, as elaborated below.
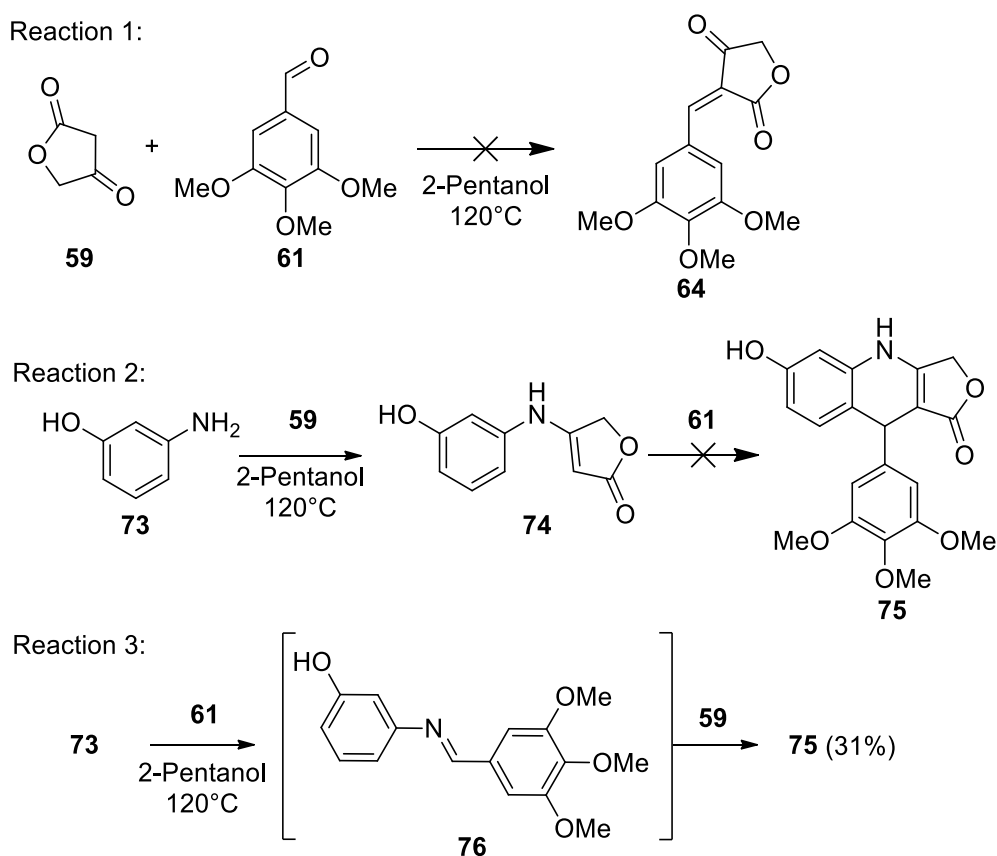
Scheme 14: Different model reactions performed by Roche and co-workers as probes into the mechanism of MCRs.[70]

To further investigate the roles played by aniline in the three-component synthesis of 4-azapodophyllotoxins, an electron-deficient aniline was used that did not fulfil the requirements set by Giorgi-Renault and co-workers, along with a "normal" aniline **73**.[58] The electron-poor 4-chloroaniline (**77**) was then utilized to first form the intermediate imine **78**, followed by the sequential addition of tetronic acid **59** and aniline **73** (Scheme 15).[70] It is important to note that after completion, only compound **75** was isolated in 31% yield and that none of the chlorine-containing product of the MCR was observed.
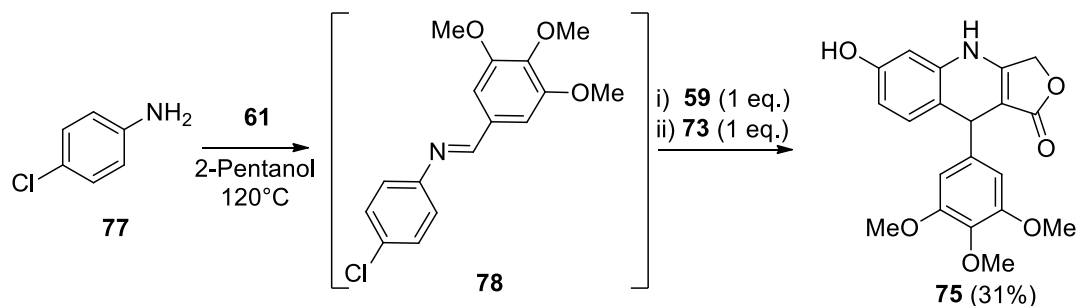
Scheme 15: Control reaction done by Roche and co-workers to support the dual-role hypothesis of aniline.[70]

Based on these experimental results, Roche and co-workers thus proposed a modified mechanism, in which the aniline first serves as a catalyst to form the Knoevenagel adduct, via the formation of an imine between the benzaldehyde and aniline, followed by reaction with the tetronic acid (**59**) (Scheme 16).[70] The initial aniline is then regenerated and reacts with the Knoevenagel adduct to form the product.

In further support of the proposed mechanism, the achiral intermediate **80** (obtained from the chiral hemiaminal **79**) explains why the products are always observed as a racemates. The intermediate **80** also explains why no enantiomeric enrichment was observed in the MCR products when a chiral ligand (L-proline) was used.[66] In summary, the work by Roche and co-workers gives a good indication of the importance of the aniline reactant in the discussed reaction, but it is clear that many nuances of this MCR are still poorly understood.[70] Further work is thus required, before the mechanistic understanding of this important reaction can be employed to expand its scope and allow modification of the reaction conditions to prepare currently inaccessible 4-azapodophyllotoxins, perhaps even enantiomerically enriched ones.
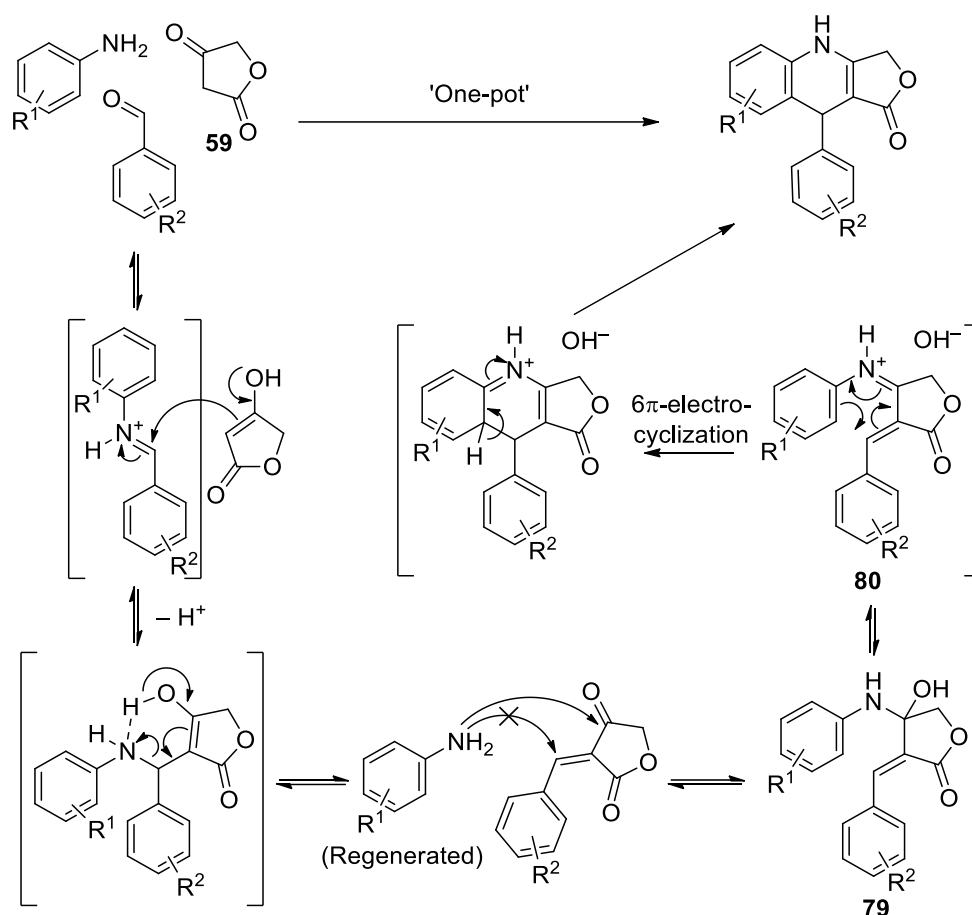
Scheme 16: Complete mechanism proposed by Roche and co-workers.[70]

Library Sytheses Azapodophyllotoxins

Due to the simplicity of MCRs, several 4-azapodophyllotoxin analogue libraries have been synthesized. The earlier projects tried to mimic the podophyllotoxin backbone, thus keeping the A, B, D, and E rings as close to the natural lignan as possible, for example, in the synthesis of 4-azadidehydropodophyllotoxin **56a** (Scheme 9).[56–58] Giorgi-Renault and co-workers also reported the synthesis of libraries of compounds that had variations in the A and E rings, as well as substitutions on the nitrogen in the C ring (Table 3).[58] These authors modified the A ring (product **81**) by annealing a benzene ring to the position 7 and 8, using 2-naphthylamine as the aniline reactant, as well as by leaving out the ring altogether (products **82**, **83**). The E ring was also modified by introducing heterocyclic (product **84**) or isomeric trimethoxyphenyl substituents (product **85**).

Table 3: Synthesis of 4-azapodophyllotoxin analogues **81–85** using MCR.[58]
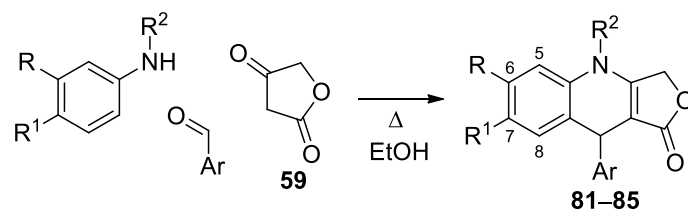
Product	R, R¹ (alkene)	R²	Ar	Yield, %
81	(o-xylene structure)	H	(trimethoxy aryl)	59
82	OH | H	H		63
83	OMe | OMe	H		94
84	(dioxane dimethyl structure)	H	(2-pyridyl)	78
85		H	(trimethoxy aryl)	83

Following these results, it is of interest that Ji and co-workers published a procedure on MCRs using microwave (MW) heating instead of conventional heating.[63] These researchers first optimized the reaction by trying various solvents at 80°C and MW power 300 W, as shown in Table 4.

Table 4: The effect of solvent on the synthesis of compound **86**.

Entry	Solvent	Time, min	Yield, %
1	Ethylene Glycol	12	86
2	Water	12	85
3	Acetic Acid	15	71
4	Dimethyl formamide	16	63
5	Ethanol	18	60

33

Since the use of ethylene glycol and water afforded the highest yields in the shortest times, the decision was made to use for further optimization water instead of ethylene glycol, as water is environmentally preferable.

86 (R^1 = Me)
87 (R^1 = H)   88a–c   89a,b   90   91a,b   92a,b
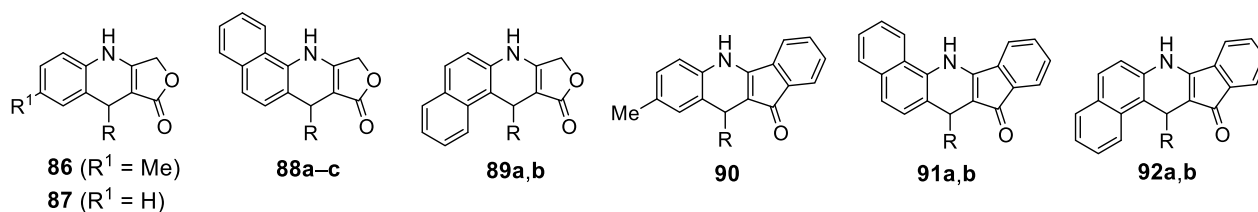
Figure 8: Novel analogues synthesized using MWI.

Table 5: Examples of reaction times and yields of the compounds (Figure 8) synthesized by Tu and co-workers under MW heating.[63]

Compound	R	Time, min	Yield, %
86	4-BrC$_6$H$_4$	5	96
87	4-FC$_6$H$_4$	6	95
88a	4-FC$_6$H$_4$	5	95
88b	Thiophen-2-yl	6	97
88c	n-C$_4$H$_9$	3	94
89a	4-FC$_6$H$_4$	5	93
89b	3,4-Cl$_2$C$_6$H$_3$	3	95
90	4-FC$_6$H$_4$	7	96
91a	4-FC$_6$H$_4$	5	97
91b	Thiophen-2-yl	6	98
92a	4-FC$_6$H$_4$	7	96
92b	Ph	3	97

Ji and co-workers carried out the reaction in water going up to 120°C in 10°C increments.[63] As the yields levelled out at higher temperatures, 100°C was chosen as the optimal value. The authors also searched for the optimal power output. It was established that the lower power

34

settings resulted in relatively poor yields. Using the optimized conditions, a library of 36 compounds was then synthesized. It is noteworthy that for this specific library, the anilines used did not have an electron-donating group in the *meta*-position. Examples included α-naphthylamine, β-naphthylamine, *p*-toluidine and aniline to vary the AB ring system. For the E ring, some variations were tried, including *para*-halogen-substituted benzaldehydes (products **86**, **87, 88a**, **89a**, **90**, **91a**, **92a**), as well as a short-chain linear aldehyde (product **88c**). All of these reactions were gave excellent yields in the range of 93–98% and some of the structures are shown in Figure 8. Benzaldehyde, 3- and 4-nitrobenzaldehyde and 4-methoxybenzaldehyde were also successfully utilized in the MW-heated MCR reactions. A few specific examples of these synthesized compounds are reported in Table 4 (antiproliferative activity of these compounds was unfortunately not described in this work). Using this method, a variety of AB-ring systems were then explored by Ji and co-workers, which included modifications to the D ring to generate indane-based podophyllotoxin analogues (**90–92**) .[63] These compounds were synthesized in excellent yields (the yields of some examples are shown in Table 5).

In 2007, Magedov, Kornienko, and co-workers investigated the use of various aminopyrazoles in MCRs with tetronic acid and 3,4,5-trimethoxybenzaldehyde to obtain the heterocyclic podophyllotoxin analogues shown in Figure 9.[71] 5-Methylpyrazol-3-amine used for the synthesis of compound **93f** gave the highest yield, as well as the best antiproliferative activity amongst those tested, having an activity similar to that of podophyllotoxin **50** (results discussed later in this review).

	R^1	R^2	Yield, %
93a	Ph	4-BrPh	45%
93b	*p*-Tol	Me	53%
93c	H	4-BrC$_6$H$_4$	54%
93d	*i*-Pr	Me	57%
93e	Me	Me	69%
93f	H	Me	80%
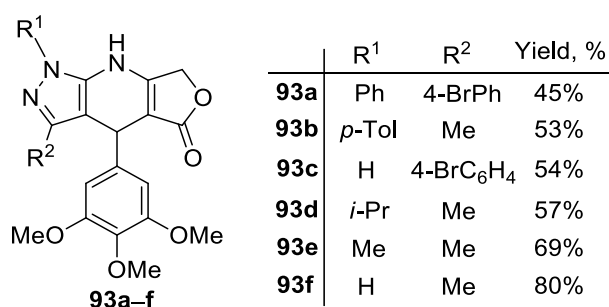
Figure 9: Various pyrazole-containing azapodophyllotoxin analogues synthesized by Magedov and co-workers with corresponding yields.[71]

Based on this result, the application of different aldehydes (26 in total) was investigated, followed by testing of the antiproliferative activity of the MCR products.[71] The promising activity of some of these 4-azapodophyllotoxin analogues prompted a further investigation by Magedov, Kornienko, van Otterlo, and co-workers in 2011, which involved the use of other aldehydes, as well as an unsubstituted aminopyrazole in the MCR.[29] In this study, a total of

47 compounds were synthesized (see representative examples **94**–**97** in Figure 10), including scaffolds using indoles and other heterocycles in the AB ring system (not shown). Four of these compounds with the pyrazole moiety in the AB ring system showed an antiproliferative activity similar to that of podophyllotoxin **50** (see later for a more detailed description of the antiproliferative activity). The yields of these dihydropyridopyrazole compounds ranged from 54–85%. In the same study, the use of α-naphthylamines in the MCR (e. g., products **96a**–**e**, **97a**–**e**).
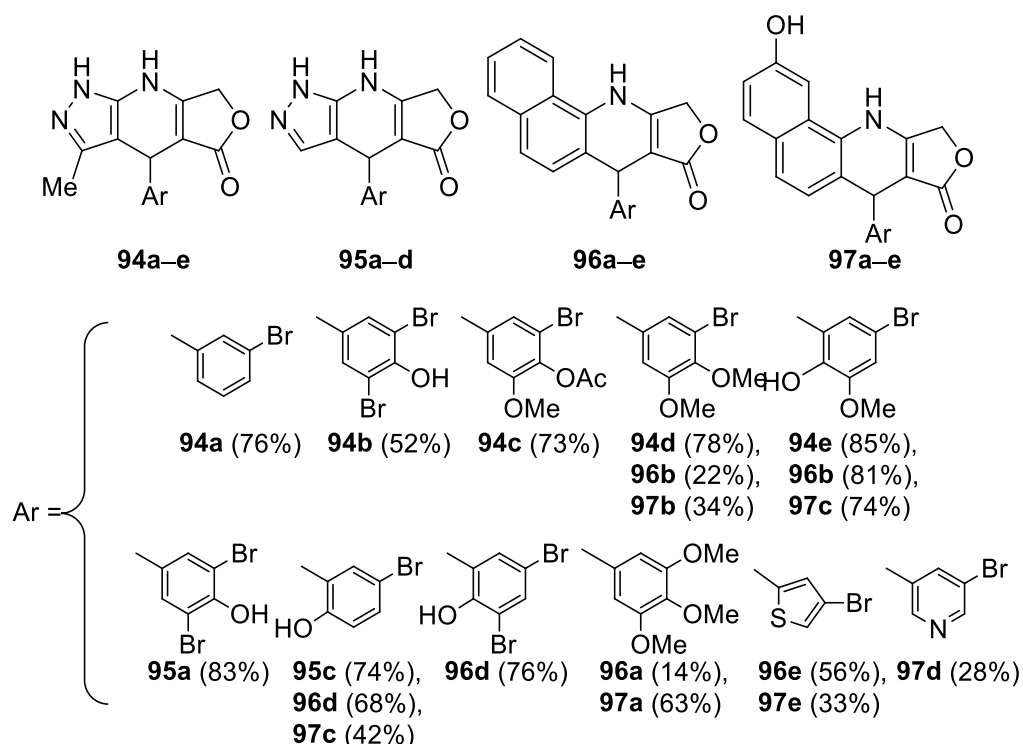
Figure 10: Azapodophyllotoxin analogues synthesized by Magedov and co-workers found to have good antiproliferative activity.[29]

Although the yields of some of these MCR products shown in Figure 10 were low, the reactions were all done under conventional heating conditions and could possibly be improved by using microwave heating. It is the high anticancer activity of these compounds that make them of interest. They exhibit antiproliferative activity similar to and greater than podophyllotoxin yet have all been generated in a one-pot, one-step reaction (the biological data of these compounds are given later in Tables 7 and 8). The lower yields of these compounds synthesized under conventional heating can probably be overcome, as Tu and co-workers did a study to compare the differences in yield when using microwave heating instead of conventional heating.[67] They reported increases in yield by 12–19%, as well as a reduction in reaction time by up to 97% when synthesizing *N*-phenyl-4-azapodophyllotoxin analogues **98a**–**f** (Table 6). These results highlight the efficiency of using microwave conditions for MCRs, both with respect to high yields of the desired products obtained, and to the use of

environmentally benign solvents, such as water.

Table 6: Reaction times and yields of syntheses of compounds **98a–f** under MW and conventional heating conditions.[74]

98a−f
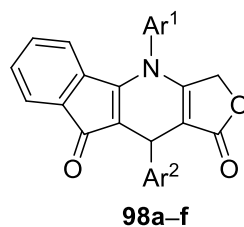
Com-pound	Ar^1	Ar^2	Time, min		Yield, %	
			MW	Conven-tional	MW	Conven-tional
98a	Ph	4-FC$_6$H$_4$	7	180	89	71
98b	Ph	Ph	10	270	74	61
98c	Ph	2,4-Cl$_2$C$_6$H$_3$	7	180	90	76
98d	4-MeC$_6$H$_4$	4-ClC$_6$H$_4$	10	210	88	71
98e	4-MeC$_6$H$_4$	4-BrC$_6$H$_4$	10	240	85	69
98f	4-ClC$_6$H$_4$	2,4- Cl$_2$C$_6$H$_3$	8	240	89	73

Recently, the group of Ghahremanzadeh and co-workers also reported the use of ionic liquids in the synthesis of *N*-phenyl-4-azapodophyllotoxin analogues such as compounds **99** (Scheme 17) which were prepared in excellent yields.[73] They demonstrated that the proposed MCRs performed in various 1-butyl-3-methylimidazolium (bmim) salt ionic liquids proceeded with great efficiency and with enhanced environmental benefits. These yields were better (75-90%) than those achieved with organic solvents (60-75%) and were obtained in a quarter of the time when compared to "normal" thermal conditions, meaning heating at reflux. The best organic solvent, ethanol, gave a yield of 75%, while the rest produced lower yields. Following this, the use of [bmim]Tf as a catalyst in was investigated and it was found that a 20 mol % loading of alum resulted in a 94% yield compared to 90% yield without the catalyst for the same reaction.

X = Tf (90%), OH (75%), Br (80%), PF$_6$ (88%) , BF$_4$ (83%)
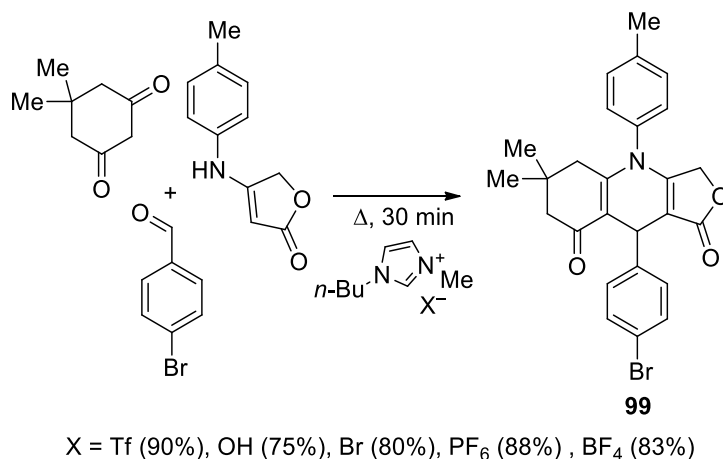
Scheme 17: Synthesis of compound **50** in different ionic solvents with respective yields.[73]

Thus, the use of a catalyst did improve the yield slightly but given the high yield of the reaction without catalyst, the use of a catalyst might only be necessary in cases where the yield is much lower. Unfortunately, compounds in this library were not tested for their ability to inhibit cell proliferation.

As regards more distantly related structures, Magedov, Kornienko, and co-workers also reported the synthesis of a dimeric analog with a pyrazole moiety in the AB ring, compound **100** (Figure 11), under conventional heating conditions in excellent yield (92%).[71] Tu and co-workers have synthesized dimeric *N*-phenyl-4-azapodphyllotoxin analog **101a-c** (Figure 11) using MW conditions.[74] The use of MW heating gave a more than two-fold increase in yield of these compounds in comparison with the conventional conditions.

These dimeric analogues only serve to show the scope of MCRs in generating 4-azapodophyllotoxin analogues, since the antiproliferative activity of compound **100** proved to be fairly weak. It should also be noted that other variations on the 4-azapodophyllotoxin scaffold have been achieved. These examples include products where the D lactone ring has been cleaved to form hydrazide, e. g., compound **102** (Fig, 11).[75] These compounds were utilized for their fluorescent properties, and their ability to induce cell death in cancer cells has not been investigated. Another example of a similar elimination of the D ring was published by Shestopalov and co-workers in which compounds having a 4-oxapodophyllotoxin scaffold lacking the D ring were produced by MCR (e. g., compound **103**, Figure 11).[76] Of interest is that these structural variations still produced compounds with good cytotoxic activity.
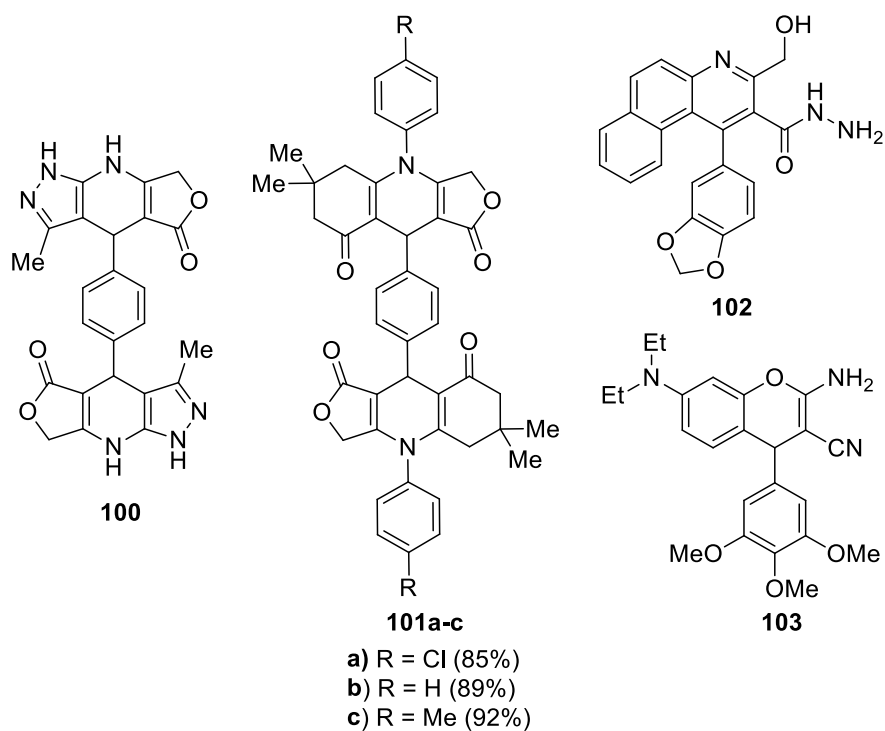
Figure 11: Dimeric 4-azapodophyllotoxin analogues **100**[71] and **101**[74]. Two examples with modified D rings (compounds **102**[75] and **103**[76]).

Even though compound **102** was not of interest for the use as an antiproliferative agent, together with compound **103** these compounds offer new avenues for exploring different structural analogues of azapodophyllotoxins as antiproliferative agents.[75,76]

**Anticancer activities of 4-azapodophyllotoxin analogues
and mode of action studies**

As described in the previous sections of this review, libraries containing a significant number of 4-azapodophyllotoxin analogues, with multiple points of variation, have been synthesized following the advent of the MCR approach to these compounds. However, it should be noted that the early libraries focused more on the synthesis of these compounds and on improving the yields of these reactions. Therefore, many of these compounds were not tested for their antiproliferative action (or, alternatively, these results were not reported in the literature). Nonetheless, it was clear from the initial studies that many of these compounds had very similar potency to the cyclolignan podophyllotoxin **50**, but with the substantial advantage that they could be generated in good to excellent yields by environmentally friendlier procedures.[71] This was in contrast to the large scale production of podophyllotoxin **50** which is still extracted from the *P. peltatum* and *P. hexandrum* species producing only 0.25 and 4% podophyllotoxin **50** by dry weight, respectively.[84] Since 4-azapodophyllotoxin derivatives with good activity could be generated in one step, Magedov, Kornienko, and co-workers used the libraries of compounds synthesized in their group to generate systematic structure activity relationship (SAR) data.[54] This group[29,71,72] had synthesized libraries of dihydropyridopyrazole analogues of 4-azapodophyllotoxin, as well as analogues based on α-naphthylamine. Table 8 shows some of the results involving the antiproliferative and apoptosis-inducing effect of some of the dihydropyridopyrazole analogues on the HeLa, MCF-7/AZ, and Jurkat cell lines.[72] The most active examples, compounds **82**, **93f**, and **94a**–**d** are shown, and their activities are compared to those of podophyllotoxin **50** and 4-aza-2,3-didehydropodophyllotoxin **56a** originally synthesized by Giorgi-Renault and co-workers[58] (Table 7).

As shown in Table 8, these compounds all have apoptosis-inducing properties comparable to that of the naturally occurring cyclolignan **50**, inducing apoptosis in more than half of the Jurkat cells in the assays performed. As to the remaining cell viability, only compound **94d** (Table 7) had activity similar to that of podophyllotoxin **50**, faring almost the same against HeLa and MCF-7/AZ cell lines than podophyllotoxin (details in Table 7). Compounds **94a**–**d** proved to be less active than the aminopyrazole analogues without the methyl group (compounds **95a**–**d**), which had GI_{50} values very similar to that of podophyllotoxin (Table 8). The naphthylamine derivatives **96** and **97**, however, showed very high potency, inhibiting HeLa and MCF-7 cells at concentrations as low as 2 nM.

Table 7: Antiproliferative and apoptosis-inducing properties of podophyllotoxin (**50**) and some 4-azapodophyllotoxin analogues synthesized by Magedov, Kornienko and co-workers.[72]

56a: R + R^1 = O(CH$_2$)$_2$O, **82:** R = R^1 = MeO
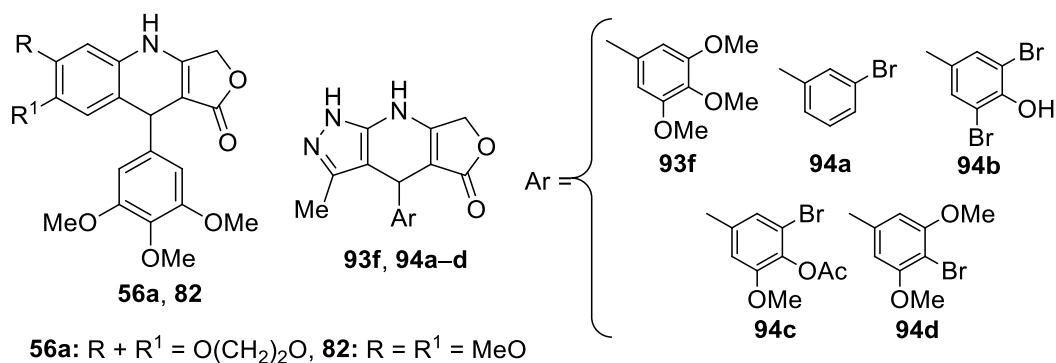
Compound	Cell viability*, %			Apoptosis**, % Jurkat
	HeLa	MCF-7/AZ	Jurkat	
50	19 ± 5	55 ± 3	18 ± 5	54 ± 2
56a	54 ± 6	52 ± 3	54 ± 1	55 ± 4
82	53 ± 5	58 ± 4	35 ± 6	49 ± 4
93f	50 ± 2	58 ± 5	47 ± 3	55 ± 4
94a	51 ± 3	63 ± 4	68 ± 3	58 ± 2
94b	58 ± 7	60 ± 6	58 ± 3	53 ± 0
94c	47 ± 2	46 ± 2	36 ± 6	58 ± 1
94d	16 ± 3	47 ± 1	29 ± 3	56 ± 1

* Percent of remaining cell viability after 48 h treatment with compounds at a final concentration of 5 μM relative to DMSO control ±SD from 2 independent experiments, each performed in 8 replicates. Determined by MTT assay.

** Percent of apoptotic cells after 48 h treatment with compounds at a final concentration of 5 μM relative to DMSO control ±SD from 2 independent experiments, each performed in 8 replicates. Determined by flow cytometric Annexin-V/propidium iodide assay.

Table 8: GI$_{50}$ values of pyrazole- and α-naphthylamine-based 4-azapodophyllotoxin analogues* by Magedov, Kornienko, and co-workers[71,72]

94a–e 95a–d 96a–e 97a–e
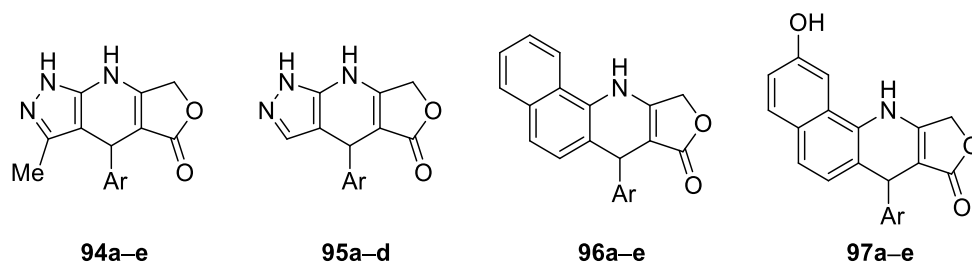
Compound	GI$_{50}$**, μM		Compound	GI$_{50}$**, μM	
	HeLa	MCF-7		HeLa	MCF-7
50	0.020 ± 0.002	0.010 ± 0.003	**96a**	0.003 ± 0	0.003 ± 0
94a	3 ± 0.1	4.0 ± 0.3	**96b**	0.003 ± 0	0.003 ± 0
94b	8 ± 2	–	**96c**	0.003 ± 0	0.003 ± 0
94c	4 ± 1	–	**96d**	0.003 ± 0	0.003 ± 0
94d	0.75 ± 0.1	1.0 ± 0.1	**96e**	0.003 ± 0	0.003 ± 0
94e	0.035 ± 0.004	0.10 ± 0.04	**97a**	0.002 ± 0	0.003 ± 1
95a	0.025 ± 0.008	0.025 ± 0.003	**97b**	0.002 ± 0	0.003 ± 0
95b	0.025 ± 0.003	0.030 ± 0.005	**97c**	0.003 ± 1	0.003 ± 1
95c	0.050 ± 0.005	0.025 ± 0.004	**97d**	0.003 ± 0	0.003 ± 0
95d	0.020 ± 0.005	0.010 ± 0.003	**97e**	0.003 ± 0	0.003 ± 0

* General structures given – for substitutions of the E ring, see Table 5.

**Concentration required to reduce the viability of cells by 50% after 48 h treatment with compounds, relative to DMSO control, ±SD from 2 independent experiments, each performed in 8 replicates, determined by MTT assay.

In terms of another set of compounds tested for their antitumor activities, it should be noted here that Kumar and Alegria also synthesized a range of 12 *N*-substituted 4-aza-analogues by MCR.[77] Representative examples of these compounds are shown in Figure 12. The group

of Kumar and Alegria then expanded this library to 18 *N*-hydroxyethyl-4-azapodophyllotoxins in a follow-up study (compounds **104**–**106**, Figure 12) and screened this library against the National Cancer Institue's 60 human tumor cell lines.[77,85] These compounds had good activity (most compounds showing GI_{50}-values in the sub-micromolar range), with compounds **105a**–**f** proving to be more active *in vitro* than their related heteroatom scaffolds **104a**–**f** and **106a**–**f**.
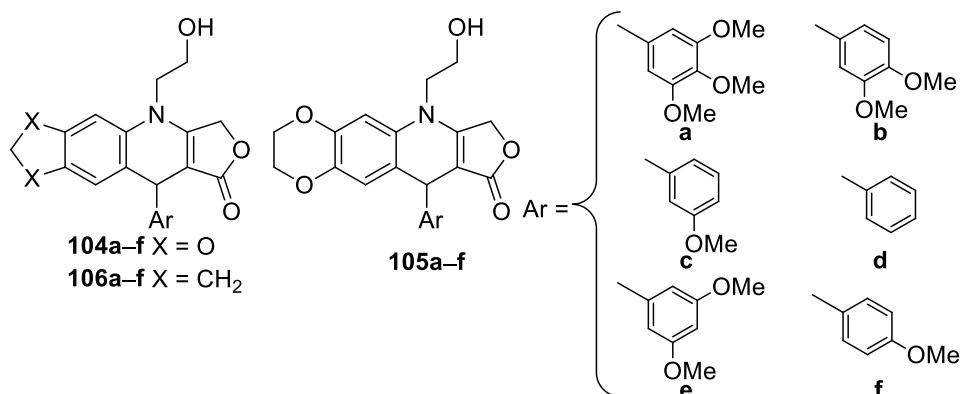
Figure 12: Library of N-hydroxyethyl-4-azapodophyllotoxins synthesized by Kumar and Alegria.[77,85]

Kamal and co-workers also synthesized a small library of 4-azapodophyllotoxin analogues and tested these against 5 human cancer cell lines (MCF-7, KB, Colo 205, A-549, and A-2780). Out of the 23 compounds contained in this library, three compounds **107**–**109** (Figure 13) had activity comparable to podophyllotoxin **50** and better than etoposide **55a** against certain cell lines (data shown in Table 9).[78] Tu and co-workers also reported the synthesis of a small library of 12 compounds with the benzothiazole-moiety in the AB ring system. These compounds were similar to compound **109**, albeit with variations in the E ring by the use of different aldehydes.[79] These compounds were then screened against three carcinonoma cell lines (M14, MCF-7, and SW1116), and exhibited cytotoxic activities ranging from moderate to strong.
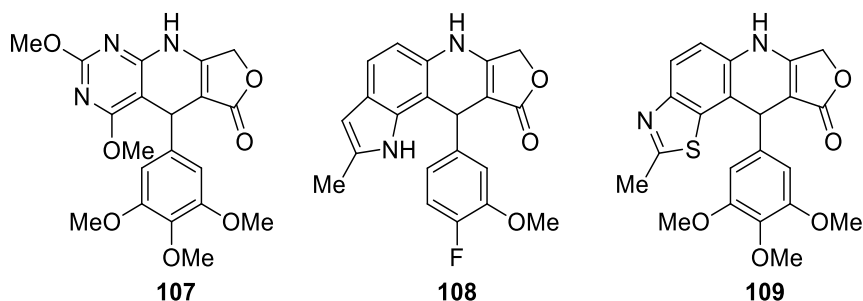
Figure 13: Three most active compounds from the library synthesized by Kamal and co-workers.[78]

Table 9: Cytotoxic activity of compounds **55a**, **107**–**109** (GI_{50}, μM) against the 5 human cancer cell lines.

Com-pound	Breast MCF7	Oral KB	Colon Colo 205	Lung A-549	Ovarian A-2780
107	2.4	0.17	0.16	2.1	–
108	2.6	–	–	2.1	2.4
109	–	2.1	2.5	2.4	2.3
55a	2.1	0.3	0.13	3.08	1.3

An interesting variation to the 4-azapodophyllotoxin scaffold was also investigated by Labruère and co-workers, where various linkers, including methylene and phenylene groups, were incorporated in between the C ring and E ring, e. g., compounds **110**, **111** (Figure 14).[80] The goal was to design novel antivascular agents that maintained a potent activity towards tubulin, but with lower toxicity towards normal, healthy cells. These compounds proved to fairly inactive in the destabilization of tubulin, thus showing that the linker has a deactivating effect.[80] Compound **110** did, however, show promising results as an antivascular agent.
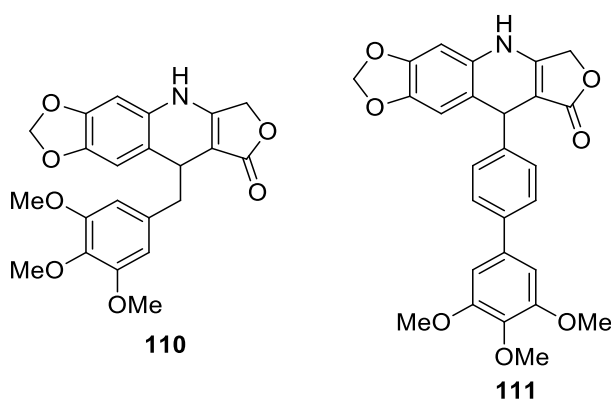
Figure 14: 4-Azapodohyllotoxin analogues with linkers between C and E rings.[80]

As mentioned earlier, podophyllotoxin **50** is known to inhibit cell mitosis through microtubule destabilization.[47] In 2011, Magedov and co-workers investigated the mode of action of the 4-azapodophyllotoxin analogues synthesized by them to see if it was similar to that of the natural product, the latter thus being mimicked by the MCR products.[29] Using flow cytometric cell cycle analysis, it was found the pyrazole-based 4-azapodophyllotoxin analogues, like compounds **94a**–**e** and **95a**–**d** (Figures 9 and 10), retained the microtubule-destabilizing mechanism of the

natural cyclolignan **50**. The retention of the microtubule-destabilizing activity was also confirmed *in vitro* using a fluorimetry-based tubulin polymerization assay. In the same study, the effect of the stereocentre in the C ring was also investigated. Using chiral HPLC to separate the enantiomers of compound **112** (Figure 15), these researchers found the *R*-isomer to be four orders of magnitude more active than the *S*-isomer.[29] The bioactivity results obtained, and shown in Figure 15, indicates that the isomer that mimics the stereochemistry of podophyllotoxin **50** clearly is the more active of the two isomers. This evidence thus adds support for the hypothesis that these particular synthetic structures mimic the natural product prototype very closely, perhaps even in terms of biological interactions with the target site.
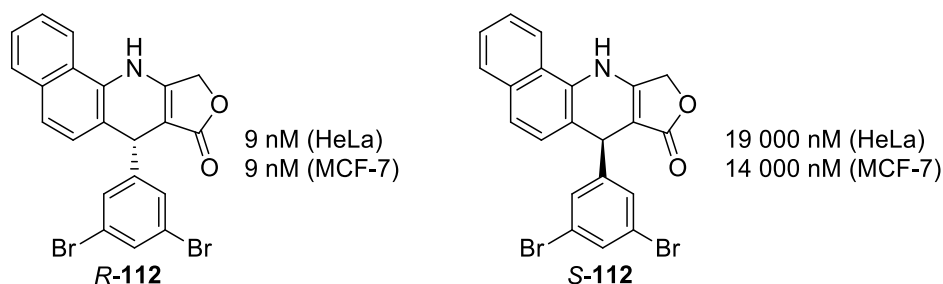
Figure 15: Comparison of GI_{50} values of the enantiomers of compound **112** against two cell lines.[29]

The application of MCR has become a powerful synthetic tool in modern drug discovery, due to its atom economy and the fact that molecular diversity is readily achievable through one-step syntheses.[81] This has been demonstrated by the advances in podophyllotoxin-inspired medicinal chemistry research, with many active 4-azapodophyllotoxin analogues being generated by way of MCRs in good to excellent yields. A fair number of research groups have thus generated libraries of new 4-azapodophyllotoxin analogues of considerable structural variety, thereby demonstrating the versatility of these reactions. The fact that these active compounds are now accessible through one-step syntheses, means that more effort can now be invested in improving the selectivity and potency of these compounds, instead of focusing on linear total syntheses to generate simple podophyllotoxin analogues. Downstream medicinal chemistry issues such as ADMET properties can now also be addressed, as many of the currently active compounds are very insoluble (see for instance the use of mimicry involving the prodrug, etopophos, by making phosphate salts of the active MCR products). Since the MCR also allows to synthesize *N*-substituted analogues, the activity of these compounds can now be compared to etoposide and teniposide; so the compounds such as compound **99** should be tested for their antiproliferative action and their mode of action. It would be interesting to see if these compounds change from inhibiting cell proliferation by inhibiting microtubule assembly to topoisomerase II inhibitors. The biggest challenge of all that still needs to be addressed is enantioselectivity, as Magedov and co-workers have shown that the

R-isomer is significantly more active than the *S*-isomer.[29] Thus, an enantioselective MCR could possibly produce active compounds with single digit nanomolar or even sub-nanomolar activities (for a recent review on advances made in asymmetric MCRs see the review published by de Graaf, Ruijter and Orru[86]).

2.2.2 Addendum to the review – new work published since February 2014

In this section, work published after our review will be discussed. The publications included will focus more on advances in 4-azapodophyllotoxin research rather than discuss any new libraries added to the literature, unless these libraries deliver new insights. Therefore, this section will discuss biological results and insight gained surrounding the method of action, as well as molecular modelling results.

1.2.2.1. Insights gained from new libraries

Kamal and co-workers considered the different libraries of 4-azapodophyllotoxins that have been reported and incorporated 1,10-phenantrholin-5-amine (**113**) into the azapodophyllotoxin scaffold as a modified AB-ring system.[87] Previous libraries, such as those done by our collaborators, remarked on the increase in anticancer potency of azapodophyllotoxins when heterocycles, pyrazoles in particular, and polyaromatic moieties, such as naphthyl groups, were incorporated in the AB-ring system.[29,71,88] The use of the 1,10-phenanthroline motif served as a hybrid of both the aforementioned moieties (Figure 16).
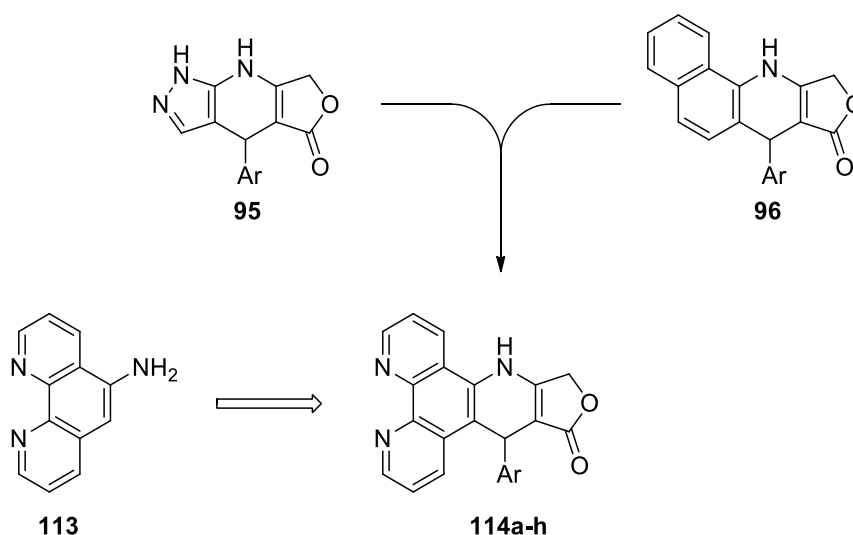
Figure 16: Hybridization of pyrazole- and naphthyl-azapodophyllotoxins into the phenanthroline-azapodophyllotoxins.[87]

The general MCR procedure, as proposed by Giorgi-Renault and co-workers[58], was employed to generate a library of phenanthroline azapodophyllotoxin (**114a-h**) analogues. Representative examples of the library are shown in Scheme 18.
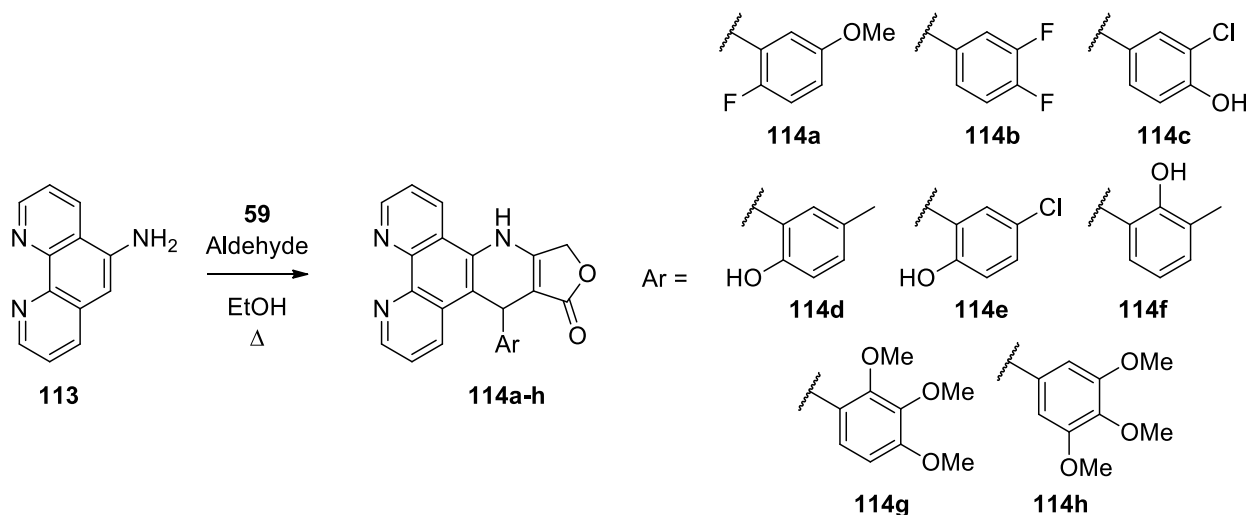
Scheme 18: Representative examples of phenanthroline-azapodophyllotoxin analogues by Kamal and co-workers.[87]

Table 10: GI_{50} values of the representative phenanthroline-based azapodophyllotoxin analogues reported by Kamal and co-workers.[87]

Compound	GI_{50} μM		
	MIAPACA	MCF-7	HeLa
50	0.5 ± 0.1	0.23 ± 0.09	0.71 ± 0.2
55a	1.3 ± 0.03	0.25 ± 0.1	0.64 ± 0.4
114a	0.02 ± 0.01	0.01	<0.01
114b	0.5 ± 0.04	<0.01	0.03 ± 0.01
114c	0.9 ± 0.07	7.7 ± 1.3	0.3 ± 0.02
114d	2.0 ± 0.9	8.2 ± 0.2	<0.01
114e	NA	NA	0.3 ± 0.1
114f	1.9 ± 1.6	NA	0.6 ± 0.09
114g	0.5 ± 0.4	10.3 ± 2.4	0.2 ± 0.1
114h	3.7 ± 0.9	8.2 ± 0.2	0.16 ± 0.01

These compounds were tested for their antiproliferative activity against pancreatic (MIAPACA), breast (MCF-7) and cervical (HeLa) cancer cell lines (Table 10). The results of compounds **114a-h** are shown in Table 10, along with the activity results for podophyllotoxin (**50**) and etoposide (**55a**). In summary, the incorporation of this polyaromatic, heterocyclic

motif delivered compounds with activity comparable to the natural compound and its semisynthetic derivative.

Interestingly, a study by Westwell and co-workers, following the same general MCR procedure, also investigated the use of 1,10-phenanthrolin-5-amine (**113**); however, they reported that the reaction did not deliver the desired 4-aza-2,3-didehydropyridophenanthroline scaffold (**114**).[87] They reported that the elimination of the water to deliver the 2,3-didehydropyrido-scaffold did not occur, instead, the reaction delivered the **C3**-hydroxy product (**115**, Scheme 19).

Westwell and co-workers determined the crystal structure of compound **115c** by means of X-ray diffraction, which showed the reported compound in the *cis*-γ–lactone conformation. The analysis showed that only two enantiomers were present and both, in fact, showed the γ-lactone ring in the *cis*-configuration (Figure 17). These compounds were analysed for their antiproliferative activity against two cancer cell lines and reported IC$_{50}$ values comparable to podophyllotoxin (**50**), etoposide (**55a**) and teniposide (**55b**), as shown in Table 11.
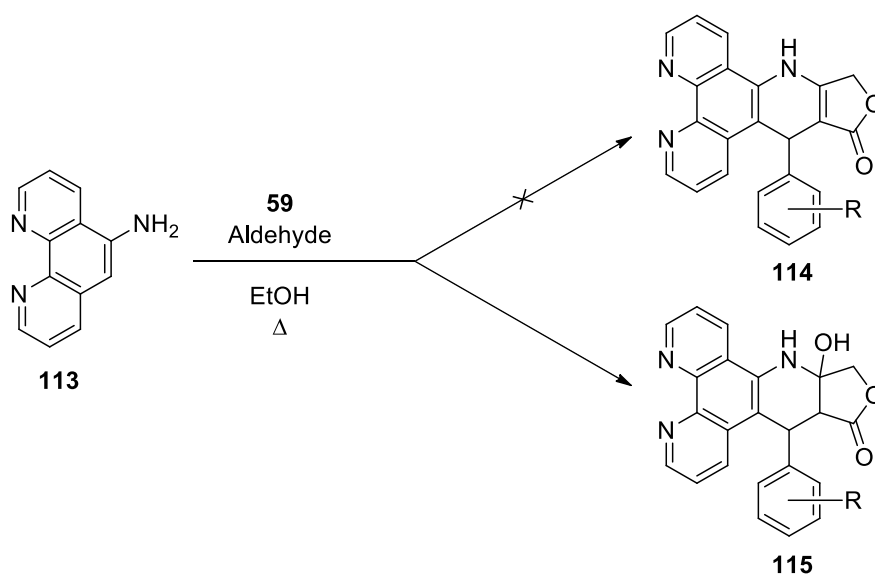
Scheme 19: C3-hydroxyazapodophyllotoxins reported by Westwell and co-workers.[89]

Westwell and co-workers performed docking studies to gain more understanding into the how these compounds interact with the colchicine binding site of the tubulin-podophyllotoxin crystal structure (PDB ID: 1SA1).

Table 11: IC$_{50}$ values of representative C3-hydroxyazapodophyllotoxins (as racemates) reported by Westwell and co-workers.[89]

Compound	R	IC$_{50}$ (μM)	
		MCF-7	22Rv1
115a	4-SCH$_3$	0.648	0.855
115b	2-OCF$_3$	0.288	0.165
115c	3-OCF$_3$	0.466	0.257
115d	4-OCF$_3$	0.424	0.239
115e	2-CF$_3$	0.209	0.107
115f	3-CF$_3$	0.825	0.510
115g	3-SF$_5$	0.589	0.311
115h	3-CH$_3$,5-OCF$_3$	0.475	0.242
115i	4-SCF$_3$	2.295	0.894
115j	3,5-*bis*-CF$_3$	0.643	0.380
115k	3-CF$_3$,4-OC$_2$H$_5$	0.355	0.295
115l	4-OCF$_2$H	0.901	0.719
115m	2-CH$_3$,5-OCF$_3$	3.307	2.842
115n	4-SF$_5$	0.857	0.590
115o	2-OCH$_3$,4-OCF$_3$	0.396	0.322
115p	5-OCH$_3$, 3,4-methylenedioxy	7.250	4.002
115q	3,4-difluoromethylenedioxy	0.910	0.520
50	Podophyllotoxin	1.264	0.364
55a	Etoposide	0.125	0.082
55b	Teniposide	0.230	-

115c
C1-*S,* **C2**-*R*, **C3**-*S*
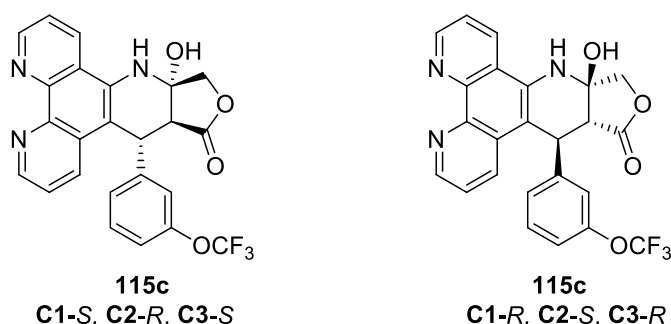
115c
C1-*R,* **C2**-*S*, **C3**-*R*

Figure 17: Two different antipodes of compound **115c**, as determined from the crystal structure.

The *cis*-γ-lactone configuration of the **C1**-*R*, **C2**-*S*, **C3**-*S* antipode (**115c**) showed a novel mode of interaction in the binding pocket, with a hydrogen bond bridge between the carbonyl oxygen

of the lactone ring and the thiol chain of βCys241 as well as a hydrogen bond between the **C3**-hydroxy group and the carbonyl group of βLys352. The **C1**-R antipode showed a more favourable docking interaction than the **C1**-S and shares the same absolute configuration as podophyllotoxin (**50**) (Figure 18).
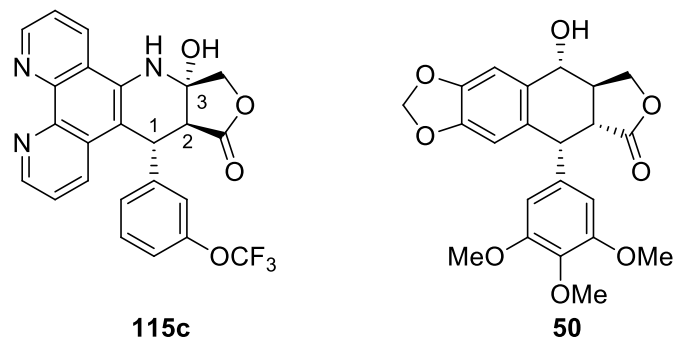
Figure 18: **C1**-R, **C2**-S, **C3**-S antipode (**115c**) and podophyllotoxin (**50**).

These two studies, the one by Kamal and coworkers[87] and Westwell and co-workers[89], did pose an interesting problem, as both studies reported different structures for the main CD-ring system (the conventional unsaturation between C2 and C3 for Kamal and co-workers, and saturated system due to the C3 hydroxy-group as reported by Westwell and co-workers). Both studies[87,89] followed the general procedure as proposed by Giorgi-Renault and co-workers and consideration of the experimental procedures of the two studies in question show no appreciable difference in execution, only in the different aldehydes employed. The reported reaction times do vary, but in terms of literature, this is common, and it would be difficult to identify as an appreciable difference. Both research groups substantiated their structures using ^{1}H NMR, ^{13}C NMR and mass spectrometry.

Westwell and co-workers stated that they have conclusively proven that the previously reported structures of Kamal and co-workers are incorrect. However, the statement was problematic in that their library of analogues[89] did not include any of the aldehydes used in the study by Kamal and co-workers[90] and neither study reported IR data. The IR data would give a clear indication of whether a hydroxyl group was present or not, as in the case of the mass spectrometry data, the researchers of both groups reported high resolution masses for their compounds that correlated to the calculated masses. This would lead to the only possible point to deliberate on for the discrepancies in structure, the differences in the electronic effects of the pendent E-rings that originate from the aldehydes.

The aldehydes used by Westwell and co-workers were all fluorinated (with the exception of the aldehyde employed in the synthesis of compound **115p**) and many contained multiple fluorine groups. Kamal and co-workers employed more varied and traditionally used

aldehydes (ether containing aromatic aldehydes). These aldehydes are shown below in Figure 19 so the two sets could be considered together. The Westwell library included many derivatives that contained the trifluoromethyl group as well as sulphur groups. When this is considered against the substitution patterns of the Kamal library, a strong difference in the electronic character could be postulated.

Kamal and co-workers
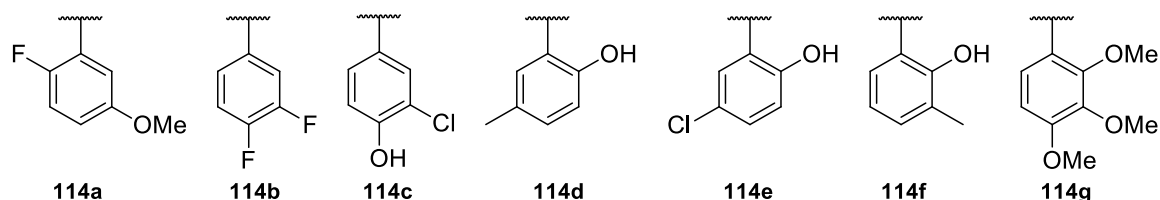
Westwell and co-workers
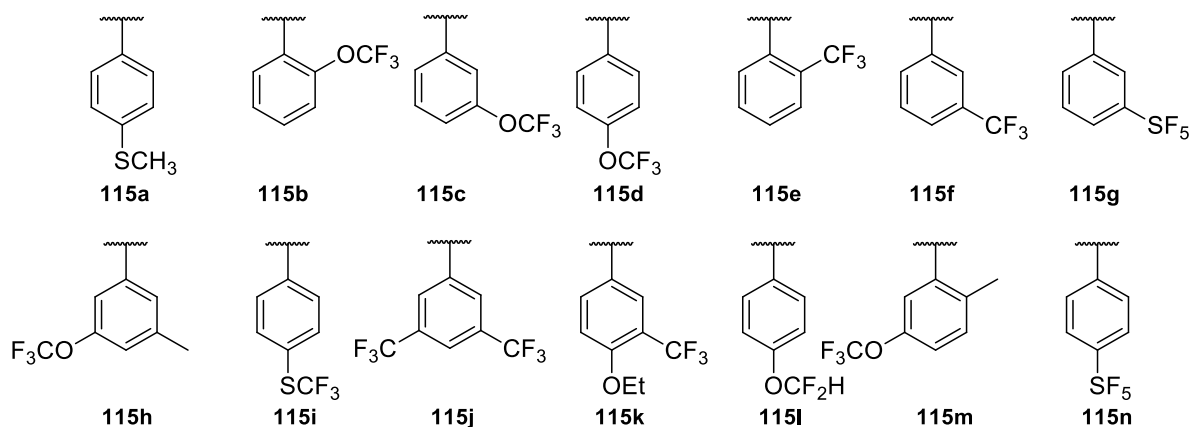
Figure 19: Aldehydes employed by the two groups, **114a-g** by Kamal and co-workers[87] and **115a-n** by Westwell and co-workers[89].

Westwell and co-workers had also suggested a mechanism why the expected elimination to furnish the 2,3-didehydropyridino scaffold did not occur. This mechanism was the same as that reported by Tu and co-workers[63,65–67] and Shi and co-workers.[68] This mechanism considered a nucleophilic attack by the *ortho*-carbon in the aromatic ring on the Michael acceptor of the Knoevenagel adduct before the attack of the amine on the 3-ketone. This mechanism has been discussed earlier on page 28 and therefore will not be discussed in depth again. Roche and co-workers also did perform a systematic probe into the mechanism of this class of compounds that did show that the nucleophilic attack by the amine on the ketone occurred first to set up a 6π electro-cyclization where the nucleophilic *ortho*-carbon would attack the electrophilic Michael acceptor (Shown below in Scheme 20).[70]
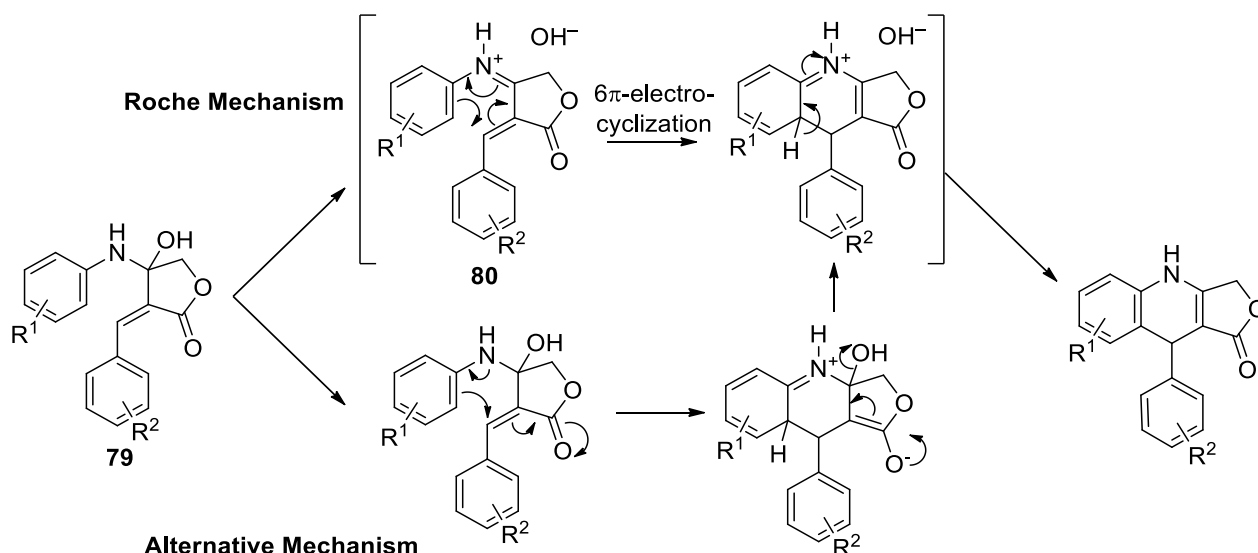
Scheme 20: Represented step in the mechanism proposed by Roche and co-workers (See page 32 for discussion of this mechanism).[70]

An alternative route can also be considered that involved the ester ketone and achieved elimination by means of an E_1CB mechanism. These proposed mechanisms account for the standard CD-ring structure reported in 4-aza-2,3-didehydropodophyllotoxin research. As we have had significant experience with these scaffolds along with our collaborators[29,71,72,88], our synthetic results concur with that reported by Kamal and co-workers.[87] Therefore, we query the results reported by Westwell and co-workers and their conclusion that they have proven the work by Kamal and co-workers incorrect. The anomalous NMR data they reported is interesting but does not hold up to an inspection of the scaffold. The *cis*-hydration over the 2,3 positions of the C-ring (as can be seen in the annotated structure in Figure 18) would give rise to two new signals. The methine proton on carbon 2 and the 3-hydroxyl-proton. Westwell and co-workers reported two such signals, with the proton on the tertiary carbon appearing at 3.5 ppm and the solvent exchangeable OH-proton at 6 ppm, both as singlets. However, the proton on the tertiary carbon would be expected to show a doublet through coupling with the hydrogen on C1. A chemical shift of δ 6 ppm for the OH proton is also fairly uncharacteristic with alcohol OH protons generally appearing in the 0.5 – 5 ppm range, as well as not appearing as a broad singlet. The researchers are ambiguous with regards to the singlet, not specifying that it is indeed a broad singlet.

As both groups had provided full characterization of their reported compounds, neither study could be called into question. The discussion with regards to discrepancies in the reported final compounds only served to show that the mechanism through which the reagents of this class of MCR products assemble into the resulting scaffolds still needs to be investigated more. The substitution pattern on the aromatic aldehyde appeared to play a significant role in

52

whether the C-3 hydroxy-elimination does take place. The crystal structures reported by Westwell and co-workers do conclusively show the presence of this hydroxy-group. However, the NMR data reported by Kamal and co-workers conform with literature in terms for the elimination product that Westwell and co-workers did not find.

Wu and co-workers also investigated the hybridization of the 4-azapodophyllotoxin scaffold, focusing on alterations of the D-ring.[91] Their study investigated substituting tetronic acid (**59**) with a different 1,3-diketone species. The researchers considered the biological activity of *para*-naphthoquinones, such as rhinacanthin C (**116**), that have been showed to have anti-inflammatory and anti-viral properties, in addition to strong anticancer properties.[92–94] To achieve this, Wu and co-workers incorporated 2-hydroxynaphthalene-1,4-dione (**117**) into the 4-azapodophyllotoxin scaffold to provide *para*-naphthoquinone-4-aza-podophyllotoxins (**118a-d**, Scheme 21). The use of 2-hydroxynaphthalene-1,4-dione (**117**) has also been reported by Pélinski and co-workers in a study that investigated the incorporation of various 1,3-diketones into the 4-azapodophyllotoxin scaffold through microwave-assisted synthesis.[95]
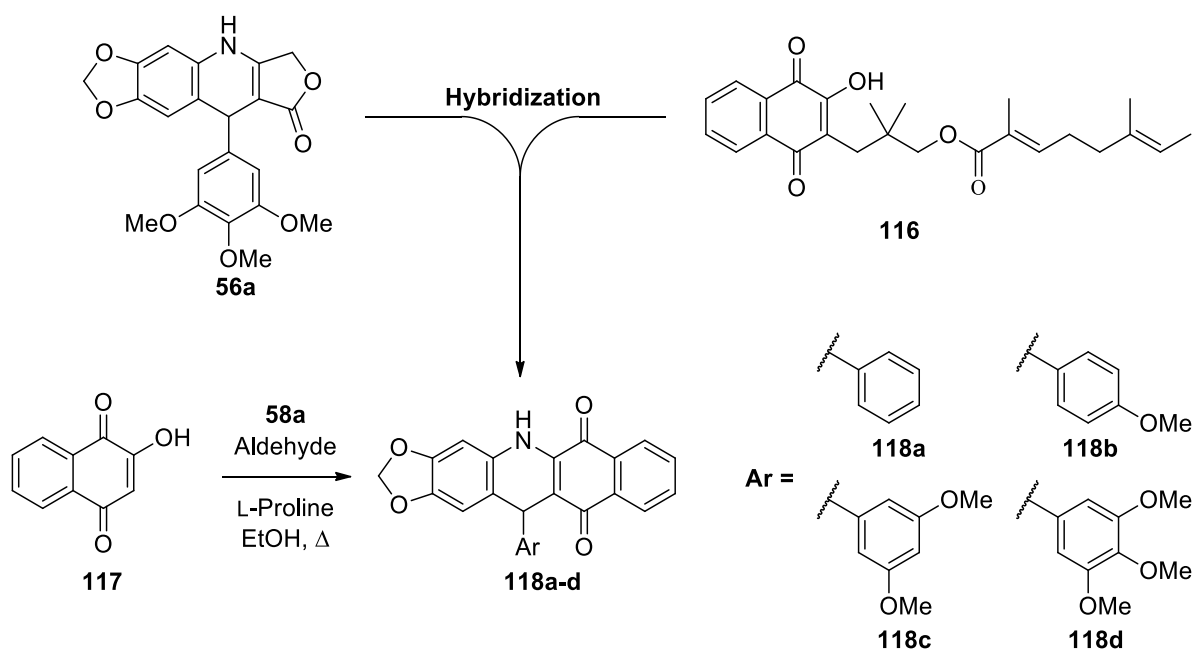
Scheme 21: Azapodophyllotoxin analogues with a modified D-ring. Representative para-naphthoquinone-hybrids reported by Wu and co-workers.[91]

Wu and co-workers determined the antiproliferative activity of these *para*-naphthoquinone-4-azapodophyllotoxins against liver (HepG2) and ovarian (HeLa) cells, as well as determining the cytotoxicity against a non-cancerous cell line (L02). The biological activity of these compounds were compared to that of the first 4-azapodophyllotoxin analogue (**56a**), reported by Giorgi-Renault and co-workers.[58] The antitumour activity of the compounds from this study that showed the greatest activity are shown in Table 12, along with the cytotoxicity values

against the non-cancerous L02 cell line. The aim was to determine whether the modification of the D-ring increased the specificity of these compounds towards the cancerous cell lines over the non-cancerous cell lines.

The greatest specificity was observed for compound **118c**. The L02/HepG2 ratio was determined to be 2.29 in comparison to 1.47 for compound **56a**. Other compounds also showed specificity ratios similar to that of compound **118c**; however, the HepG2 cytotoxicity of these compounds were also lower than that of the representative compounds discussed.

Table 12: Activity values of the representative naphtoquinone azapodophyllotoxin analogues reported by Wu and co-workers.[91]

Compound	IC$_{50}$ (μM)		
	HepG2	**HeLa**	**L02**
118a	32.83 ± 5.80	25.05 ± 5.51	60.12 ± 7.40
118b	28.58 ± 9.13	21.61 ± 5.94	51.34 ± 6.73
118c	23.75 ± 4.37	26.75 ± 7.76	54.33 ± 5.25
118d	14.56 ± 4.37	26.75 ± 4.05	27.44 ± 3.57
56a	28.78 ± 2.95	36.11 ± 5.98	42.22 ± 3.32

Another library that was of interest, was the library reported by Pettit and co-workers.[96] Figure 20 shows representative examples from this library. Kumar and Alegria were the first researchers to generate libraries that focused on gaining understanding into the activity of these *N*-functionalized azapodophyllotoxins with their research into the hydroxyethyl derivatives.[46,97] This library by Pettit and co-workers represented the first efforts into more diversified *N*-functionalized derivatives and investigations into their antiproliferative activities.

The library included non-*N*-functionalized azapodophyllotoxins, such as compounds **119a** and **119f**, as well as *N*-alkyl-azapodophyllotoxins, such as compounds **119b-d**. Of particular interest, was compound **119e**. This was the first study in literature that introduced the *N*-benzyl functionality in the 4-position of the azapodophyllotoxin scaffold. This compound also employed the 4-fluorobenzyl motif inspired by an etoposide-derivative that has shown great promise as an antiproliferative agent. The inhibitory data reported for this compound (shown below in Table 13) was also amongst the most active agents reported in this study.
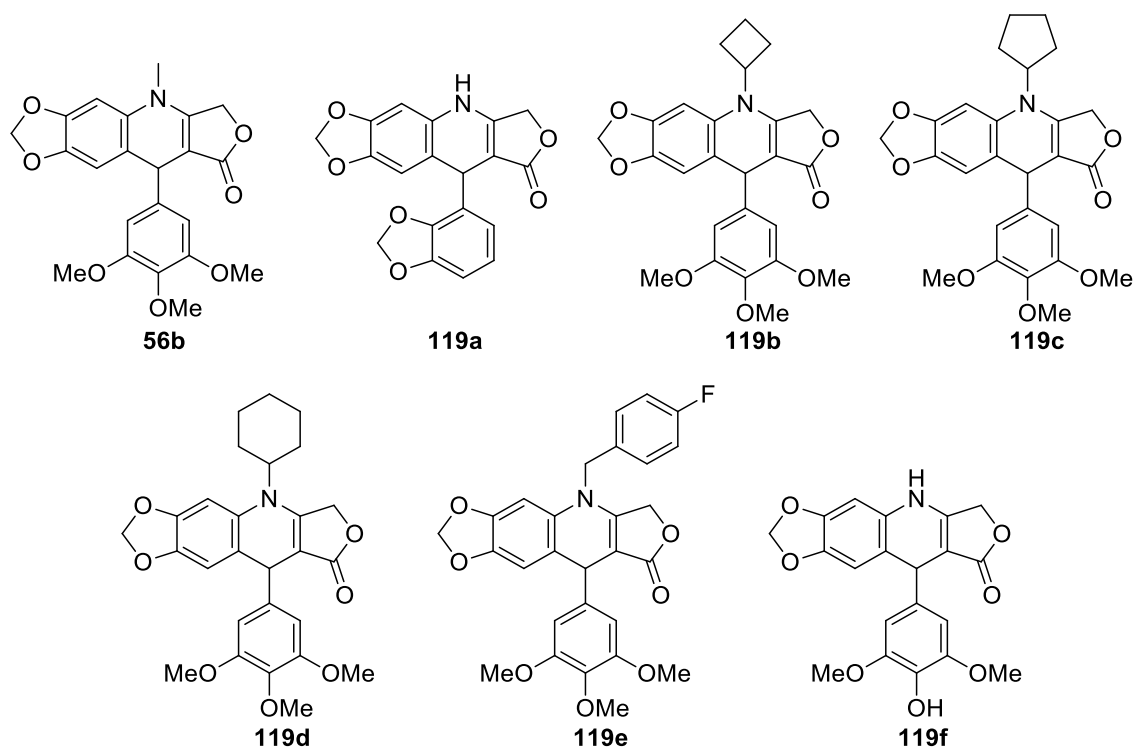
Figure 20: Representative examples reported by Pettit and co-workers.[96]

Pettit and co-workers reported the antiproliferative activity data of their library against various cell lines (shown in Table 13). The activity data for podophyllotoxin (**50**), deoxypodophyllotoxin (**51a**) and picropodophyllotoxin (**52**) was also reported (Table 13, Figure 21 shows the structure of compounds **50**, **51a** and **52**).

Table 13: Activity data for the representative azapodophyllotoxin analogues reported by Pettit and co-workers.[96]

	ED$_{50}$ (µg.mL^{-1})	GI$_{50}$ (µg.mL^{-1})					
	P388	**BXPC-3**	**MCF-7**	**SF268**	**NCI-H460**	**KM-20L2**	**DU-145**
119a	0.17	0.065	0.0039	0.0089	0.021	ND	0.041
119b	0.24	0.040	0.026	0.026	0.028	0.032	0.047
119c	15.3	0.083	0.045	0.062	0.16	0.12	0.27
119d	3.4	0.17	0.052	0.066	0.27	0.24	0.27
119e	1.9	0.046	0.037	0.030	0.031	0.033	0.047
119f	0.028	0.028	0.025	0.026	0.027	0.032	0.033
56b	0.027	0.049	0.034	0.029	0.032	0.032	0.026
50	0.0043	ND	ND	ND	ND	ND	ND
51a	0.029	0.00044	0.0027	0.00056	0.0018	0.0014	0.0017
52	0.0031	0.0012	0.00055	0.00040	0.00077	0.0076	0.0021

55
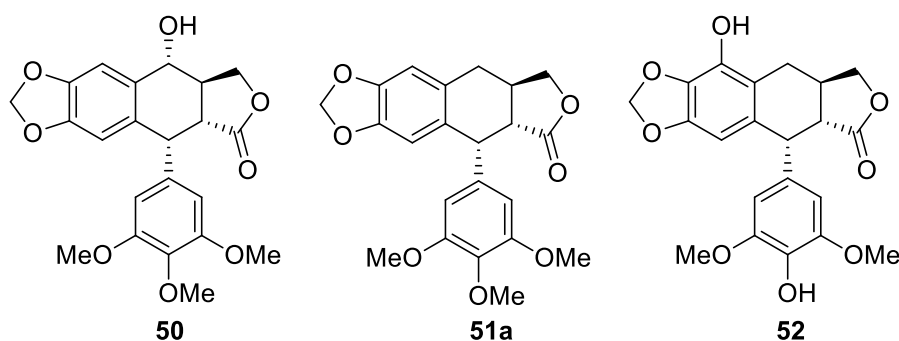
Figure 21: Podophyllotoxin (**50**), deoxypodophyllotoxin (**51a**) and picropodophyllotoxin (**52**).

The activity data for the most active analogues are shown in Table 13, but it can be noted that even the most active analogues are still not as active as the natural cyclolignans (Figure 21).

These libraries have highlighted and delivered new insights into the effects of the A-, B-, D- and E-ring systems. The phenanthroline-derivatives again highlighted the importance of the polyaromatic AB-ring systems.[87,89] This conformed with the naphthylamine based libraries as reported by Magedov and co-workers, where the naphthyl-4-azapodophyllotoxins were amongst the most potent analogues in the study.[29] These types of scaffold decorations were also reported by groups such as Ji and co-workers.[63] These systems have The work by Westwell and co-workers also reiterated that the mechanism of these MCRs still need more investigation, as the method did not produce the desired 4-aza-2,3-didehydro scaffold, but instead produced the **C3**-hydroxy antipode.[89] The key insight here was, however, that this still produced compounds with anticancer activity comparable to the natural product and its semisynthetic derivatives. The library of Pettit an co-workers showed that the *N*-functionalization of 4-azapodophyllotoxins produced compounds with good anticancer activity, however, not comparable to the activity of the natural compounds.[96]

New libraries of azapodophyllotoxins were also reported by Roche and co-workers[98] and Raju and co-workers[99], however, they will not be discussed here as these libraries offered no additional insight into this class of compounds and merely followed the routine exploration of different aromatic amines and aryl aldehydes along with tetronic acid in MCRs. These novel 4-azapodophyllotoxins were analysed for their antiproliferative activities, which ranged from inactive compounds to compounds with activities comparable to podophyllotoxin (**50**).Roche and co-workers did consider the effect of the electron density of the E-ring and its correlation to the inhibitory activity of the compound, with the ring motifs arranged by decreasing electron density on the aryl ring (Figure 22). A clear trend was not apparent throughout the entire library, with the trimethoxy-, methylenedioxy- and phenyl ring systems varying in activity. The only consistent trend was that the pentafluoro-analogues were generally inactive.[98]
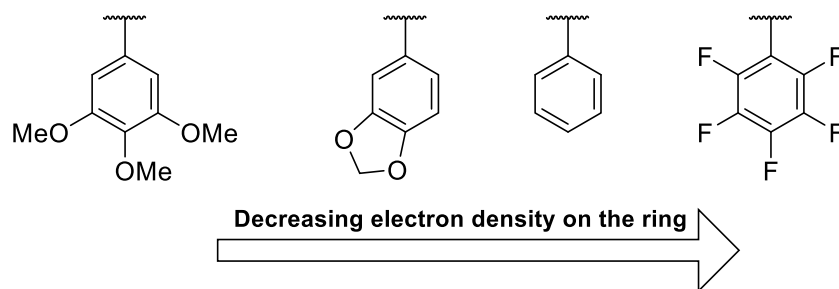
Figure 22: Various E-ring decorations explored by Roche and co-workers organised according the electron density on the aryl ring.[98]

What could be noted is that the researchers employed a sacrificial aniline, as reported in their earlier work on the investigation into the mechanism of these compounds,[70] in the synthesis of the novel library of analogues. Raju and co-workers also introduced different AB-ring systems in the novel analogues synthesized in their study, however, the antiproliferative activity data is only reported for some of these.[99] A more interesting aspect of their study was the *in silico* modelling studies performed on the more active analogues. This will be discussed in the next section.

1.2.2.2. Studies of HPFQ and Docking Studies

Some of the most interesting work on 4-azapodophyllotoxins have been focused on HPFQ (**106d**, Figure 21), the most structurally simplified azapodophyllotoxin, initially reported by Kumar and Alegria.[77] Kumar and co-workers[100] and Kumar Ghosh and co-workers[101–103] have focused their efforts on gaining understanding into the method of action of these *N*-hydroxyethyl analogues. The study by Kumar, Vélez and Zayas looked at the effect of these compounds on the cell cycle of COLO 205 cancer cells. They reported that compound **106d** caused effects similar to that of etoposide (**55a**), such as DNA fragmentation and cell cycle arrest at the S-phase. Compound **106d** also appeared to cause autophagy, similar to etoposide (**55a**).[100]

A further study by Kumar Ghosh and co-workers[101] investigated the photophysics of HPFQ (**106d**, Figure 23), in hopes of gaining more understanding into the factors that influence its physiochemical properties.
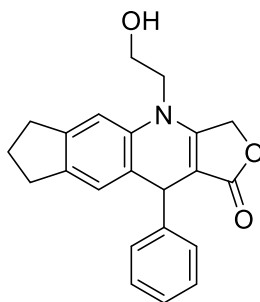
Figure 23: 4-(2-Hydroxyethyl)-10-phenyl-3,4,6,7,8,10-hexahydro-1*H*-cyclopenta[*g*]furo[3,4-*b*]quinoline-1-one (HPFQ) (**106d**), initially reported by Kumar and Alegria.[77]

A summary of the H-bonding interactions in the solvation studies is shown in Figure 24. The hydroxyl-group of the *N*-hydroxyethyl substituent acted as a hydrogen bond donor with solvents such as 1,4-dioxane, acetonitrile and tetrahydrofuran (THF). The carbonyl group of the lactone ring acted as a hydrogen bond acceptor in polar protic solvents and compounds such as cyclohexane showed no interaction with HPFQ (**106d**). These interactions were based on the fluorescence energy maxima determined in various binary solvent mixtures (consisting of polar and apolar solvents). Other analyses conducted in this study included frontier molecular orbital (FMO) analysis to look at the ground and excited states of the molecule, as well as probes into the fluorescence quantum efficiency, time resolved fluorescence anisotropy, and steady-state absorption and emission of HPFQ.

The study highlighted that the interesting fluorescent properties of this class of compounds can be potentially exploited in biomedical research to offer new insights into how they interact with biological systems.[101]

Kumar Ghosh and co-workers followed up this study by investigating the interaction between HPFQ (**106d**, Figure 24) and bovine serum albumin (BSA), using the photophysical properties identified in their previous study.[102] BSA was chosen for this study as it has been extensively employed as a transport vehicle for a wide array of drugs and enzymes. Specific residues within BSA were investigated, namely the tryptophan residues that show significant emission in the 310-350 nm range. The fluorophore properties of HPFQ have now been established and the Fluorescent Resonance Energy Transfer (FRET) between the active compound and the tryptophan residues were investigated. Along with the measurements of steady state absorption and fluorescence, *in silico* docking studies against the BSA crystal structure (PDB ID: 3V03) were also employed.
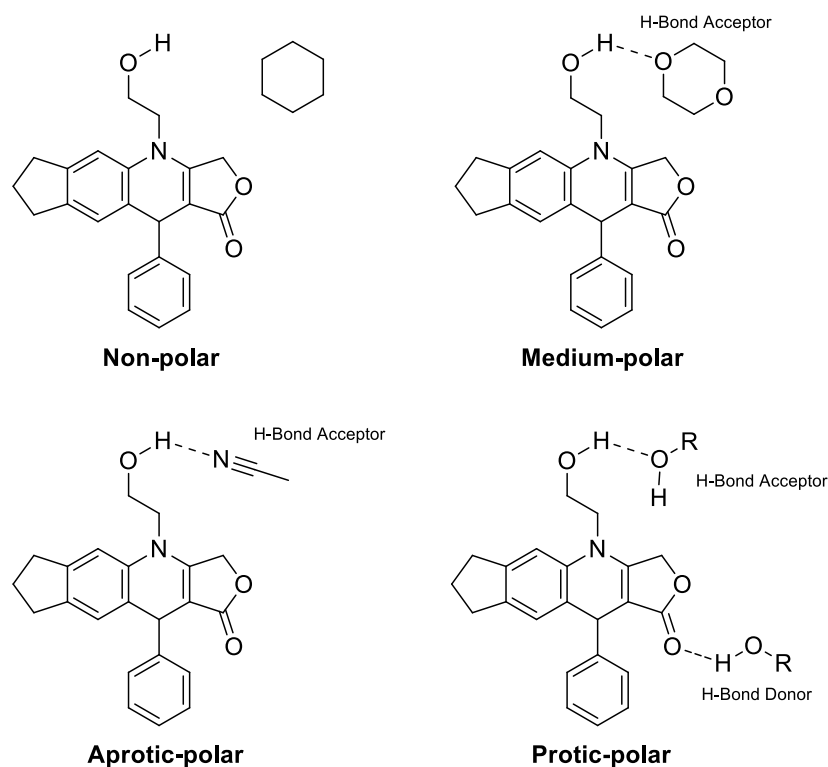
Figure 24: Interactions between HPFQ (**106d**) and different solvents as reported by Kumar Ghosh and co-workers.[101]

To investigate whether HPFQ (**106d**) would occupy the conventional pharmacophore pocket (subdomain IIA, also known as the Sudlow site I), HPFQ was titrated against a solution containing the Warfarin-BSA complex. Warfarin (**120**, Figure 25) and Ibuprofen (**121**, Figure 25) generally occupy this subdomain. During the experiments the displacement of warfarin was observed as HPFQ concentration increased.
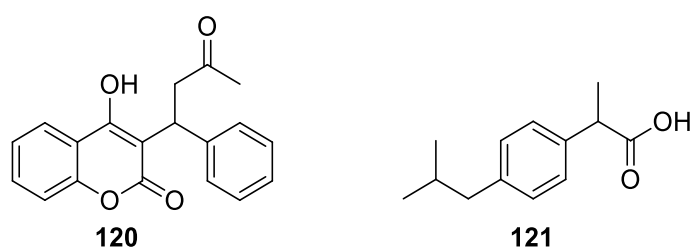
Figure 25: Structures of Warfarin (**120**) and Ibuprofen (**121**).

The complexation of compound **106d** into the hydrophobic site could be confirmed as FRET was observed from the Trp-213 fluorophore to HPFQ. *In silico* docking visualization also showed the interaction between the tryptophan amino-group and the hydroxyl-group of HPFQ. Kumar Ghosh and co-workers did a follow-up study to investigate if the same interactions would be observed in human serum albumin (HSA).[103] The BSA study showed a hydrogen bonding interaction, whereas a similar interaction was not observed in HSA. HPFQ was found

59

to occupy the Sudlow site I in HSA as well, but *in silico* docking studies suggested that the interaction was stronger with the hydrophobic side chains. The apolar phenyl ring of HPFQ showed a strong interaction with the benzene ring of the Trp-214 indole, and the formation of a hydrogen bond between hydroxyethyl group of HPFQ and Arg257 of the protein backbone was proposed. Fluorescence studies supported this hypothesis.[103]

The azapodophyllotoxins can therefore be well accommodated in biological systems such as these, as these compounds generally exhibit hydrophobic characteristics in the A-, B- and E-ring systems and more polar characteristics in the D-ring. The interactions of the hydroxyethyl group showed how the characteristics of the *N*-4-aza substituents can therefore also dictate how these compounds interact within the binding pocket.

Raju and co-workers performed *in silico* docking studies against the etoposide/topoisomerase II crystal structure (PDB ID: 3QX3) for two of their most potent azapodophyllotoxin analogues, compounds **124** and **125** (Figure 26).[99]
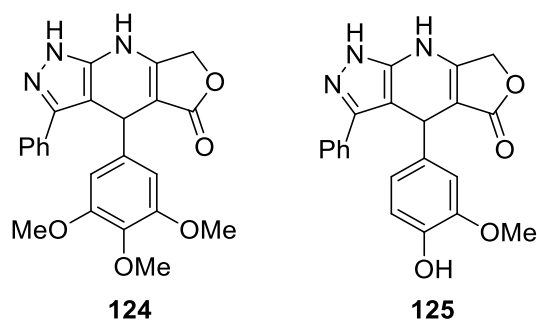
Figure 26: Two 4-azapodophyllotoxins generated by Raju and co-workers that showed the best antiproliferative activity.[99]

The different possible ligand structures of the two analogues were generated and docked into the etoposide cavity in the crystal structure of topoisomerase II. Only three conformational ligands satisfactorily docked into the active site, one ligand for compound **124** and two ligands of compound **125**. The most favourable ligand pose of compound **124** that docked into the active site had a *R*-configuration at the **C1** position of the C-ring and the proton in the 2N position of the pyrazole ring. The poses of compound **125** that docked into the active site exhibited alternate configurations at the **C1** position and showed two different tautomers of the pyrazole ring. The three ligands that docked successfully (with the hydrogens of interest drawn in) are shown in Figure 27.

124-*C1*-*R*   **125-*C1*-*S***   **125-*C1*-*R***
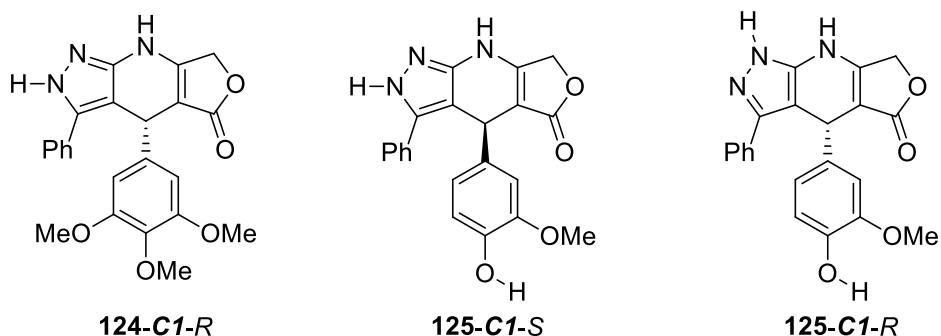
Figure 27: The three different successfully docked conformers.

The *in silico* docking results confirm observations mentioned earlier, that podophyllotoxin and etoposide have different methods of action, podophyllotoxin acting through the destabilization of microtubule formation whereas etoposide is considered a topoisomerase II poison.[49] The *para*-hydroxy group is cited as an important functional group due to its interaction with the active site, as is evidenced through the hydrogen-bonding interaction with the arginine residue, Arg503A (Figure 28). This is notably absent for compound **124**. The study only performed *in silico* docking studies on the crystal structure of the etoposide-topoisomerase II complex and not on the podophyllotoxin-tubulin complex.

124-*C1*-*R*   **125-*C1*-*S***
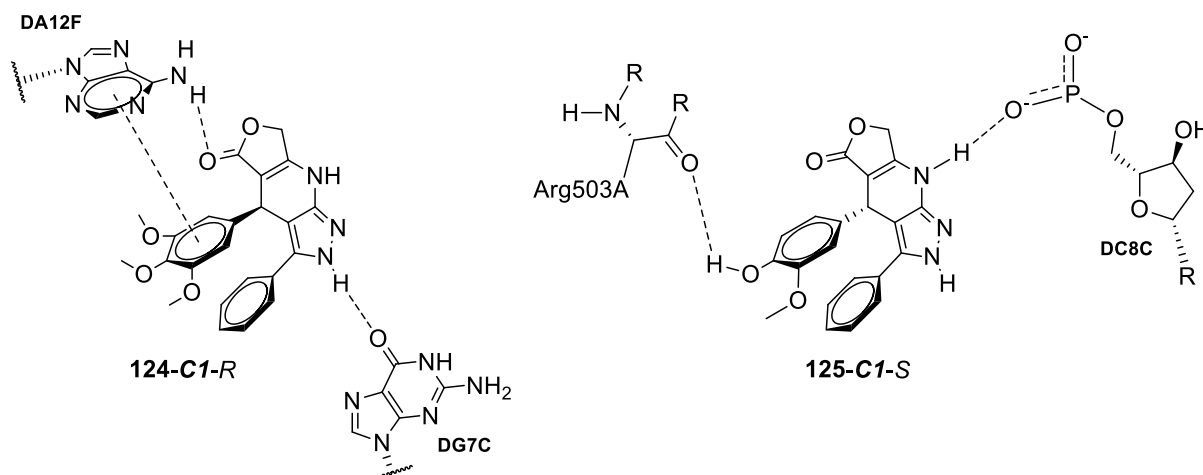
Figure 28: Simplified representations of the docking poses in the active site of the etoposide/topoisomerase II crystal structure (PDB ID: 3QX3) of compounds **124** and **125**, as reported by Raju and co-workers.[99]

This small structural difference leads to different means of interacting in the active site, as shown by the simplified docking representations of the two different compounds in Figure 27. Compound **124** primarily showed interaction with the adenosine and guanine groups of DNA within the active site, with a π-π stacking interaction between the hydrophobic E-ring and the

61

pyrimidine ring of the adenosine nucleotide, as well as a hydrogen bond between the 2N proton of the pyrazole ring and guanine.

Compound **125**, on the other hand, docked into the active site with different interactions. The 4-hydroxygroup on the E-ring formed a hydrogen bonding interaction with Arg503A of topoisomerase II and the proton of the 4-aza moiety in the C-ring showed a hydrogen bond with phosphate group on the DNA backbone (Figure 27). This, once again, lends more insight into the importance of the substitution pattern of the E-ring and how the method of action could possibly be affected by this.

Azapodophyllotoxins have also been to be shown to be effective agents in targeting resistant cancer cell lines. Malhotra, Ferlini, Fattorusso and co-workers investigated the use of employing *N*-hydroxyethyl 4azapodophyllotoxins in targeting the resistance pathways in paclitaxel-resistant ovarian cancer cell lines.[104] They produced a library of these *N*-hydroxyethyl analogues and focused the investigation on the analogue that produced the most promising results, compound **127** (shown in Figure 29, along with paclitaxel (**126**)).
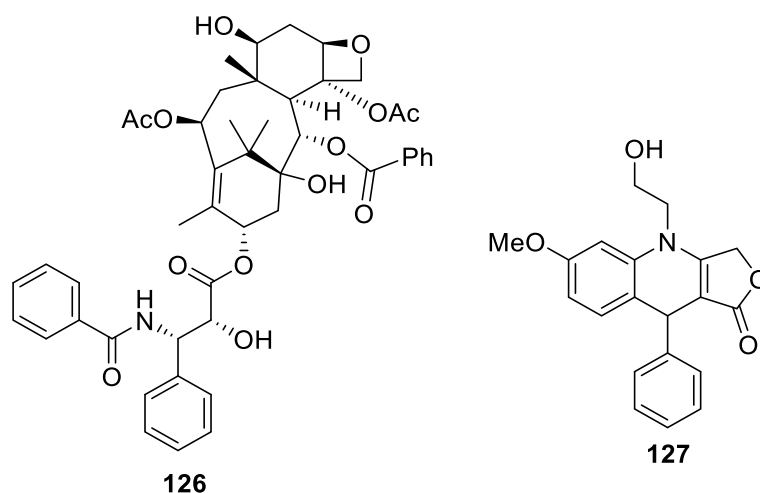
Figure 29: Paclitaxel (**126**) and the *N*-hydroxyethyl analogue (**127**) investigated by Malhotra, Ferlini, Fattorusso and co-workers.[104]

Malhotra, Ferlini, Fattorusso and co-workers investigated this by identifying the most potent analogue in their library, followed by *in silico* docking studies against the active site of the GTP kinase, GBP1. GBP1 has been shown to signal the activation of kinases attributed to the development of drug resistance.[105,106] PIM1 is such a prosurvival kinase, which is activated by the GBP1 GTPase to induce resistance to microtubule targeting agents (MTAs), such as paclitaxel (**126**). The study found that compound **127** sufficiently stabilized GBP1 during complexation, and that the ability of the kinase to activate the PIM1 pathway was significantly inhibited. This study, therefore, confirmed the utility of this class of compounds, as

azapodophyllotoxins seem to possess more qualities simply beyond acting as antiproliferative agents, but also as a complementary drug class for combatting drug resistance.[104]

Finally, it must be mentioned that a number of patents have been filed for this class of compounds as well, either with MCRs as the method of generating the compounds of interest for anticancer treatment or forming a key step in the production thereof.[107–109] Representative examples of compounds enclosed in these patents are shown in Figure 30.
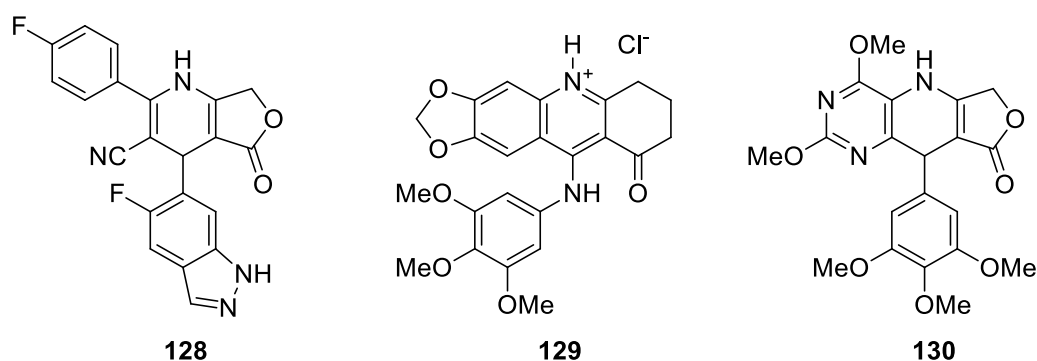
Figure 30: Patented 4-azapodophyllotoxins: Compound **128** by Michels *et al.*[107], compound **129** by Chabot et al.[108] and compound **130** by Ahmed et al.[109]

The patent by Michels *et al.* disclosed 1,4-didehydropyridine derivatives (such as compound **128** amongst others) for the treatment of c-Met-mediated diseases and conditions, which included the use of these compounds as antiproliferative agents.[107] The patented compounds by Chabot *et al.* were synthesized by employing a MCR as the first step in the synthesis to ultimately produce water soluble 4-azapodophyllotoxins, such as compound **129**, as anticancer drugs.[108] Finally, Ahmed *et al.* patented 4-azapodophyllotoxins that included substituted pyrimidines in the AB-ring system as potential antitumour agents.[109]

In summary, the different libraries were thoroughly considered in the design of the compounds synthesized in this project. In terms of the AB-ring system of novel analogues reported by different researchers, it is evident that many different decorations offered promising antiproliferative activity despite apparent different molecular interactions with the active site. Aryl systems, with or without heteroatoms, have been the most ubiquitous in the reported libraries, however, the potency of pyrazole-based 4-azapodophyllotoxins have shown that the interaction in this pocket is not yet fully understood. The *in silico* modelling studies by Raju and co-workers showed hydrogen bonding interactions between the pyrazole ring and the guanine base pair of the DNA fragment in the active site. To gain pointed insight, only certain AB-ring systems were considered for this study and the naphthyl-derived analogues reported by Magedov and co-workers were chosen.[29] The low nanomolar activities of these compounds held promise as starting points for further exploration of the scaffold.

The *in silico* studies only focused on the crystal structure of either podophyllotoxin-tubulin (PDB ID: 1SA1)[29,110] or etoposide-topoisomerase II (PDB ID: 3QX3).[99] In studies on the 4-azapodophyllotoxin analogues with no substituents in the 4-azaposition, the use of the podophyllotoxin-tubulin complex crystal structure is an adequate model, as these compounds are known to be tubulin poisons.[29] The introduction of substituents in the 4-azaposition does pose the question whether the same change in mechanism of inhibition will be observed as in the case of podophyllotoxin (**50**) and etoposide (**55a**). For this reason, we explored the crystal structures of both complexes, as the work by Raju and co-workers showed that interactions with the residues in the active site are still present, even in the absence of the *para*-hydroxy group on the E-ring (compounds **124** and **125**, Figure 28).[99] The E-ring substitutions investigated in this study therefore included both the podophyllotoxin-inspired (3,4,5-trimethoxyphenyl) and etoposide-inspired (3,5-dimethoxy-4-hydroxy-phenyl) E-rings.

The promising anticancer activity of the 4*N*-hydroxyethyl analogues reported by Malhotra and co-workers[85] and the 4*N*-alkyl analogues reported by Pettit and co-workers[96] further strengthened the interest in introducing different substituents in the 4-azaposition, so as to mimic etoposide (**55a**). The nature of these substituents will be discussed next in the section, *Aims and Objectives*.

3.1 Aims and Objectives

The focus of this study is on the exploration of 4-*N*-functionalized 4-azadidehydropodophyllotoxins (hereafter generally referred to as 4-azapodophyllotoxins) by means of multicomponent reactions (MCRs), as well as synthetic methods for the functionalization of these compounds through alkylations, reductive aminations and "click" chemistry. Etoposide (**55a**, Figure 31) will serve as the main inspiration for drug design, with the A and B ring systems and the 4-aza-position the primary focus for variation.

Etoposide, **55a**: R^1 = Me
Teniposide, **55b**: R^1 = thiophene
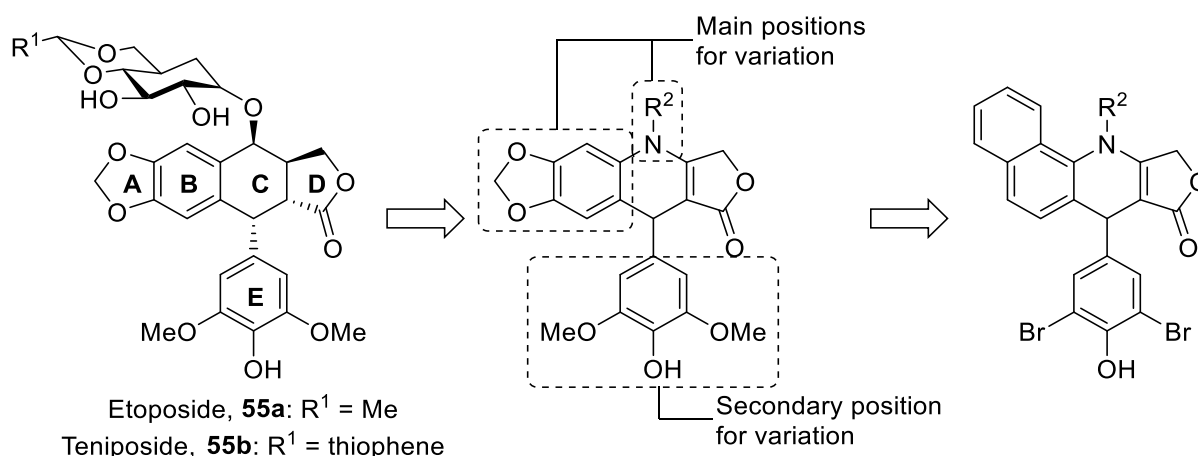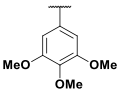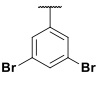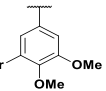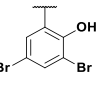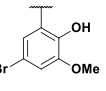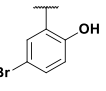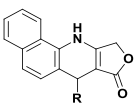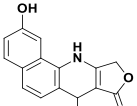
Figure 31: Proposed positions on the 4-azapodophyllotoxins that will be varied for this study.

3.1.1 AB ring variations

In a 2011 study, our group along with our collaborator, Prof Alexander Kornienko, a range of naphthylamine-based 4-azapodophyllotoxins were synthesized and tested for their antiproliferative activity against both HeLa and MCF-7 cells.[29] These compounds were shown to have IC$_{50}$ activities in the nanomolar range. The bioactivity results for these compounds are summarized in Table 14 below:

Therefore, due to the potent inhibitory action against HeLa and MCF-7 cancer cell lines exhibited by these analogues, the naphthyl-1-amine (**131**, Figure 31) moiety will be incorporated into our proposed libraries. Along with naphthyl-1-amine (**131**), its isomer, naphthyl-2-amine (**132**, Figure 32) will also be used, as it mimics the 5-6-6-5 linear ring system of the natural product podophyllotoxin (**50**) and its semisynthetic derivatives (etoposide **55a** and teniposide **55b**, Figure 31).

Table 14: IC$_{50}$ (nM) values of the compounds generated by Magedov *et al.*[29]

Naphthyl Scaffold	R							
	Yield	14	39	22	41	74	68	35
	HeLa	3±0	16±2	3±0	18±2	3±0	3±0	7±2
	MCF-7	3±0	14±1	3±0	21±1	3±0	3±0	13±3
	Yield	63	50	34	42	58	42	28
	HeLa	2±0	6±1	2±0	7±4	6±1	3±1	3±0
	MCF-7	3±1	3±0	3±0	3±0	3±0	3±1	3±0

Figure 32: Generalized structures of the naphthyl-1-amine (**131**) and naphthyl-2-amine (**132**)-derived analogues to be synthesized in this study.

The motivation for the use of naphthyl-2-amine (**132**), as mentioned, lay in its generation of 4-azapodophyllotoxin analogues that mimic the linear ABCD ring system. This is founded upon work done by our collaborators,[29,54] that showed the naphthyl-based 4-azapodophyllotoxin analogues to be potent antiproliferative agents (the compounds are shown in Figures 9 and 10 on pages 35 and 36, and the antiproliferative activity can be found in Tables 9 and 10 on pages 40 to 42). Results published by Lee and co-workers on the generation of podophyllotoxin analogues that employ similar linear systems lent further credence to our interest in the use of napthyl-2-amine. They synthesized phenazine-derived podophyllotoxins (**133a-c**, Figure 33) that showed comparable inhibition of cancer cell proliferation in comparison with etoposide.[111]

133a   **133b**   **133c**
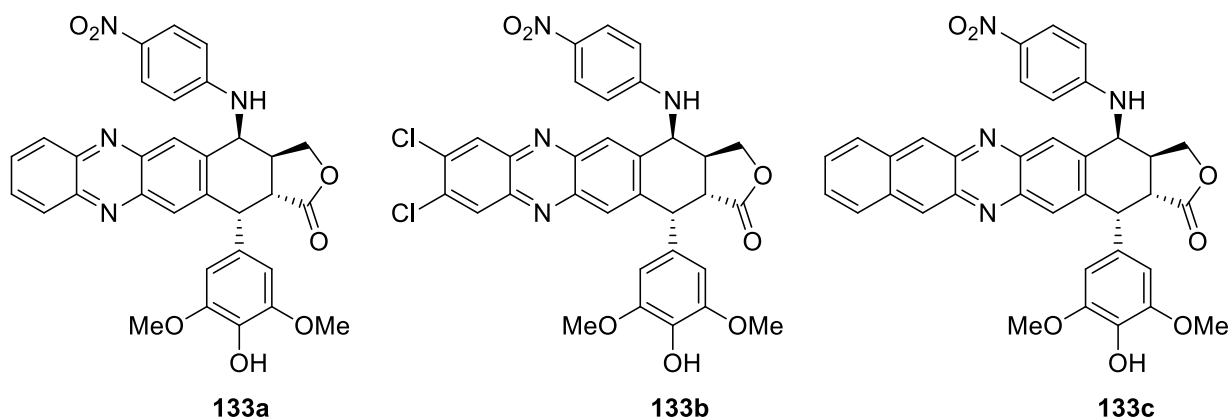
Figure 33: Phenazine podophyllotoxin analogues (**133a-c**) generated by Lee and co-workers.[111]

The growth inhibitory activities of these compounds were determined against the KB and KB/7d cancer cell lines. KB/7d is an etoposide-resistant cell line, as can be seen from the reduction in toxicity when compared with the KB cell line (Table 15 below). The inhibitory data shows the potency of the phenazine-derivatives. What is especially noteworthy is that compound **133b** shows an almost negligible reduction in activity against the etoposide-resistant cell line, KB/7d, compared to etoposide and the other two analogues.

Table 15: Antiproliferative activities of the Phenazine analogues generated by Lee and co-workers.[111]

	IC$_{50}$ (μM)	
	KB	KB/7d
Etoposide	0.164±0.044	23.8±1.5
133a	0.42±0.05	16.58±13.79
133b	0.11±0.03	0.56.8±0.13
133c	0.48±0.17	10.59±3.98

This could be attributed to the intercalatory interaction between the left-hand side of the drug and the DNA fragment in the DNA-Topoisomerase II complex.[112] This interaction had been well documented in literature and can also be observed in modelling studies. We have undertaken modelling studies using the Schrödinger Maestro Docking suite and a π-π interaction between the adenosine base pair and the fused biphenyl AB-ring systems of these analogues could be seen when the library of naphthyl-2-amine-based analogues were docked into the etoposide pocket in a crystal structure of Topoisomerase II (PDB ID: 3QX3). These results will be discussed in more detail in a subsequent chapter, but for now a ligand-enzyme interaction of a representative analogue synthesized during this project is shown to illustrate

this interaction (Figure 34). The diagram below shows strong interactions between adenosine and guanine residues on the DNA strand with the A and B rings of the corresponding *N*-functionalized 4-azapodophyllotoxin analogue. The modelling software generated identifiers for each base pair on the DNA fragment contained within the enzyme-compound complex. The identifier D referred to DNA and the accompanying letter identified the corresponding base pair (A for Adenosine, C for cytosine, G for Guanine and T for Thymidine). Finally, the third letter followed by a number denoted chain fragment and which number the base pair was on that chain.
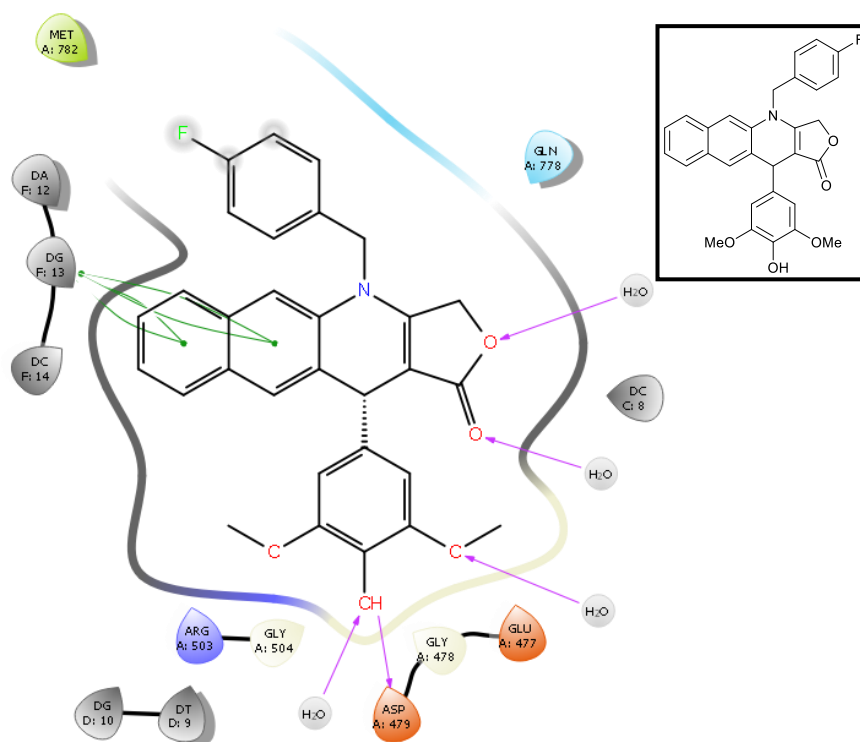
Figure 34: Ligand interaction diagram (LID) of a proposed *N*-functionalized 4-azapodophyllotoxin analogue.

Thus, the π-π stacking interaction between the AB-ring system of the 4-azapodophyllotoxin analogue was identified to be with adenosine, DA F:12, and guanine, DG F:13. These interactions were visualized by the green lines in Figure 34.

This same interaction was seen between the methylenedioxy-ring of etoposide (**55a**) and the same base pairs, DA F:12 and DG F:13, on the DNA fragment (as shown in Figure 35) of the refined crystal structure of the etoposide-topoisomerase II complex (which showed the interactions of etoposide in the active pocket). The fact that these interactions were present for the novel analogue as well as the known active originally crystallized into this enzyme, did suggest that our novel libraries could prove to have promising antiproliferative activity. In the

68

chapter, *Biological Evaluation*, we will discuss these assumptions in more detail alongside the biological activity results attained against an oesophageal cancer cell line, WHCO1.
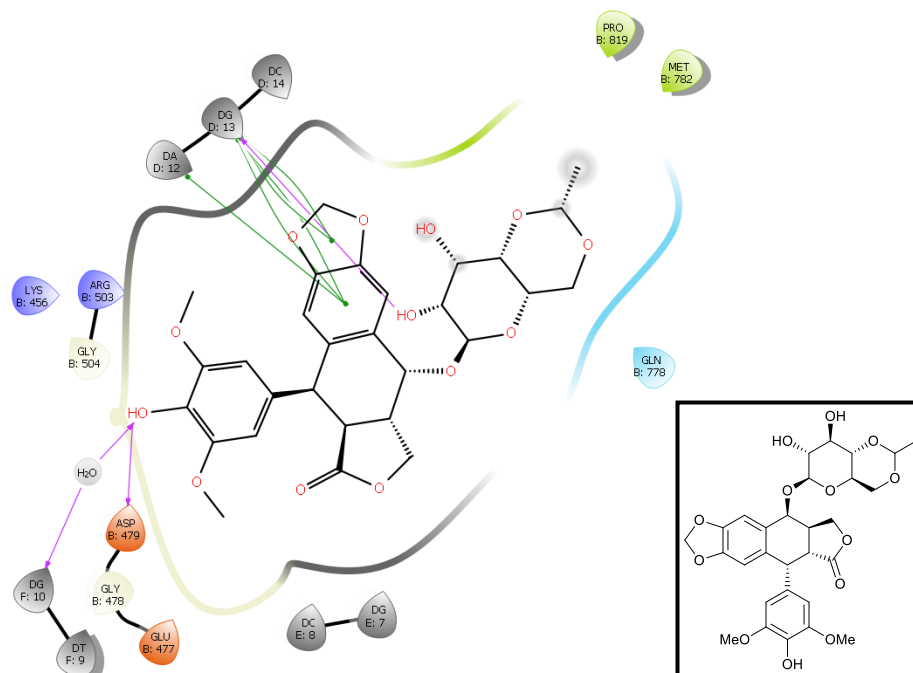
Figure 35: Ligand interaction diagram of etoposide (**55a**) in the active site of the refined crystal structure of the etoposide-topoisomerase II complex.

3.1.2 4-*N*-functionalization

The second major point for variation will be the 4-aza-position on the C-ring of our proposed analogues. Two main classes of variations have been considered for this position: i) the introduction of a propargyl group as a precursor for "click" chemistry and ii) functionalized benzyl groups. The rationalization behind the *N*-functionalization of the 4-position of the azapodophyllotoxins was of interest due to the effect observed when the semisynthetic derivatives, etoposide (**55a**) and teniposide (**55b**), were generated from podophyllotoxin and a change in the mechanism of inhibition was observed. The natural cyclolignan acted through the destabilization of microtubule formation during the mitotic phase, whereas the new semisynthetic derivatives induced apoptosis through the stabilization of the topoisomerase II-DNA complex, thus acting as topoisomerase poisons.[113]

The *N*-propargyl analogues will serve as the basis for etoposide mimics, as glycosyl azides will be used to introduce glucoside moieties into this position. The *N*-benzyl analogues will serve to explore 4-azapodophyllotoxin analogues that mimic more recent etoposide-derived topoisomerase II poisons currently undergoing clinical trials – GL331 (**134**, Figure 36) and NPF (**135**, Figure 36). The antiproliferative activity of these two derivatives indicated that this

position of the C-ring could accommodate substituents with diverse chemical properties and still maintain potent inhibitory activity and were therefore seen as interesting motifs to include into the proposed library of novel 4*N*-functionalized 4-azapodophyllotoxins. This would serve to explore the chemical space in in this region and provide new insight into the structure-activity relationships of these compounds.

55a
Etoposide

GL331, **134**: R = NO$_2$
NPF, **135**: R = F
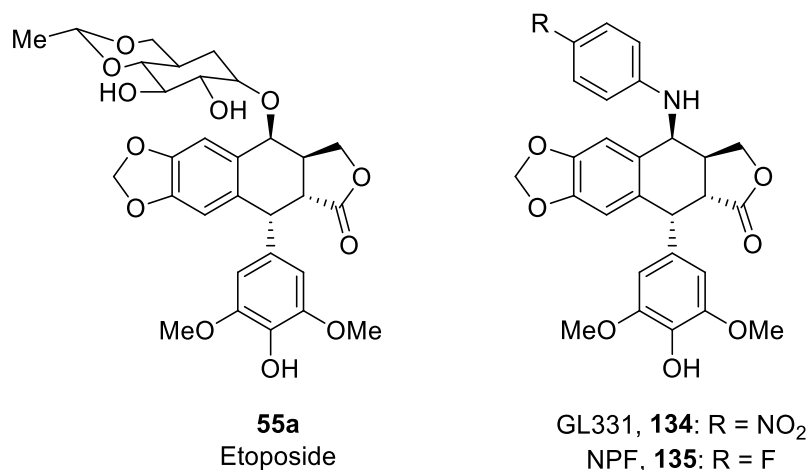
Figure 36: Etoposide (**55a**) and the new N-benzyl derivatives, GL331 (**134**) and NPF (**135**) currently undergoing clinical trials.

The investigation of the mechanism of action of topoisomerase poisons did, however, show that the 4-position of podophyllotoxin analogues are tolerant to a wide variety of different substituents.[112] This has been highlighted through the generation of analogues such as compounds **136a** and **136b** by Zou and co-workers[114] and compounds **137a** and **137b** by Chen and co-workers (Figure 37).[115]

The antiproliferative activities of these four compounds are given in Table 16 below. The efficacy of these compounds were analysed against three different cell lines – HeLa, K562 and K562/A02 (a multidrug resistant cell line variant of K562).[114,115] The furan derivatives (**136a** and **136b**) of the Zou research group fared well against HeLa cells, but no measurable difference was observed for K562 and K562/A02 compared to etoposide.[114] The 4'-triazole-analogues (**137a** and **137b**) of the Chen group, however, showed very potent inhibition of these cell lines, with the activity against the multi-drug resistant K562/A02 especially noteworthy, as essentially no reduction in activity is observed for these compounds.
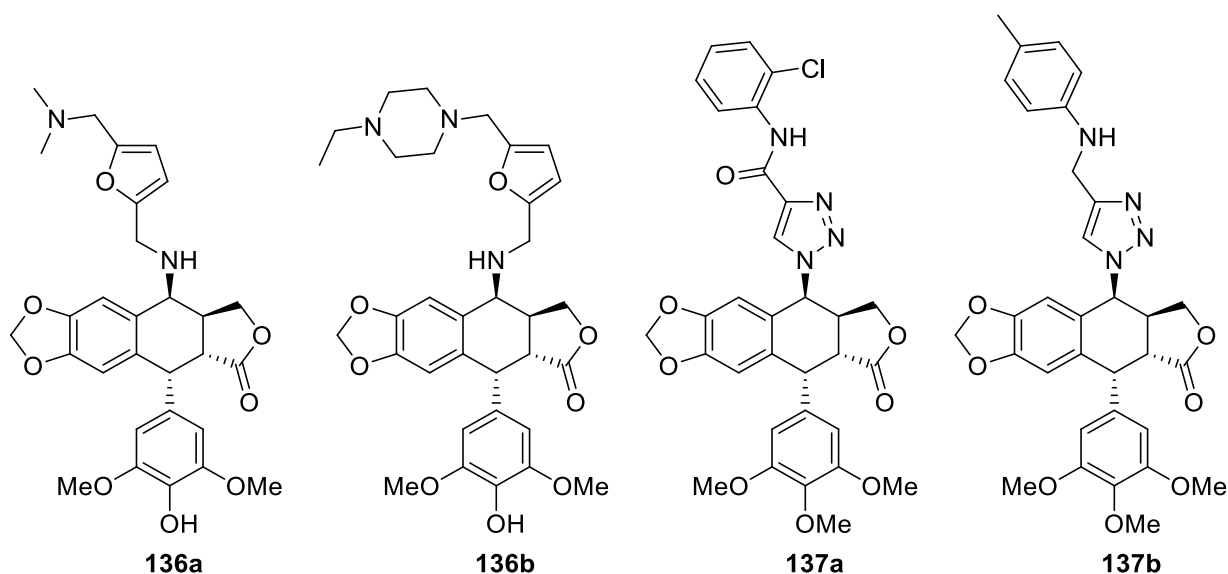
Figure 37: Furan derivatives (**136a** and **136b**) by Zou and co-workers[114] and triazole derivatives (**137a** and **137b**) by Chen and co-workers.[115]

Table 16: Anticancer activities of the different analogues generated by Zou and co-workers (**136a** and **136b**)[114] and Chen and co-workers (**137a** and **137b**).[115]

Compound	IC$_{50}$ (μmol/L)		
	HeLa	K562	K562/A02
136a	0.51	7.89	70.12
136b	0.67	7.45	123.21
137a	0.85	0.47	0.52
137b	0.08	0.05	0.06
55a	6.27	3.39[114] 2.11[115]	234.7[114] 151.69[115]

Along with the potent 4'-triazole derived podophyllotoxins synthesized by Chen and co-workers, Kumar and co-workers also generated a library of 4'-triazole-based podophyllotoxins (**138a-d**, Figure 38) that exhibited highly potent cytotoxicity against human cancer cell lines such as HT-29, 502713, A549, MCF-7 and SF-295.[116] These were colon (HT-29 and 502713), lung (A549), breast (MCF-7) and central nervous system (SF-295) cancer cell lines (the antiproliferative activities of the four representative examples are shown in Table 17).

138a   138b   138c   138d
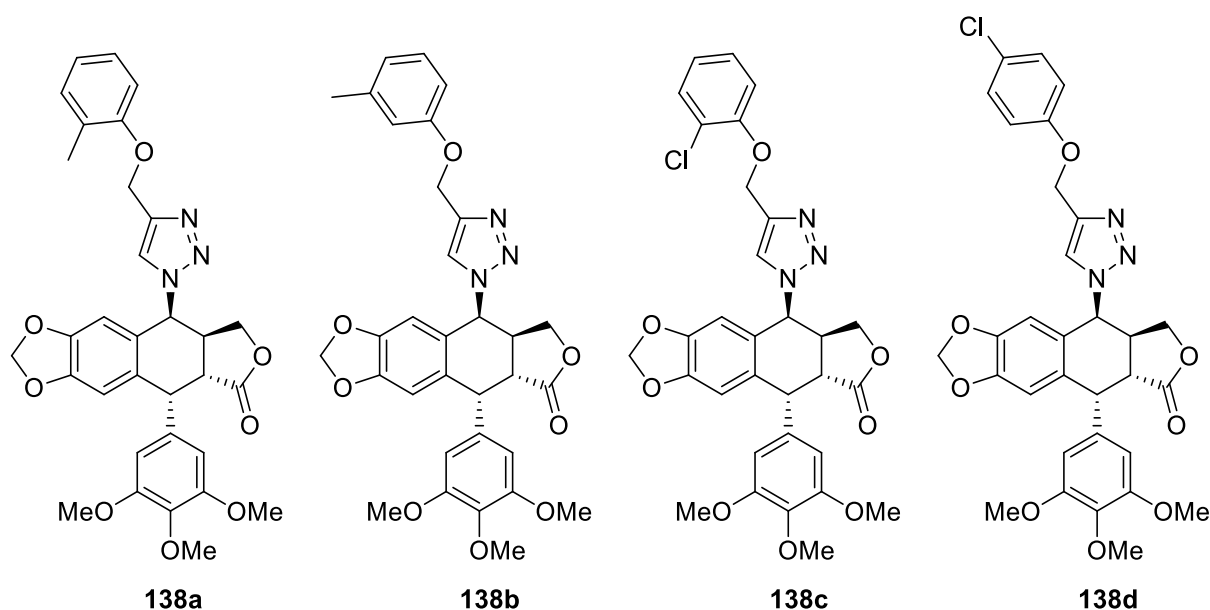
Figure 38: 4'-Triazole derivatives synthesized by Kumar and co-workers.[116]

Table 17: Antiproliferative activities of the representative analogues by Kumar and co-workers.[116]

Compound	IC$_{50}$ (μM)				
	HT-29	502713	A549	MCF-7	SF-295
138a	0.34	0.32	1.42	1.60	3.79
138b	0.53	0.72	1.67	1.87	8.86
138c	0.34	0.41	0.64	0.79	1.00
138d	0.35	0.43	0.56	1.60	1.67
55a	5.31	3.88	7.63	2.51	5.69

What all these podophyllotoxin derivatives have in common is that all of them contain heteroatoms in the 4′-position, leading to the assumption that there may be a requirement for a heteroatom in this position. However, the potency of analogues such as TOP-53 (**139**, Figure 39) shows that the tolerance of this region does not require a heteroatom in the 4′-position.[117] TOP-53 (**139**) has proved to be more effective in inhibiting tumour growth than etoposide (**55a**) against certain tumour cell lines. TOP-53 inhibited the cell growth of two human tumour cell line, LX-1 and Lu-99, with IC$_{50}$ values of 0.64 μM and 0.26 μM, respectively. This is in comparison to etoposide (**55a**) with IC$_{50}$ values of 4.9 μM and 2.1 μM, respectively.[118] Initial *in silico* modelling studies have also not shown any notable interactions in this position and therefore was not considered as a design parameter in the novel library.

139
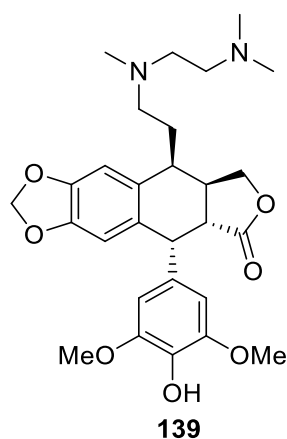
Figure 39: TOP-53 (**139**), an etoposide analogue.[117]

3.1.3 Etoposide Mimics

The first *N*-functionalized 4-azapodophyllotoxins in this study focused on the *N*-alkylation of the naphthylamines, both naphthyl-1-amine (**131**) and naphthyl-2-amine (**132**), with a propargyl moiety at the 4*N*-postion. The purpose of the propargyl group was to open up the 4-azapodophyllotoxin analogues to a "click" chemistry library of derivatives (as shown by Figure 40).
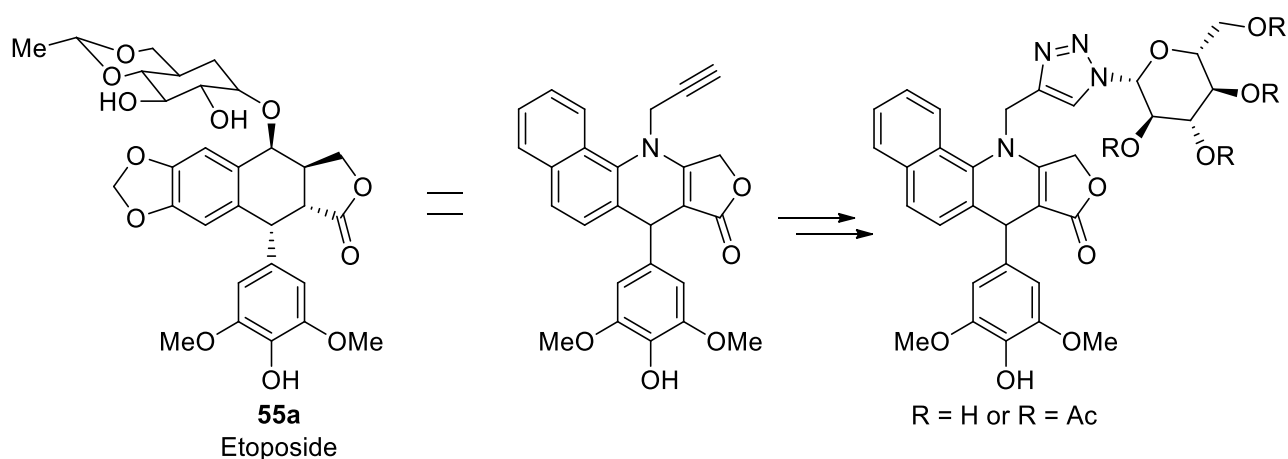
Figure 40: Etoposide (**55a**) and how the glycosyl derivatives would be generated.

These etoposide mimics were to explore not only the efficacy of the glycoside moiety in the 4-position, but also to investigate the effect of a triazole linker on the activity of these compounds. The use of the triazole linker in medicinal chemistry has been widely documented, with its bioisosteric properties cited as an important factor.[119] The triazole moiety has been shown to be a bioisostere for amide bonds, with the 1,4-cycloaddition product acting in a similar manner to the *Z*-isomer of amide bonds. Figure 41 shows that the configuration of the 1,4-triazole has

an electrophilic carbon and H-bond acceptor in the same positions as the *Z*-isomer of the amide.
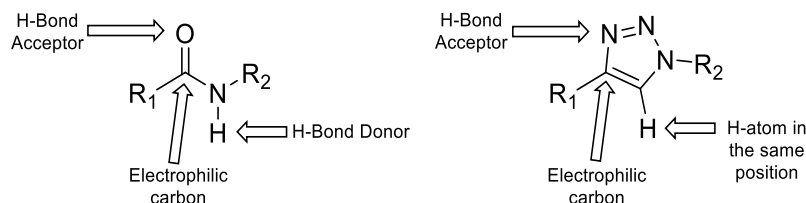
Figure 41: Bioisosteric properties of the triazole group in comparison with an amide group.

Therefore, as shown earlier, the incorporation of a triazole onto the 4'-position of podophyllotoxin analogues has been met with production of highly potent antiproliferative agents, and, thus, the same moiety will be incorporated in the 4-azapodophyllotoxin scaffold.[114,116]

The propargylated analogues, as well as the triazole products will be evaluated for their antiproliferative activity, thus giving more insight into the role this substitution plays in the efficacy of these compounds.

3.1.4 GL331 and NPF mimics

The second push to the exploration of the 4-position of the 4-azapodophyllotoxin class of compounds is based on the novel class of topoisomerase II inhibitors such as GL331 (**134**) and NPF (**135**, Figure 42). These compounds are currently undergoing clinical trials against gastric carcinoma, colon cancer, non-small cell carcinoma and etoposide resistant malignancies, as these compounds have shown greater pharmacological profiles than its parent compound etoposide.[120] NPF (**135**) is especially interesting, as it has exhibited a 10-fold greater potency at inhibiting human topoisomerase II, as well as a 113% increase in the formation of the topoisomerase II-DNA complex.[121] These C-4β *N*-aryl derivatives have also been reported to have better water solubility and could counter drug resistance.[122,123]

GL331, **134**: R = NO$_2$
NPF, **135**: R = F

R = NO$_2$, F or H
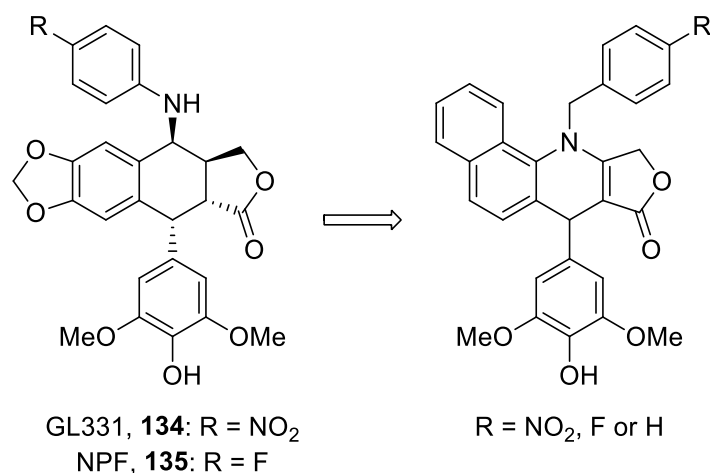
Figure 42: C-4β-Aryl derivatives of podophyllotoxin as inspiration for new 4-azapodophyllotoxin analogues.

Based on this, the naphthylamines will be functionalised with different benzyl substituents. 4-Nitrobenzyl- and 4-fluorobenzyl-substituents will be generated, as well as non-functionalized benzyl groups. The use of a non-functionalized benzyl group will serve as a method of probing the importance of the *para*-substitution on the 4'-aryl pendent group.

3.1.5 E-ring variation

The final part of the podophyllotoxin scaffold that will be varied is the pendent E-ring. The variation of this region will only be a minor focus of this study, as the E-ring will be kept very similar to that of the natural product, podophyllotoxin, which has a trimethoxy-substituted E-ring and the etoposide configuration, which contains a *para*-hydroxy group.

Podophyllotoxin-derived

Etoposide-derived
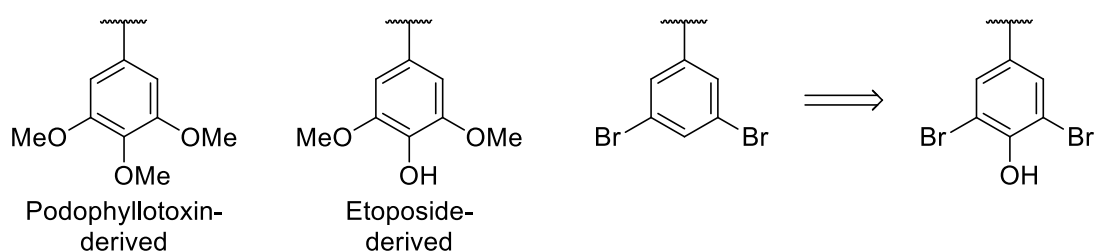
Figure 43: Variation of the E-ring.

Besides the two established ring systems, a 3,5-dibromo variation will also be used (Shown in Figure 43). This is based on the potency shown by this ring system in previous studies done in our group.[29] The importance of the *para*-hydroxy group has been highlighted through SAR studies done on podophyllotoxins[112] and through molecular modelling studies we have conducted, which show the hydroxyl group of etoposide interaction with an aspartate residue

75

in the active site, as well as an interaction with DNA through the hydrogen bonding water bridge (Figure 44).
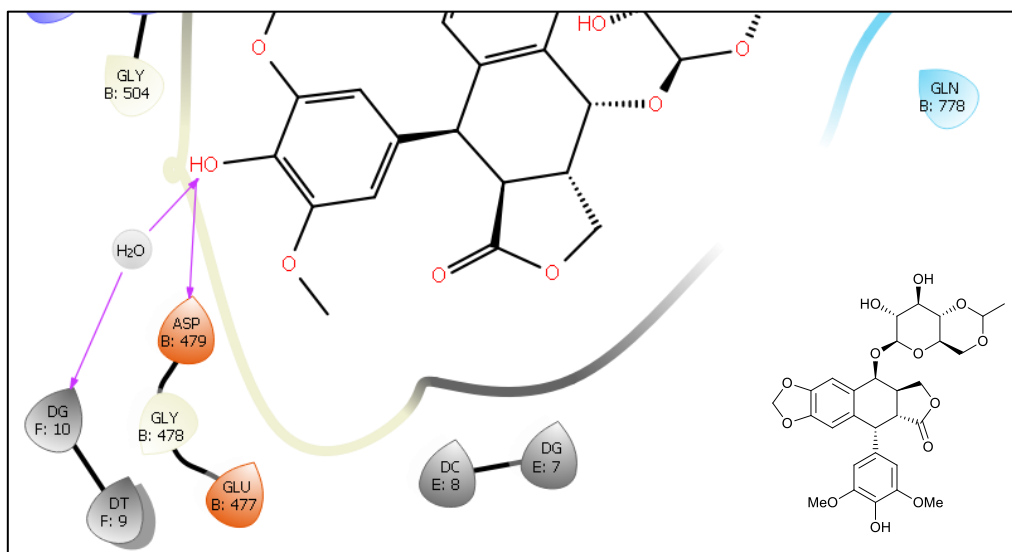
Figure 44: Motivation for including the 4-hydroxygroup on the E-ring.

For this reason, the 4-hydroxy group will be maintained in specific analogues and 3,5-dibromo-4-hydroxy substitution pattern will be incorporated into the novel analogues.

The synthesis of these novel analogues will be discussed: firstly through the preparation of *N*-functionalized arylamines – the *N*-propargyl- and *N*-benzyl derivatives, followed by the incorporation of these compounds into 4-azapodophyllotoxins by MCRs. The synthesis of various azides will also be discussed, which were incorporated onto the *N*-propargyl 4-azapodophyllotoxins through "click" chemistry.

The section on *Biological Evaluation* (Section 8.1) will discuss the different methods of inhibitions of podophyllotoxin and etoposide (destabilization of microtubule formation and topoisomerase II-DNA cleavage complex stabilization, respectively) as well as *in silico* molecular modelling studies of the two different methods of inhibition. The differences in these two mechanisms of inhibition will be elaborated on and we will discuss why it is important to understand both when this class of compounds is considered. This is due to the history of podophyllotoxin (**50**) and how its hemisynthetic derivative, etopoiside (**55a**) was developed. Along with this, the antiproliferative activities of our library of synthesized compounds against the oesophageal cancer cell line, WHCO1, will be reported and discussed. The *in silico* docking studies will also be discussed in terms of these biological activity results, so as to determine whether this method is effective as a predictive tool for biological activity.

4.1 Synthesis of *N*-Functionalized Arylamines

4.1.1 Exploration of the 4-aza-position

As discussed in the chapter, *Aims and Objectives*, the etoposide-mimicking 4-azapodophyllotoxins we aimed to synthesize, contain a glycoside moiety with a triazole linker to the 4-aza-position (Figure 45).

55a
Etoposide
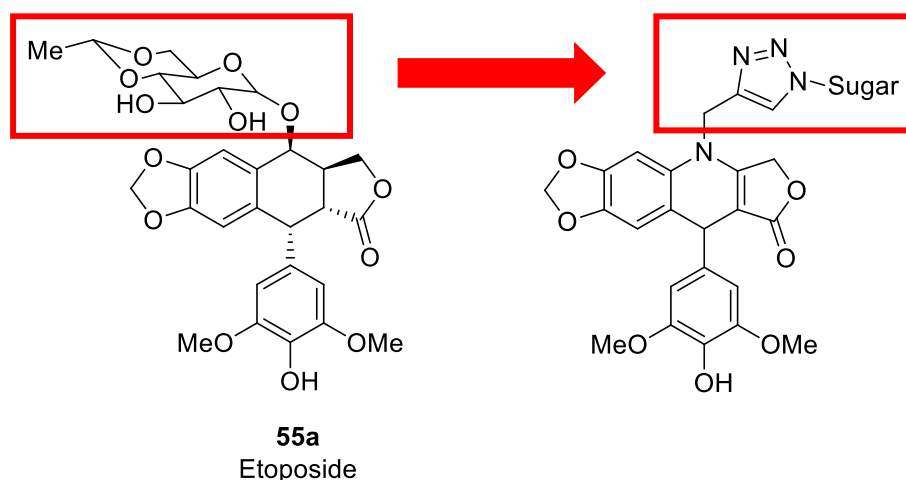
Figure 45: Incorporation of the glycoside moiety onto the 4-azapodophyllotoxin scaffold.

The retrosynthetic analysis of the proposed library involved the introduction of the triazole-linked glycoside moiety through a 1,4-dipolar cycloaddition of a glycosyl azide onto an alkyne. This required an alkyne in the 4-aza-position of our compounds of interest. These compounds were accessed through the established multicomponent reaction (MCR) method, as reported by Giorgi-Renault and co-workers.[58] As explained earlier, the MCR was tolerant to the use of the *N*-substituted anilines, therefore, we proposed to functionalise our arylamines of interest before synthesizing the desired natural product analogues by means of MCRs (Figure 45).

The retrosynthetic analysis, as shown in Figure 46, provides generalised structures of our intended strategy. The desired triazole-linked glycoside derivative (**G1**) could be readily accessed through a 1,4-dipolar cycloaddition of a glycosyl azide with the 4*N*-propargyl 4-azapodophylloton (**G2**). This scaffold (**G2**) could be attained through the modified Hantzsch dihydropyridine multicomponent reaction, as had been well-documented in literature and was discussed earlier. The other two components were commercially available benzaldehydes and tetronic acid (**59**). Therefore, the initial step required the synthesis of an *N*-functionalized arylamine (**G3**) from commercially available arylamines (**G4**).
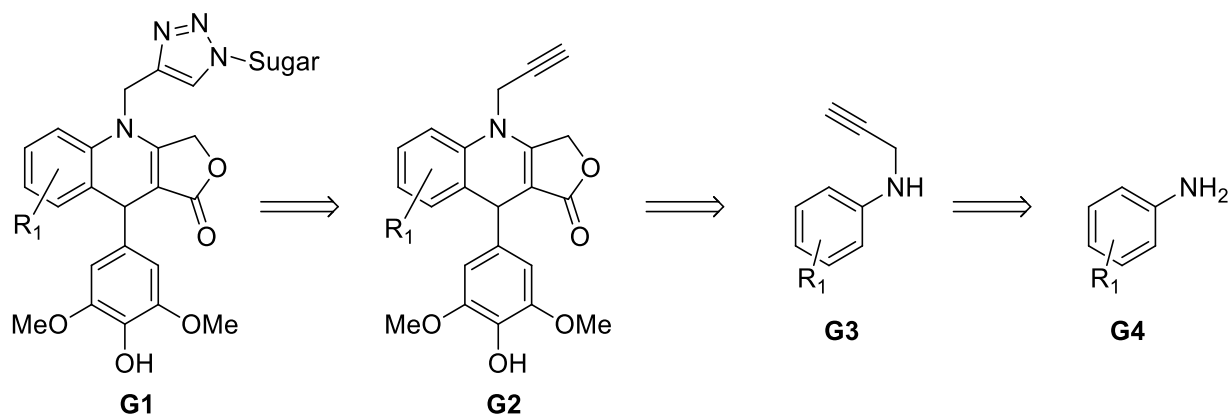
Figure 46: Retrosynthetic design of the glycoside 4-azapodophyllotoxin derivatives.

Thus, the first step in generating the desired library of analogues involved the *N*-alkylation of our naphthylamines, naphthyl-1-amine (**131**) and naphthyl-2-amine (**132**).

4.2 Synthesis of *N*-functionalized Arylamines

4.2.1 Synthesis of *N*-propargyl aryl amines

The propargylation of the naphthylamines was achieved by the simple *N*-alkylation of the corresponding arylamines with propargyl bromide (**136**) and potassium carbonate in *N,N*-dimethyl formamide (DMF).[124] The first reaction of naphthyl-1-amine (**131**) under these conditions was monitored with thin layer chromatography (TLC), and in the reaction lane, two major products were visualized as two spots under 254 nm UV light and with potassium permanganate stain (with R_f values of 0.65 and 0.4) when the reaction). Upon completion of the reaction, these products were separated by means of gravity-assisted column chromatography and the *N*-propargylated product **137** was afforded in a reasonable 73% yield (Scheme 22).
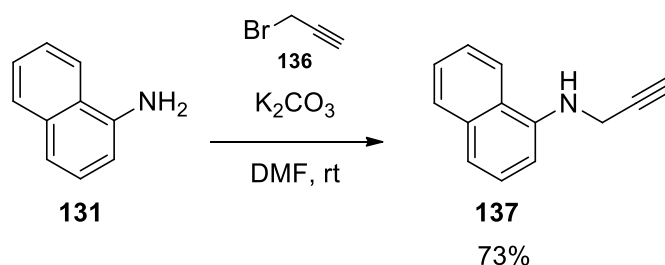
Scheme 22: Synthesis of *N*-propargyl-naphthyl-1-amine (**137**).

The successful synthesis of *N*-propargyl-naphthyl-1-amine (**137**) was confirmed by means of NMR spectroscopy (both ^{1}H and ^{13}C NMR) and high resolution mass spectrometry. The NMR spectra were recorded in deuterated chloroform (CDCl$_3$). In the proton spectrum, the broad

singlet of the amine proton is visible at δ 4.6 ppm, as well as the methylene protons of the propargyl group appeared as a doublet at δ 4.1 ppm and the methine proton as a triplet at δ 2.3 ppm. The seven aromatic protons of the naphthyl-ring can be seen in the region between δ 6.7 ppm and 8.0 ppm as multiplet signals. This is due to the planar nature of the fused phenyl rings that leads to finer splitting between the different protons.
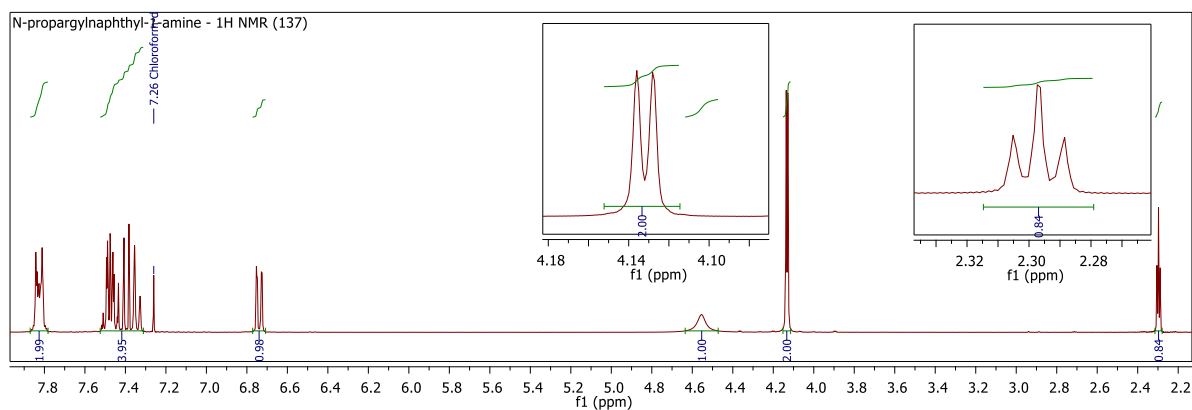
Spectrum 1: ^{1}H NMR spectrum of compound **137**.

The ^{13}C NMR spectra (Spectrum 2) also showed the expected signals for the product. The internal carbon of the triple bond can be seen at δ 81 ppm and the terminal (methine) carbon at δ 34 ppm. The methylene carbon can be seen at δ 72 ppm. The high resolution mass spectrometry data also confirmed the successful synthesis of the mono-propargylated product, with the [M + H]$^+$ adduct calculated as 182.0970 and the recorded mass found to be 182.0963. The data compared well to the literature reported data.[125]
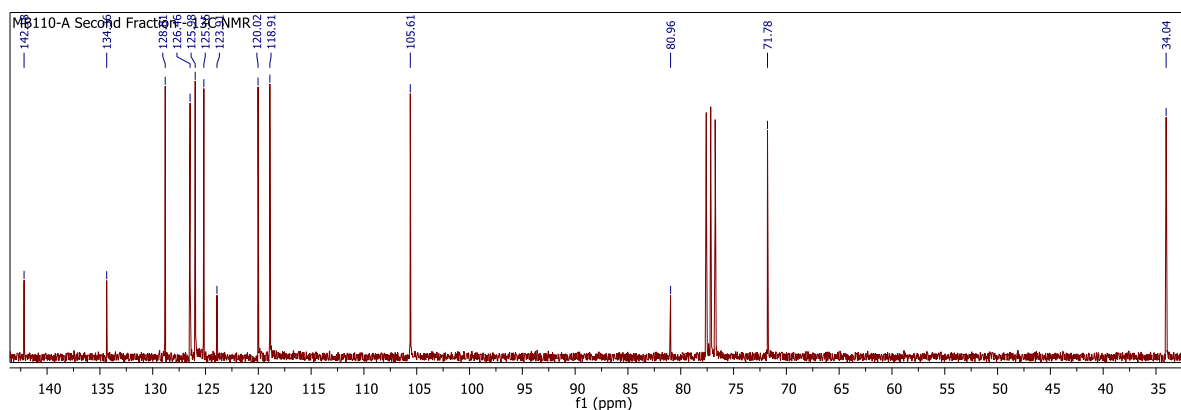
Spectrum 2: ^{13}C NMR of compound **137**.

The propargylation of the naphthylamines required extended reaction times when compared to work done previously in our group on the propargylation of various anilines. The additional compounds utilized included the unsubstituted aniline (**138**) and 8-aminoquinoline (**139**), as well as the more electron-rich 3,4-dimethoxyaniline (**140**) (Scheme 23).
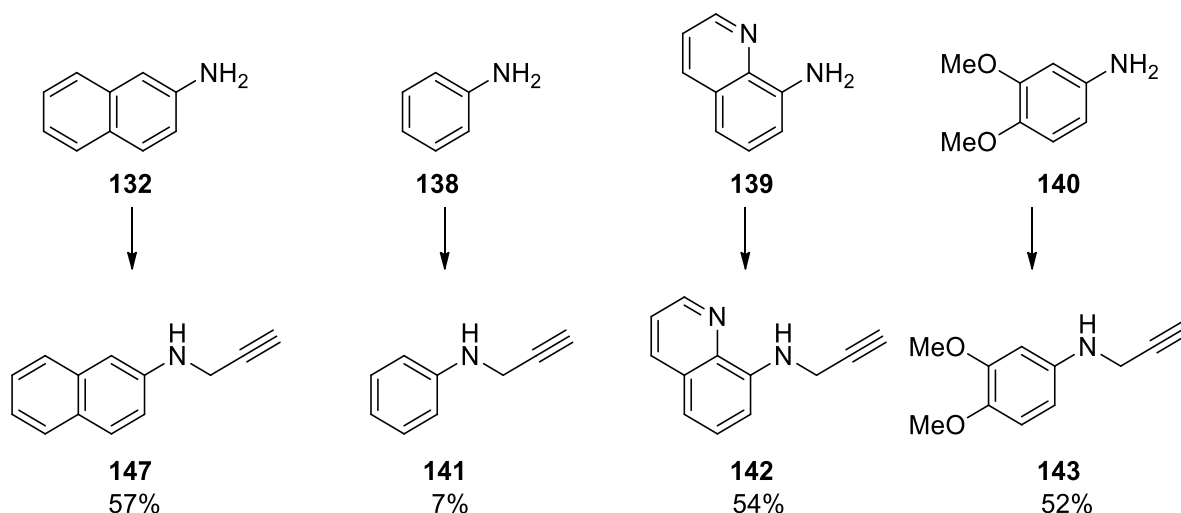
Scheme 23: Other *N*-propargyl arylamines and yields. Conditions: **136**, K₂CO₃, DMF, rt.

The corresponding *N*-propargylated products **141**-**143** (shown in Scheme 23) were all attained in 2-6 hours whilst stirring at room temperature in moderate (**142**, **143**, **147**) to poor (**141**) yields. The successful synthesis of these compounds were confirmed by means of ¹H NMR, as the propargylation of the arylamine was easily observed. Compounds **141**,[126] **142**[127] and **143**[128] all compared well to literature reported spectra. The reactions with naphthylamines (**131** and **132**) needed between 72 and 96 hours at room temperature to reach completion. As these reaction times were very long, it was decided to increase the temperature so as to increase the rate of conversion and shorten reaction times. Heightened temperature led to reduced yields, however, as the increased temperature favoured the *bis*-propargylation product.

The propargylation reactions were repeated on certain substrates, in attempt to optimise the conditions to favour the *mono*-alkylated product. The effect of temperature was the first condition to be investigated. The first substrate to be used, was 3,4-dimethoxyaniline (**140**, Scheme 24) and, subsequently, the analogous 3,4-methylenedioxyaniline (**58a**) was used (Scheme 25).
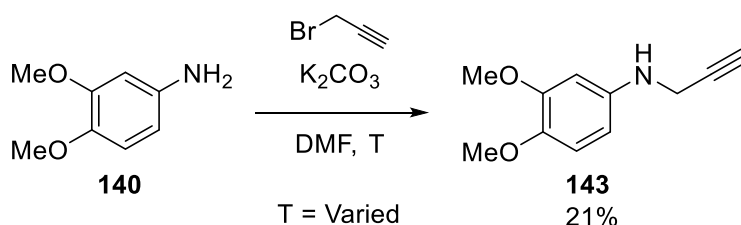
Scheme 24: Propargylation of 3,4-dimethoxyaniline (**140**).

The reaction was first performed at 15 °C, as the ambient temperature in the lab was not at 25 °C and the reaction was done without heating under these conditions. The *mono*-propargylated product was isolated in 21% yield, without any other major by-products. The

80

reaction was then repeated, with the temperature maintained at 25 °C by means of heating in an oil bath with a temperature probe. The yield was then recorded as 49%, similar to what had previously been achieved. A secondary product appeared to be forming, as a second spot was more visible on the TLC plate. As this spot was observed to be less polar that the primary spot, this spot was theorized to be the *bis*-propargylated product. The reaction was then repeated a third time, with the temperature elevated to 50 °C. The desired product was now isolated in a poor yield of 28%, with the secondary product fluorescing very strongly on the TLC plate. A similar trend was observed when 3,4-methylenedioxyaniline (**58a**) was used as substrate, with product **144** (Scheme 25) isolated in a yield of 22% when the reaction was performed at 15 °C and a yield of 48% at 30 °C.
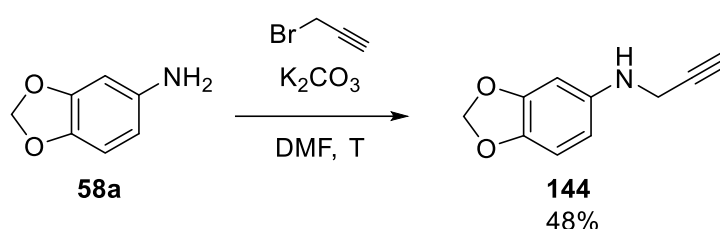
Scheme 25: Propargylation of 3,4-methylenedioxyaniline (**58a**).

The NMR spectra (Spectrum 3) below confirm the formation of the *bis*-propargylated product **145**, as the N-H peak of the *mono*-alkylated species (**144**) at 3.70 ppm is not visible in the top spectrum.

All propargylation reactions were performed for 6 hours. Longer reaction times led to reduced yields, as the formation of the secondary *bis*-propargylated product appeared to be favoured. This was also attributed to the more nucleophilic character of the resulting secondary amine, which would then outcompete the primary amine. The increased nucleophilic character is due to the alkyl group increasing the electron density on the nitrogen. Thus, the conclusion was drawn that heightened temperature were unfavourable in generating the *mono*-propargylated product.

Secondly, different bases were considered as another way of optimising the alkylations and the use of DIPEA as an organic base was first explored. The propargylation of 3,4-methylenedioxyaniline (**140**) was repeated with DIPEA as base, monitoring the reaction first at 15 °C and then again at 30 °C. Under both conditions, the *bis*-propargylated product **145** still formed in significant amounts and yields for the *mono*-propargylated product **144** still only ranged between 45-50%.
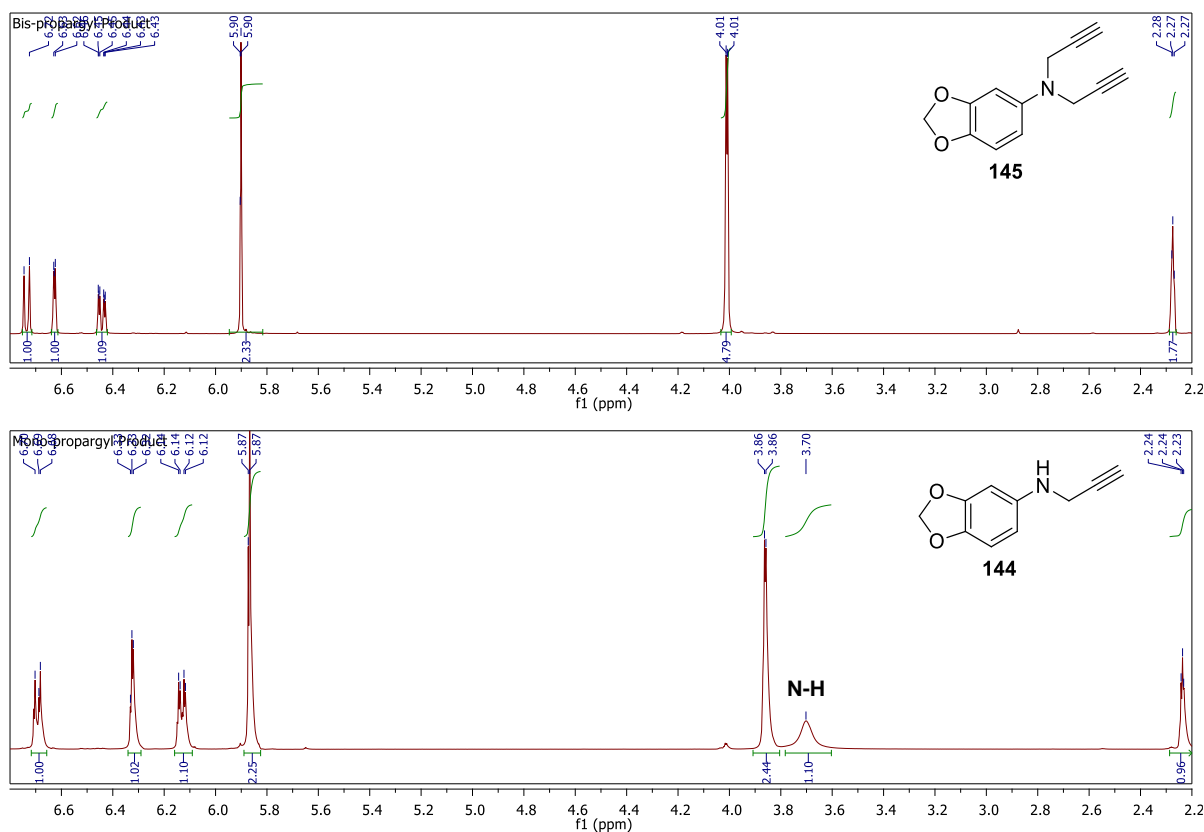
Spectrum 3: ^{1}H NMR spectra of the *bis*-propargylated product **145** (Top) and the mono-propargylated product **144** (Bottom).

As increased temperatures, along with the use of a base, resulted in *bis*-propargylation, it was theorized that employing high temperatures without a base, could lead to improved yields and more selectivity towards the *mono*-product. This could favour the nucleophilic attack on the alkylhalide by the aniline (which could also act as a base), would lead to the formation of the anilinium bromide salt of compound **144** (Scheme 26).
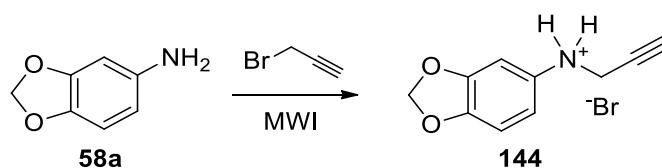
Scheme 26: Propargylation under MWI conditions.

The reaction was therefore redone by charging a microwave vial with 3,4-methylenedioxyaniline (**58a**) and propargyl bromide (**136**) (80% w/v in toluene) and heated under microwave irradiation at 110 °C for 2 hours. Upon quenching and isolation, the mixture was purified by means of automated column chromatography. Both the *mono*- and *bis*-alkylated products were isolated in a ratio of 6.1:1, with a 24% yield recorded for the desired product.

82

As the use of potassium carbonate as a base seemed to give the best yields, in spite of the formation of the undesired *bis*-propargylated, this method was employed in the propargylation of our compounds of interest, naphthyl-1-amine (**131**) and naphthyl-2-amine (**132**). What should be noted, is the reduced activity of these naphthylamines in comparison to the more electron-rich compounds such as 3,4-dimethoxyaniline (**140**) and 3,4-methylenedioxyaniline (**58a**), with much longer reaction times required for conversion.
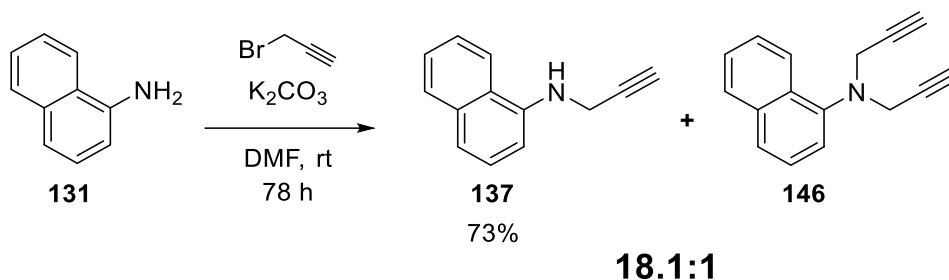
Scheme 27: Propargylation of α-naphthylamine (**131**).

For naphthyl-1-amine (**131**), the reaction reached completion after 78 hours. After purification it was found that a minor amount of the undesired *bis*-functionalized naphthylamine (**146**) had formed, in a ratio of 18.1:1 for *mono*-functionalized to the *bis*-functionalized species (Scheme 27). The same selectivity was, however, not observed in the synthesis of the *N*-propargyl naphthyl-2-amine variant. The *mono*-propargylated product (**147**) was isolated in 57% yield, in a ratio of 2.5:1 to the *bis*-functionalized product (**148**) (Scheme 28).
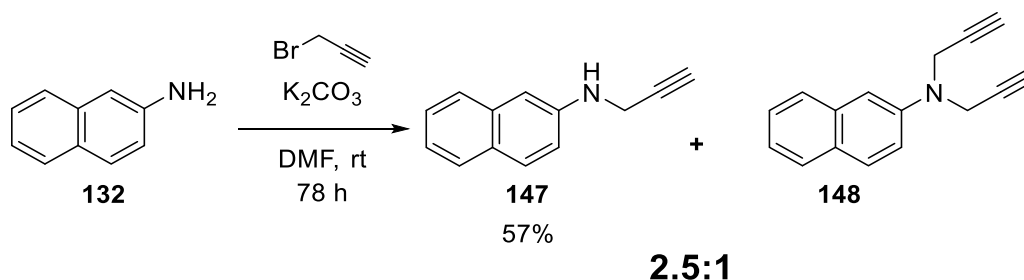
Scheme 28: Propargylation of β-naphthylamine (**132**).

The use of the aminonaphthols, 8-aminonaphth-2-ol (**149**) and 5-aminonaphth-1-ol (**150**), were also considered and explored (Figure 47), but the stability of these two compounds led to significant synthetic challenges and degradation problems. The degradation was more noticeable during the reductive amination approach, which will be discussed later.
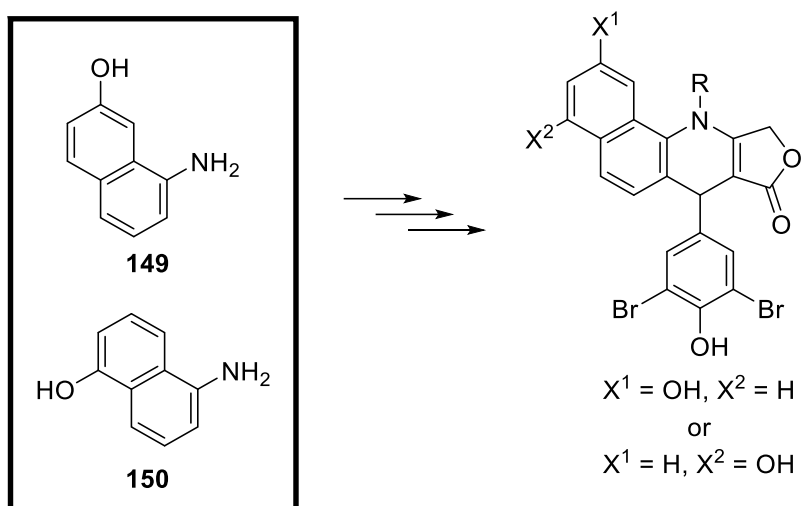
Figure 47: Aminonaphthols considered for incorporation onto the 4-azapodophyllotoxin scaffold.

The synthetic challenges associated with the exploration of the aminonaphthol variations included low yields for the desired mono-alkylated product or multiple alkylations when exploring the use of alkyl halides for functionalization (Scheme 29).

When the reaction was performed at room temperature, the mono-propargylated product (**151**) was isolated in very poor yields, which did not improve when the temperature was increased to 50 °C. At the higher temperatures the mono-propargylated product was not observed in measurable amounts, and the *bis*- (**152**) and *tris*-propargylated (**153**) products were favoured (Scheme 29).
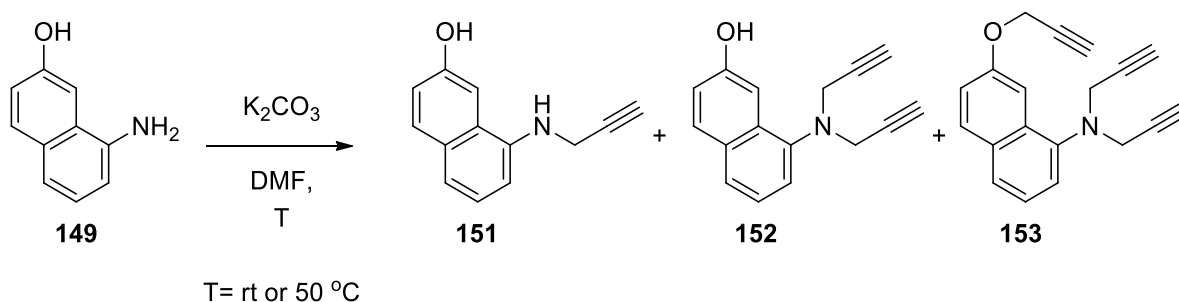
Scheme 29: Propargylated products of 8-aminonaphthalen-2-ol (**149**).

For the purposes of our study, only the naphthyl derivatives **137** and **147** were utilized in MCRs so as to synthesize the corresponding *N*-functionalized 4-azapodophyllotoxins. Compounds **142**, **143** and **144** were not used for the generation of 4-azapodophyllotoxin analogues in this study and originally served as scaffolds for the optimization of the propargylation reactions. Compounds **143** and **144** were, however, used in a different study conducted in our group. Next, the synthesis of various *N*-benzyl naphthylamines will be discussed.

84

4.2.2 Synthesis of *N*-Benzyl Naphthylamines

Building on the premise of exploring variations of the general 4-azapodophyllotoxin scaffold which focused on mimicking etoposide in its mechanism of action, rather than the natural cyclolignan, podophyllotoxin, two potential compounds were identified as inspiration. These were two C4-anilino analogues of etoposide (**55a**), named GL331 (**134**) and NPF (**135**) (shown in Figure 48). GL331 (**134**) was submitted for clinical trials and is reported to be in Phase II. It has been shown to have good antiproliferative activity against gastric carcinoma and colon cancer cell lines, as well as showing potency against various etoposide resistant cancer cell lines.[129] Similar to etoposide (**55a**), GL331 (**134**) has also been reported to act as a topoisomerase II poison by effecting DNA damage.[130] NPF (**135**) is a newer C4-*N*-arylderivative of etoposide that has shown great promise as a potential anticancer drug, with a 10-fold more potent inhibition of topoisomerase II and showing 100-fold higher cytotoxicity against many cell lines in comparison to etoposide (**55a**).[129]

55a
Etoposide

GL331, **134**: R = NO$_2$
NPF, **135**: R = F
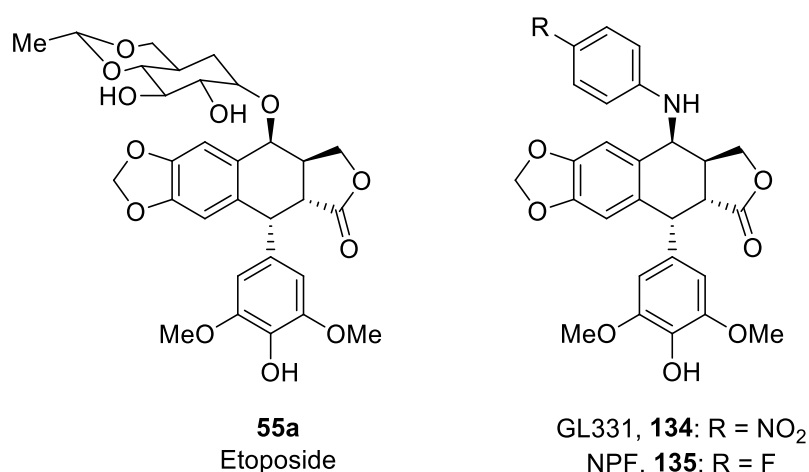
Figure 48: Etoposide (**55a**) and novel derivatives, GL331 (**134**) and NPF (**135**).

Due to these examples, we decided to investigate the 4*N*-(4-nitrobenzyl) and −(4-fluorobenzyl) groups as substituents on the 4-position of the 4-azapodophyllotoxin scaffolds, with primary focus placed on the α- and β-naphthylamine (naphthyl-1-amine (**131**) and naphthyl-2-amine (**132**), respectively) -derived scaffolds. Along with the 4-nitrobenzyl- and 4-fluorobenzyl-analogues, the corresponding *N*-benzyl analogues were also to be synthesized. This was to be able to probe the importance of the electron-withdrawing groups in the 4-position of the pendant benzyl-group, to be assessed later by analysing the biological activity data along with *in silico* molecular modelling results. Figure 49 below shows the target *N*-benzyl derivatives, with the E-ring containing the *p*-hydroxy-group. Similar to what was discussed earlier in the chapter with the retrosynthetic analysis of the propargylated analogues, the *N*-benzyl 4-azapodophyllotoxin analogues were accessed through the multicomponent reaction of a

suitable *N*-functionalized naphthylamine with an aromatic benzaldehyde and tetronic acid. Thus, the first step would involve introducing the benzyl group to the amine, as can be seen below in Figure 49.

Based on GL331: R = NO$_2$
Based on NPF: R = F
SAR Study: R = H
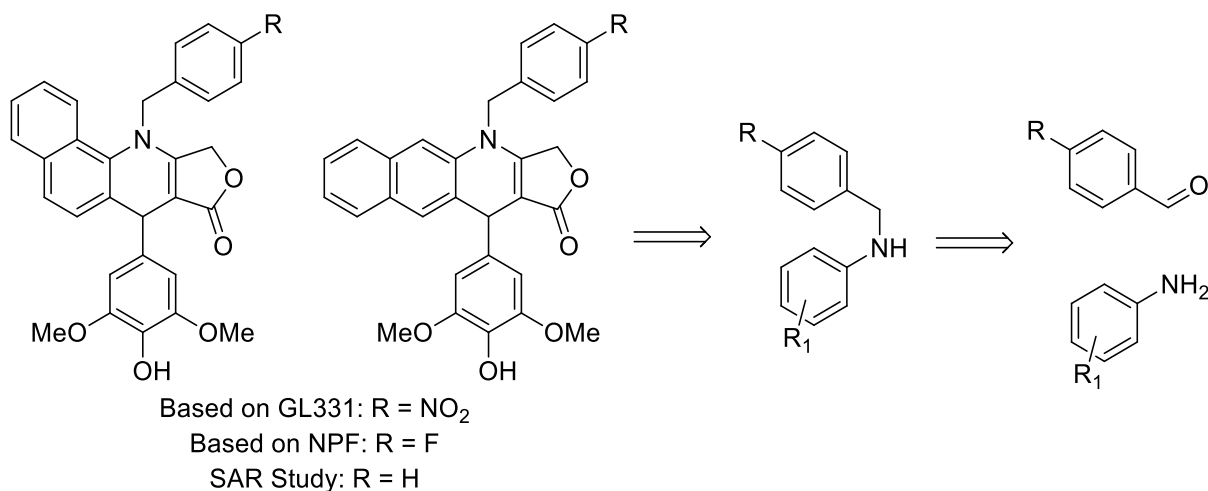
Figure 49: *N*-benzyl derivatives to be synthesized.

Other E-ring variations that were investigated were the podophyllotoxin-derived trimethoxy-subsituted E-ring, as well as two bromo-substituted E-rings, 3,5-dibromo-4-hydroxy-substituted and 5-bromo-2-hydroxy-substituted (shown in Figure 50).
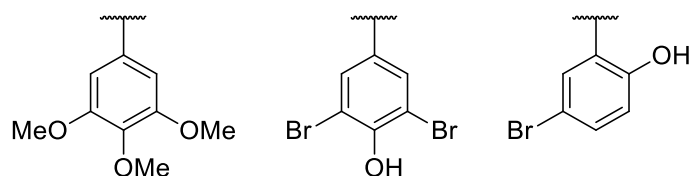
Figure 50: Different substitution patterns of interest for this study.

The synthesis of the GL-331 4-azapodophyllotoxin derivatives started with the derivatization of the naphthylamine substrates (**131** and **132**) with a *p*-nitrobenzyl moiety. The first strategy attempted was a simple substitution using *p*-nitrobenzylbromide (**154**), in THF (Scheme 30). Initially, the reaction mixture was stirred overnight at 35 ⁰C, but very little conversion was observed through TLC analysis after 12 hours. The reaction mixture was then heated to 50 ⁰C for 24 hours, but starting material was still observed and the reaction was left to stir for another 12 hours. When full conversion was still not achieved after this time, the reaction was worked up and the resultant residue was purified by column chromatography. The product (**155**) was recorded in only 5% yield.
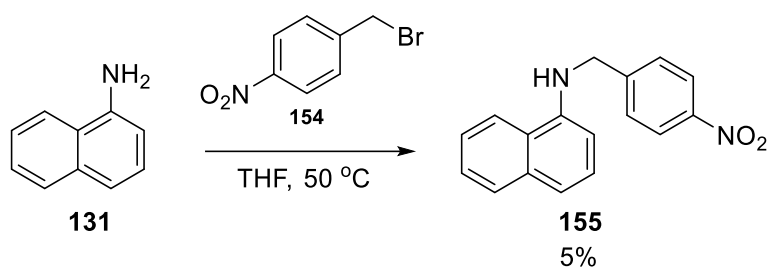
Scheme 30: *N*-benzylation of α-naphthylamine (**131**) with *p*-nitrobenzylbromide (**154**).

As a simple substitution without any additive was not yielding acceptable conversion, the reaction was repeated with different bases and the temperatures were varied. As the work synthesis of the *N*-propargyl arylamines showed that high temperature favoured *bis*-alkylation, high boiling point solvents were not considered for the benzylation reactions. Only THF as a polar, aprotic solvent was investigated. These results are summarized in Table 18.

Table 18: Summary of different conditions used for *N*-benzylation of α-naphthylamine (**131**).
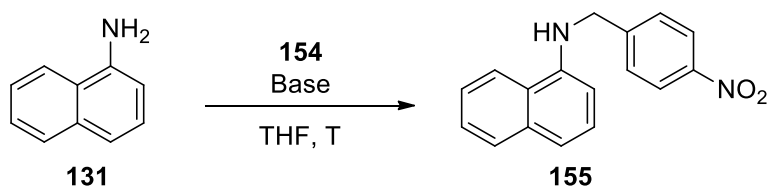
Solvent	Base	Temp. (°C)	Time (hours)	Yield (%)
THF	-	35	12	-
THF	-	50	24	5
THF	K$_2$CO$_3$	25	12	8
THF	K$_2$CO$_3$	25	24	14
THF	K$_2$CO$_3$	50	24	19
THF	DIPEA	35	12	10
THF	DIPEA	35	24	13

As can be seen from Table 18, yields increased but remained poor for the benzylation reactions of α-naphthylamine (**131**). Also noticed was that during the propargylation of α-naphthylamine, naphthylamines were slower to react than more electron-rich arylamines. For this reason, a different approach was considered, as the reaction times for the benzylation by means of benzylhalide substitution proved inefficient and resulted in poor to moderate yields. Reductive amination was therefore considered as an alternative approach and a solid state reaction between a suitable naphthylamine and a corresponding benzaldehyde was considered based on work done by Cho and Kang.[131]
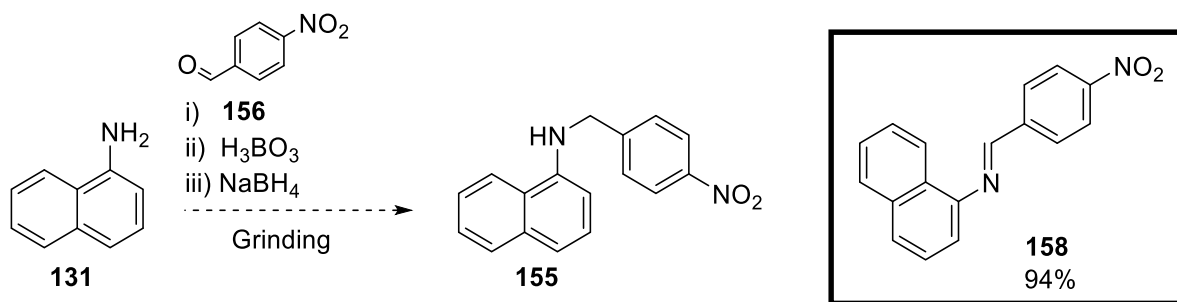
Scheme 31: Mortar and pestle grinding reaction of α-naphthylamine (**131**) based on work by Cho and Kang.[131]

Firstly, naphthyl-1-amine (**131**) and *p*-nitrobenzaldehyde (**156**) were ground together in a mortar and pestle for 30 minutes, after which boric acid was added and finally sodium borohydride (Scheme 31). This mixture was ground for another 30 minutes before the reaction was slowly quenched with saturated sodium bicarbonate in the mortar and then washed with ethyl acetate. The reaction gave a single product, but analysis by means of ^{1}H NMR spectroscopy proved that the reaction had not reached completion and the desired product (**155**) was not formed. The corresponding imine (**158**) was, however, collected in 94% yield. The reaction was repeated, and the grinding time extended for the addition of boric acid and sodium borohydride, but the reaction again did not go to completion. The boric acid and sodium borohydride were used in equimolar amounts to the naphthylamine and benzaldehyde species, thus poor homogeneity was thought to be the problem. However, even when adding small amounts of diethyl ether while grinding to improve homogeneity, the reaction still only yielded the imine (**158**).

The use of grinding in a mortar and pestle delivered the imine in excellent yield, but the reaction proved challenging upon repetition. This was due to contamination from the mortar in subsequent reactions, as methods to clean the bowl proved mostly ineffective – even when soaked in *aqua regia* overnight. Several attempts proved that the contamination was going to be a problem when using this method, especially when using compounds that are similar in both structure and polarity [such as naphthyl-1-amine (**131**) and naphthyl-2-amine (**132**)], as purification by means of column chromatography was not feasible. To overcome this limitation, the reaction was conducted by conventional means, using dry diethyl ether as solvent at room temperature (Scheme 32).

The same step-wise approach was followed, reacting the aldehyde (**156**) and naphthylamine (**132**) species first, followed by the subsequent addition of boric acid and sodium borohydride. The naphthylamine and benzaldehyde species were stirred at room temperature for 30 minutes, followed by the addition of boric acid and sodium borohydride and left to stir at room

temperature overnight. A precipitate had formed, which was collected and analysed by means of ^{1}H NMR spectroscopy.
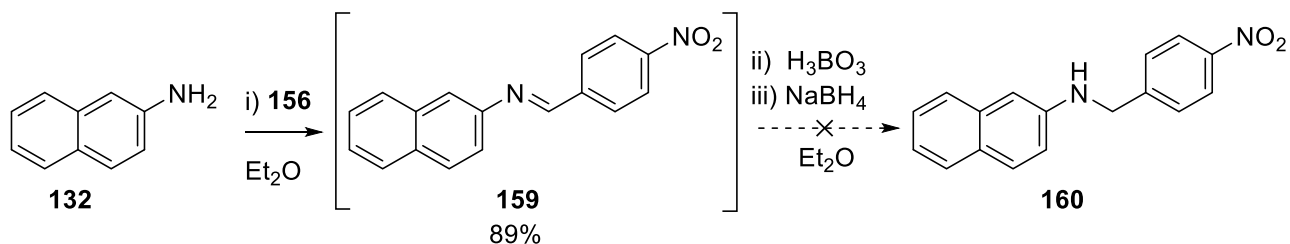
Scheme 32: Modified reductive amination approach.

The expected peaks of the benzyllic and amine protons between 4 - 5 ppm were not observed in measurable intensities; however, the proton signal for the imine (**159**) was observed at 8.69 ppm, confirming that the reduction had not been successful in delivering the desired product (**160**) (Spectrum 4). The imine (**159**) was, however, again synthesized in a very good yield of 89%.
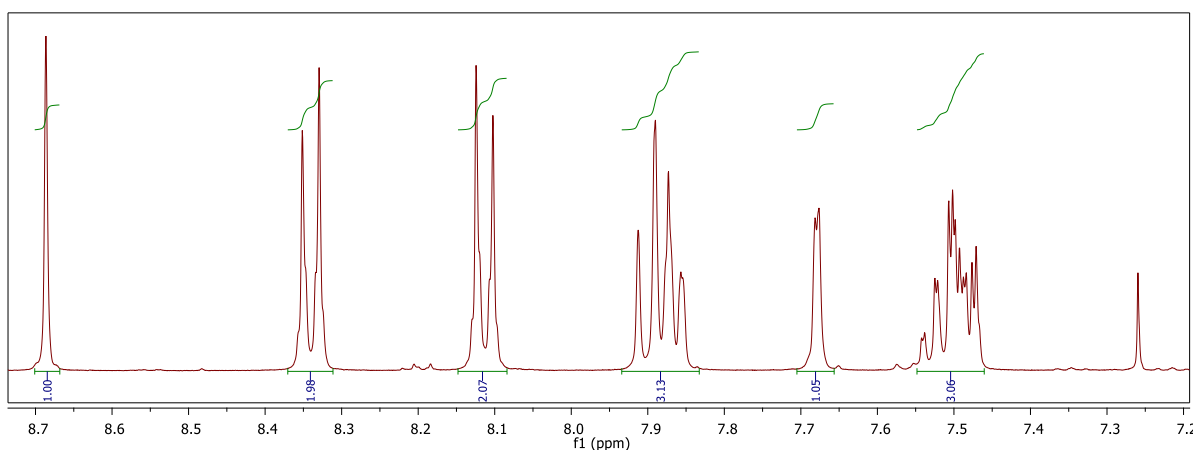
Spectrum 4: ^{1}H NMR spectrum of the imine (**159**).
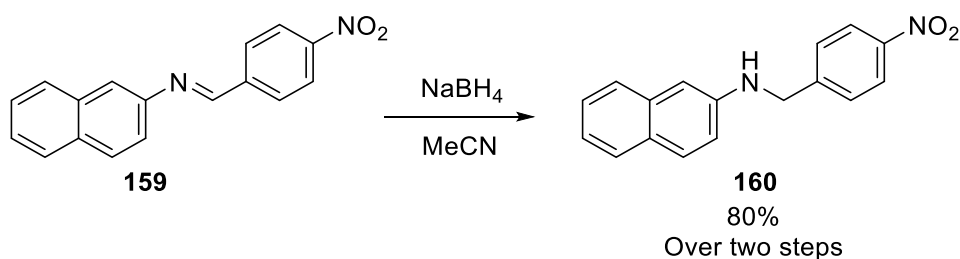
Scheme 33: Reduction of the imine (**159**) to afford the desired *N*-benzyl naphthylamine (**160**).

The imine (**159**) was then dissolved in acetonitrile and NaBH$_4$ was added. Once analysis by means of thin layer chromatography confirmed the full consumption of the imine, the reaction mixture was quenched and the product isolated. The desired product, *N*-4-

89

nitrobenzylnaphthyl-1-amine (**160**), was subsequently isolated in 90% yield, thus 80% over two steps (Scheme 33).

Considering that all previous methods resulted in producing the corresponding imines in good yield, but that a successive reduction step was always necessary, a literature search on the reduction of imines led to the discovery of work done by Okamoto and co-workers.[132] These researchers employed calcium hydride as a reductive hydride species in the presence of a zinc halide at room to deliver *N*-substituted amines (such as compound **162**) from the corresponding imine **161** in quantitative yields (Scheme 34).
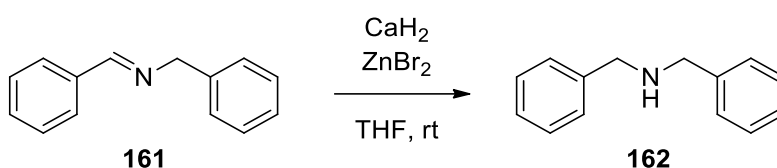
Scheme 34: Reductive amination reported by Okamoto and co-workers.[132]

As their study started with the imine, we followed a modified approach of their work by forming the imine first.
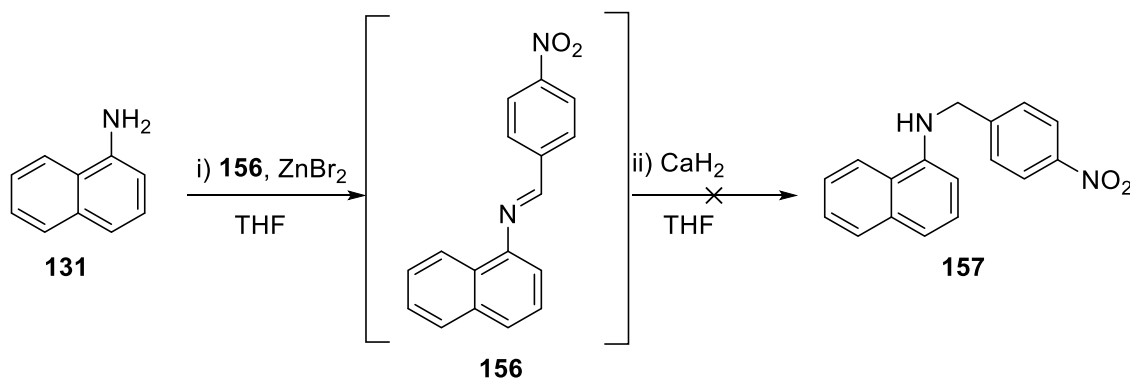
Scheme 35: Lewis acid mediated reductive amination approach.

As Lewis acids also facilitate the formation of imines, 4-nitrobenzaldehyde (**156**) was dissolved in tetrahydrofuran (THF) and zinc bromide was added.[133] Once all solid material had dissolved, naphthyl-1-amine (**131**) was added and analysis by means of thin layer chromatography after one hour showed the consumption of the naphthylamine. Calcium hydride was then added and the reaction stirred for 12 hours at room temperature (Scheme 35). However, TLC showed that no reduction had occurred and analysis of the crude mixture by means of ^{1}H NMR spectroscopy, confirmed this as no methylene peak was observed in the spectrum with the imine peak still at 8.70 ppm. The imine (**158**) was, however, synthesized in 96% yield. The reaction was repeated, but upon the addition of the calcium hydride, the reaction was heated to 50 °C. Unfortunately, after 12 hours, again no reduction had occurred.

90
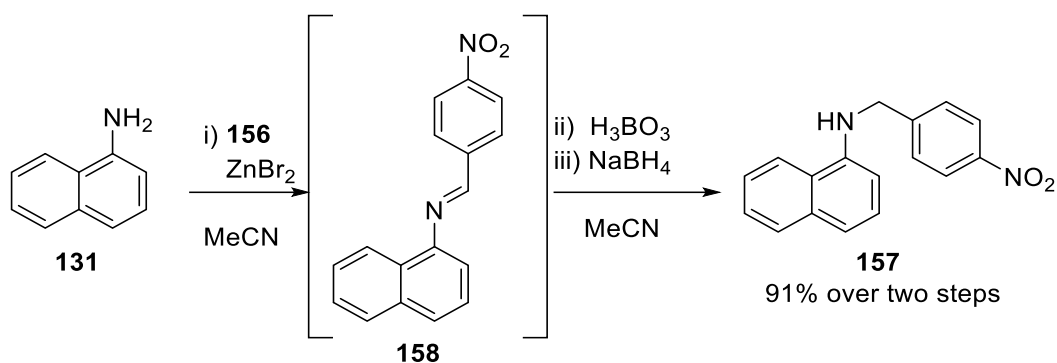
Scheme 36: New approach that combined the work of Okamoto and co-workers[132] and Cho and Kang.[131]

The two approaches were thus combined as the formation of the imine (**158**) was easily achieved, especially with the use of zinc bromide as Lewis Acid. The subsequent reduction of the imine (**158**) with boric acid and sodium borohydride was also successful, thus it was decided to combine the approaches in a two-step one pot synthesis. The reaction was repeated in dry acetonitrile and heated to 65 °C and left to cool to room temperature upon addition of sodium borohydride (Scheme 36). This was done with both naphthyl-1-amine (**131**) and naphthyl-2-amine (**132**) and the corresponding 4-nitrobenzyl functionalized naphthylamines (**157** and **160**) were successfully synthesized. This was confirmed by means of NMR spectroscopy (spectra shown below in Spectrum 5) and high resolution mass spectrometry.

The changes that could be noted from the spectrum of the imine, was the appearance of the N-H proton signal at δ 5.9 ppm for compound **157** and δ 4.4 ppm for compound **160**. Both spectra also showed the methylene peaks of the benzyl group, with a signal in the aliphatic region that integrated for two protons. These signals appeared at δ 4.6 ppm for both compounds **157** and **160**. The doublets corresponding to the *p*-substituted benzyl group could also be seen in the aromatic region, with integration values of two per signal. The calculated [M + H]$^+$ mass for both 279.1134 and the observed masses were 279.1132 for compound **157** and 279.1125 for compound **160**.
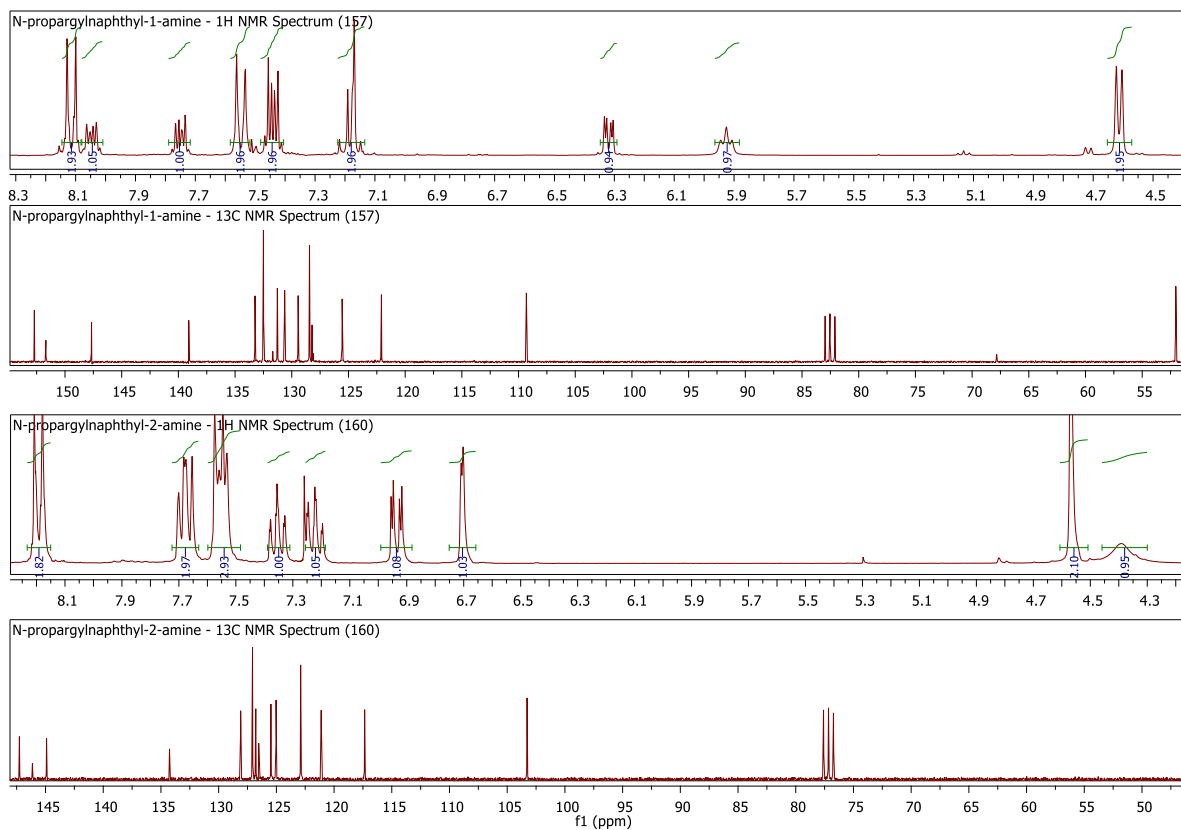
Spectrum 5: ^{1}H and ^{13}C NMR spectra of compounds **157** (top two spectra) and **160** (bottom two spectra)

The same general reaction (shown below in Scheme 37) procedure was then followed using benzaldehyde (**163**) and 4-fluorobenzaldehyde (**164**).
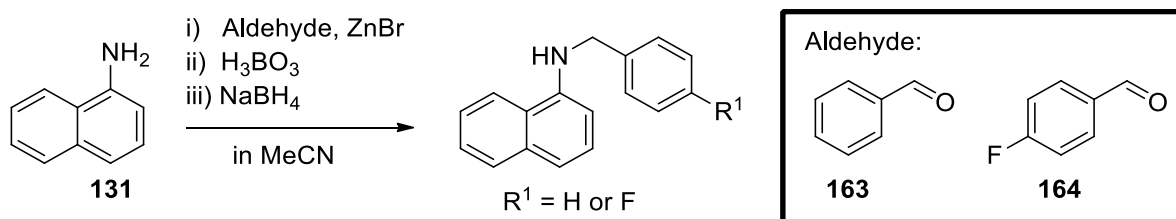
Scheme 37: Synthesis of the benzyl- and 4-fluorobenzyl derivatives.

The yields for the different products are given in Figure 51 below.
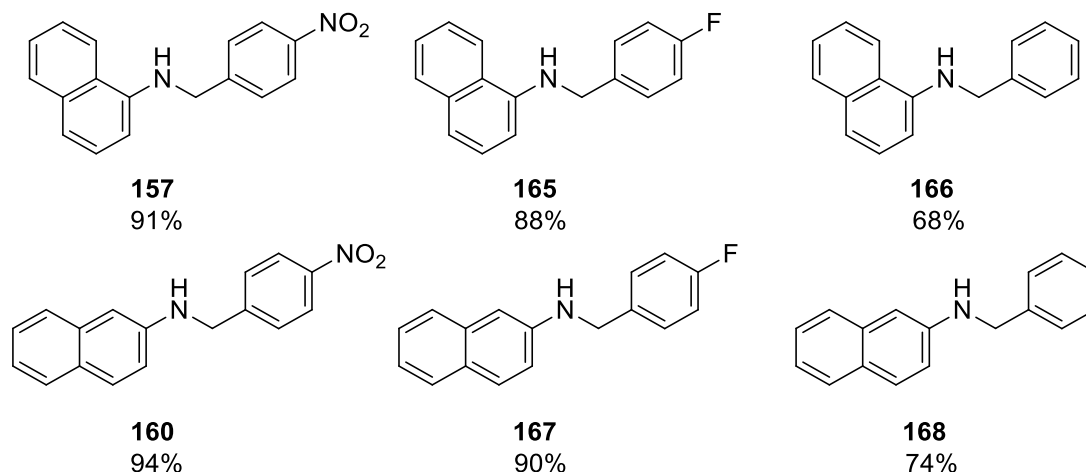
Figure 51: N-benzyl derivatives successfully synthesized.

Compounds **166**[134] and **168**[135] have been reported in literature and the spectra recorded in this study compare well. Compounds **165** and **167** were satisfactorily characterized by means of NMR spectroscopy (^{1}H and ^{13}C) and high resolution mass spectrometry.

As mentioned earlier, the use of aminonaphthols (**149** and **150**) were explored for propargylation as well as benzylation. The problem with multiple propargylations through the use of propargyl bromide, coupled with instability of the aminonaphthols during the reductive amination approach, led to the abandonment of these two compounds for this study. Synthetic issues with the incorporation of *N*-functionalized α-naphthylamines (**137**, **157**, **165** and **166**) into the novel 4-azapodophyllotoxin scaffolds also contributed to this, due to position of the amino groups on compounds **149** and **150**. This will be discussed in the following chapter, *Multicomponent Reactions*.

5.1 Multicomponent Reactions

5.1.1 Synthesis

The main synthetic method used in this study, was the employment of the multicomponent reaction (MCR) proposed by Giorgi-Renault and co-workers.[58] The generalised reaction scheme is shown below in Scheme 38, where the method was reported to also accommodate R-groups such as methyl groups.
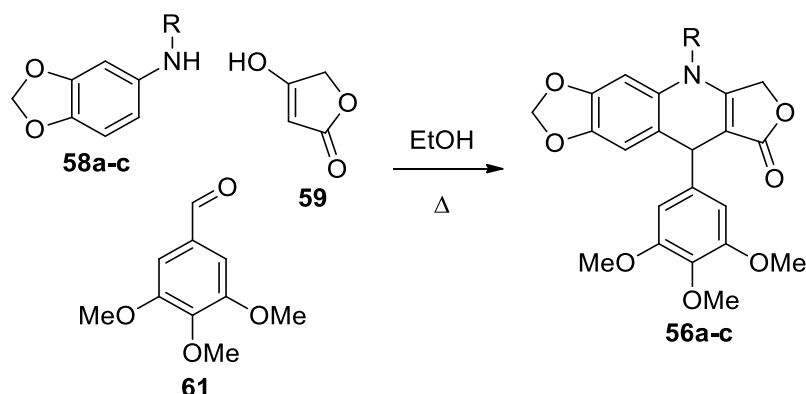
Scheme 38: Multicomponent as reported by Giorgi-Renault and co-workers.[58]

A study by Malhotra and co-workers also extended the aniline R-group to include hydroxyethyl chains and these compounds were analysed for their antiproliferative activity against the NHI 60 Cancer Cell line library. The GI_{50} values for these were determined and shown to be very active, with compounds **104a**, **105a** and **106a** in Figure 52 as examples, with values below 1 μM for more than 75% of the cell lines.[46]
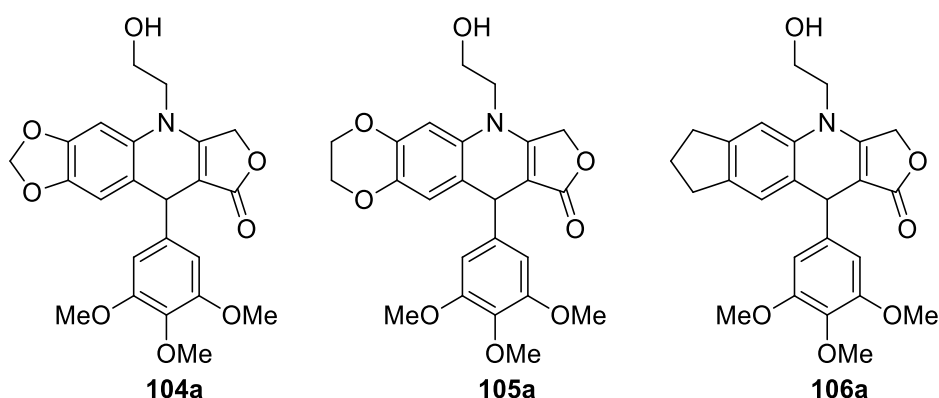
Figure 52: Representative examples of compounds generated by Malhotra and co-workers.[46]

As our proposed library considered the introduction of R-groups onto the 4-aza position, the *N*-functionalized naphthylamines that were previously synthesized were utilized in MCRs. To

optimize the reaction conditions, the reaction depicted in Scheme 39 was used as a model reaction.
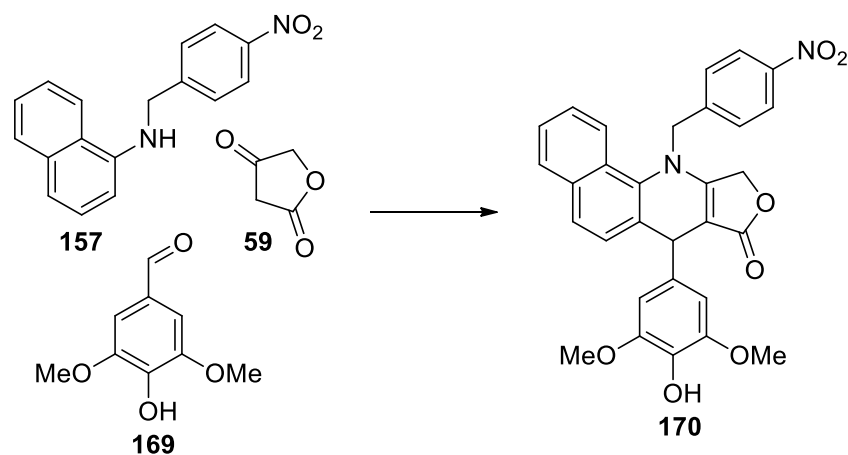
Scheme 39: Model reaction to be used for optimization of MCR for the generation of a novel library. Conditions are summarized in Table 19.

Table 19: Summary of the conditions used in the Model MCR studies (as shown in Scheme 39).

Method of heating	Catalyst	Solvent	Temp. (°C)	Time (h)	Product
Conventional	None	Ethanol	85	144	None
Conventional	4-Chloroaniline	Ethanol	85	120	None
Microwave Irradiation	None	Ethylene Glycol	110	2	None
Microwave Irradiation	None	Ethylene Glycol	110	4	None
Microwave Irradiation	None	Ethylene Glycol	190	2	None
Microwave Irradiation	4-Chloroaniline	Ethylene Glycol	110	2	None
Microwave Irradiation	4-Chloroaniline	Ethylene Glycol	110	4	None
Microwave Irradiation	4-Chloroaniline	Ethylene Glycol	190	2	None

To find the best conditions, *N*-(4-nitrobenzyl)-naphthyl-1-amine (**157**) was used along with tetronic acid (**59**) and syringaldehyde (**169**). The initial reaction conditions initially set forth by Giorgi-Renault and co-workers was used first, as we previously had success with this in our research group and that of our collaborators.[29,58,72] This method involved stirring the three reagents at reflux in ethanol so as to furnish the desired 4-azadidehydropodophyllotoxin analogues as a precipitate. The solubility of the starting materials and the insolubility of the resulting 4-aza-scaffold is also one of the benefits of MCRs, as purification becomes much easier. The MCR product tends to precipitate from the reaction mixture in high purity and filtration and washing with cold ethanol removes most of the unreacted starting material. However, when the 4-nitrobenzyl naphthalene derivative (**157**) was used, no precipitate was

observed after 96 hours at reflux. The reaction was monitored at 12 hour intervals after this point for another 48 hours and even though TLC indicated the formation of a fourth spot, none of the starting materials were consumed. This suggested that the reaction was still incomplete, but so as to confirm that product had in fact started forming (as suggested by the visualization of a new fourth spot under 254 nm UV light), the reaction was then stopped and cooled on ice. As had been noted by previous reports on 4-azapodophyllotoxin MCRs, a precipitate was expected, yet no precipitate formed even when the reaction mixture was stored in the freezer overnight. The abundance of chromophores on the product suggested that even trace amounts of the desired product could appear on TLC, however, it could also have been the Knoevenagel adduct of the benzaldehyde and tetronic acid. As purification was unfeasible due to the scale of the reaction, optimization for better conversion was considered instead.

As described earlier, the proposed mechanism of MCRs involves the dual role of the amine as both catalyst (to form the Knoevenagel adduct) and reagent. It was therefore hypothesized that the electronics of the secondary amine of *N*-(4-nitrobenzyl)-naphthyl-1-amine (**157**) could be impeding its ability to act as a catalyst and the reaction was repeated with a sacrificial aniline, 4-chloroaniline (**171**) (10 mol%).

The reaction was again stirred at reflux for 96 hours and the same result was observed as in the reaction without the catalyst. Extending the reaction time did not change the result. As neither of these attempts afforded the desired product **170**, it was decided to repeat the reaction (both without and with a sacrificial aniline) under microwave irradiation. This would make it possible to increase the temperature beyond that which is possible under conventional heating.

The compounds were added to a microwave reaction vial (without 4-chloroaniline (**171**) as sacrificial aniline) and ethylene glycol was added. The reaction mixture was then heated to 110 °C under microwave irradiation (MWI) for two hours. The reaction mixture was cooled in an ice bath and no precipitate was observed. Analysis by means of TLC showed that none of the starting material had been consumed and no appreciable amount of product had formed. The reaction was then repeated under MWI at 110 °C for four hours, yet no difference was observed. The temperature was then increased to 190 °C and the reaction repeated and again no product was observed. The use of a sacrificial aniline yielded the same results. These results are summarised in Table 19 above.

As none of the attempts yielded the desired product, the problem appeared to be with the *N*-functionalized naphthylamine. To investigate whether the benzyl group on the naphthylamine led to the reagents not assembling into the desired scaffold, the *N*-propargyl naphthylamine was engaged in the reaction under the same conditions. The propargyl group is well tolerated

in microwave irradiated MCRs, as it was used previously by an MSc student, Sebastien Depaifve, that did research in our group. A representative MCR, employing *N*-propargyl-3,4-methylenedioxyaniline (**144**), performed by the researcher is shown below in Scheme 40. The reaction furnished compound **172** in a good yield of 72% (Scheme 40).
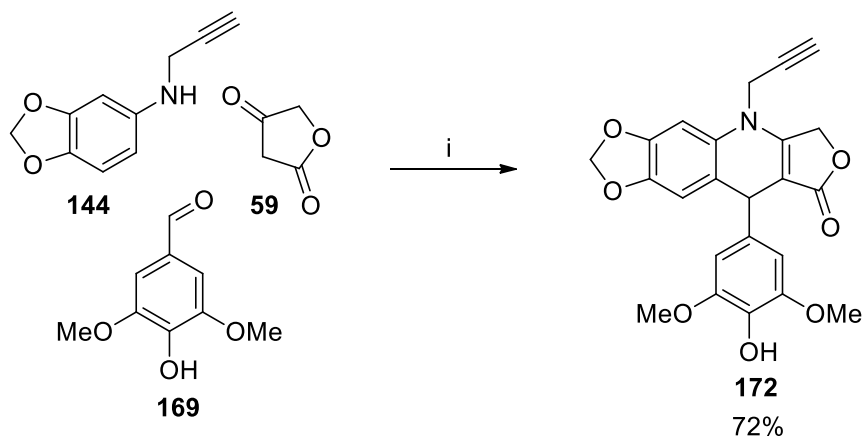
Scheme 40: Microwave Irradiated MCR. i) Ethylene Glycol, 110 °C, 35 min, MWI.

The same procedure used for compound **172** was then used for two different *N*-propargyl naphthylamines, *N*-propargylnaphthyl-1-amine (**137**) and *N*-propargylnaphthyl-2-amine (**147**). Going forward, the naphthyl-1-amine and naphthyl-2-amine derivatives will be referred to as the α-naphthylamine and β-naphthylamine derivatives, respectively. This will extend to the *N*-benzyl derivatives as well.
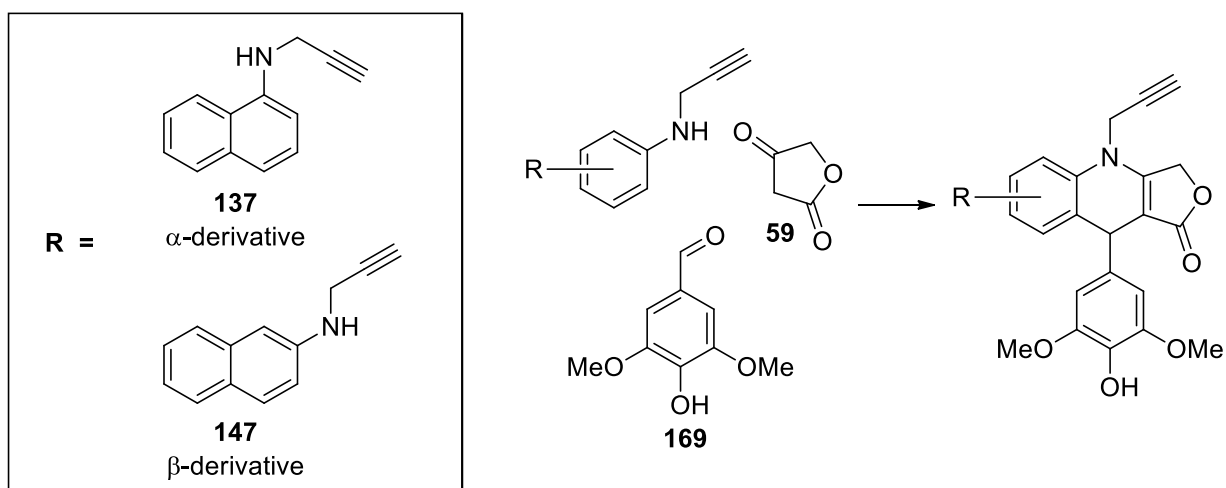
Scheme 41: Generalised Microwave Irradiated MCR.

Both *N*-propargylnaphthylamines (**137** and **147**), along with tetronic acid (**59**) and syringaldehyde (**169**), were stirred under microwave irradiation at 110 °C for 35 minutes. Interestingly, after the reaction mixtures had cooled down to room temperature, the one involving β-naphthylamine MCR (**174**, Scheme 42) showed a precipitate whereas the mixture

97

with α-naphthylamine MCR showed no precipitate. Even upon cooling, no precipitate formed and analysis by means of TLC showed that the starting material had not been consumed and no appreciable product had formed (as the visualization of a fourth spot under UV light would imply that at least some desired product had formed). Even at extended reaction times under MWI, no appreciable product had formed (as no reduction in the intensity of the reagents under UV were visible, nor any new products visualized as spots under UV light).
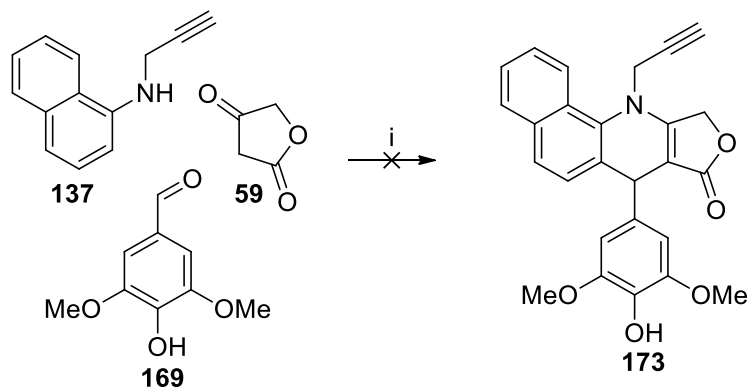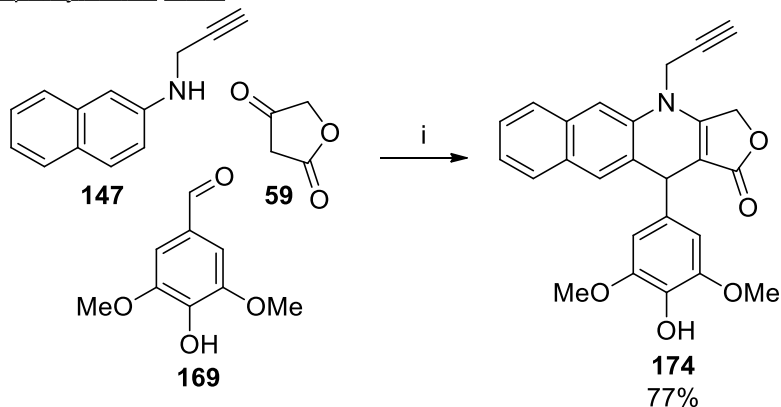
Scheme 42: Microwave Irradiated MCR. i) Ethylene Glycol, 110 °C, 35 min, MWI.

The β-naphthylamine product (**174**) was isolated by vacuum filtration and the resulting solid washed with cold ethanol to furnish the desired product yield in good yield (77%) as confirmed by means of ^{1}H NMR, ^{13}C NMR, IR spectroscopy and high resolution mass spectrometry. The analysis by means of NMR spectroscopy and HRMS showed that the product was isolated in good purity, therefore, no further purification was deemed necessary. The ^{1}H NMR spectrum of compound **174** is shown in Spectrum 6 below.
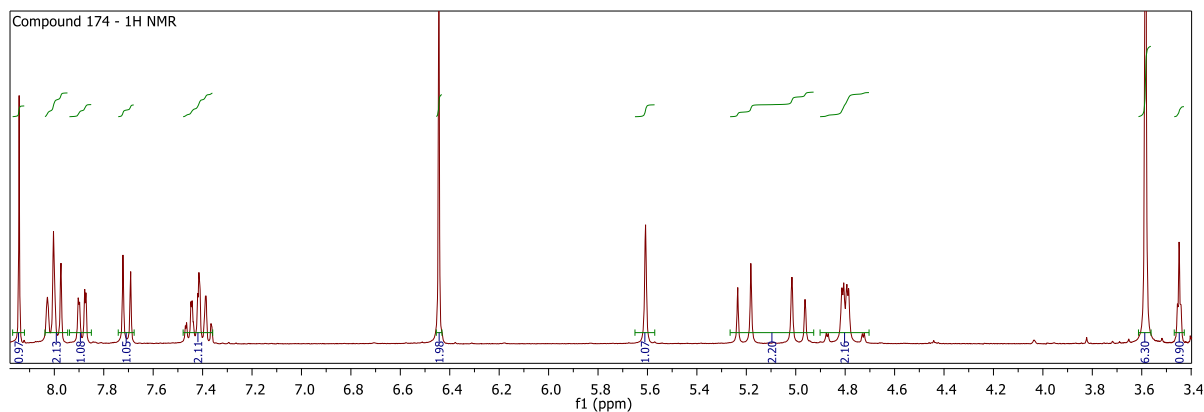
Spectrum 6: ^{1}H NMR Spectrum of compound **174**.

The proton spectrum showed the methoxy group protons of the newly incorporated pendant R-ring at δ 3.6 ppm and the *ortho*-protons of the ring at δ 6.54 ppm. The phenolic OH-signal could also be seen at about δ 9 ppm. This was in addition to the signals for the propargyl group (methylene, δ 4.8 ppm, and methine, δ 3.45 ppm) and the aromatic signals of the naphthyl ring. The most diagnostic signal was the signal of the C1 proton of the C-ring, which produced a singlet at δ 5.6 ppm. This correlated with work reported by Professor van Otterlo and our collaborators, which focused on similar naphthylamine analogues.[29] The tetronic acid methylene signal was usually recorded as a double of doublets that integrated for 2 protons with a *J*-coupling of 15 Hz at a chemical shift of δ 5.0 ppm. However, we observed two doublets (δ 5.2 ppm and δ 5.0 ppm), with similar *J*-coupling values, that integrated for one proton each. This was still hypothesized to be the tetronic acid-derived methylene signal and was confirmed by the ^{13}C NMR spectrum (Spectrum 7), where the expected signal was observed at δ 56 ppm, as had been commonly reported. The splitting pattern of the methylene protons of the tetronic acid can be explained by the diastereotopicity of these two protons, with the second order effects introduced by the propargyl substituent leading to asymmetry in the resulting doublets. Malhotra and co-workers reported a similar occurrence in synthesis of a library of 4-*N*-hydroxethyl derivatives.[46]
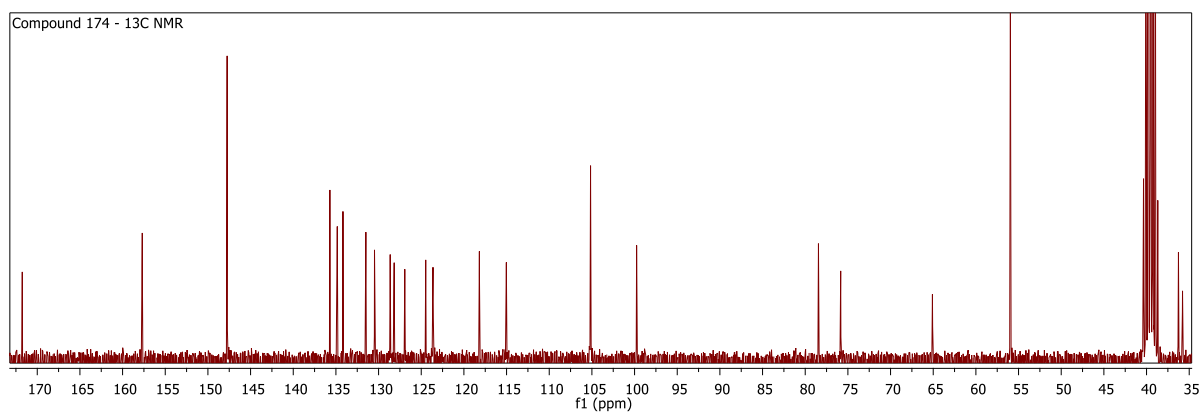
Spectrum 7: ^{13}C NMR of compound **174**.

The successful synthesis of compound **174** was further confirmed by means of high resolution MS, as the proton adduct was recorded at a mass to charge ratio (m/z) of 428.1490 and the calculated mass was 428.1498.

The β-naphthylamine MCR was repeated at a higher temperature, 135 °C, for 35 min and yielded the desired product (**174**) in a 72% yield. When the reaction was repeated at 45 minutes and one hour, the yields did not markedly improve, with the product isolated in yields of 77% and 76%, respectively. The results for the different arylamine MCRs are summarised in Table 20 below.

Table 20: Summary of *N*-propargyl arylamines used in MWI MCRs.

N-Functionalized Arylamine	Product	Catalyst	Temp. (°C)	Time (min)	Yield (%)
144	**172**	-	110	35	None
147	**174**	-	110	35	68
		-	135	35	72
		-	135	45	77
		-	135	60	76
137	**173**	-	110	35	NP*
		-	110	60	NP*
		-	110	120	NP*
		-	135	120	NP*
		-	170	240	NP*
		4-Chloroaniline	170	240	NP*

* NP: No Product Isolated

100

An interesting correlation between the two model studies was that neither the *N*-(4-nitrobenzyl)-napthyl-1-amine (**157**) nor the corresponding *N*-propargyl analogue (**137**) yielded any of the respective desired products. This was observed both with and without the use of a sacrificial aniline catalyst, at increased temperatures and extended reaction times. As compound **147** assembled readily into the desired scaffold under these conditions, in good yield as well as in shortened reaction times, the same procedure was considered for the *N*-benzyl β-naphthylamine derivatives.
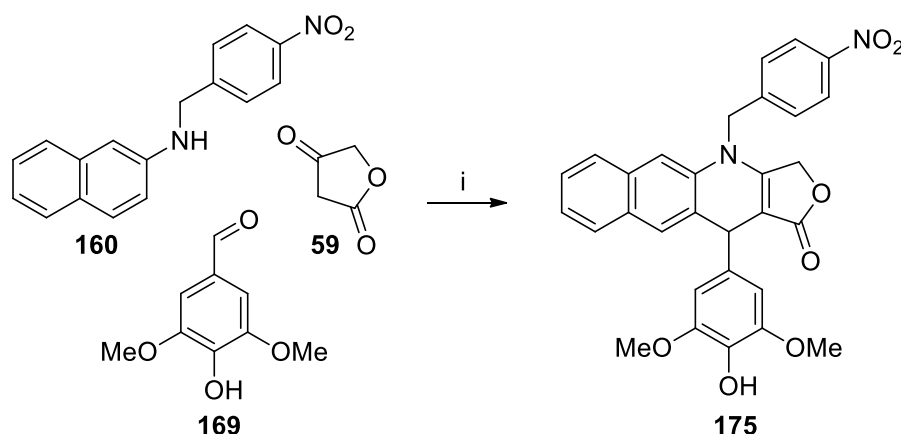
Scheme 43: MCR with *N*-(4-nitrobenzyl)-naphthyl-2-amine. MWI: i) 4-Chloroaniline (20 mol%), Ethyene glycol, 130 °C, 30 min or i) Ethyene glycol, 130 °C, 30 min. Conventional heating: i) EtOH, Δ or i) 4-Chloroaniline (20 mol%), EtOH, Δ.

The same procedure which successfully delivered the *N*-propagyl-4-azapodophyllotoxins (such as compound **174**) was used then followed to synthesise the desired *N*-benzyl-4-azapodophyllotoxins. A microwave vial was charged with *N*-(4-nitrobenzyl)-naphthyl-2-amine (**160**), syringaldehyde (**169**), tetronic acid (**59**) and ethylene glycol and heated to 130 °C for 30 minutes. Upon cooling, some precipitate seemed to have formed and the reaction mixture was diluted with cold ethanol. A negligible amount of solid was obtained during filtration, however not enough for analysis.

When the procedure was repeated with the addition of 4-chloroaniline as catalyst, a more appreciable amount of precipitate was isolated during the filtration. Analysis by means of ^{1}H NMR spectroscopy confirmed that it was the desired product (**175**), albeit in a poor yield of 6%. The product was confirmed by means of ^{1}H NMR spectroscopy, which showed the expected signals for the D-ring methylene peak at δ 5.0 ppm (as was observed for compound **174**) along with the singlet for the C1 proton of the newly formed C-ring at δ 5.7 ppm. The signals for the *p*-nitrobenzyl group were also observed, with the protons of the benzyl methylene group showing at δ 5.3 ppm and the two signals for the aromatic ring showing at δ

8.2 ppm and δ 7.6 ppm. The ^{13}C NMR and high resolution MS spectra also confirmed the successful formation of the product.

The reaction was repeated, and the temperature increased to 150 °C. After 30 minutes of stirring, however, no more precipitate was visible than was in the first attempt at 130 °C. The reaction time was then increased to 3 hours. This furnished the desired product (**175**) in an improved, yet still poor yield of 15%.

The use of MWI appeared to offer a method of producing the *N*-benzyl analogues, although in poor yield. The reaction was then repeated using conventional heating. The reaction mixture was stirred in ethanol at reflux and the reaction monitored over 4 days. The reaction that was performed without the use of the sacrificial aniline, only afforded the product **175** in a 22% yield, whereas the product was isolated in a 52% yield when 4-chloroaniline (**169**) was used as catalyst.

β-Naphthylamine MCR
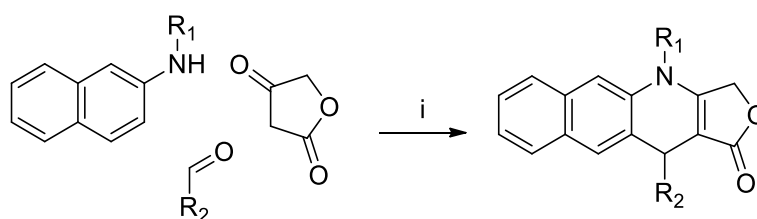
α-Naphthylamine MCR
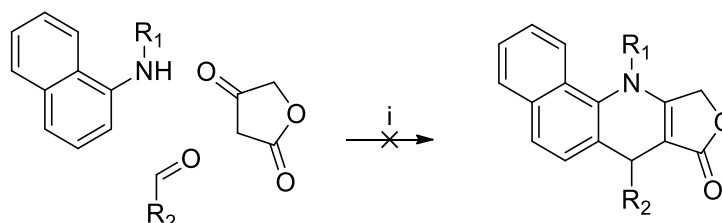
R$_1$ = 4-nitrobenzyl, Propargyl

i) Conventional Heating or MWI

R$_2$ = 3,5-Dimethoxy-4-hydroxyphenyl

The difference between the two strategies, MWI and conventional heating, could be explained by the increased steric bulk of the *N*-benzyl group in comparison to the *N*-propargyl group. Even though the resulting 4-azapodophyllotoxin is clearly a thermodynamically favoured product, increasing bulk of the substituent seemed to markedly slow down the reaction.

The assembly of the β-naphthylamine derivatives into the desired scaffolds (even in poor yields under MWI and fair yields under conventional heating for the *N*-benzyl analogues)

suggested that the inability of the α-naphthylamine derivatives to deliver the corresponding products, may in fact have to do with the reactivity of the *N*-functionalized α-naphthylamines. This was confirmed when the β-naphthylamine analogues (*N*-propargyl- (**147**) and *N*-(4-nitrobenzyl) substituted (**160**)) were investigated under both MWI and conventional heating, both with and without the use of 4-chloroaniline (**171**) as sacrificial aniline (as shown in Scheme 43), even though the *N*-benzyl naphthylamines were slow to assemble into the desired scaffold under MWI.

This posed an interesting question. The *N*-substituted β-naphthylamines assembled into the desired *N*-derivatized 4-azapodophyllotoxins under both conventional heating and MWI conditions, whereas the *N*-substituted α-naphthylamines did not. In a 2011 study that Professor van Otterlo was part of along with our collaborators, the unsubstituted α-naphthylamines were successfully incorporated into 4-azapodophyllotoxin scaffolds in poor to moderate yields.[29]

Given the structural similarity of the two different naphthylamines, different reasons were postulated for the differences observed in activity (Figure 53). Mechanistically, especially according to the insights into the dual role of the of the aniline as reported by Roche and co-workers, the *N*-functionalized naphthylamines could be less effective in their role as catalyst for the formation of the Knoevenagel adduct, as the formation of the needed iminium might be prohibited by the bulk of the benzyl substituent.[70] The bulk of this substituent could then prove to be problematic in the cyclization that leads to the formation of the didehydropyridine scaffold (mechanism on page 32). The inherent nucleophilicity of the amine was considered in terms of the orientation of the relative orientation of the phenyl rings. The effect of the propargyl- and 4-nitrobenzyl substituents were first ignored as it was postulated that the contribution of these substituents would be relatively minor.

Figure 53: α-Naphthylamine and β-naphthylamine.

It was expected that there might be a significant difference in the electron density on the nitrogen atoms that resulted in the difference in nucleophilicity. No appreciable difference in the electron density on the two nitrogens was observed during a computational study

performed by Dr Bernard Dippenaar, however, an interesting interaction was observed in the calculation of α-naphthylamine.
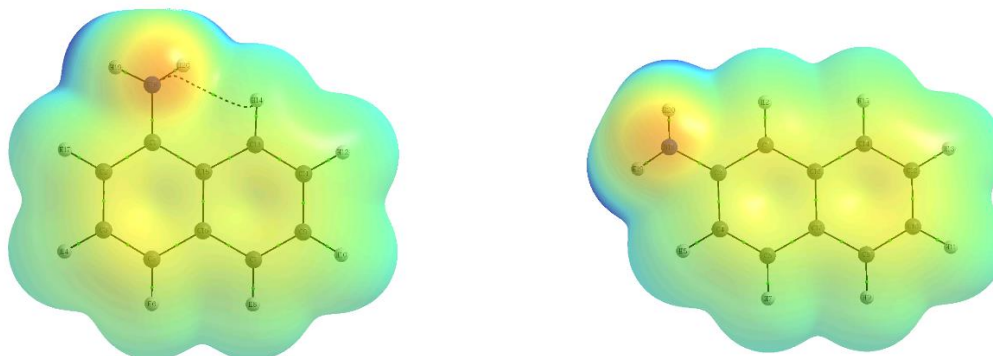
Figure 54: Electostatic potential on α-naphthylamine (left) and β-naphthylamine (right).

A Bond Critical Point (BCP) was observed between the nitrogen and hydrogen on the neighbouring aromatic ring in the case of the α-naphthylamine, whereas no such interaction was observed for the β-naphthylamine (Figure 54). The presence of this BCP in the α-naphthylamine analogue suggests the sharing of electrons between the nitrogen and the hydrogen. The ring contraction present in fused phenyl systems, such as those in the naphthylamine scaffolds, have been documented. This contraction would bring the nitrogen and hydrogen atoms into closer proximity when the electron rich atom is in the 1-position of the naphthyl ring, whereas it would have less effect on an electron rich atom on the 2-position. The ^{1}H NMR spectra of the *N*-functionalized naphthylamines were then investigated.
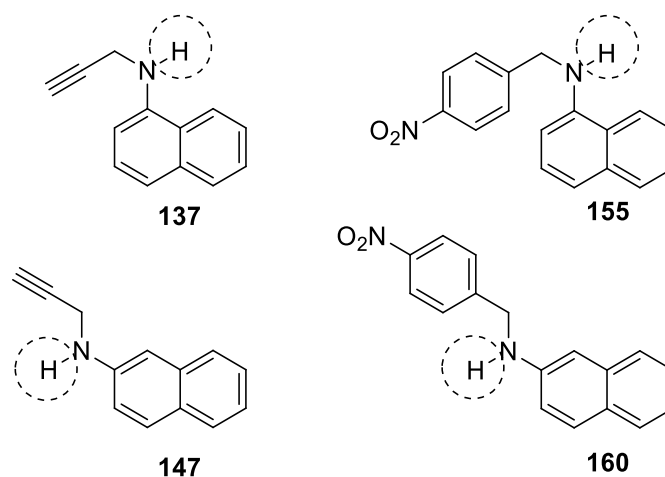
Figure 55: *N*-functionalized naphthylamines.

The N-H shifts of the four analogues were investigated. The ^{1}H NMR spectra of these four compounds were recorded in CDCl$_3$ (shown below in Spectrum 8).
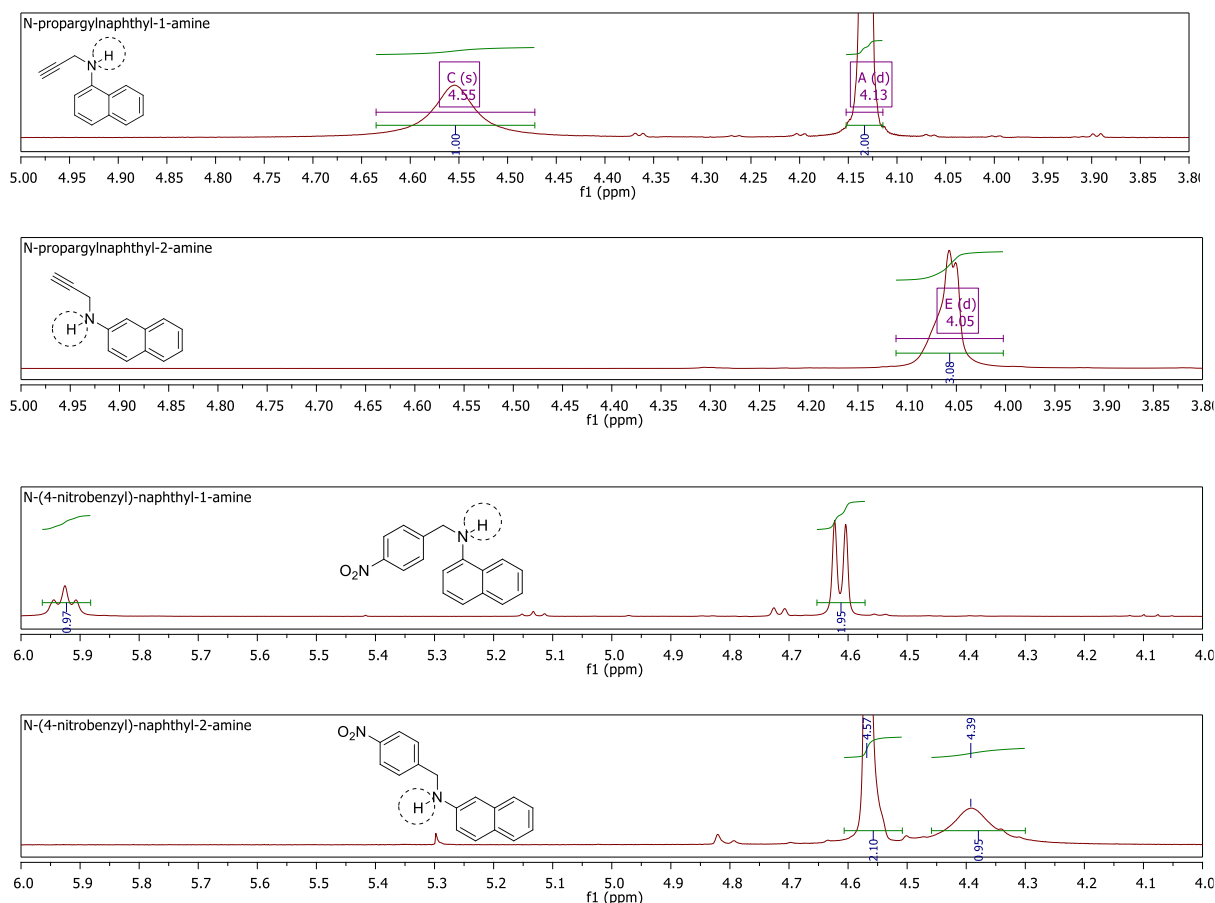
Spectrum 8: Broad singlets of the N-H protons of compounds **137**, **147**, **155** and **160**.

The N-H proton shift is significantly downfield in the case of the α-naphthylamine compared to the β-naphthylamine. The same trend can be observed for the *N*-(4-fluorobenzyl) and *N*-benzyl analogues (Spectrum 9). A shift of at least 0.5 ppm is consistently observed (a larger shift was observed in the case of the *N*-(4-nitrobenzyl) analogue).

The N-H proton on the α-naphthylamine analogues therefore is more deshielded than the corresponding proton on the β-naphthylamine analogues. When this is rationalized in terms of the BCP observed in the computational study, the interaction between the lone pair on the nitrogen atom and the proton on the neighbouring ring leaves the nitrogen more electropositive and thereby leading to a downfield shift for the N-H proton.
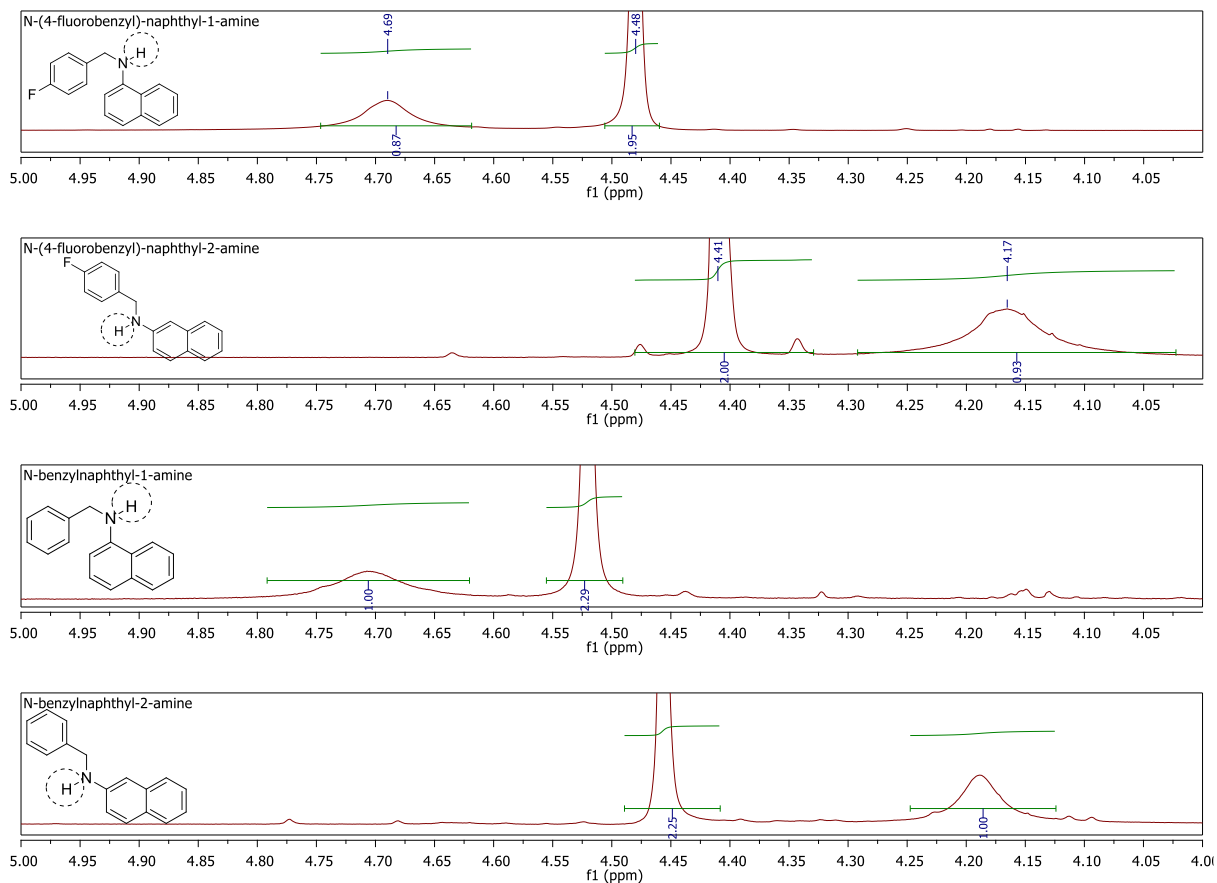
Spectrum 9: Spectra of the broad singlets of the different *N*-functionalized amines.

106

5.1.2 First set of *N*-functionalized 4-azapodophyllotoxins

The success of the MCR method with regards to the β-naphthylamine derivatives resulted in the synthesis of 14 novel *N*-functionalized 4 azapodophyllotoxins. The *N*-propargyl derivatives were synthesized by means of MWI and the *N*-benzyl derivatives were synthesized by employing 4-chloroaniline as a sacrificial aniline under conventional heating. The yields for the 14 novel compounds are summarized below (Figures 57 on the next page). These analogues were all analysed by means of ^{1}H NMR, ^{13}C NMR, IR spectroscopy and high resolution MS to confirm the successful synthesis of these compounds. As had been discussed earlier, certain signals in the NMR spectra were inspected for confirmation of the formation of the 4-azapodophyllotoxin scaffold. These were, again, the signal for the C1 proton of the C-ring (a singlet integrating for one proton at a chemical shift of δ 5.6 ppm), the signal for the methylene protons in the tetronic acid based D-ring (a doublet of doublets signal at a chemical shift of δ 5.0 ppm) and the methylene protons of the group in the 4*N*-azaposition (either the propargyl group or the various benzyl groups). In all cases the calculated m/z ratio of the proton adducts in the high resolution MS was also found. The full characterization data of these compounds are recorded in the chapter, *Supplementary Information* (10.2).

These 4 *N*-propargyl analogues were evaluated for their antiproliferative properties as well as serving as precursors to triazole-based derivatives of these compounds. The synthesis of the azides to be used in conjunction with these compounds will be discussed in the following chapter.

The analogues were all synthesized in fair to good yields, along with two 4-azapodophyllotoxin analogues with no substitution in the 4-aza position, **187** and **188** (Figure 56) as reference structures.
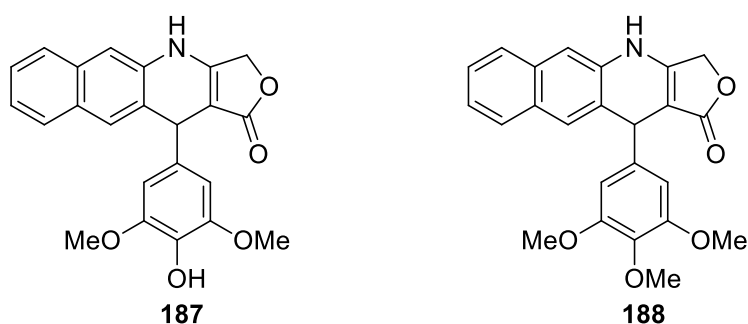
Figure 56: Unsubstituted 4-azapodophyllotoxin analogues.
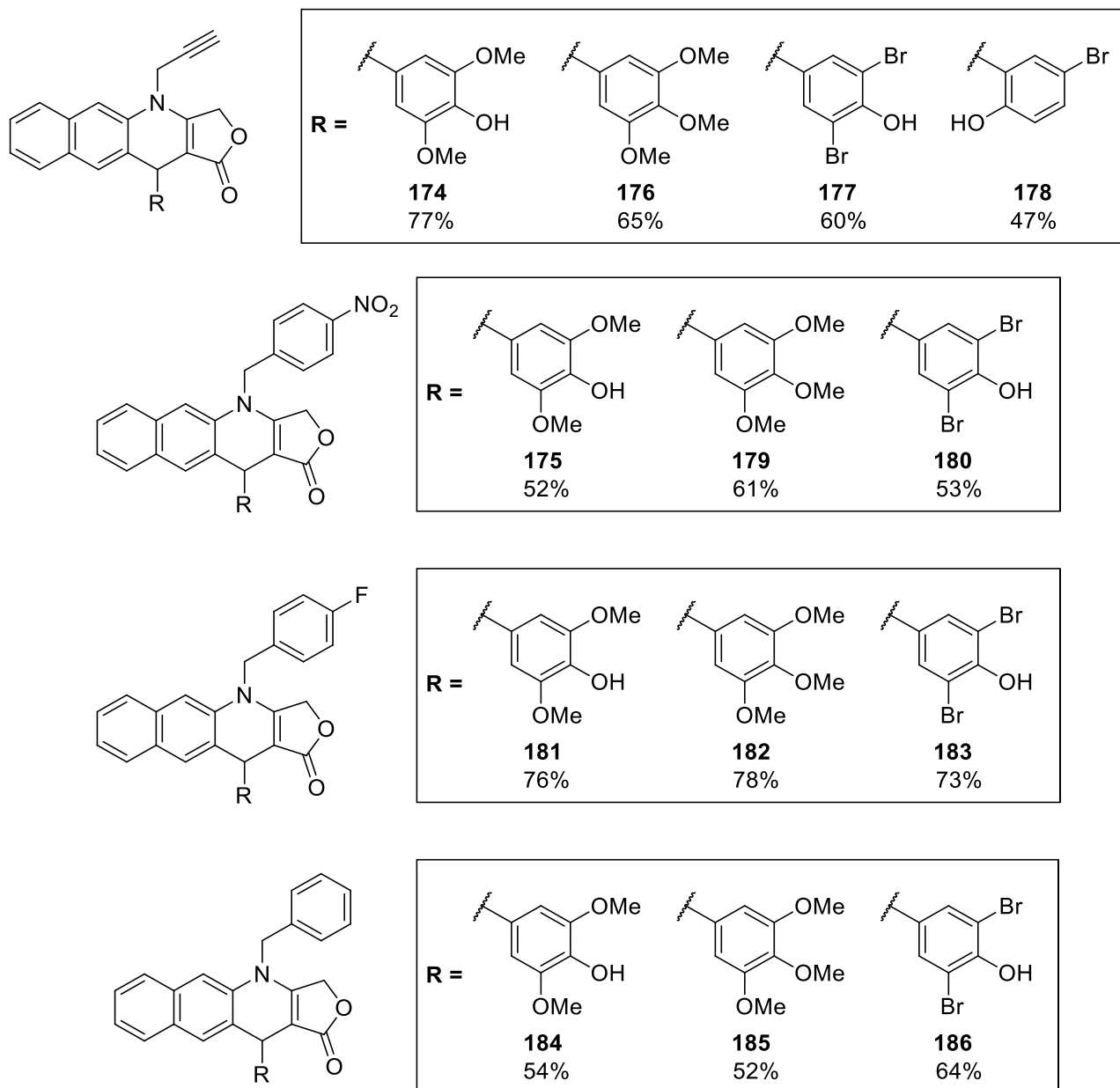
Figure 57: *N*-benzyl 4-azapodophyllotoxin analogues successfully synthesized and corresponding yields.

6.1 Synthesis of Azides for the functionalization of 4*N*-propargyl azapodophyllotoxins

6.1.1 Azide Syntheses

As discussed in the chapter, *Aims and Objective*, 4-azapodophyllotoxin analogues based on etoposide (**55a**) were of great interest in this study. Two representative examples of compounds synthesized in this study that contain a triazole-linked sugar group in the 4*N*-aza position (**189** and **190**) are shown in Figure 58.
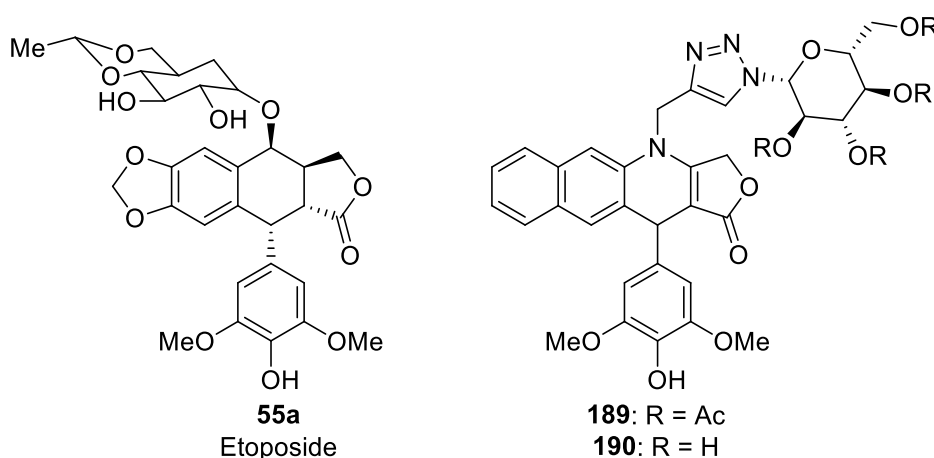
Figure 58: Etoposide (**55**a) and two proposed novel analogues (**189** and **190**).

The introduction of the propargyl group in the 4-position (as discussed in the previous chapters) opens up this area of the scaffold to the exploration with various azides. This section will discuss the synthesis of various azides that were synthesized throughout this study. These azides formed part of the final compounds of both our first- and second-generation libraries.

As our initial interest was focused on the glucosyl moiety, the first azides to be synthesized were the tetra-acylated and deacylated glucosyl azides.

The synthesis of the glucosyl azide followed an established procedure by Len and co-workers, by employing D-glucose (**191**, Scheme 44) in a successive acylation and bromination procedure to afford the desired tetraacetyl glucosyl bromide (**192**) as a white solid. The researcher noted that bromination of the anomeric position proceeds to give the axial product, as larger groups preferentially react from the less sterically crowded axial direction.[136] Compound **192** was engaged into the next step without purification to give the tetraacetyl glucosyl azide (**193**, Scheme 44) upon work-up. Compound **193** was purified by recrystallization from ethanol and isolated in yield of 88% over two steps
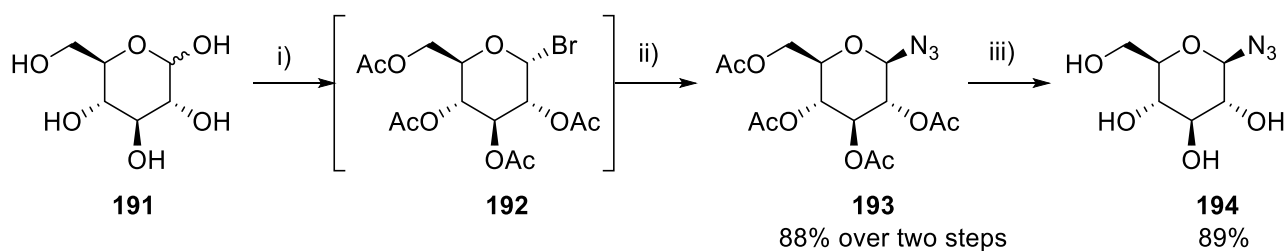
Scheme 44: Preparation of the glucosyl azides. i) Ac_2O, pyridine then HBr, AcOH (glacial); ii) NaN_3, DMSO, rt.; iii) Et_3N, 50% MeOH (aq.), rt.

Analysis by means of NMR spectroscopy and compared well with the literature reported values.[136] The acylated glucosyl azide was used in in the synthesis of analogues such as compound **189** (Figure 58).

As the body has many esterases that could cleave off the acyl groups, compound **189** could be viewed as a prodrug of its deacylated counterpart, compound **190** (shown in Figure 58). Compound **193** was deacylated to afford compound **194** according to a procedure reported by Ogihara and co-workers (Scheme 44),[137] in a yield of 89%. A research student in our group had also previously used the deacylated glucosyl azide (**194**, Figure 59) to synthesize compound **195** (which forms part of as of yet unpublished work done in our group), so as to mimic the analogous sugar group present in etoposide (**55a**)(Figure 58). Compound **194** was also to be used in click reactions.
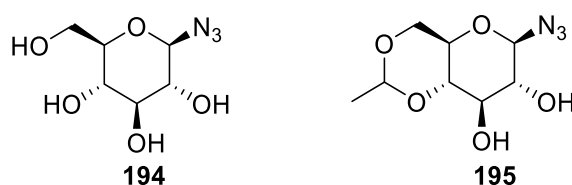
Figure 59: Glucosyl azide (**194**) used in this study and the etoposide-like analogue, compound **195**.

Along with these glucosyl azide, two azidobenzoic acids were also synthesized as part of our first generation library. The aim of introducing these carboxylic acid groups onto the 4-azapodophyllotoxin scaffold by means of a triazole linker is to offer a potential attachment point for polypeptide drug delivery systems. Our group has been in contact with the research group of Prof. Beck-Sickinger for possible collaboration. Their research group has investigated the use of polypeptide delivery systems for clinically approved drugs, such as methotrexate (**196**, Figure 60), that have been met with drug resistance.[138]

110

196
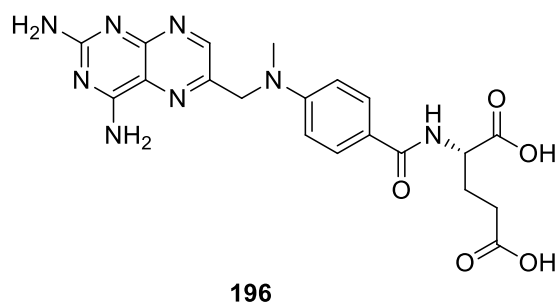
Figure 60: Methotrexate (**196**).

Beck-Sickinger and co-workers employed a modified analogue of neuropeptide Y as a targeting moiety and their research group found an increase in cytotoxicity against the MDA-MB-231 breast cancer cell line, as well as overcoming drug resistance of the cell line towards methotrexate (**196**). This cell line has shown resistance to compound **196** as a free molecule. However, when attached to the modified targeting peptide, the mechanism of resistance of this cell line was overcome through efflux of the drug into the cell *via* the carrier protein.

Azides with a carboxylic acid were then considered for incorporation onto the 4-azapodophyllotoxin scaffold, as the polypeptides employed by Beck-Sickinger and co-workers were coupled to methotrexate (**196**) at the carboxylic acid terminals. Therefore, should these novel compounds (to be discussed in the next chapter) prove to possess cytotoxic activity, the carboxylic acid moieties of these substituents could provide a point of attachment to such a carrier peptide and a possible collaboration.

The azides were synthesized using 3-amino- and 4-aminobenzoic acid as starting materials, by following a procedure that involved the diazotization of the amine and subsequent aromatic substitution with sodium azide, as reported by Kutonova.[139] The desired products were isolated in good yields of 83% and 77% for compounds **197** and **198**, respectively (Scheme 45).

197
83%

198
77%
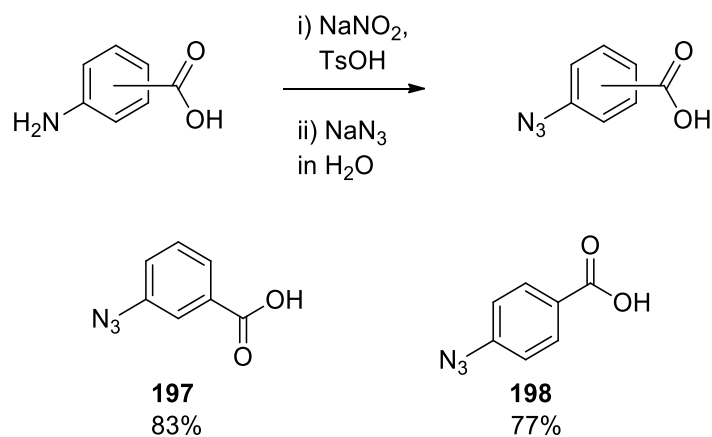
Scheme 45: Synthesis of 3- (**195**) and 4-azidobenzoic acid (**196**).

The NMR spectra of compounds **197** and **198** both showed the expected chemical shifts and compared well to literature reported values.[139] The IR spectra for these compounds correlated well with what was reported in literature, with the characteristic N_3 peaks of 2127 cm^{-1} for compound **197** and 2099 cm^{-1} for compound **198** clearly visible.[140]

So as to further show the versatility of introducing a propargyl group onto the 4-azapodophyllotoxin scaffold, a second generation library of compounds were also envisaged. For this library, the azides of various groups of interest were synthesized. These compounds can be viewed as biological targeting agents or as tools to explore which groups are tolerated in this position. Diverse groups were selected, such as alkyl groups with hydrophobic characteristics, nucleosides and biologically-relevant groups such as fatty acids.

To investigate the effect of hydrophobic moieties such as alkyl chains have on biological activity, simple nucleophilic substitutions were performed on 1-bromoheptane (**199**, Scheme 50) and 6-chlorohexan-1-ol (**200**, Scheme 46) in preparation of the corresponding azides for use in subsequent click reactions to investigate the effects of these groups on the biological activity of the corresponding 4*N*-triazolo-4-azapodophyllotoxin analogues.

$$Br\diagup\diagdown\diagup\diagdown\diagup R \xrightarrow[\text{overnight}]{\substack{NaN_3 \\ DMF,\ 75\ ^oC}} N_3\diagup\diagdown\diagup\diagdown\diagup R$$

199: R = CH₃
200: R = OH

201: R = CH₃, 32%
202: R = OH, 99%
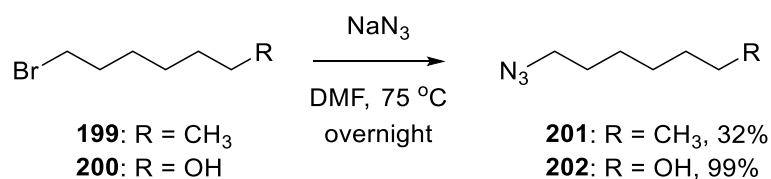
Scheme 46: Synthesis of alkyl azides.

1-Azidoheptane (**201**, Scheme 50) was synthesized in a poor yield of 32% yield and analysis by means of ¹H NMR and IR spectroscopy compared well to literature reported values.[141] Despite the poor yield, no efforts were made to improve the yield, as enough pure product was isolated to engage in click reactions. The synthesis of 6-azidohexan-1-ol (**202**, Scheme 46) proceeded well and the product was isolated in a yield of 99%, also confirmed by means of ¹H NMR and IR spectroscopy that compared well to the literature.[142] Other hydrophobic moieties that were considered were cholesteryl- and fatty acid groups. These groups are known to be used in the construction of cell walls and other structures.

The first step in the synthesis of these compounds was the synthesis of an azidoethyl linker. The proposed linker was synthesized from 2-bromoethanol (**203**, Scheme 47) in a two-step synthetic sequence to afford 1-azido-2-(methylsulfonyl)ethane (**204**, Scheme 47) in a 93% yield.
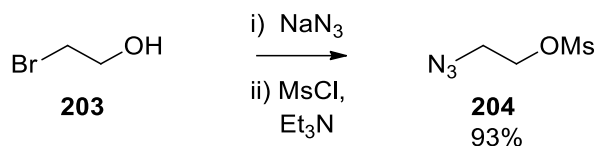
Scheme 47: Synthesis of the azidoethyl linker.

The desired product, compound **204**, was isolated in a much better yield over two steps than the method by Ilien and co-workers.[143] The method reported by this group involved the initial *bis*-mesylation of ethylene glycol and the subsequent mono-substitution with sodium azide to give compound **204** in a yield of 44%.[143] The ^{1}H NMR and IR spectra compared well to that reported by Ilien and co-workers.

This azidoethyl mesolate (**204**) was incorporated as the linker for different biological moieties. It was first incorporated as the linker to a fatty acid group. Firstly, 3-aminopropanol (**205**) was Boc-protected under mild conditions to afford the desired product, *N*-Boc-3-aminopropanol (**206**, Scheme 48), in a yield of 69%, as compared to the literature reported ^{1}H NMR spectra.[144]
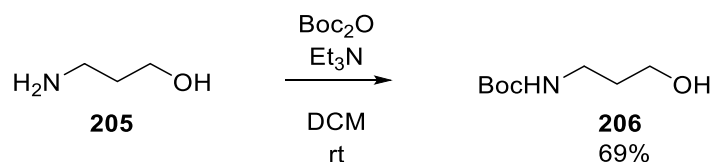
Scheme 48: Boc-protection of 3-aminopropanol.[144]

Next, the Boc-protected product **206** was reacted with palmitoyl chloride (**207**) to give compound **208** (Scheme 49), as a waxy white solid in 68% yield.
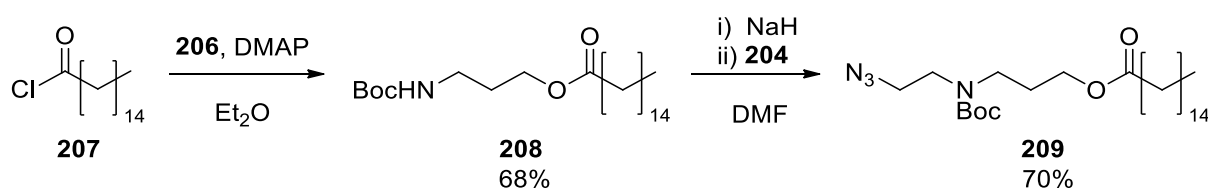
Scheme 49: Synthesis of the fatty acid with alkyl linker.

Compound **208** was then reacted with 1-azido-2-(methylsofonyl)ethane (**204**) to deliver the desired product (**209**, Scheme 49) in a yield of 70%.

113
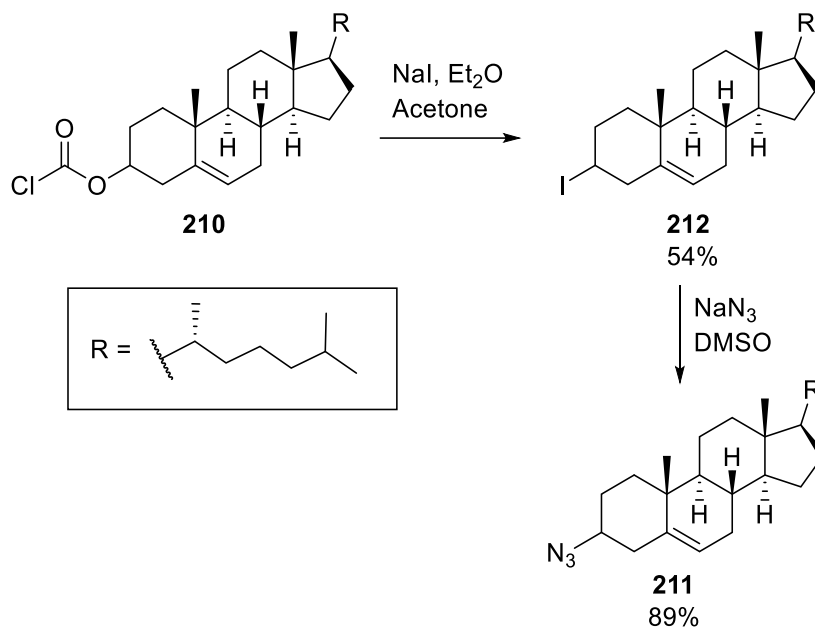
Scheme 50: Synthesis of cholesteryl azide (**211**)

The use of a cholesteryl moiety was also of interest, therefore commercially available cholesteryl chloroformate (**210**, Scheme 50) was conversion to cholesteryl azide (**211**) was attempted through a two-step sequence. Cholesteryl chloroformate (**210**) was converted to the corresponding iodide (**212**) using a method reported by Kevill and Weitl.[145] The melting point of the isolated product was determined and the range of 107 – 109 °C corresponded with the literature reported value.[145] The isolated solid (**212**) was reacted with sodium azide to obtain the corresponding azide (**211**, Scheme 50). Analysis by IR spectroscopy showed a characteristic azide peak at 2129 cm^{-1}(Spectrum 11), however, the presence of the peak at 1726 cm^{-1} suggests that the previous conversion to the iodide (compound **212**) was unsuccessful.
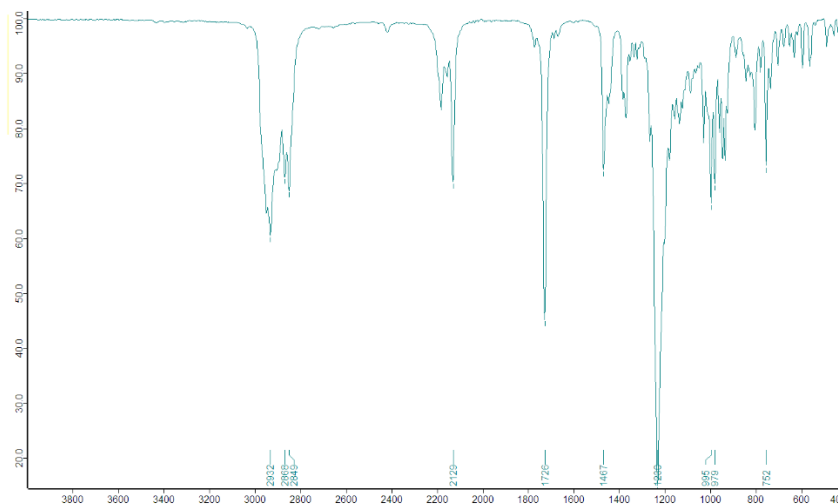
Spectrum 10: IR spectrum of compound **211**, suggesting that the synthesis of the iodide (compound **212**) was unsuccessful.

Along with these azides, zidovudine (azidothymidine, AZT) (**213**, Figure 61) was also purchased to be used in the synthesis of the representative triazole linked compounds, which will be discussed in the following chapter.

213
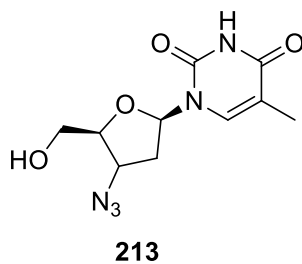
Figure 61: Zidovudine (Azidothymidine, AZT) (**213**).

Click Chemistry

6.2.1 Mechanistic discussion

This section will discuss the use of compounds **174** and **176-178** in copper-catalyzed 1,3-dipolar cycloaddition reactions with various azides to generate a set of 1,4-disubstituted triazole derivatives of the *N*-functionalized 4-azapodophyllotoxin analogues (Scheme 51). The azides that were employed are those discussed in the previous section, *Azides* (Chapter 6.1), and shown later in Figure 62. These reactions will be referred to as "click" reactions, as termed by Sharpless and co-workers, by the tendency of these reactions to be wide in scope and delivering products in good yields under mild conditions.[146–148]
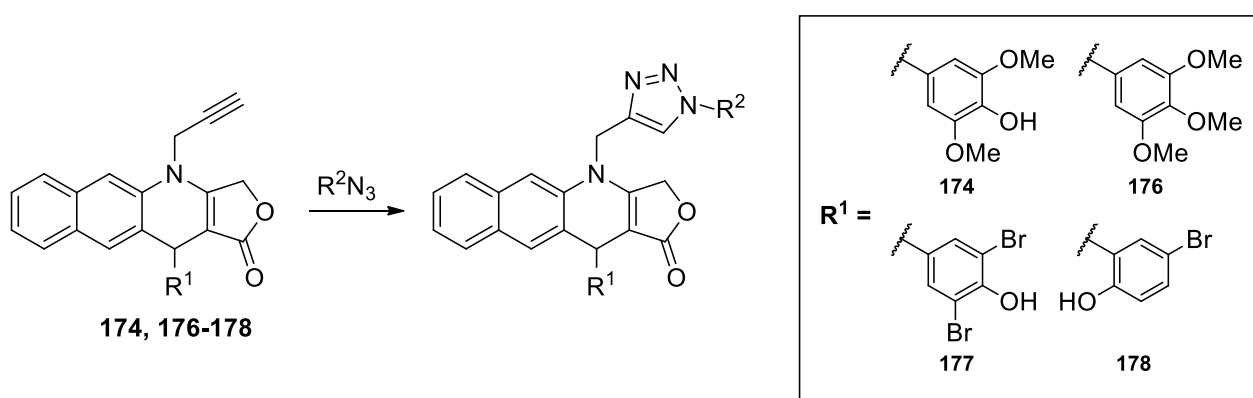
Scheme 51: Generalised scheme of the "click reaction" used to synthesise the 4*N*-triazole 4-azapodophyllotoxin analogues.

The click method employed a cuprous catalyst in *tert*-butanol and water at room temperature, as initially reported by Sharpless, Fokin and co-workers (a representative reaction is shown in Scheme 52). The cuprous catalyst was formed *in situ* by the reduction of the copper (II) salt by sodium ascorbate. The copper(I) catalyst served to improve the dipolarophilicity of the terminal alkyne (**214**) and therefore take advantage of the "spring-loaded" nature of the azide (**215**) as noted by the authors.[147] For the reaction shown, the product (**216**) was isolated in a yield of 91%.
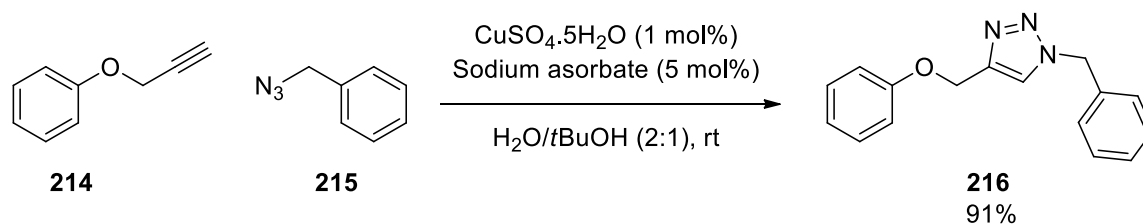
Scheme 52: A representative reaction reported by Sharpless, Fokin and co-workers.[147]

In this study, they also proposed a mononuclear mechanism for the formation of the desired 1,4-disubstituted triazole (Scheme 53). The proposed mechanism commences with the complexation of the cuprous salt with the terminal alkyne (**217**) and subsequent formation of the acetylide cuprous complex (**218**). This was followed by a step-wise, annealing sequence with the azide (**219**) centered on the copper centre, leading to the subsequent formation of intermediate (**221**) *via* complex **220**. The copper-containing cyclic intermediate **221** then rearranged to the more energetically favourable triazole **222**. The religation of the cuprous ligand produced the desired 1,4-triazole and the catalyst was reintroduced into the cycle.
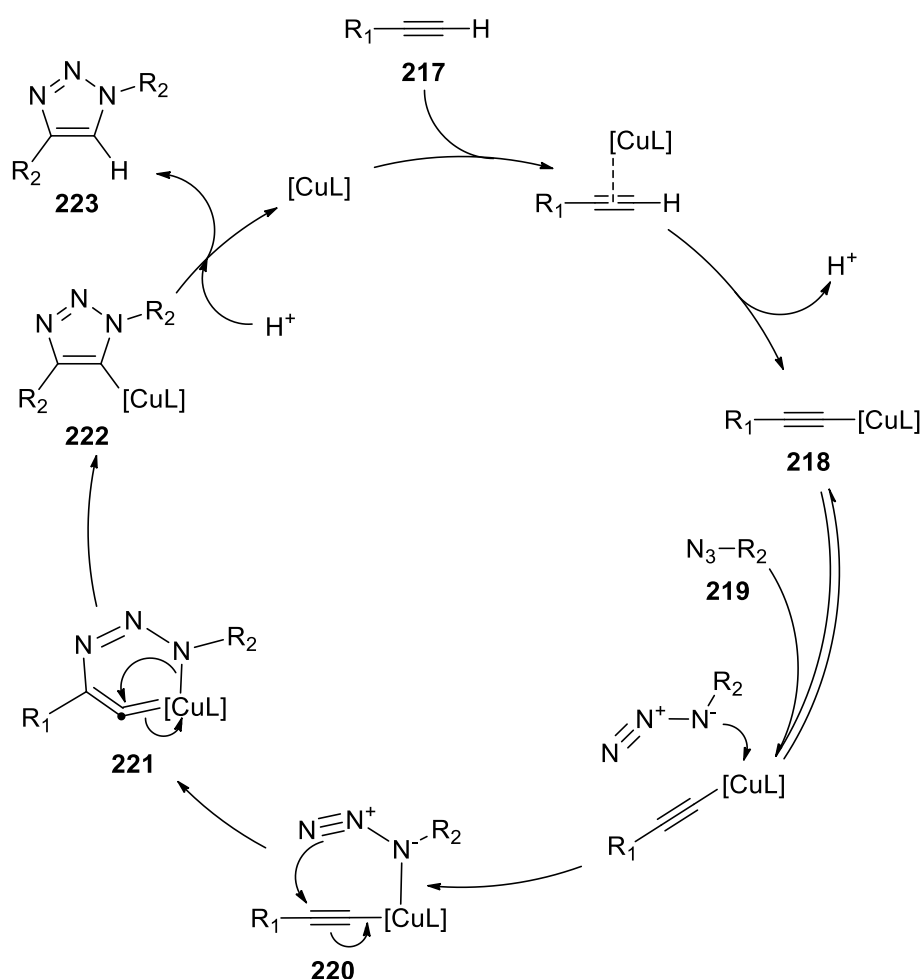
Scheme 53: Mononuclear mechanism for the 1,4-addition "click" reaction.[147]

The researchers performed density functional theory (DFT) calculations to determine the energetic favourability of the subsequent steps in the mechanism, which showed that a concerted [2+3] cycloaddition between complex **218** and azide **219** to form complex **222** is too unfavourable to be feasible.

Further probes into the mechanism by Fokin and co-workers,[149] however, has suggested that the mononuclear mechanism initially proposed in his work with Sharpless is not completely

accurate.[147] Fokin and co-workers conducted heat-flow reaction calorimetry to investigate the activity of the copper acetylide complex toward the employed azide. They found that the mononuclear species (**218**) was not sufficiently reactive towards the azide for the ligation steps to occur. Through the use of isotopically enriched copper salts, they were able to establish that the mechanism was reliant on the formation of a dinuclear copper species (**224**, Scheme 54) for the acetylide to be sufficiently reactive towards the azide.[149] They therefore proposed an updated mechanism with functionally equivalent dinuclear species, as shown in Scheme 54.
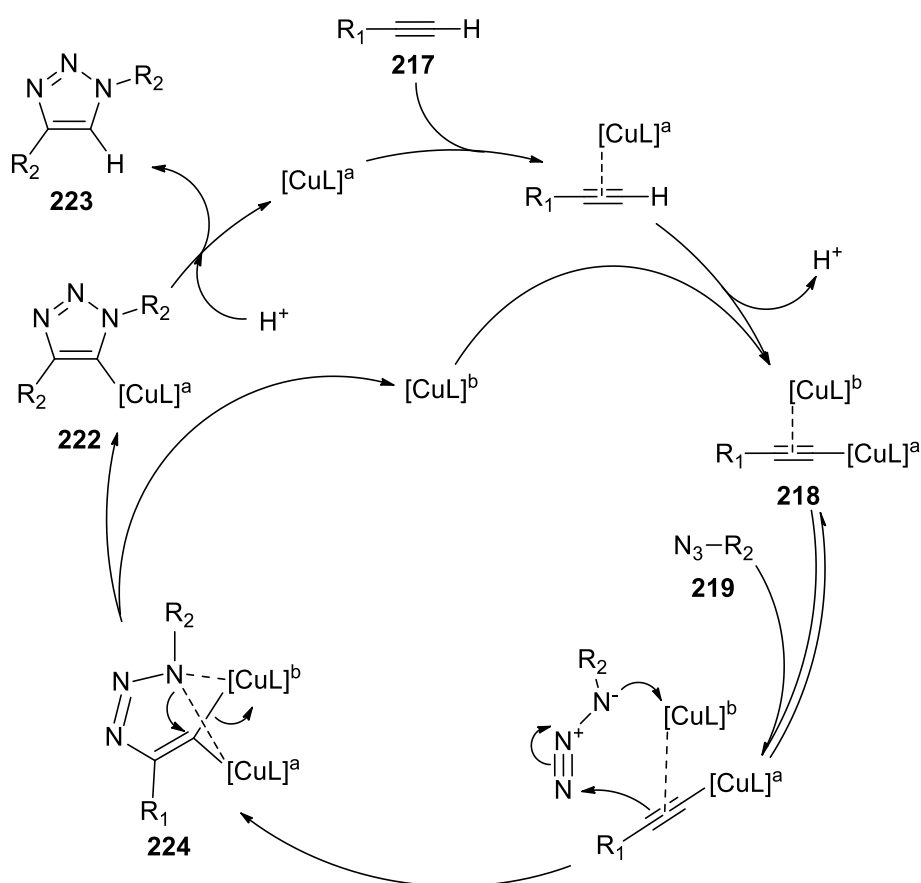
Scheme 54: Updated mechanism proposed by Fokin and co-workers.[149]

6.3 Synthesis of 4*N*-methylene-triazolo derivatives of 4*N*-propargyl 4-azapodophyllotoxin analogues

The azides (Figure 62) previously synthesized were then employed in "click" reactions to generate a set of 4*N*-triazole 4-azapodophyllotoxin analogues. These analogues served to explore the activity of this novel class of analogues.
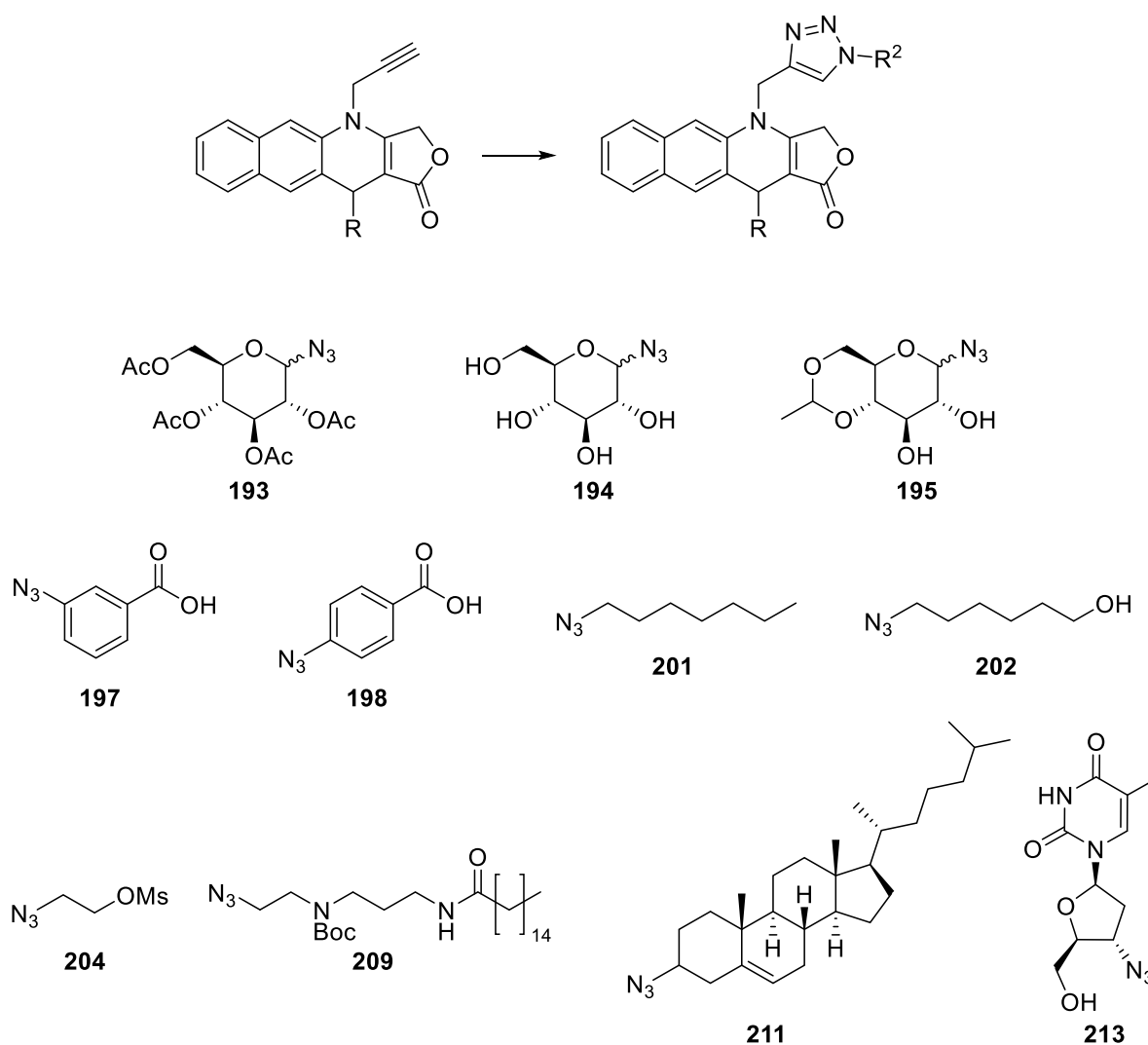
Figure 62: Azides employed in the "Click" reactions

The method reported by Sharpless, Fokin and co-workers (as shown in Scheme 52) was used for the synthesis of the novel 4-azapodophyllotoxin analogues. Earlier work done in our group showed that this method worked well in the reaction of 4-azapodophyllotoxin **225** with compound **193** to generate analogue **226** (Scheme 55) in a yield of 95%.
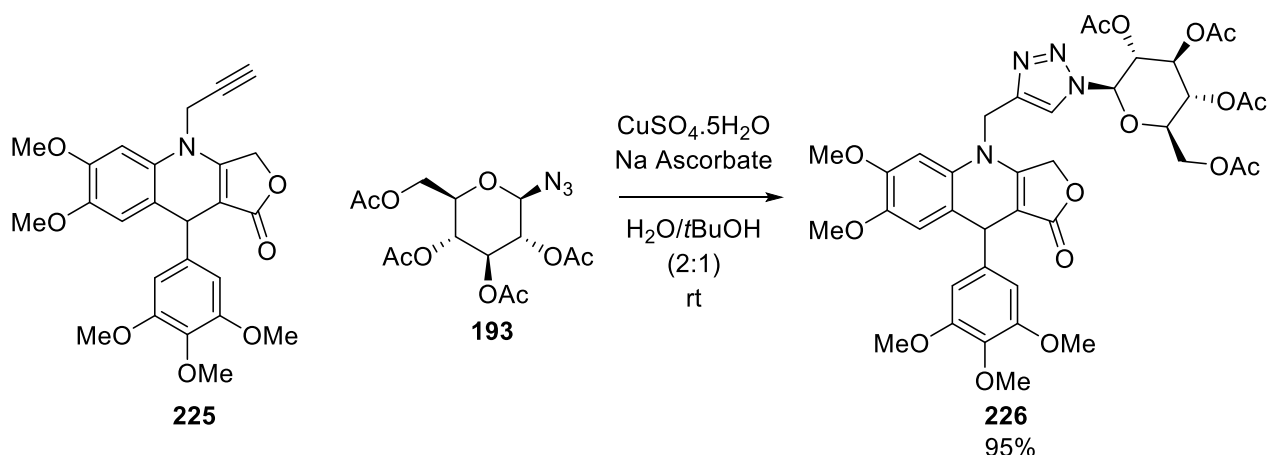
Scheme 55: 4-Azapodophyllotoxin analogue (**226**) previously synthesized in our group by Mr Sebastien Depaifve as part of unpublished work.

Compound **226** was characterized by means of ^{1}H and ^{13}C NMR spectroscopy. The characteristic C-H peak of the newly incorporated triazole linker can be seen at δ 7.99 ppm, as well as the acetate peaks of the glucoside group between δ 1.86 ppm and 1.74 ppm (Spectrum 11).
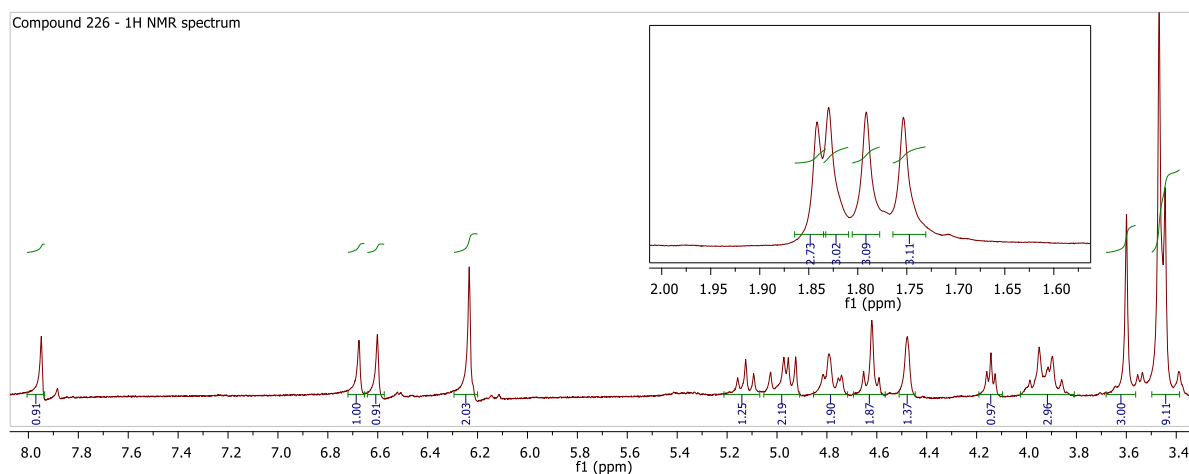
Spectrum 11: ^{1}H NMR spectrum of compound **226**.

The same conditions were repeated using the novel analogues synthesized during this study. However, when the synthesis was performed to obtain compounds **174** and **176**, lower yields were observed. The solubility of the substrates seemed to be a problem, as it has been noted that the 4-azapodophyllotoxin analogues are soluble in only a limited range of solvents. For this reason, the reactions were repeated in DMSO rather than the water/*tert*-butanol mixture (Scheme 56).

120
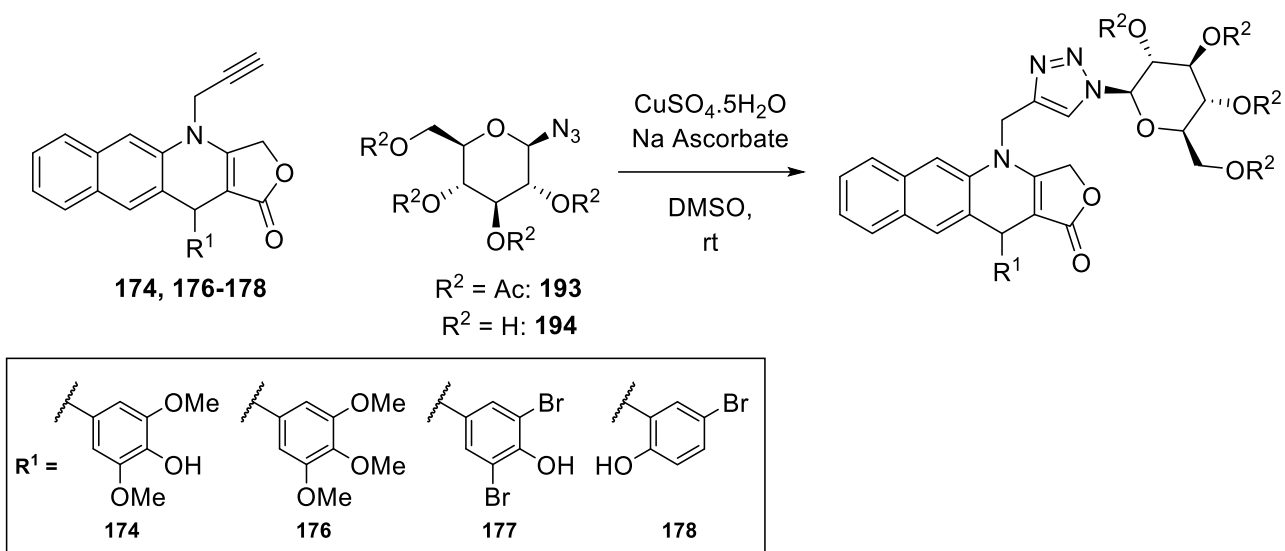
Scheme 56: Glucosyl click derivatives of compounds **174**, **176**-**178**.

The ^{1}H and ^{13}C NMR spectra of compound **227** confirmed the successful introduction of the glucosyl group onto the scaffold, as the signals for the acetate groups were observed at 2.03 ppm as four overlapping singlets in the proton spectrum and at 20.8 ppm in the carbon spectrum, as observed for compound **226**. A new proton signal was also observed in the aromatic region in the as part of a multiplet at 7.8 ppm that was attributed to the triazole. This region contains several multiplets that belong to the naphthyl-ring system that collectively integrate for 6 protons. The newly observed signal leads to 7 protons in this region. The triazole C-H carbon peak can however be observed 123.2 ppm in the ^{13}C NMR spectrum.

Significant overlap of signals also occur in region between 4.5 and 5.5 ppm than can be attributed to the newly introduced glycoside group overlapping with the signals from the tetronic acid-ring methylene signal, however, the expected signals for the glycoside ring can be observed in the ^{13}C NMR spectrum. The signal for the anomeric carbon was observed at 98.8 ppm and the signals for the C3, C4, C5 and C6 carbons of the ring at 68.2, 70.6, 72.2 and 76.4 ppm respectively.

The successful synthesis of compound **227** was further confirmed by means of high resolution mass spectrometry. The successful synthesis of compounds **228**, **231** and **232** were confirmed in the same manner, except with the absence of the signals of the acyl groups in compounds **231** and **232**. The HRMS data also confirmed this.

The corresponding yields for the different compounds formed are shown below in Figure 63.
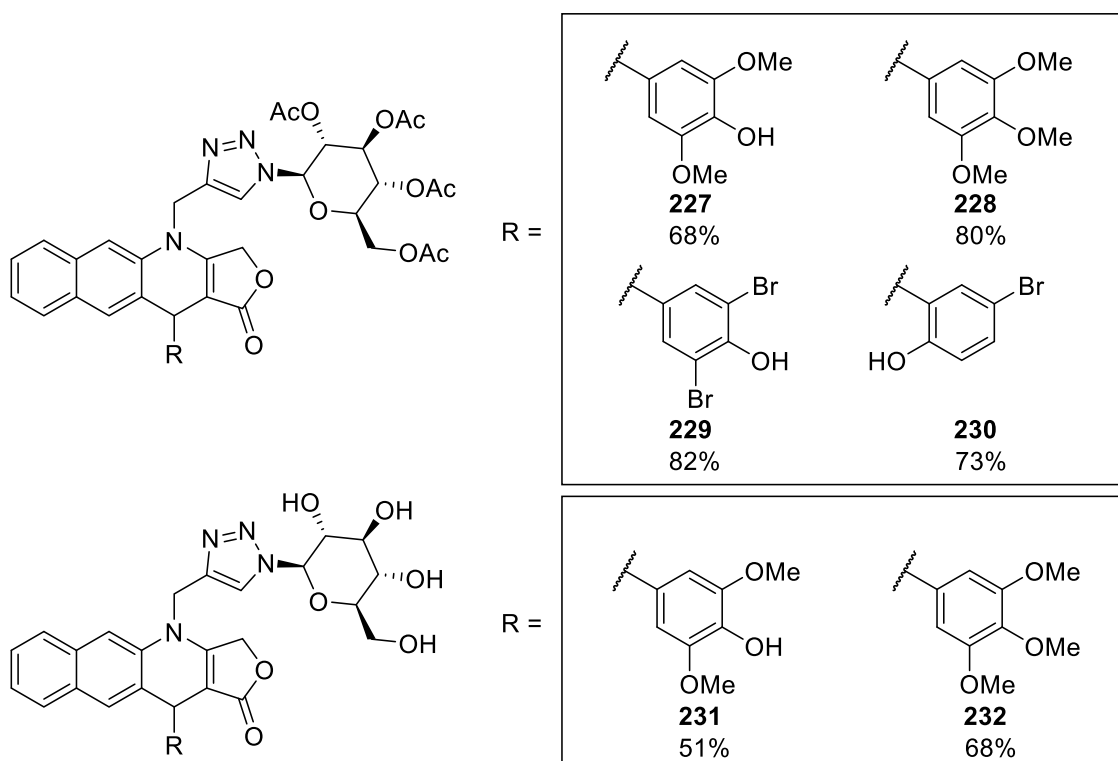
Figure 63: Glucosyl triazole derivatives of compounds **174**, **176-178** and corresponding yields.

The glucosyl derivatives formed part of the initial library for testing, as the glucosyl moiety closely mimics the sugar group on etoposide (**55a**).

The second smaller library served to explore the tolerance of the active site towards a variety of different substituents. These compounds were also synthesized using the method reported by Sharpless, Fokin and co-workers with DMSO as solvent. The products were isolated in moderate to good yields. The yields of these compounds are reported in Figure 64.
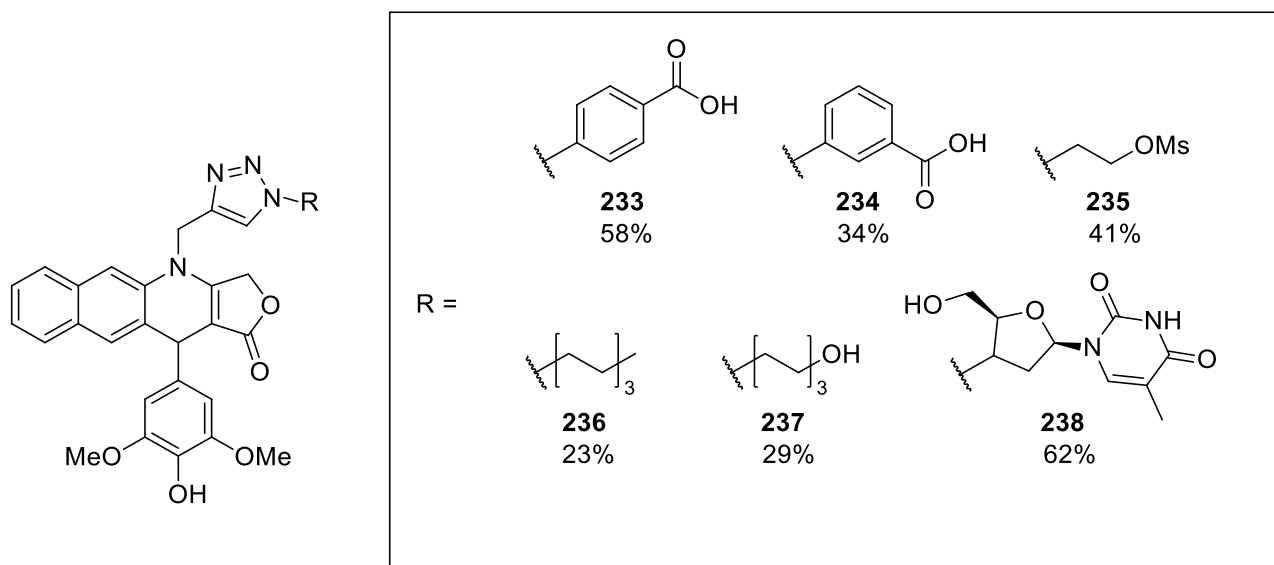
Figure 64: Extended library of triazole derivatives and corresponding yields.

7.1 Biological Targets

7.1.1 Introduction to the relevant biological targets

The literature review in the section, *Natural Products in Chemistry*, focused primarily on the promise of the MCRs to deliver compounds with promising antiproliferative activity. The *in vitro* inhibition activity of these compounds were discussed in terms of proving how valuable a tool MCRs are in the development of novel chemotherapeutic agents. The mechanism of inhibition of the podophyllotoxin (**50**) and the structurally simplified 4-azapodophyllotoxins have been noted to act primarily as tubulin poisons and the hemisynthetic derivatives, such as etoposide (**55a**), inhibit cell growth by acting as topoisomerase II poisons. This was not discussed in depth, as the focus was primarily on the design and synthesis of novel agents that could give SAR insights. The biological targets will now be discussed, as it gives better insight into the biological evaluation and *in silico* molecular modelling results obtained during this project.

7.1.2 Background to the two different biological targets

The section, *Natural Products in Chemistry*, noted that many of the analogues showed good to excellent activity towards various cancer cell lines, especially in comparison to the naturally occurring cyclolignan, podophyllotoxin (**50**). As has been shown by Magedov and co-workers by the use of flow cytometric cell cycle analysis, analogues such as compound **242** (Figure 65) act through the inhibition of microtubule polymerization.[29] These unsubstituted 4-azapodophyllotoxin analogues therefore inhibit cancer cell proliferation through the same mechanism as podophyllotoxin (**50**). However, as mentioned previously in the section *Natural Products in Chemistry* (Section 2.1), podophyllotoxin (**50**) did not fare well in clinical trials due to severe gastrointestinal side-effects. Considering the inhibitory activity of the methanolic extract of the *Podophyllum* genus, the researchers at the Sandoz Company theorized that the antiproliferative activity of this extract might stem from glucosyl derivatives present in the extract that were never identified due to the lability of such groups during the separation processes.[49] Confirmation of the validity of this hypothesis came through the report of podophyllotoxin glycosides isolated from plants of *Podophyllum emodi*.[150–152] The efficacy of the novel glycoside derivative led to the synthesis of over 600 semisynthetic derivatives that included glucosyl moieties in various positions, the screening process of these derivatives eventually leading to the discovery of two semisynthetic compounds, VM-16 and VM-26 – which would later be named etoposide (**55a**) and teniposide (**55b**), respectively.[49]
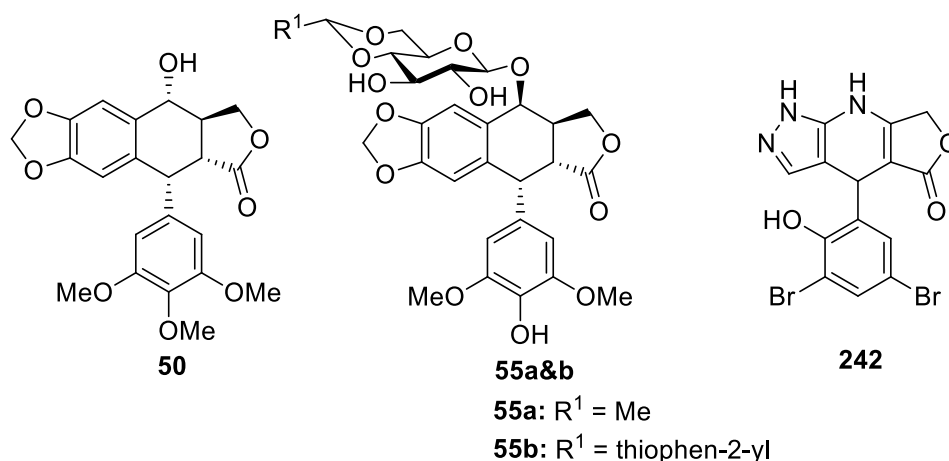
Figure 65: Podophyllotoxin (**50**), its semisynthetic derivatives (**55a** and **55b**) and an analogue reported by Magedov and co-workers (**242**).[29]

These novel compounds with improved water solubility showed decreased off-target toxicity compared to the parent cyclolignan (**50**), but were also reportedly less active.[49,150–152] During the analysis of the antineoplastic activity of these compounds, the researchers noted discrepancies between the *in vitro* inhibitory activity of these compounds and the *in vivo* inhibition of tumour growth. Studies on the effect of these compounds on chick embryonic fibroblasts showed that the mechanism by which they inhibit cell proliferation was distinctly different from that of podophyllotoxin (**50**). As mentioned, podophyllotoxin had been well documented to be a tubulin destabilizing agent.[49]

7.1.3 Tubulin Destabilizing Agents

Tubulin destabilizing agents (also referred to as tubulin poisons) are a class of compounds that inhibit cell proliferation through the destabilization of the microtubules during mitosis. Other compounds in this class are compounds such as colchicine (**243**, Figure 66) and combrestatin (**244**, Figure 66). These compounds tend to bind in the same pocket, referred to as the colchicine-binding domain. It is of interest to note that these compounds are all hydrophobic in nature and have a trimethoxy-substituted phenyl ring in common.

125
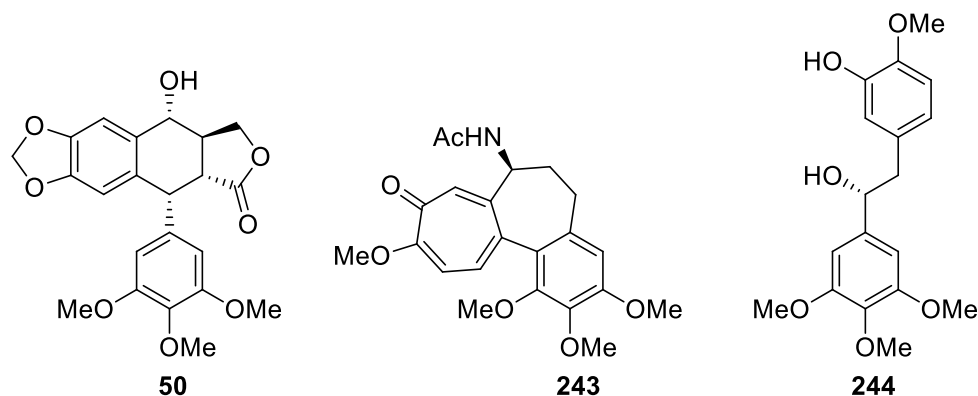
Figure 66: Representative examples of tubulin poisons.

In Figure 67, a simplified comparison between normal microtubule assembly and the disrupted assembly caused by antimitotic agents (such as **50**, **243** and **244**) can be seen. The top diagram shows the ordered assembly of the α- and β-tubulin subunits into linear tubulin polymers which are finally ordered into microtubules during mitosis. The bottom diagram shows how these microtubule (MT) destabilizing agents distort the growth of these tubulin polymers through insertion between the alternating $\alpha\beta$-dimers and divert the direction of growth. This leads to a failure for these polymer strands to assemble into a microtubule and, ultimately, leads to mitotic failure.

For the purpose of these studies, the protein databank (PDB) crystal structures of the anticancer agents in the corresponding active sites of the biological targets were investigated. These results will be discussed in depth later, and for the sake of this discussion, the disrupted growth of the microtubules can be shown, as it was evident in the refined protein databank crystal structures. The disrupted direction of growth as shown in the diagrammatic representation in Figure 67, can be seen in the refined protein structures in Figure 67. Normal tubulin growth is linear, however when these destabilizing agents are introduced, the growth diverts. The PDB structures that were used in our *in silico* docking studies for the investigation of the tubulin-destabilizing agents were PDB ID: 1SA1 (podophyllotoxin/tubulin complex) and PDB ID: 1SA0 (colchicine/tubulin complex).

a) **Normal Microtubule Formation**
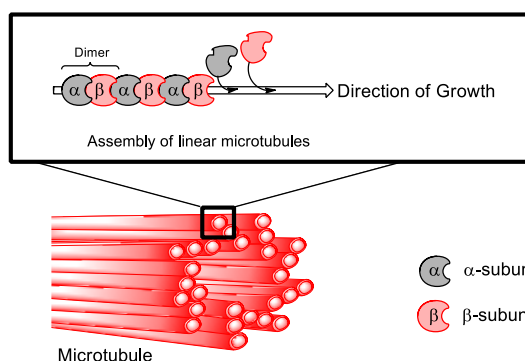
b) **Microtubule Formation disrupted by tubulin targeting compounds**
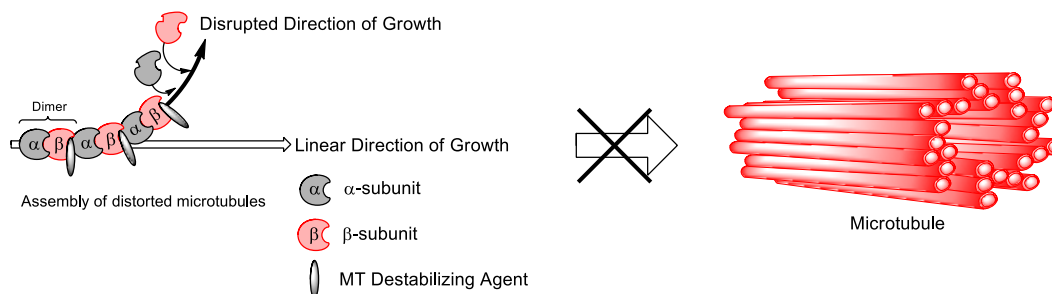
Figure 67: Diagramatic representations of a) Normal microtubule formation during mitosis; and b) the disruption of microtubule assembly by tubulin poisons. a) and b) reproduced from Ravelli and co-workers.[153]

Refined images generated in the Schrödinger Maestro suite are shown in Figure 68, with podophyllotoxin (**50**) in the active site (Top image, Figure 68) and colchicine (**243**) in the active site (Bottom image, Figure 68). The disrupted growth can be seen in the non-linear nature of the refined complexes.

The mechanism of inhibition of podophyllotoxin (**50**) has been clearly documented and from initial studies into the novel semisynthetic derivatives (etoposide (**55a**) and teniposide (**55b**)), it was evident that these compounds inhibited cell growth by a different mechanism. The semisynthetic derivatives exhibited potent cytostatic effects and induced apoptosis before the start of the mitotic cycle, unlike podophyllotoxin (**50**) which had a clear destabilizing effect on the formation of microtubules.[49]
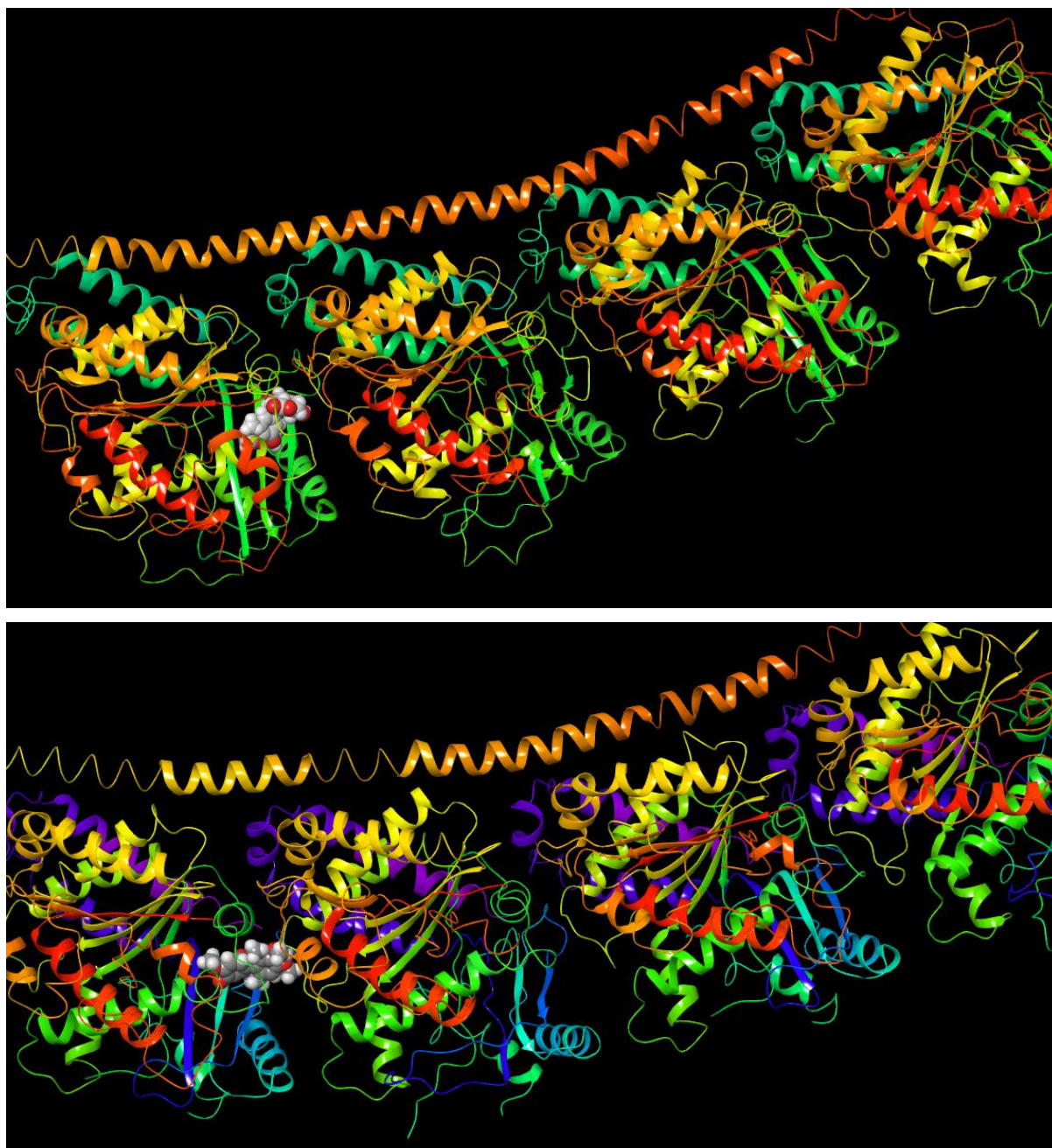
Figure 68: Top image shows podophyllotoxin (**50**) in the colchicine domain (PDB ID: 1SA1). The bottom image shows colchicine (**243**) in the colchicine domain of the tubulin polymer (PDB ID: 1SA0). Images generated using Schrödinger Maestro[154] from the crystal structures reported by Ravelli and co-workers.[153]

The investigation into the library of over 600 novel derivatives revealed that certain characteristics played a pivotal role in whether the mechanism of inhibition was similar to that of the natural cyclolignans or by means of a novel and distinct mechanism.

Two principal characteristics identified were the stereochemistry of the substituent in the 4-position of the C-ring and the absence of a methyl group in the 4'-position of the E-ring.

Compounds such as etoposide (**55a**) and teniposide (**55b**) had an inverted stereochemistry at the 4-position and were also demethylated in the 4'-position of the E-ring.[49] These compounds were later classified as topoisomerase II poisons.

7.1.4 Topoisomerase II Poisons

Topoisomerase II poisons exhibit cytostatic effects by inhibiting the cell from entering the mitotic cycle. Many late-stage chemotherapeutic agents act *via* this mechanism of inhibition. Along with compounds such as etoposide (**55a**) and teniposide (**55b**), compounds such as doxorubicin (**245**, Figure 69) and amsacrine (**246**, Figure 69) are included in this class.

55a&b
55a: R^1 = Me
55b: R^1 = thiophen-2-yl

245

246
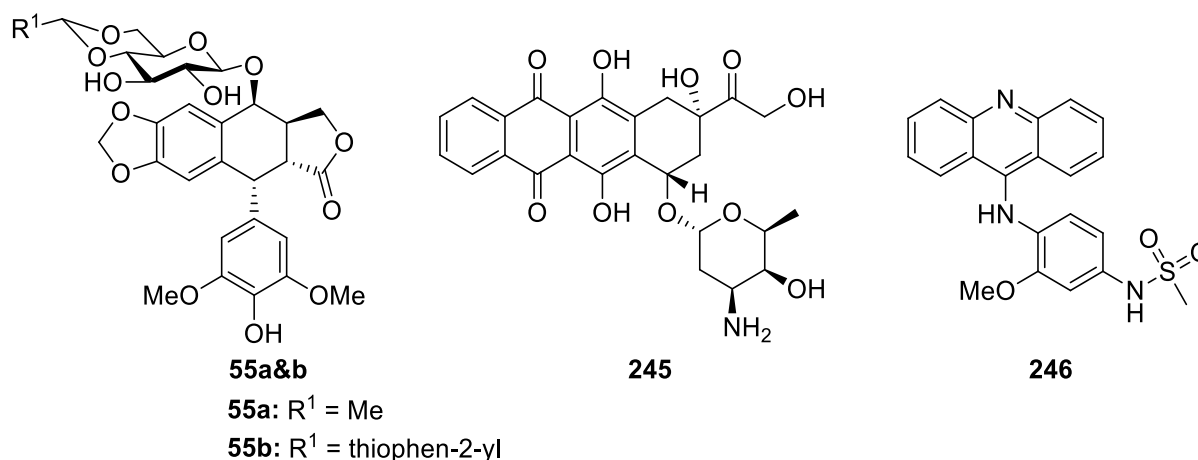
Figure 69: Representative examples of topoisomerase II poisons.

The topoisomerases play an important role in healthy cell function, as these enzymes serve to remove DNA supercoiling and resolve DNA strand entanglements through single-stranded (topoisomerase I) and double-stranded (topoisomerase II) DNA cleavage and recombination. Thus, their primary function is to maintain the topology of the DNA structure and allow for RNA transcription to commence unimpeded. As the 4-*epi*-4'demethylpodophyllotoxin glycoside derivatives primarily act as topoisomerase II poisons, topoisomerase I will not be discussed here and focus will be on the discussion of topoisomerase II. Topoisomerase II exists in the cell nucleus in two distinct isoforms – the α- and β-isoforms, with the β-isoform about 10 kDa larger than the α-counterpart.[155]

 A diagrammatic representation of the double stranded DNA breakage to remove supercoiling in DNA strands is shown in Figure 70. Supercoiling results from the unwinding of the DNA double helix during transcription and this unwinding leads to increased tension further down the DNA strand, as DNA strands are typically anchored to chromosomal structures of the nucleic membrane. This increase in tension results in the formation of positive or negative coiling, which can limit transcription from those segments of DNA and compromise normal

meiotic or mitotic function. Topoisomerase II relieves this tension by effecting a double-stranded breakage and subsequent unwinding of the coil. The DNA strand is then recombined during the religation of the enzyme-DNA complex.[155]
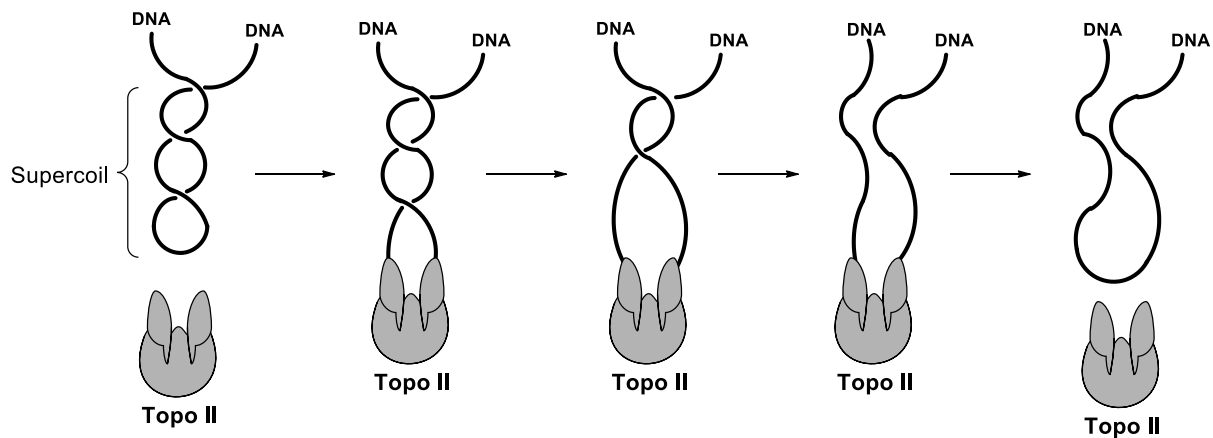
Figure 70: Diagrammatic representation of supercoiling resolution by topoisomerase II, copied from work reported by MacDonald and co-workers.[112]

The same double-stranded DNA breakage is employed to disentangle DNA strands, as shown in Figure 71 below.
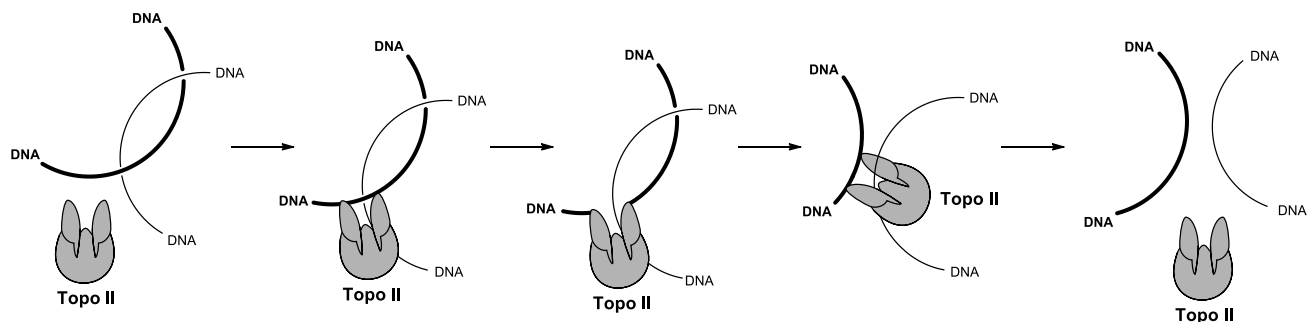
Figure 71: DNA disentanglement through double-stranded DNA breakage, copied from work reported by MacDonald and co-workers.[112]

This DNA cleavage-religation equilibrium is finely maintained during the normal cell cycle, as the DNA-topoisomerase II cleavage complex only accounts for only 0.5-1% of the absolute concentration of topoisomerase II in the intra-nucleus matrix. An increase in nuclear concentration of the DNA-topoisomerase II complex therefore leads signals a breakdown in function and leads to apoptosis, whereas a decrease leads to mitotic failure and also, ultimately, cell death (Figure 72).[155]
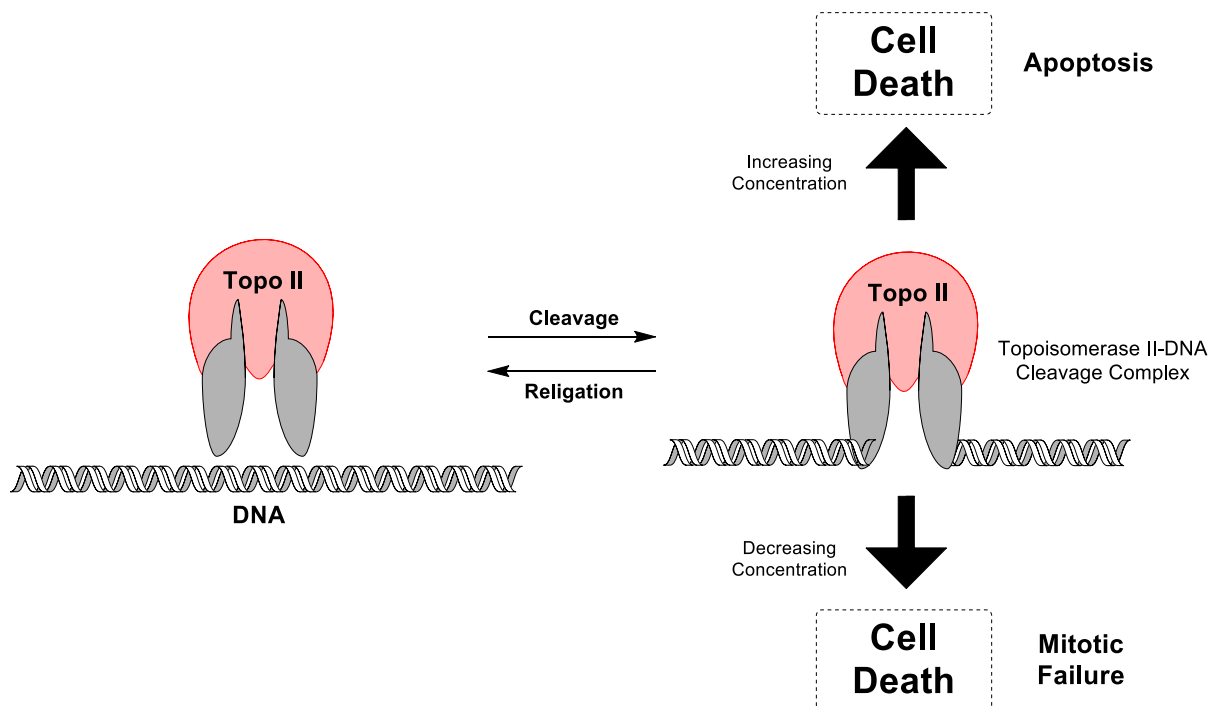
Figure 72: Simplified diagram of the DNA-topoisomerase II cleavage complex, reproduced from work reported by Deweese and Osherhoff.[155]

Topoisomerase II poisons exploit this mechanism by stabilizing the DNA-topoisomerase II cleavage complex and thereby inhibiting the religation of the enzyme. This leads to an increase in concentration of the complex in the nuclear matrix and thereby induces apoptosis (Figure 73).
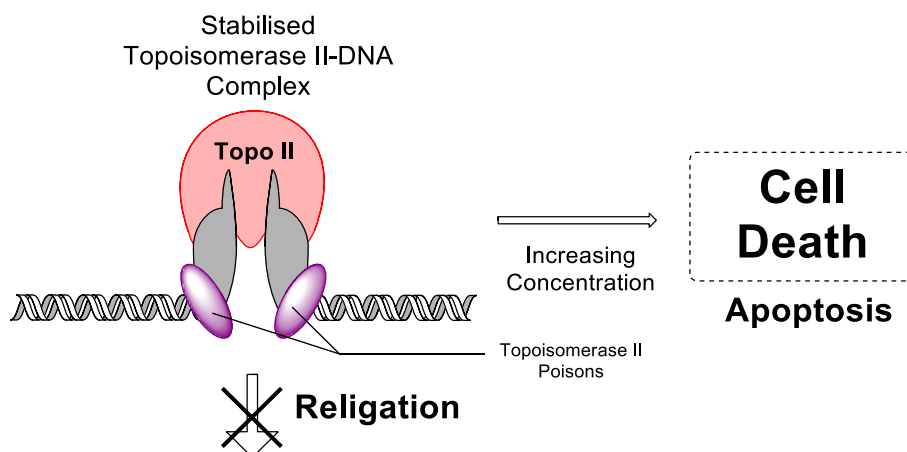
Figure 73: Effect of the stabilized DNA-topoisomerase II complex on cellular concentration reproduced from work reported by Deweese and Osherhoff.[155]

The effect of demethylation in the 4′-position of the E-ring on the novel glycosidic podophyllotoxin derivatives had been reported to be more pronounced on the activity of these compounds, in comparison to that of the substituents in the 4-position of the C-ring. This

131

happens through the same enzyme-drug interaction as initially identified by MacDonald *et al.*[112] and has subsequently been confirmed by other studies on derivatives such as GL-331[156] (**134**, Figure 74) and TOP-53[117](**139**, Figure 74). This observation was also made by Yuan and co-workers in their study on 4β-heterocyclic derivatives of epipodophyllotoxin and 4'-demethylepipodophyllotoxin.[129] Two derivatives of interest in this study were the derivatives of epipodophyllotoxin (**247a**, Figure 74) and 4'-demethylepipodophyllotoxin (**247b**, Figure 74).
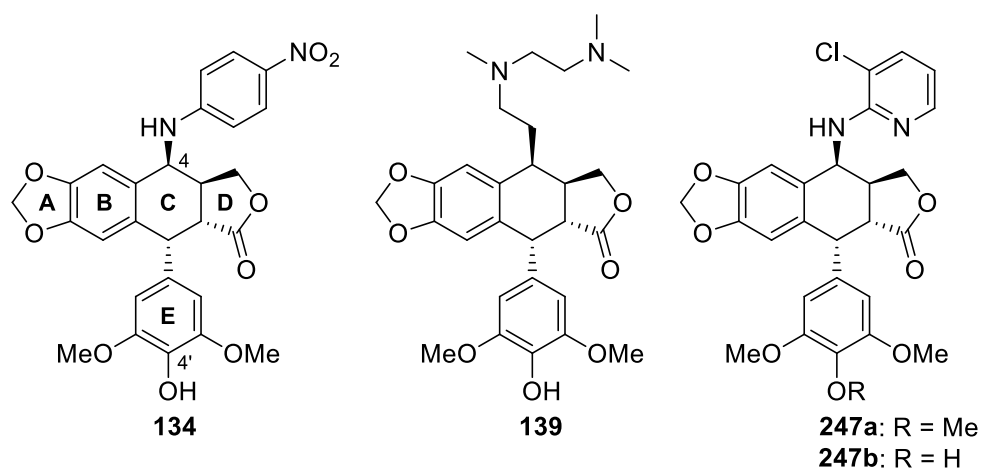
Figure 74: 4β-Functionalized podophyllotoxin derivatives, GL-331 (**134**) and TOP-53 (**139**), as well as novel derivatives reported by Yuan and co-workers.[129]

Both derivatives exhibited antiproliferative activities greater than that of the natural compounds and etoposide when compared to various cell lines. The researchers did however show that the substitution pattern on the E-ring was far more significant in determining the method of inhibition than whether or not there was a substituent in 4-position of the C-ring. Compound **247a** showed a more potent microtubule destabilizing effect at 1 μM dosage than colchicine (**243**), when considering the immunofluorescence images of cell lines stained with an anti-α-tubulin antibody. Whereas, on the other hand, compound **247b** exhibited potent cytostatic effects in the treated cell lines. At 1 μM dosage, 75% of the treated HeLa cells were suspended in the G_2/M phase, thus inhibiting the initiation of the mitotic cycle.[129]

The 4-position on the C-ring was, however, found to be tolerant to a much greater variety of substituents (as has been mentioned earlier in Section 3.1, *Aims and Objectives*). The comparative IC_{50} values against HeLa cells of etoposide (**55a**), along with two representative examples of derivatives reported by Zou and co-workers (compounds **136a** and **136b**),[114] and compound **247b**, as reported by Yuan and co-workers,[129] are shown in Figure 75.
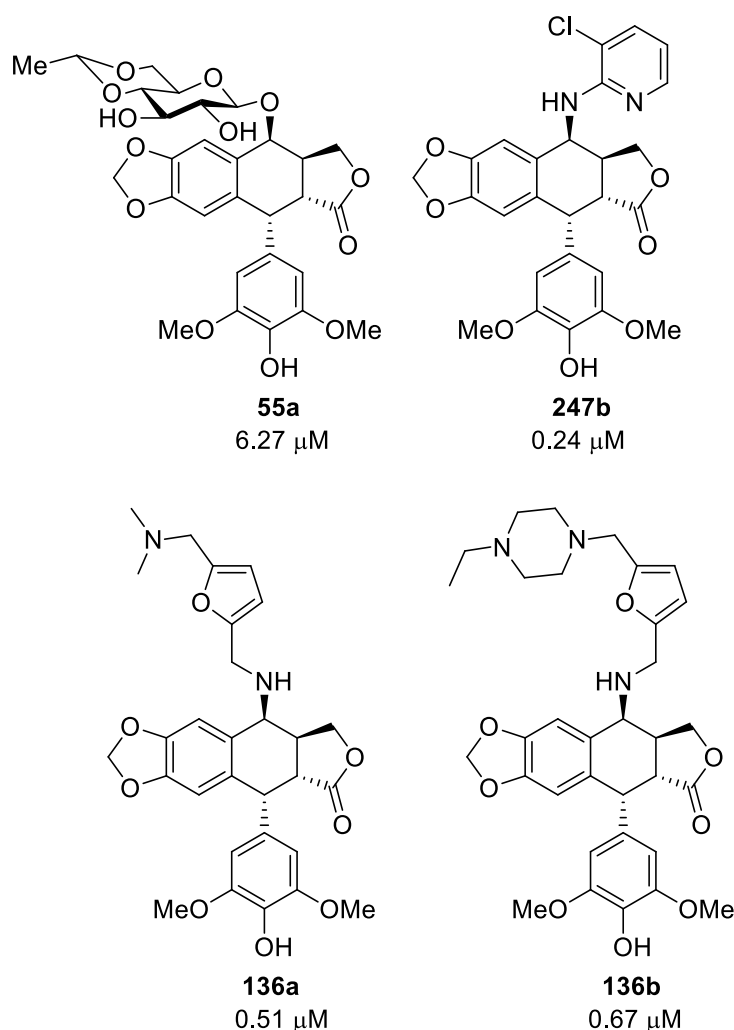
Figure 75: Etoposide (**55a**) and three semisynthetic derivatives with corresponding IC$_{50}$ values against HeLa cancer cell lines.

Thus, with all of this considered, the first library of compounds were evaluated for their antiproliferative action against a WHCO1 oesophageal cancer cell line. *In silico* molecular modelling docking studies were then performed against various PDB structures as complimentary insights into the active sites of interest. The anticancer activity of our first library of compounds will be discussed next, followed by a molecular modelling discussion.

7.1.5 Summary

To understand the effect the 4*N*-functionalization of 4-aza-2,3-didehydropodophyllotoxins had on the activity of this class of compounds, it was important to compare the 4*N*-functionalized compounds to the analogous non-functionalized compounds (**187** and **188**, Figure 77). By mimicking the etoposide (**55a**) and podophyllotoxin (**50**) E-ring substitution patterns, the same rationale followed by previous researchers was also employed. The library will be discussed in different subsections, so as to group the related compounds and consider their respective

antiproliferative activities in comparison to that of compounds **187** and **188**. The subsections will be grouped by means of the 4*N*-substituent, i.e. the GL-331/NPF mimics, the propargylated derivatives, and the etoposide mimics (Figure 77). These antiproliferative activities will also be shown in comparison to the literature reported activity of the well-known chemotherapeutic agent, cisplatin.

It should also be noted that at the commencement of this study, 4*N*-functionalized 4-azapodophyllotoxin analogues had not received much attention in literature, with only the hydroxyethyl derivatives reported by Kumar, Malhotra and co-workers garnering attention (these compounds were discussed in more depth earlier in Section 2.1, *Natural products in Chemistry*).[46,85,100] In terms of compounds more similar to the clinically viable agents, such as etoposide (**55a**) and its derivatives (**134**, **135** and **139**), published synthetic and biological evaluations were focused more on semisynthetic approaches and the antiproliferative activity of these derivatives.[117,120,121,123,157,158]
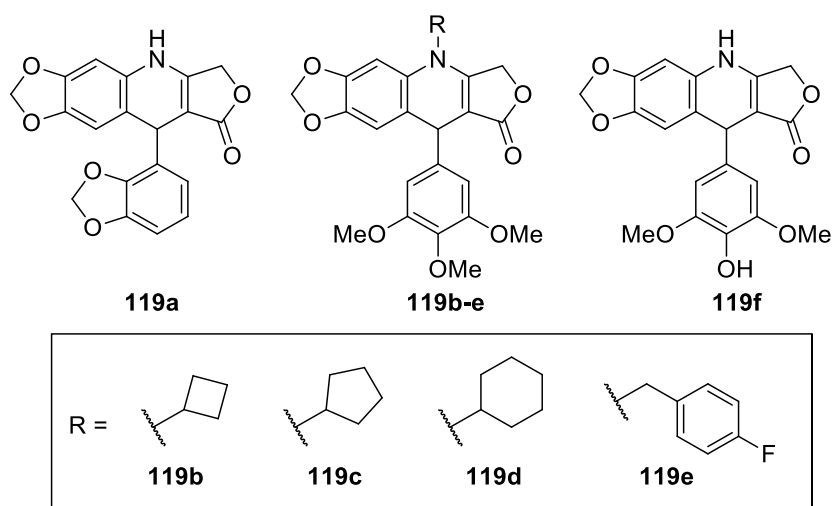
Figure 76: Representative examples reported by Pettit and co-workers.[96]

The library of more diversified *N*-functionalized derivatives (**119a-f**, Figure 76) by Pettit and co-workers, that was also discussed in Section 2.1, *Natural Products in Chemistry*, showed interesting cytostatic biological activity (GI$_{50}$ data for the MCF-7 and SF268 cell lines shown in Table 21).[96]

Table 21: Antiproliferative activity data for the representative azapodophyllotoxin analogues reported by Pettit and co-workers.[96]

| | GI$_{50}$ | | | |
| | µg/mL | | nM | |
	MCF-7	SF268	MCF-7	SF268
119a	0,0039	0,0089	11,10	25,33
119b	0,0260	0,0260	57,59	57,59
119c	0,0450	0,0620	96,67	133,19
119d	0,0520	0,0660	108,44	137,64
119e	0,0370	0,0300	73,20	59,35
119f	0,0250	0,0260	65,21	67,82

This study did not, however, investigate the method of action of these compounds, so as to determine whether these analogues were microtubule destabilizers or topoisomerase II poisons. A common structural motif amongst some of the representative analogues (**119b-e**,[96] Figure 76) was the 3,4,5-trimethoxyphenyl pendent ring, which had been shown in other studies to encourage tubulin destabilization over G$_2$/M cell cycle arrest.[129] It can be noted though that the analogues with cyclopentyl- (**119c**) and cyclohexyl-rings (**119d**) showed slightly lower activity against certain cell lines (such as the central nervous system (CNS) cancer cell line, SF268, shown in Table 21), in comparison to the unsubstituted analogues and those with smaller substituents. Compound **119e**, in our opinion, could benefit from more study, due to its structural similarity to the drug, NPF (**135**), which is currently undergoing clinical trials.

7.2 Biological Evaluation and results

Biological evaluation of our compounds were performed by Dr Catherine Kaschula and co-workers. Those results will be discussed next, in terms of the different subsets as mentioned previously. All compounds were tested as racemates against an oesophageal cancer cell line, WHCO1 – a cell line derived from a South African patient.[37]

7.2.1 Antiproliferative activity of novel compounds

The novel compounds that were analysed for their antiproliferative activity were divided into smaller sub-groups, namely the clinical compounds that served as the inspiration for the design of the compound. These were GL331/NPF mimics, the propargylated derivatives and etoposide mimics. The sub-groups are shown below in Figure 77.

GL-331/NPF Mimics:
175, 179-186

187: R$_1$ = H
188: R$_1$ = CH$_3$

Propargylated Derivatives:
174, 176-178

Etoposide Mimics:
227-234
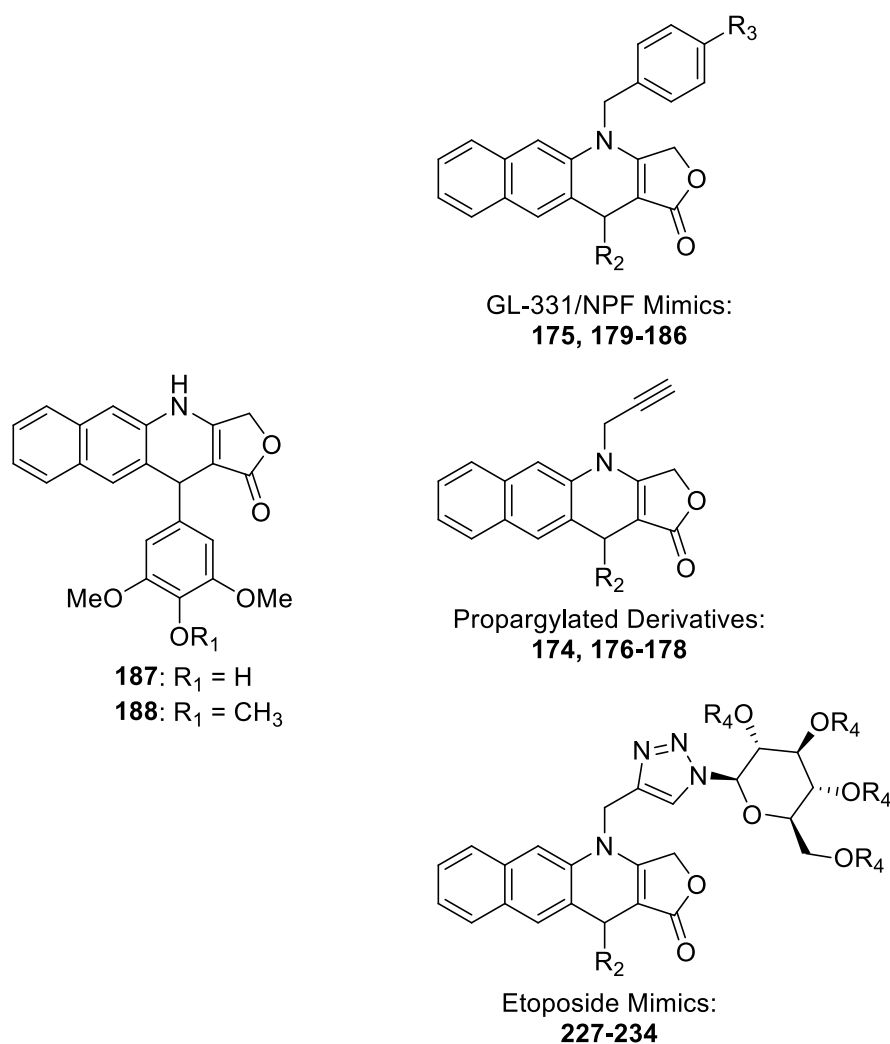
Figure 77: Different subsets of the novel library of 4-azapodophyllotoxins.

GL-331/NPF Mimics

Two of the novel analogues, compounds **180** and **181**, as shown below in Table 22, showed good antiproliferative activity against the oesophageal cancer cell line (WHCO1) and another two were also fairly potent, in comparison to the known chemotherapeutic agent, cisplatin. Compounds **180** and **181** were closest in activity to cisplatin (9.2 μM), with IC$_{50}$ values of 15.33 μM and 11.65 μM, respectively. Compounds **184** and **185** also showed low micromolar activities, at inhibitory concentrations of 16.61 μM and 12.85 μM, respectively. These compounds did not, however, compare well in activity to compounds **187** and **188**, which had sub-micromolar activity values. These activity values are in line with that of literature reported values for 4-azapodophyllotoxins and also correlates with observations in literature that 4β-functionalized podophyllotoxin derivatives have lower *in vitro* activity than their non-functionalized parent compounds.[49] An interesting trend that was noted in this subset was that the analogues with a 3,5-dibromo-4-hydroxy substitution pattern on the pendent E-ring (**180**, **183**, **186**) generally scored fairly good IC$_{50}$ values. The compounds with an etoposide-derived E-ring (4-hydroxy-3,5-dimethoxyphenyl) had a two-fold higher activity than their podophyllotoxin-derived counterparts (3,4,5-trimethoxyphenyl E-ring) in the analogues with 4*N*-benzyl substituents based on GL-331 (**134**) and NPF (**135**). This was different for compounds **184** to **186**, with all three analogues showing similar activity values. The comparable activities of the three *N*-benzyl derivatives (**184** – **186**) suggested that there is more significance to the 4-aza-functionalization than necessarily from the pendent E-ring.

These novel analogues have thus showed good activity, considering the fact that known actives are also active in the low micromolar region. The results for this subset are contained in Table 22 below.

Table 22: Antiproliferative activity data of GL-331/NPF (**134**, **135**) mimics against oesophageal cancer cell line, WHCO1. [a] Single experiments in triplicate, due to comparatively potent activity values. [b] IC_{50} value as reported by Hunter, Kaschula and co-workers for the same cell line.[159]
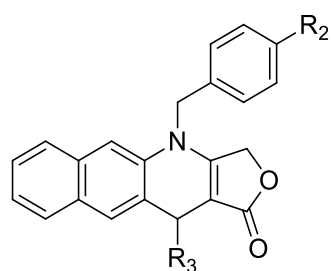
Generalized Structure
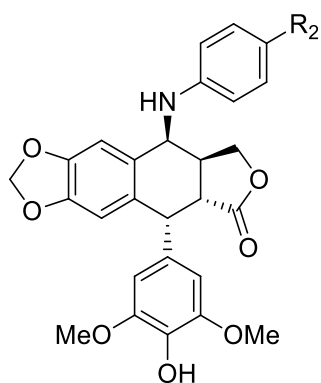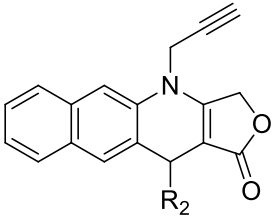
GL-331 **134**: R_2 = NO$_2$
NPF **135**: R_2 = F
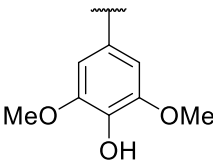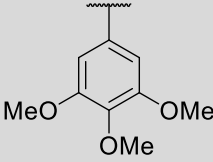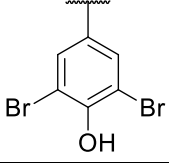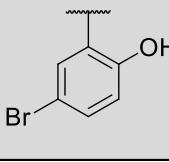
Compound	R^2	R^3	WHCO1 IC$_{50}$ (µM)
175	NO$_2$	MeO—/—OMe, OH (3,5-dimethoxy-4-hydroxyphenyl)	47.18 ± 10.8
179	NO$_2$	MeO—/—OMe, OMe (3,4,5-trimethoxyphenyl)	86.50 ± 21.2
180	NO$_2$	Br—/—Br, OH (3,5-dibromo-4-hydroxyphenyl)	15.33 ± 2.1
181	F	MeO—/—OMe, OH	11.65 ± 2.7
182	F	MeO—/—OMe, OMe	34.83 ± 21.6
183	F	Br—/—Br, OH	22.43 ± 10.8
184	H	MeO—/—OMe, OH	16.61 ± 8.8
185	H	MeO—/—OMe, OMe	12.85 ± 7.3
186	H	Br—/—Br, OH	20.94 ± 16.6
187			0.177 [a]
188			0.318 [a]
Cisplatin			9.20 ± 0.1 [b]

138

Propargylated Derivatives

The 4*N*-propargylated analogues served as precursors to the triazole-linker containing compounds; however, determining the antiproliferative activity of these analogues was postulated to give insight into how the activity of the compounds would change with ever increasing substituent size. As show in Table 23, two of the propargylated compounds were essentially inactive.

Table 23: Antiproliferative activity data of 4N-propargylated mimics against oesophageal cancer cell line, WHCO1. [a] Single experiments in triplicate, due to comparatively potent activity values. [b] IC_{50} value as reported by Hunter, Kaschula and co-workers for the same cell line.[159]

Compound	R^2	WHCO1 IC_{50} (μM)
174		>200
176		>200
177		2.70 ± 0.8
178		23.28 ± 13.7
187		0.177 [a]
188		0.318 [a]
Cisplatin		9.20 ± 0.1 [b]

The bromine-containing compounds **177** and **178**, on the other hand, showed good antiproliferative activies, inhibiting cancer cell growth at concentrations of 23.28 μM and 2.70 μM, respectively. The activity of the bromine-containing compounds hold to the literature-observed trend of brominated 4-azapodophyllotoxin analogues exhibiting potent cytotoxicity in comparison to the non-brominated analogues.[29,54] As noted with the previous subset, which

mimics GL-331 (**134**) and NPF (**135**), these propargylated analogues were also less active than the unsubstituted 4-azapodophyllotoxin analogues **187** and **188**.

Etoposide Mimics

The glycoside-containing 4-azapodophyllotoxin analogues were synthesized as potential etoposide mimics, as the inclusion of sugar moieties on the 4-azapodophyllotoxin scaffold were theorized to potentially produce the same effect in this class of compounds as was originally observed in the 1950's in the work of Stoll and von Wartburg (as mentioned earlier in this chapter).[150–152] Compounds **227**-**230** incorporated a tetraacylated glycoside group in the 4-azaposition. Deacylated compounds **231** and **232** contained the unprotected glycoside groups in the same position.

Table 24: Antiproliferative activity data of Etoposide (**55a**) mimics against oesophageal cancer cell line, WHCO1. [a] Single experiments in triplicate, due to comparatively potent activity values. [b] IC_{50} value as reported by Hunter, Kaschula and co-workers.[159]

Compound	R^2	R^4	WHCO1 IC_{50} (μM)
227	MeO, OMe, OH (R2 group)	Ac	29.0 ± 13.5
231		H	8.8 ± 3.6
228	MeO, OMe, OMe (R2 group)	Ac	12.9 ± 6.1
232		H	8.3 ± 4.1
229	Br, Br, OH (R2 group)	Ac	13.9 ± 1.7
230	OH, Br (R2 group)	Ac	23.8 ± 11.0
187			0.177 [a]
188			0.318 [a]
Cisplatin			9.20 ± 0.1 [b]

As there are many esterases present in the extra- and intracellular matrices, compounds **227**-**230** could be viewed as prodrugs and the determination of the antiproliferative activities of these could be viewed as complementary to that of their deacylated derivatives. As is shown in Table 24, the tetraacylated analogues (**227**-**230**) fared well against the oesophageal cancer cell line, with inhibitory concentrations determined between 13 – 29 μM. Deacylated

compounds **231** and **232** were, however, found to be the most active compounds in this subset (as well as some of the most active in this library as a whole). The activity of these two compounds, the closest mimics to etoposide (**55a**), also compared well to that of cisplatin.

7.2.2 Molecular Modelling studies

Concurrently with the biological evaluation of our library of compounds, we also undertook *in silico* molecular modelling docking studies using the Schrödinger Maestro Suite.[154] Along with the Maestro Suite, Canvas[160] was used to predictively calculate the properties of our compounds of interest. As podophyllotoxin is known to be a microtubule destabilizing agent that interferes with tubulin polymerization by binding to the colchicine domain, the protein data bank (PDB) structures of colchicine-tubulin (PDB ID: 1SA0)[153] and podophyllotoxin-tubulin (PDB ID: 1SA1)[153] were used. The semisynthetic analogues are known to act as topoisomerase II poisons and the most commonly investigated PDB structure for this is the etoposide-topoisomerase II β-isoform (PDB ID: 3QX3).[161] Along with the β-isoform, the etoposide-topoisomerase II α-isoform (PDB ID: 5GWK)[162] was also used for *in silico* docking studies. The use of these for different crystal structures served to explore whether these molecular modelling studies were good model systems and how well the biological results compared to the XP Glide[163] scores of the various PDB structures.[164] All crystal structures were refined and prepared for docking (described in *Supplementary Information*, Section 10.1) and the active reference compounds were docked into the different protein structures. The compounds will be referred to as known actives from here on in the text, as these compounds have been shown to be active in the designated pocket and have been used as the references in studies on similar compounds.[29,49,94,117,153,161,162,165] These known actives are shown in Figure 78. To this end, podophyllotoxin (**50**), along with compounds **56e** and **97e** as reported by Magedov and co-workers,[29] were docked as the known tubulin poisons, whereas etoposide (**55**a), its analogues (**134**, **135** and **139**), doxorubicin (**245**) and amsacrine (**246**) were docked as topoisomerase II poisons.

Thus, for these PDB structures to serve as adequate models, it was expected that the tubulin poisons would dock the most favourably into crystal structures 1SA0 and 1SA1, with the known topoisomerase II poisons generating less favourable docking scores. Alternately, the inverse was expected for 5GWK and 3QX3, with compounds such as etoposide (**55a**) and its derivatives generating lower energy docking scores than the known tubulin poisons. This offered a good comparison between the novel library of compounds and the known active compounds in terms of how well they fit into the active site pockets.
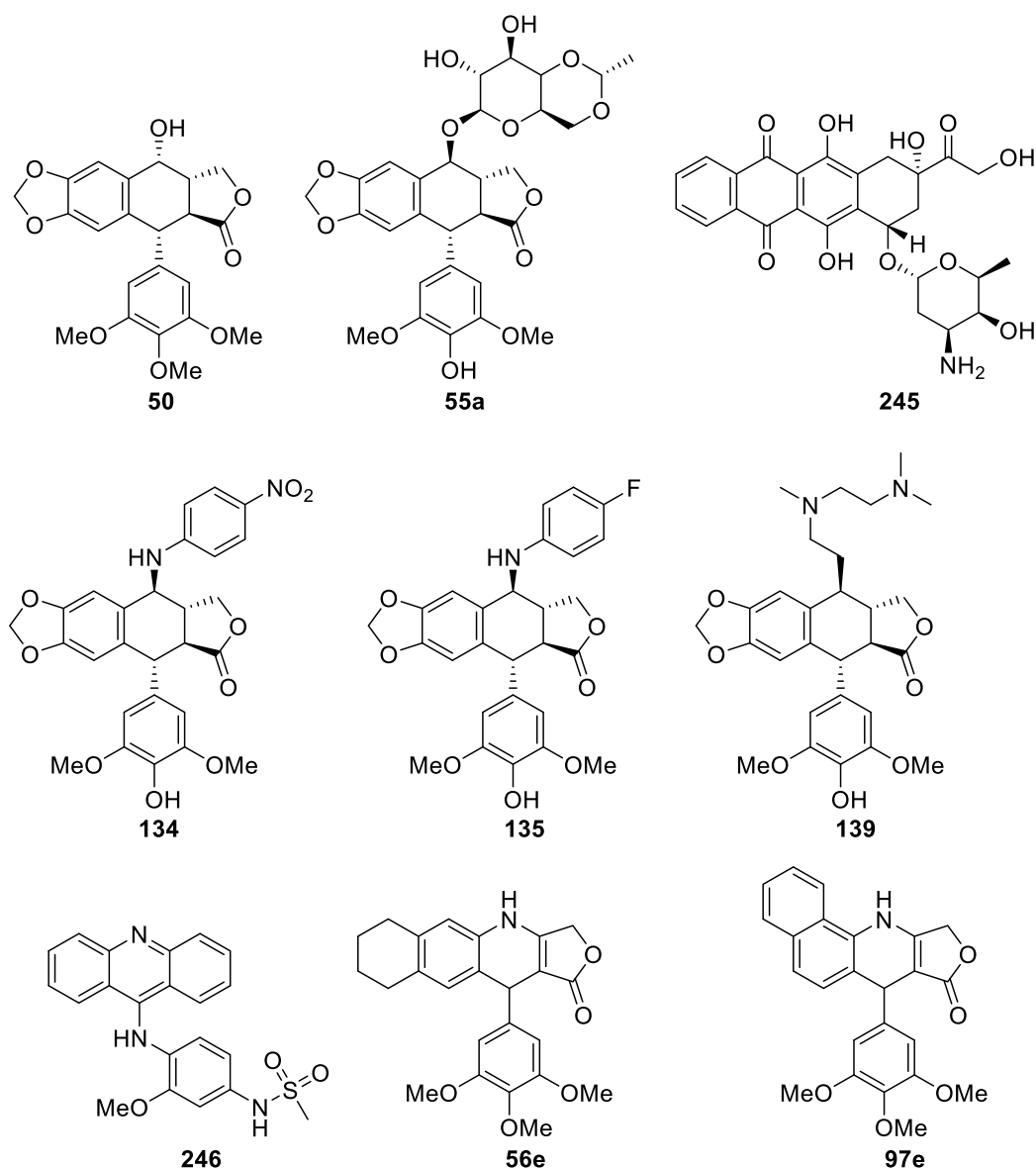
Figure 78: Known active compounds used as reference compounds in the *in silico* molecular modelling docking studies.

As podophyllotoxin is known to dock into the colchicine site of the β-tubulin dimer, it was expected that the compound would generate a favourable docking score when docked into the refined and prepared 1SA0 protein crystal structure. Unfortunately, this was not the case, and since podophyllotoxin (**55a**) did not dock into the colchicine pocket of this crystal structure, it cannot be considered as an adequate model system. The inability of podophyllotoxin to dock into the colchicine-pocket could be attributed to the hydrophobic nature of this domain. The 1SA0 protein crystal was also recorded with colchicine in the active site, therefore it should always be considered that this is a low energy complex and not fully representative of the dynamic environment of normal cellular function. This was further reaffirmed through the inability of compounds **56e** and **97e** to dock successfully into the colchicine pocket. This

inability of compounds that are known to exploit the colchicine pocket for the destabilization of microtubule assembly (as discussed earlier) to successfully dock into this crystal structure, shows that it may not be an adequate model for comparison.
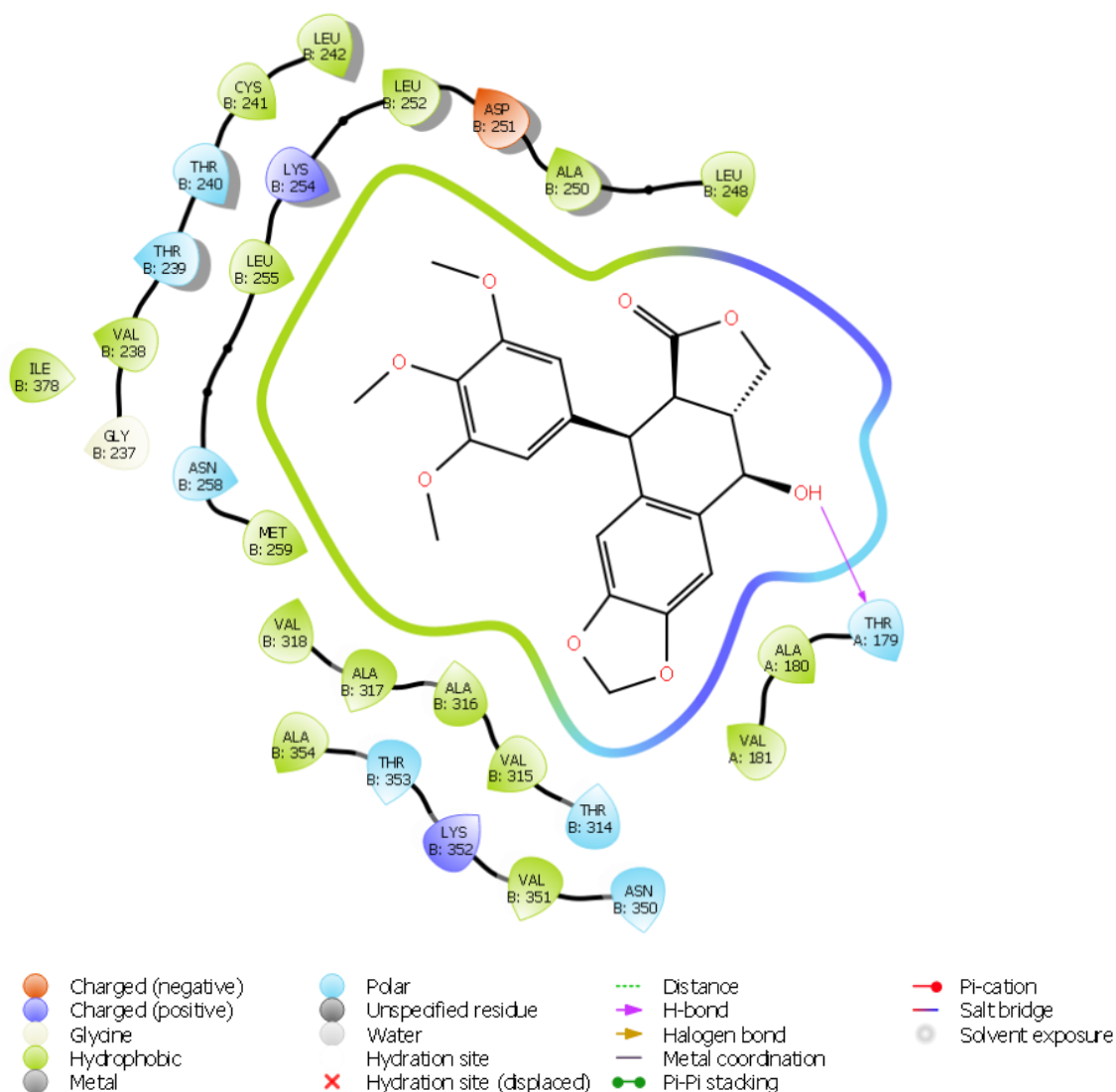
Figure 79: Ligand interaction diagram (LID) of podophyllotoxin in the active site of the 1SA1 crystal complex (with legend).

The data from this calculation will be shown in the section, *Supporting Information*, but 1SA0 will not be discussed further from here on, as it could be eliminated as a potential model system. The crystal structures for 1SA1, 3QX3 and 5GWK generated results that made them more reliable model systems for the purposes of this study – this will be discussed in the following sections.

143

The ligand interaction diagram (LID)[166] of podophyllotoxin (**50**) in the active pocket of the podophyllotoxin-tubulin complex (1SA1) showed the pocket to be very hydrophobic, which again highlighted the role played by the 3,4,5-trimethoxyphenyl group (Figure 79).

Therefore, using the Schrödinger Canvas Suite, we also calculated the ALogP values of all compounds of interest. The ALogP value indicates the hydrophobicity (or lipophilicity) of a compound by means of atomic contribution calculations.[167] The ALogP value has been shown to be the best prediction tool for small molecules.[168] When plotting the ALogP against the XP Glide docking score (XP GScore), a clear trend is not immediately observable. As can be seen in Figure 79 (Top graph), there is no discernable linear increase in Glide score as hydrophobicity increased. The same is observed when the Glide Score is considered against the reported IC_{50} values (Bottom Graph, Figure 80).

The lack of a linear trend can be attributed to the dual nature of the active site. Although the active site seems to express preference for more hydrophobic molecules, there are also some areas in the pocket more favourable to charged and polar functional groups – as can be seen in Figure 76. The hydrophobic pocket is governed by apolar groups such as valine 318 (VAL 318), methionine 259 (MET 259), leucine 255 (LEU 255), alanine 250 (ALA 250), leucine 248 (LEU 248), cysteine 241 (CYS 241) and leucine 242 (LEU 242). On the polar side, the 4α-hydroxygroup of podophyllotoxin (**50**) can be seen to form a hydrogen bond with threonine 149 (THR 149).

These same interactions were also present when 4-azapodophyllotoxin analogues, such as those reported by Magedov and co-workers[29] (compound **97e**) and Giorgi-Renault[58] and co-workers (compound **56a**), were docked into the refined 1SA1 crystal complex. These interactions can be seen in the ligand interaction diagrams in Figure 81 (Left: Compound **97e**, Right: Compound **56a**).
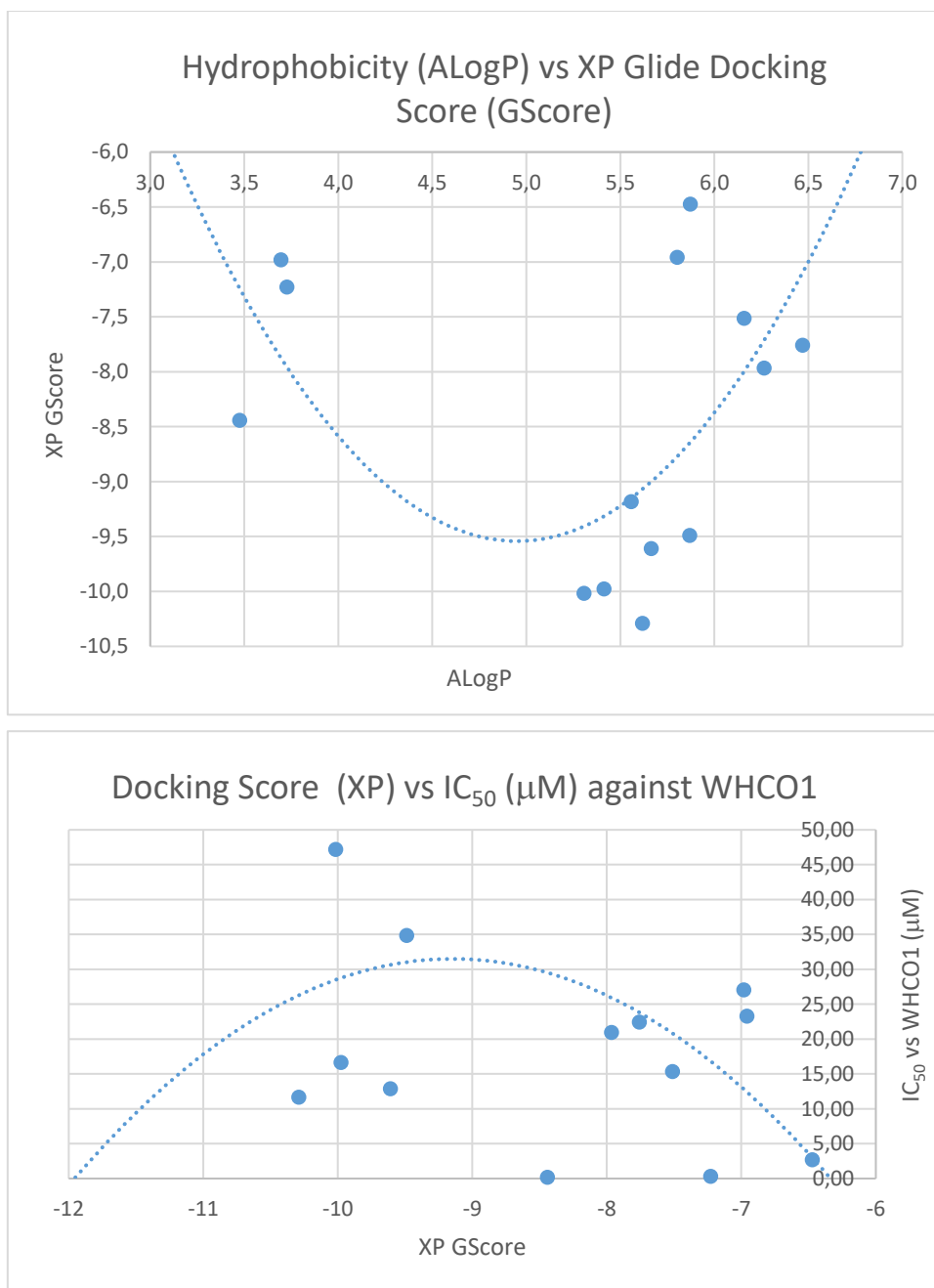
Figure 80: Graphs of our in silico molecular modelling data and anticancer activity data. Top: Hydrophobicity vs Docking Score. Bottom Docking Score vs IC_{50} values determined against WHCO1.

The most interesting result of this calculation was that the cationic species of doxorubicin (**245**) scored the most favourable docking score. (Top results from this study are shown and discussed further on in Table 25). Other than doxorubicin (**245**), a number of our novel analogues scored comparatively favourable docking GScores. These include representatives from the GL-331/NPF subset of molecules, such as compounds **181**, **175**, **184**, **185** and **182**.
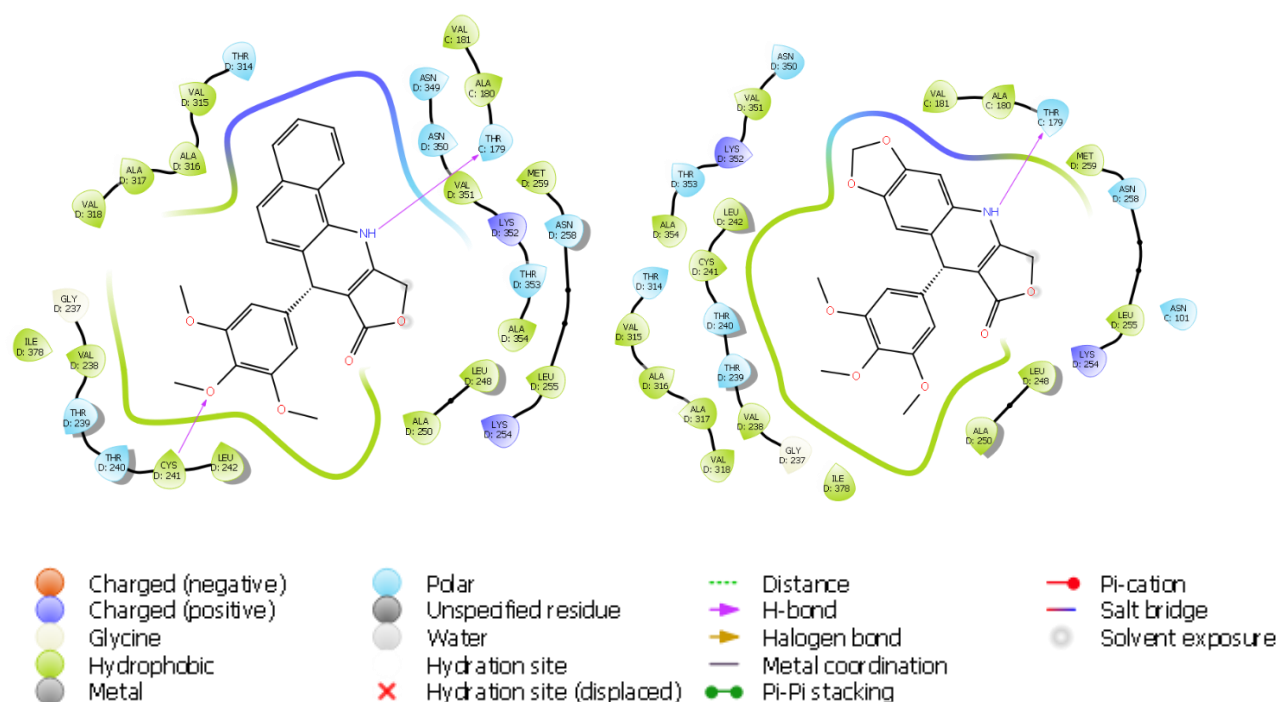
Figure 81: Ligand Interaction Diagrams of compounds **97e** (by Magedov and co-workers[29]) and **56a** (by Giorgi-Renault and coworkers[58]) in the active site of the podophyllotoxin-tubulin crystal complex (1SA1).

The ligand interaction diagrams of these compounds show that they bind into the active pocket in a different manner to that of the previously shown compounds (**50**, **97e** and **56a**).

During the calculations of the lowest energy conformations and most likely species to exist in biological conditions, two conformations were generated for doxorubicin (**245**). One conformer was the *N*-protonated cationic species, which was incidentally the conformer that scored the best Glide docking score of the two (LID shown in Figure 82). The successful docking of this conformer, again, ties in to the previously mentioned dual nature of the active site. It should also be noted that the polar interaction with threonine 179 (as can be seen with the compounds in Figures 79 (**50**) and 81 (**97e** and **56a**), was absent and the molecule, instead, formed hydrogen bonds with the threonine 353 and glycine 176 residues through the β-hydroxyketone moiety. The naphthaquinone rings on doxorubicin (**245**) did dock into the same hydrophobic pocket governed by CYS 241 and LEU 255, as was observed previously. Another hydrogen bond was also observed between the hydroxyl group on the pendent ring and the glutamine 11 (GLN 11) residue.
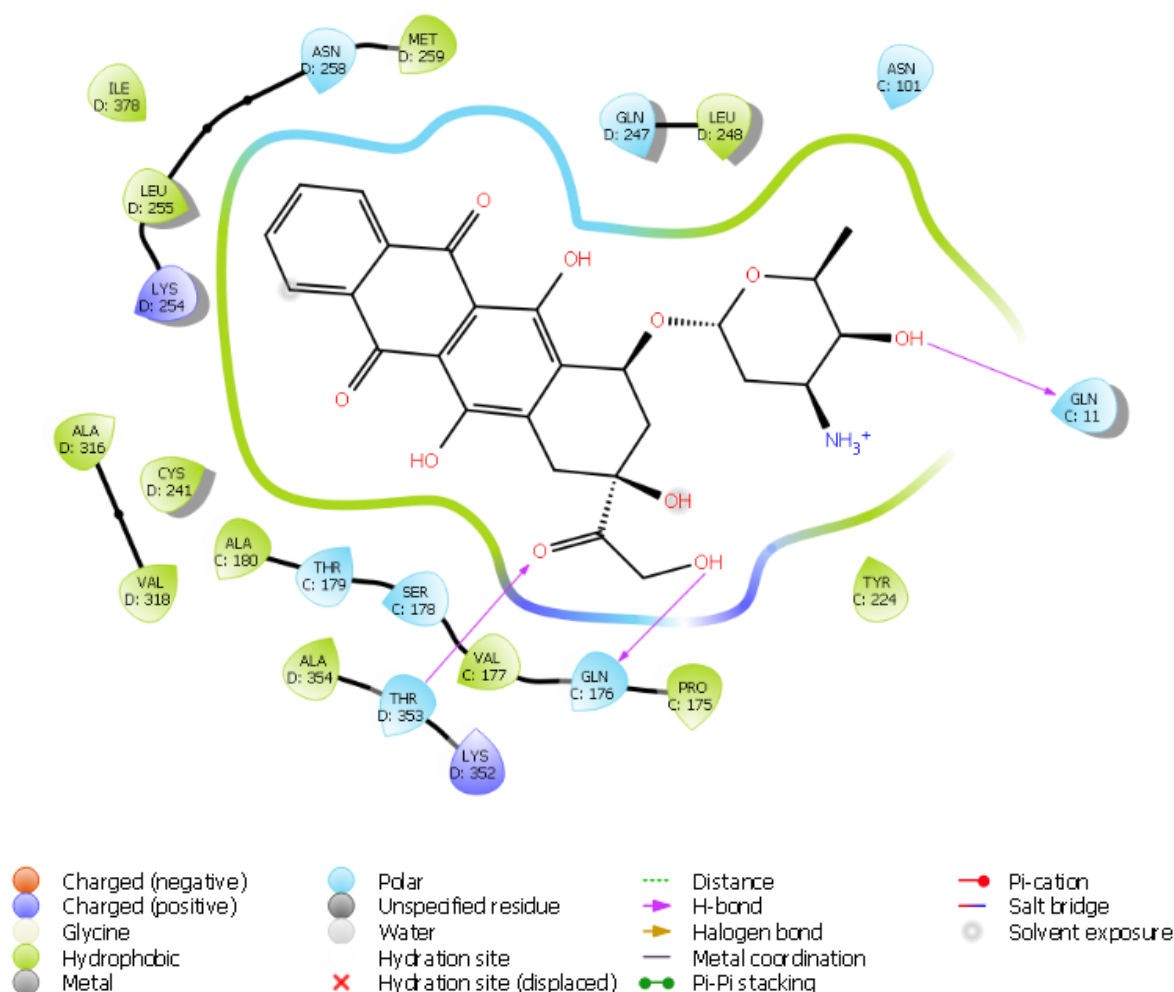
Figure 82: Ligand Interaction Diagram of doxorubicin (**245**) in the active site of the podophyllotoxin-tubulin crystal complex (1SA1).

Although no activity data had been reported for doxorubicin (**245**) against the WHCO1 cell line as of the writing of this dissertation, the active representative analogues reported values between 11-48 μM, with three of these compounds inhibiting cancer cell growth at concentrations between 11-17 μM. These activity results are tabulated in Tables 22-24 earlier in this chapter.

The ligand interaction diagrams for compounds **181** (**A**), **185** (**B**), **187** (**C**) and **188** (**D**,) can be seen in Figure 83, along with the respective antiproliferative activity values for these compounds. The novel *N*-functionalized analogues **181** and **185**, docked into the same hydrophobic pocket as the pendent E-ring of podophyllotoxin (**50**), also governed by the apolar residues VAL 318, MET 259, LEU 255, ALA 250, LEU 248, CYS 241 and LEU 242. Notably, the hydrogen bonding interaction with threonine 179 is absent and, instead, a π-cation interaction with the lysine 352 (LYS 352) was observed in the case of these *N*-benzyl analogues.

147
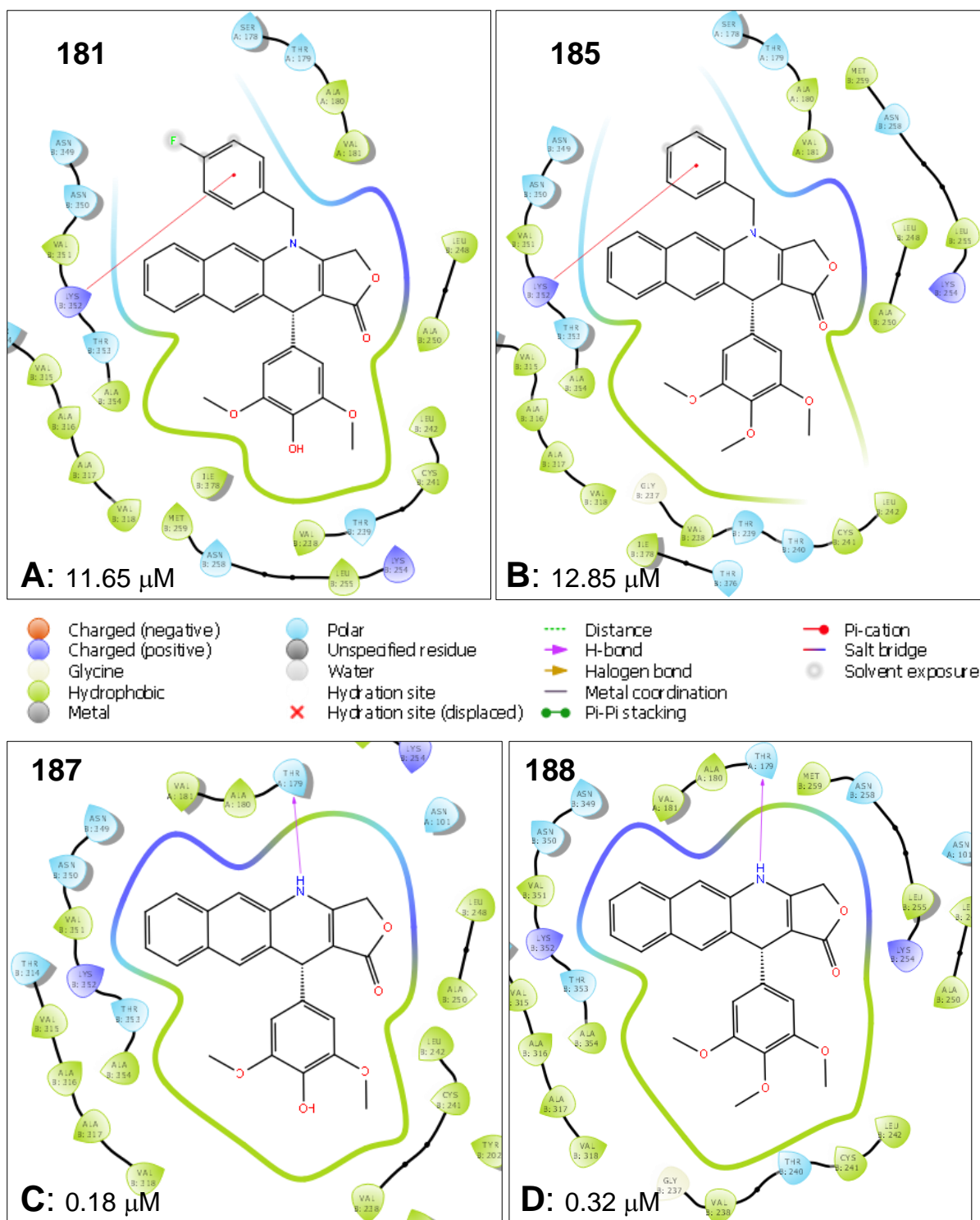
Figure 83: Ligand interaction diagrams (LID) of 4 active compounds docked into the active pocket of the 1SA1 Crystal Structure. These compounds are **181** (**A**), **185** (**B**), **187** (**C**) and **188** (**D**), with IC$_{50}$ values against the WHCO1 cell line.

This tied into the same observation made when the LID of podophyllotoxin (**50**) in Figure 79 was considered. Compounds **187** and **188** (**C** and **D**, respectively, Figure 83) aligned with the observations made on the interactions of the 4-azapodophyllotoxins **97e** and **56a** (Figure 81)

148

in the active pocket, namely, the hydrogen bond with THR 179 and the pendent E-ring that docked into the hydrophobic pocket.

Selective data from the 1SA1 docking study is shown in Table 25. The representative set only shows the docking data for the average of the *R*- and *S*-isomers (RS Ave.) that scored better (or fairly similar) XP Glide GScores to that of podophyllotoxin (**50**).

Table 25: Representative data from the 1SA1 *in silico* docking study. RS Ave. is an average of the Glide Score of the *R*- and *S*-isomers.

Compound		1SA1 RS Ave.	ALogP	WHCO1 IC$_{50}$ (μM)
245	DXR C	-11.152	-1.239	*No Data* [a]
181	2-1	-10.2915	5.617	11.65 ± 2.7
175	1-1	-10.0175	5.306	47.18 ± 10.8
184	3-1	-9.978	5.412	16.61 ± 8.8
139	TOP53 C3	-9.856	1.695	*No Data* [a]
185	3-2	-9.61	5.663	12.85 ± 7.3
182	2-2	-9.4895	5.868	34.83 ± 21.6
179	1-2	-9.1825	5.557	86.50 ± 21.2
174	4-1	-9.147	5.021	>200
176	4-2	-8.642	5.272	>200
50	PPT	-8.592	2.112	*No Data* [a]
187	9-1	-8.4415	3.475	0.18
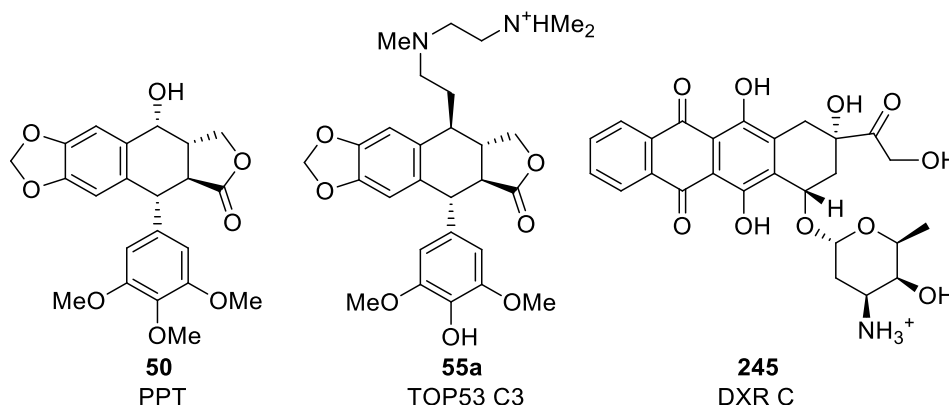
50
PPT

55a
TOP53 C3

245
DXR C

[a] No biological activity data against WHCO1 is available for these compounds. Compounds were not in hand to be tested and no literature values are available as of yet, thus they only served as comparative actives.

A common trend that can be observed in the computational data is that most of these compounds scored high ALogP values and can be considered as fairly hydrophobic compounds. The actual activity data delivered mixed results for these compounds though –

as five of the compounds in this set can be deemed as compounds with lesser inhibitory activity. Compound **187**, which was one of the only compounds with sub-micromolar activity, scored a XP Glide GScore close to that of podophyllotoxin (**50**). However, compound **187** appears to be slightly more hydrophobic, as suggested by its higher ALogP score.

When the data for the 1SA1 docking study was analysed in terms of the compounds that scored poorer docking scores or did not dock into the active site at all, an interesting trend was noted. The methylene triazolo-glycosides did not dock into the active site, which led us to postulate that there might be a size limitation to the binding pocket. To determine whether there could be validity to this theory, the molecular mass ratio of the compounds of interest was determined with regards to podophyllotoxin (**50**). The same was done in terms of the Glide docking scores. Dividing this by the molar mass ratio would give an activity to size correlation.

$$\left.\frac{XP\ GScore\ (Compound)}{XP\ GScore\ (Podophyllotoxin)}\middle/\frac{Molar\ Mass\ (Compound)}{Molar\ Mass\ (Podophyllotoxin)}\right. = Activity\ Ratio$$

This value would therefore be proportional to the magnitude of the XP GScore and inversely proportional to the molar mass of the compound. When this was plotted against the IC_{50} values of these compounds against the WHCO1 cancer cell line (Figure 84), this interpretation of the results seemed to hold promise. However, more biological data is necessary for this observation to be conclusive, as there are still many compounds that tend to give outlier values.
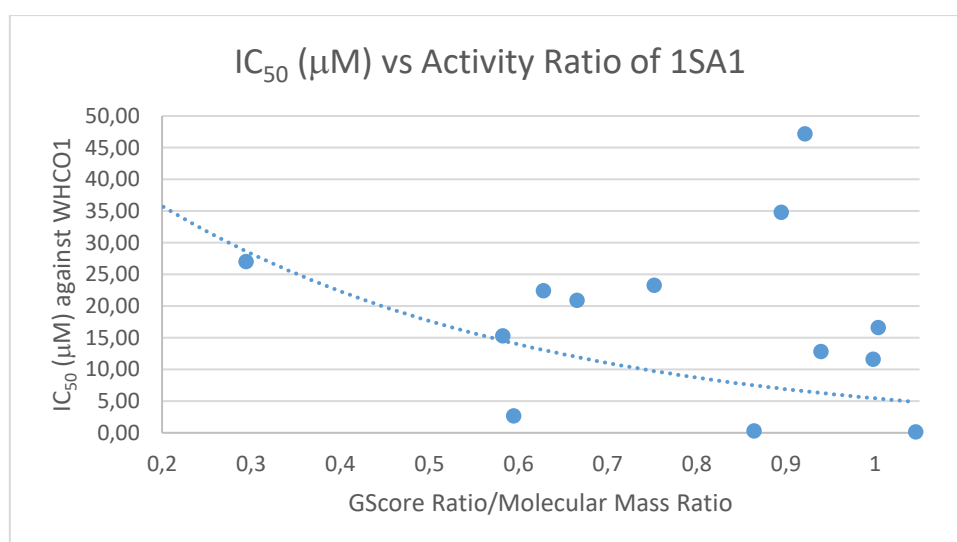
Figure 84: Correlation between the anticancer activity data and molecular modelling data expressed as the Activity Ratio, as defined earlier.

150

Due to this correlation between size and the ability of the compound to dock into the active site, there would be value in conducting studies into analogues that link the glucoside moiety directly to the 4-azapodophyllotoxin scaffold, thus with the extensive linker motif. Since such a compound would not be easily accessible through MCRs, they were not considered for this study.

Considering the *in silico* docking results against the α- and β-isoforms of topoisomerase II (PDB IDs: 5GWK and 3QX3, respectively), these crystal structures could be viewed as better predictive models for our library of compounds. The most commonly used isoform of topoisomerase II in molecular modelling studies, is the β-isoform (3QX3), so our discussion will focus more on these results than on that of the α-isoform. The contributions of the two isoforms to the antiproliferative activity of topoisomerase II poisons have not been fully determined; however, the expression of topoisomerase IIα is known to be significantly down-regulated during the interphase, whereas the β-isoform is not. This increased expression of topoisomerase IIβ is also attributed to the increased off-target toxicity of this class chemotherapeutic agents.[155] There is, however, no difference in the activity of chemotherapeutic agents on these two isoforms. The greater abundance of the β-isoform in all phases of the cell-cycle has led to it serving as the main PDB model used for topoisomerase II molecular modelling. The results of both are, however, tabulated in Table 26 on the next page. The table was ordered in terms of the most active to least active in terms of GScore (5GWK RS Ave. and 3QX3 RS Ave.). Therefore the column for the compounds contained the number of the compound as referred to in the text and the identifier used in Maestro. Multiple different GScores are also generated for certain compounds, as the ligands (as they are referred to in Maestro) are optimized to generate low energy states. This can lead to states where acidic or basic functional groups are deprotonated or protonated, respectively, and these states are regarded as different entries. The known actives shown earlier in Figure 75 are included in the data.

Notably, our two active analogues, **231** and **232** (Figure 85), docked very well into the active sites of both isoforms, scoring comparable XP Glide GScores to that of etoposide (**55a**).

Table 26: In silico docking results against the two Topoisomerase II isoforms

α-Isoform			β-Isoform		
Compound	5GWK RS Ave.	WHCO1 IC$_{50}$ (µM)	Compound	3QX3 RS Ave.	WHCO1 IC$_{50}$ (µM)
139 TOP53 C2	-14.111	*No Data[a]*	**231** 5-2	-11.542	8.80 ± 3.6
55a ETP	-12.863	*No Data[a]*	**232** 6-2	-11.496	8.25 ± 4.1
139 TOP53 C3	-12.167	*No Data[a]*	**139** TOP53 C1	-11.413	*No Data[a]*
245 DXR C	-12.078	*No Data[a]*	**139** TOP53 CC2	-11.122	*No Data[a]*
231 5-2	-11.601	8.80 ± 3.6	**139** TOP53 C3	-11.052	*No Data[a]*
134 GL331	-10.891	*No Data[a]*	**245** DXR C	-10.784	*No Data[a]*
139 TOP53 C1	-10.446	*No Data[a]*	**139** TOP53 CC1	-10.533	*No Data[a]*
135 NPF	-10.341	*No Data[a]*	**135** NPF	-10.373	*No Data[a]*
139 TOP53 CC2	-10.115	*No Data[a]*	**55a** ETP	-10.290	*No Data[a]*
232 6-2	-10.047	8.25 ± 4.1	**55a** ETP	-10.203	*No Data[a]*
187 9-1	-9.865	0.18	**139** TOP53 C2	-10.053	*No Data[a]*
55a ETP	-9.292	*No Data[a]*	**187** 9-1	-9.120	0.18
246 AMSA C	-8.418	*No Data[a]*	**186** 3-3	-8.961	20.94 ± 16.6
184 3-1	-8.300	16.61 ± 8.8	**233** 5-3	-8.888	157.97 ± 53.1
233 5-3	-8.256	157.97 ± 53.1	**174** 4-1	-8.852	>200
176 4-2	-8.197	>200	**50** PPT	-8.665	*No Data[a]*
139 TOP53 CC1	-7.904	*No Data[a]*	**245** DXR	-8.527	*No Data[a]*
50 PPT	-7.788	*No Data[a]*	**183** 2-3	-8.073	22.43 ± 10.8
97e IM3	-7.655	*No Data[a]*	**177** 4-3	-8.061	2.70 ± 0.8
180 1-3	-7.565	15.33 ± 2.1	**175** 1-1	-8.023	47.18 ± 10.8
186 3-3	-7.415	20.94 ± 16.6	**246** AMSA C	-7.964	*No Data[a]*
183 2-3	-7.354	22.43 ± 10.8	**97e** IM3	-7.945	*No Data[a]*
175 1-1	-7.325	47.18 ± 10.8	**179** 1-2	-7.942	86.50 ± 21.2
178 4-4	-7.316	23.28 ± 13.7	**185** 3-2	-7.821	12.85 ± 7.3
181 2-1	-7.120	11.65 ± 2.7	**56e** IM5	-7.797	*No Data[a]*
177 4-3	-7.107	2.70 ± 0.8	**234** 5-4	-7.427	27.04 ± 16.0
234 5-4	-6.606	27.04 ± 16.0	**176** 4-2	-7.268	>200
245 DXR	-6.435	*No Data[a]*	**181** 2-1	-7.147	11.65 ± 2.7
185 3-2	-6.304	12.85 ± 7.3	**228** 6-1	-7.138	12.86 ± 6.1
179 1-2	-6.300	86.50 ± 21.2	**134** GL331	-7.125	*No Data[a]*
182 2-2	-5.921	34.83 ± 21.6	**178** 4-4	-7.071	23.28 ± 13.7
56e IM5	-5.907	*No Data[a]*	**188** 9-2	-7.002	0.32
230 8-1	-5.890	23.85 ± 11.0	**180** 1-3	-6.752	15.33 ± 2.1
246 AMSA	-5.788	*No Data[a]*	**184** 3-1	-6.633	16.61 ± 8.8
188 9-2	-5.734	0.32	**182** 2-2	-6.577	34.83 ± 21.6
174 4-1	-4.438	>200	**246** AMSA	-5.993	*No Data[a]*
227 5-1	-2.484	29.00 ± 13.5	**227** 5-1	-5.280	29.00 ± 13.5
228 6-1	-1.170	12.86 ± 6.1	**230** 8-1	-2.741	23.85 ± 11.0
229 7-1	0.509	13.87 ± 1.7	**229** 7-1	0.116	13.87 ± 1.7

[a] No biological activity data against WHCO1 is available for these compounds. Compounds were not in hand to be tested and no literature values are available as of yet, thus they only served as comparative actives by computation.

231, R = H IC_{50} = 8.80 μM
232, R = CH_3 IC_{50} = 8.25 μM
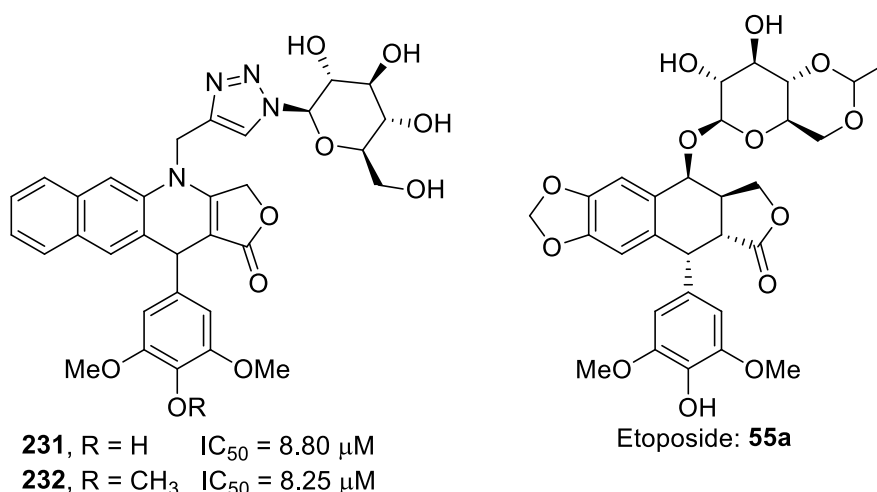
Etoposide: 55a

Figure 85: Active analogues 231 and 232 and etoposide (55a).

The ligand interaction diagrams of etoposide (55a) in the active sites of the crystal structures of both topoisomerase II isoforms (Figure 86) conform to interactions identified in previous literature reports.[169,170] Strong intercalatory interactions can be seen between the A and B-rings and guanine (DG: 13) by π-π stacking.

The 4-hydroxy group on the E-ring forms a hydrogen bonding interaction with the aspartate residues in the enzyme, ASP 463 in 5GWK and ASP 479 in 3QX3. The sugar-group also showed interactions with the solvent exposed region at the interface between the DNA fragment and the enzyme.

The hydrophobic acetyl moiety of the etoposide (55a) sugar group also appeared to interact with a hydrophobic region of the enzyme, governed by proline and methionine residues. The hydroxyl groups of this sugar group interacted with the solvated region. These same interactions with the residues of interest are also shown in the 3D rendered images in Figure 87.

When the LIDs (Figure 86) of compounds 231 and 232 are considered, the same intercalatory π-π stacking between the biphenyl AB-ring systems of the active compounds and the guanine base of the DNA strand can be seen (DG F:13). The 4-hydroxygroup of the 3,5-dimethoxy-4-hydroxyphenyl pendent ring of compound 231 can be seen to form a hydrogen bond with the same aspartate residue (ASP 479) as is seen with etoposide (55a).

153
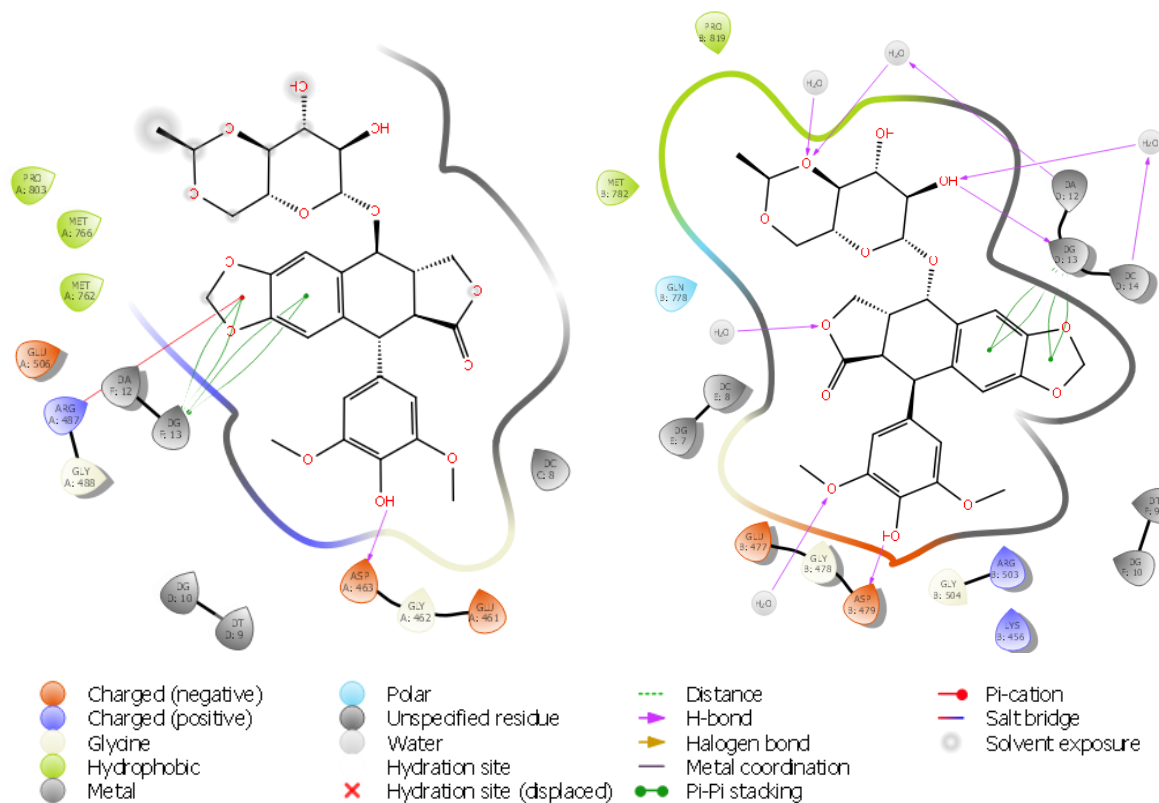
Figure 86: Ligand interaction diagrams of etoposide (**55a**) in the active sites of 5GWK (Left) and 3QX3 (Right).
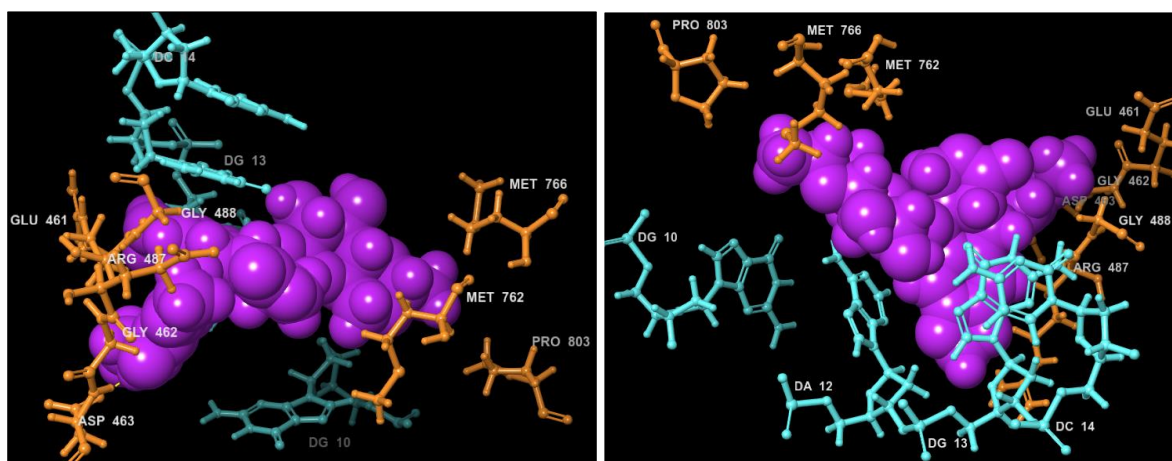
Figure 87: 3D renderings of etoposide (**55a**) (purple) with DNA (turquoise) and the enzyme (orange).

This interaction is understandably absent in the LID of compound **232** and, instead, the compound formed a water-bridged hydrogen bonding interaction with serine 480 (SER 480). The introduction of the triazole linker did seem to bring some benefits to the interactions of these novel compounds as well. This interaction was seen to be especially beneficial in the

154

case of compound **232**, as in the absence of the interaction with ASP 479, the water-bridged interaction with SER 480 slightly shifted the molecule within the active pocket. This shift introduced a π-π stacking interaction between the triazole linker and the adenosine base (DA F:12), as can be seen in the LID of compound **232** (Bottom LID, Figure 88).

The glycoside moieties of both compounds **231** and **232** also interacted with the solvent exposed region (similar to that of etoposide (**55a**)) and were involved in hydrogen bonds with the water molecules in this region. In the docking conformations of both compounds (**231** and **232**), hydrogen bonding interactions were calculated to be present between the tetronic acid-derived D-ring and *intra*-enzyme water molecules.

As with etoposide (**55a**, LIDs in Figure 86 and 3D renderings in Figure 87), the LIDs (Figure 88) of compounds **231** and **232** are accompanied by 3D rendered views of the molecules in the active pockets (Figure 89).

As was discussed in the section, *Natural Products in Chemistry* (Section 2.1), 4-aza-didehydropodophyllotoxins proved to be very promising anticancer agents due to many of the structurally diverse analogues inhibiting cancer cell growth at sub-micromolar concentrations. These compounds were found to be more active than their natural inspiration, podophyllotoxin (**50**). However, as we noted earlier in this section, the semisynthetic analogues were found to be less active, but more viable as therapeutic agents. For this reason, etoposide (**55a**) and teniposide (**55b**) have been employed as therapeutic agents for the past four decades.[49]

Thus, when the activity profile of our novel library of 4-*N*-functionalized 4-azapodophyllotoxin analogues are considered against their non-functionalized counterparts (IC_{50} values shown in Table 27, arranged from most to least active), the decreased activity does seem to make sense. Even though these compounds are slightly less active than compounds **187** and **188**, they still have very promising antiproliferative activity.
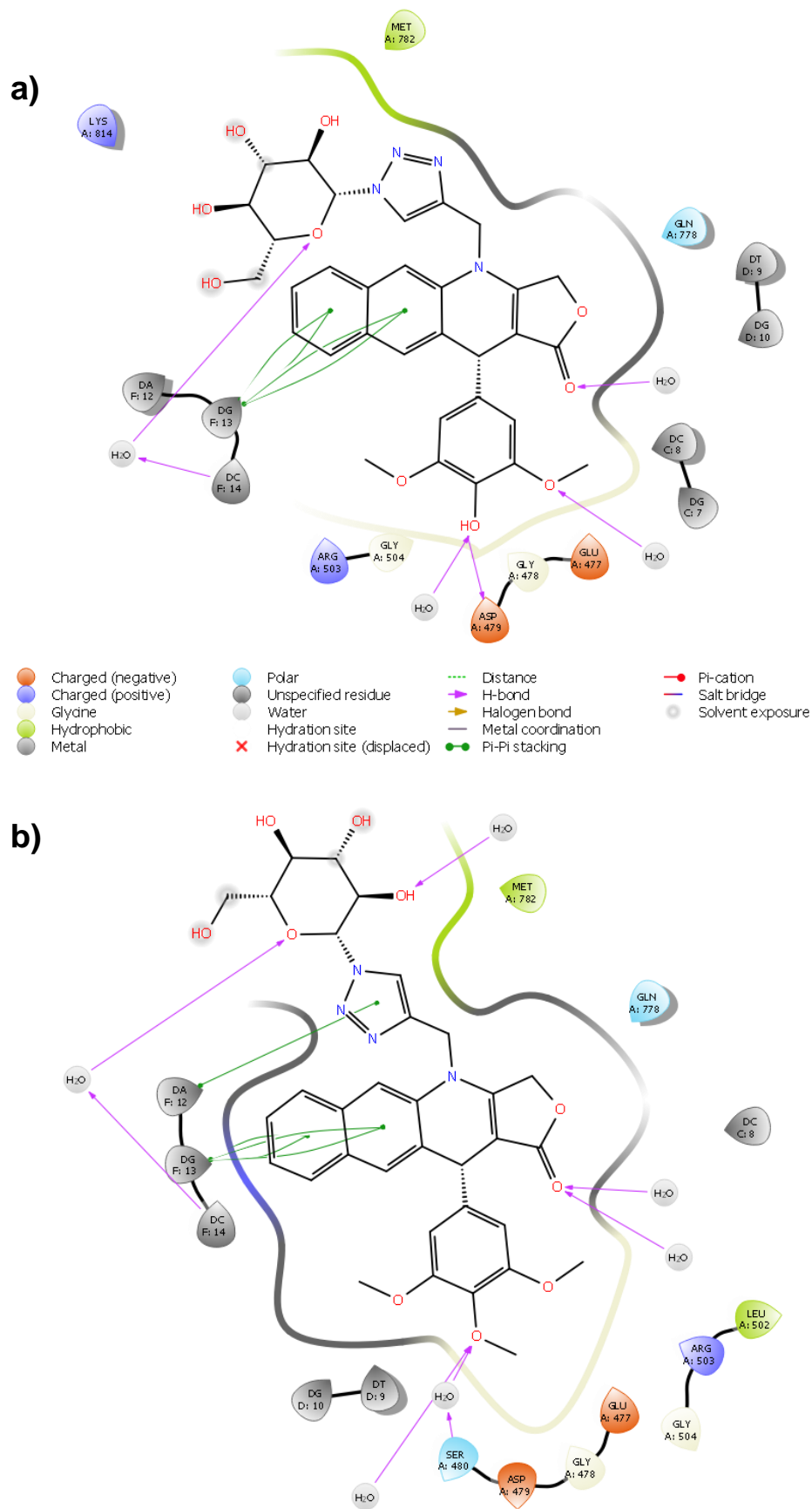
Figure 88: Ligand interaction diagrams of compounds **231** (a) and **232** (b) docked into the active site of 3QX3.
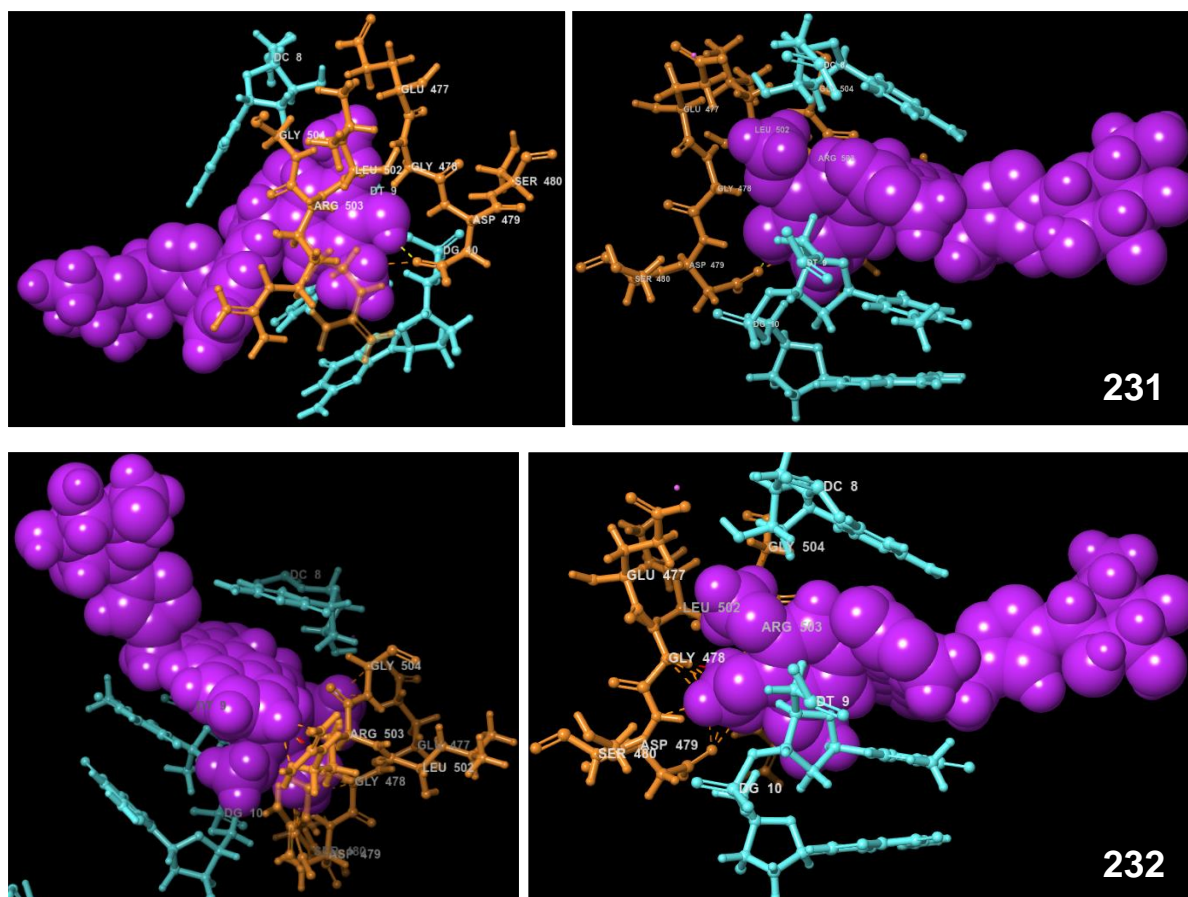
Figure 89: 3D renderings of compounds **231** (Top) and **232** (Bottom). Two different views are shown for each compound, with the molecule shown in purple, DNA in turquoise and the enzyme in orange.

Though there is no WHCO1 IC_{50} antiproliferative activity data available for podophyllotoxin (**50**) and etoposide (**55a**) against the WHCO1 oesophageal cancer cell line, the activity against certain commonly tested cancer cell lines can be considered for comparison (see Table 28).

As can be seen in Table 28, the IC_{50} values for podophyllotoxin (**50**), demethylepipodophyllotoxin (**51c**) and etoposide (**55a**) against cervical (HeLa), breast (MCF-7) and lung (A549) cancer cell lines all range from 15 – 70 μM. Our compounds can, therefore, be considered as active compounds. From the biological evaluation, one group of scaffolds did deliver consistently good activities.

Table 27: IC$_{50}$ values of our novel library of analogues, arranged from most to least active.

Compound	WHCO1 IC$_{50}$ (μM)	Compound	WHCO1 IC$_{50}$ (μM)
187	0.18	183	22.43 ± 10.76
188	0.32	178	23.28 ± 13.67
177	2.70 ± 0.79	230	23.85 ± 10.99
232	8.25 ± 4.07	234	27.04 ± 15.95
231	8.80 ± 3.64	227	29.00 ± 13.45
181	11.65 ± 2.67	182	34.83 ± 21.63
185	12.85 ± 7.33	175	47.18 ± 10.77
228	12.86 ± 6.10	179	86.50 ± 21.21
229	13.87 ± 1.72	233	157.97 ± 53.08
180	15.33 ± 2.05	174	>200
184	16.61 ± 8.76	176	>200
186	20.94 ± 16.64		
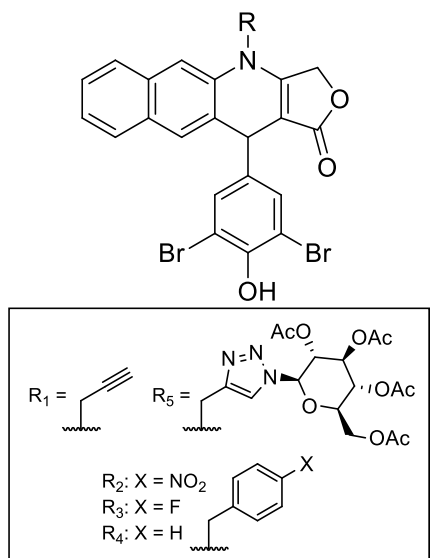
Table 28: Antiproliferative activity of podophyllotoxin (**50**), demethylepipodophyllotoxin (**51c**) and etoposide (**55a**) against cervical (HeLa), breast (MCF-7) and lung (A549) cancer cell lines.
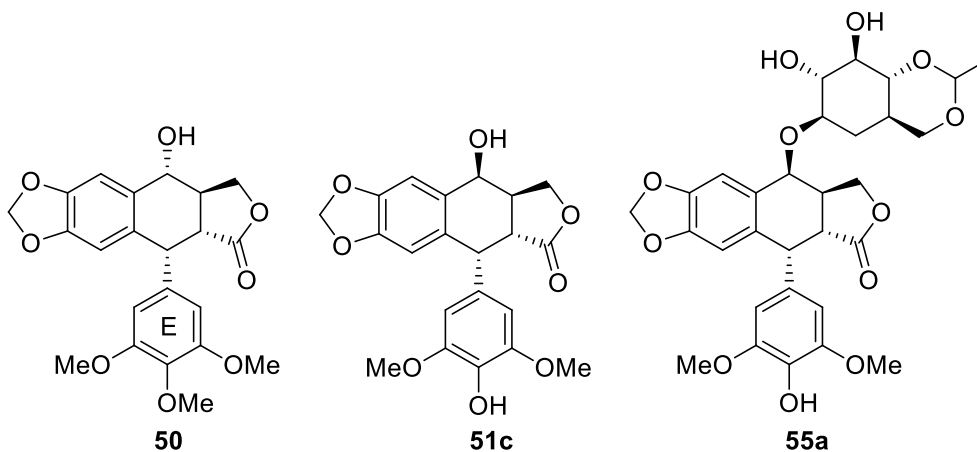
Compound	IC$_{50}$ (μM)		
	HeLa	MCF-7	A549
50	20.52 ± 1.38	36.77 ± 2.47	67.45 ± 2.24
51c	15.96 ± 1.22	20.36 ± 1.26	52.86 ± 3.85
55a	59.38 ± 0.77	28.29 ± 1.96	67.25 ± 7.05

The analogues with the 3,5-dibromo-4-hydroxyphenyl E-ring all inhibited cancer cell growth of the WHCO1 cell line at concentrations below 23 μM (Table 29). As discussed in the chapter,

Aims and Objectives (Section 3.1), this 3,5-dibromo substitution pattern was noted by Magedov and co-workers as a particularly effective motif on the E-ring.[29]

Table 29: IC_{50} values of the dibromo-containing analogues generated in this study.

Compound	R	WHCO1 IC_{50} (μM)
177	R_1	2.70 ± 0.8
180	R_2	15.33 ± 2.1
183	R_3	22.43 ± 10.8
186	R_4	20.94 ± 16.6
229	R_5	13.9 ± 1.7

The potency this substitution pattern on the E-ring introduced can be seen in the propargylated subset. Whereas, compounds **174** and **176** (Figure 90) were inactive, bromination on the E-ring retained activity. The mono-brominated analogue **178** was still fairly active, but the dibromo analogue **177** was the most active of all the novel 4*N*-functionalized analogues.

177

2.70 μM

178

23.28 μM

174: R = H
176: R = CH_3
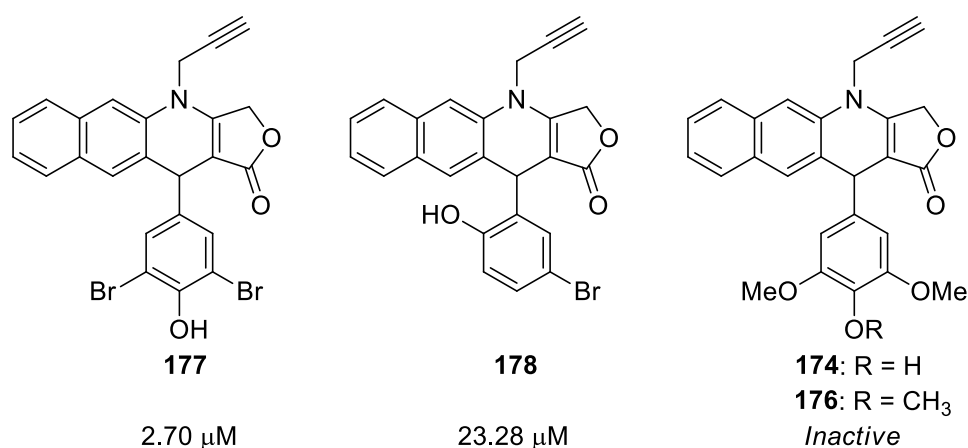
Inactive

Figure 90: 4*N*-propargylated analogues and their activity against the oesophageal cancer cell line, WHCO1.

The bromide substituents generally add hydrophobic character and when the LIDs of compound **186** in the active sites of topoisomerase II and tubulin are considered (Figure 91), this hydrophobic character appears to play a role when the molecule is docked into the crystal

159

structure of the podophyllotoxin-tubulin complex (Right, Figure 91). The pendent E-ring strongly favours the hydrophobic pocket.
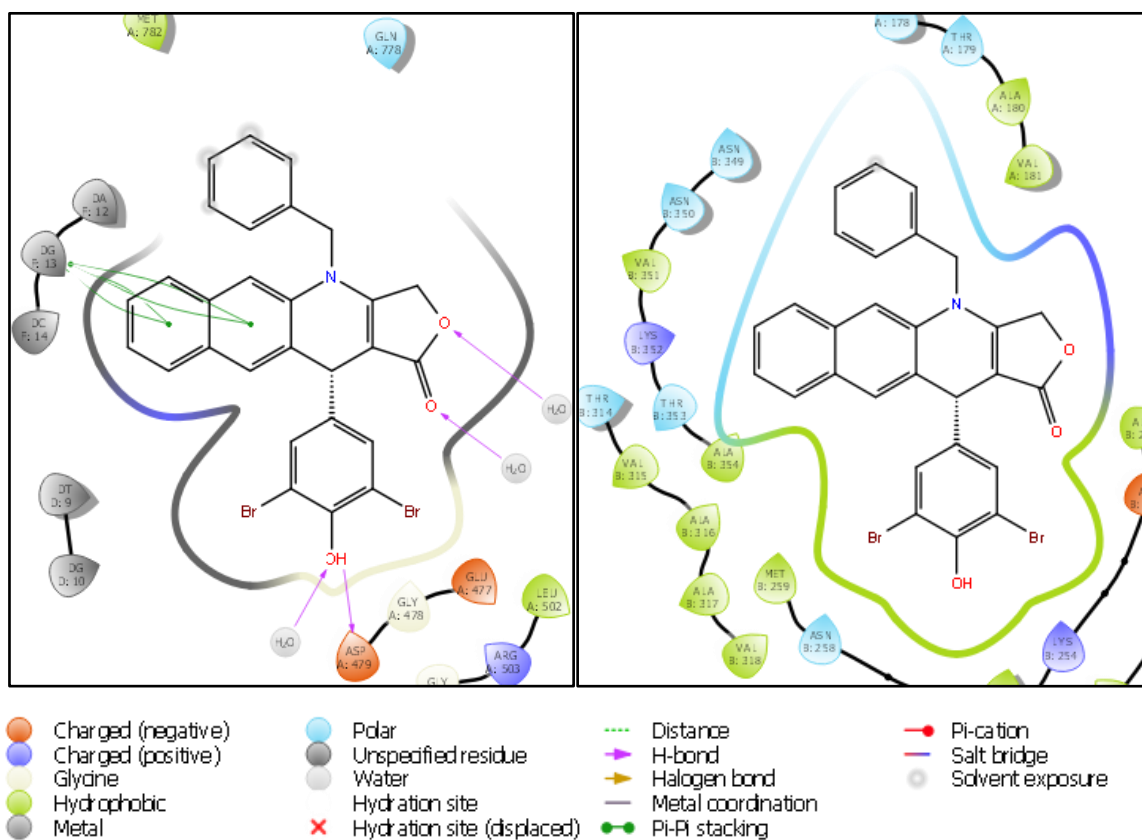
Figure 91: LIDs of compound **186** in the active sites of Topoisomerase II (left) and tubulin (right).

A similar trend is not observed in the etoposide-topoisomerase II crystal structure LID (left, Figure 91); however, this active site is not defined by strong hydrophobic character. An aspect that possibly influenced the activity of these compounds could be halogen bonding. Boeckler and co-workers have reported on the significance in this interaction in medicinal chemistry.[171] Halogens (excluding fluorine) can interact with nucleophilic residues or water molecules in the active site. Although this was not identified explicitly in all of the *in silico* modelling results, it is highly likely to play a role. The prevalence of bromide substituents on the E-ring of some of the more active 4-azapodophyllotoxin analogues reported in literature suggests that this could be a worthy line of enquiry in future studies.

Employing this E-ring in the analogues of further studies could, therefore, produce even more promising antiproliferative compounds. The potential of these compounds will be discussed in the section, *Future Work* (Section 9.1).

7.3 Conclusion

In conclusion, the aim of this study was to test whether the 4*N*-functionalization of 4-aza-2,3-didehydropodophyllotoxin analogues could generate compounds with good antiproliferative activities. We also aimed to generate these compounds through short synthetic routes and robust synthetic steps with fair to good yields. We managed to generate a library of compounds with good inhibitory activity, comparable to that of compounds such as etoposide (**55a**) and cisplatin.

During the investigations into the active pocket through *in silico* molecular modelling studies, the importance of the 4-hydroxy group on the pendent E-ring of this class of compounds was highlighted and identified as a promising substitution pattern, based on a combinatorial approach of E-rings that formed part of very active agents and the importance of the 4-hydroxy group. As most of the compounds that produced the best IC_{50} values had a 3,5-dibromo-4-hydroxy substitution pattern on the E-ring, this could be employed to generate more novel compounds with greater antiproliferative activity.

Furthermore, the methylene triazolo-glycoside group in the 4-aza position also proved to be an effective group in generating active compounds. The tetraacylated analogues were slightly less active than their deacylated counterparts (Figure 92), as can be seen in the discussion of biological activity results earlier in this chapter, *Etoposide Mimics* (Table 24), and shown again below in Figure 92.

227: R₁ = H, R₂ = Ac IC_{50} = 29.0 μM   **231**: R₁ = H, R₂ = H IC_{50} = 8.8 μM
228: R₁ = CH₃, R₂ = Ac IC_{50} = 12,9 μM   **232**: R₁ = CH₃, R₂ = H IC_{50} = 8.3 μM
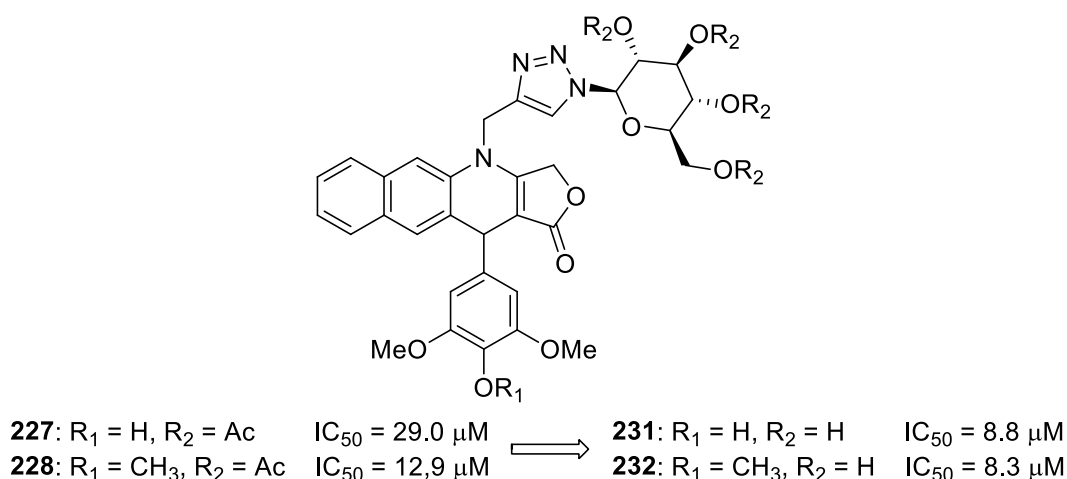
Figure 92: The novel glycoside 4-azapodophyllotoxin derivatives and the IC_{50} values of the tetraacylated and deacylated derivatives.

As mentioned, however, this acylation could be beneficial in terms of prodrug potential, as the lower activity can be utilized in the same manner as with the initial studies into the glycoside derivatives of podophyllotoxin (**50**).[150–152] The are many examples of where this strategy being

employed in the literature. Ang and co-workers reported on the effect of carboxylate ligands on oxoplatin (**243**, Figure 93), a Pt(IV) derivative of cisplatin (**242**).[172] This was to address the toxicity of cisplatin (**242**) through the introduction of acyl moieties onto *trans*-oxo groups on oxoplatin (**243**). Two representative examples, compound **244** (an asymmetric derivative with a benzoate and acetate groups) and compound **245** (a *bis*-acetate derivative) are shown in Figure 93 below. These examples serve to not only overcome the inherent toxicity of cisplatin (**242**), but also to overcome cisplatin-resistance and improve biological characteristics such as lipophilicity and cytotoxicity towards the cancer cells.[172] These derivatives displayed a ten-fold increase in cytotoxicity as well as increase activity against cisplatin-resistant cell lines.
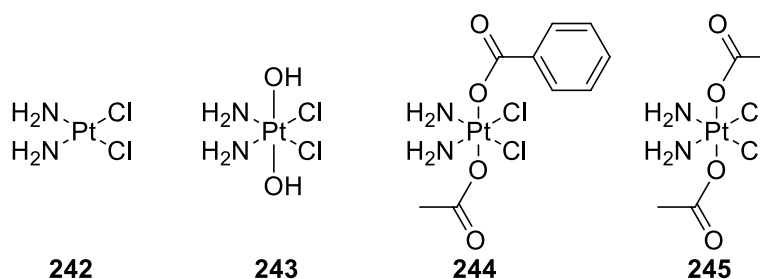
Figure 93: Cisplatin (**242**), oxoplatin (**243**) and two acyl derivatives as reported by Ang and co-workers.[172]

The prodrug applications of acyl groups were also highlighted in work on γ-glutamyl-cysteamine (**246**, Figure 94) reported by Anderson and co-workers.[173] An increase in lipophilicity, so as to improve cellular uptake of the prodrug was also cited as a reason for the introduction of these acyl groups, as well as to address gastric and duodenal ulceration – well-known side-effects of this drug.[174]
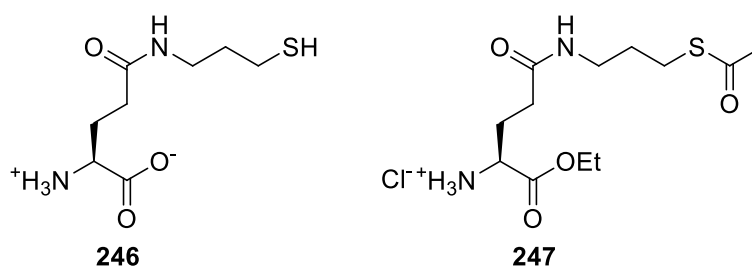
Figure 94: γ-Glutamyl-cysteamine (**246**) and an acyl derivative (**247**) as reported by Anderson and co-workers.[173]

This approach has even been used in patents for prodrugs of therapeutics such as acyclovir (**248**).[175] The patent by Bigorra Llosas *et al.* addresses the low bioavailability of acyclovir (**248**) through the acylation of the hydroxy-ethyl ether side chain (acetate derivative compound **249** as a representative example, Figure 95).

162

239   **240**
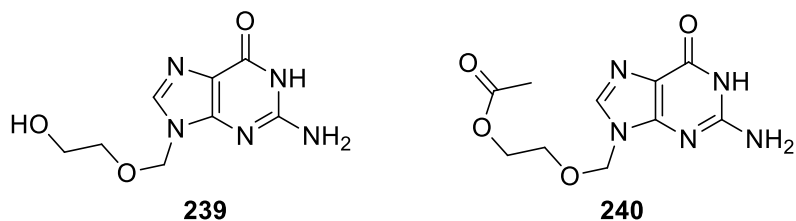
Figure 95: Acyclovir (**248**) and a patented derivative, compound **249**.[175]

The GL-331/NPF subset also produced a number of potent compounds. Only one of the GL-331 inspired analogues was active, with the two natural product-inspired analogues (**175** and **179**) proving to have lesser activity than the 3,5-dibromo-4-hydroxyphenyl analogue. This analogue also counted amongst the most active analogues generated overall, with an IC_{50} value of 15.33 μM. The compounds with the 4-fluorobenzyl and benzyl groups in the 4-*N* position of the novel analogues were fairly active in general, with activities ranging from 11 – 35 μM. The activity of these compounds is especially encouraging as they are accessible through a two synthetic sequence in very good yields.

The results of the biological evaluation confirm that this class of compounds present significant promise as anticancer agents. As these compounds have only been evaluated against one cancer cell line so far, more testing will likely only strengthen this view.

8.1 Future Work

Firstly, to properly confirm the potency of this class of compounds as potentially viable anticancer agents for clinical use, these compounds will have to be assessed against more cancer cell lines such as the most commonly used cervical (HeLa), breast (MCF-7, MDA-MB-231), colon (HCT-116) and central nervous system (A549) cancer cell lines. This will show how well these compounds compare to the known clinical (etoposide (**55a**)) and pre-clinical (GL-331 (**134**) and NPF (**135**)) agents.

We will also conclusively determine the mechanism of inhibition of these compounds, as so far we can only make inferences from structural and *in silico* molecular modelling data. To determine whether these compounds inhibit cell growth by means of microtubule destabilization or topoisomerase II poisoning, flow cytometric cell cycle analysis can be used to determine during which cycle of the mitotic phase the inhibition occurs. Tubulin poisons are known to cause cell cycle arrest in the M-phase,[29] whereas topoisomerase II poisons prohibit cells from entering into the mitotic cycle altogether. The microtubule destabilization (or lack thereof) can also be confirmed through the fluorescent microscopy of a fluorescent dye-stained cell line.[29] This can then be compared to our molecular modelling results and further determine the accuracy of these models.

The 2nd generation library of novel analogues will also be tested for their anticancer activity, further investigating the effect of the triazole linker on the activity of these compounds as well as how biological moieties, such as the cholesteryl group, contribute to this.
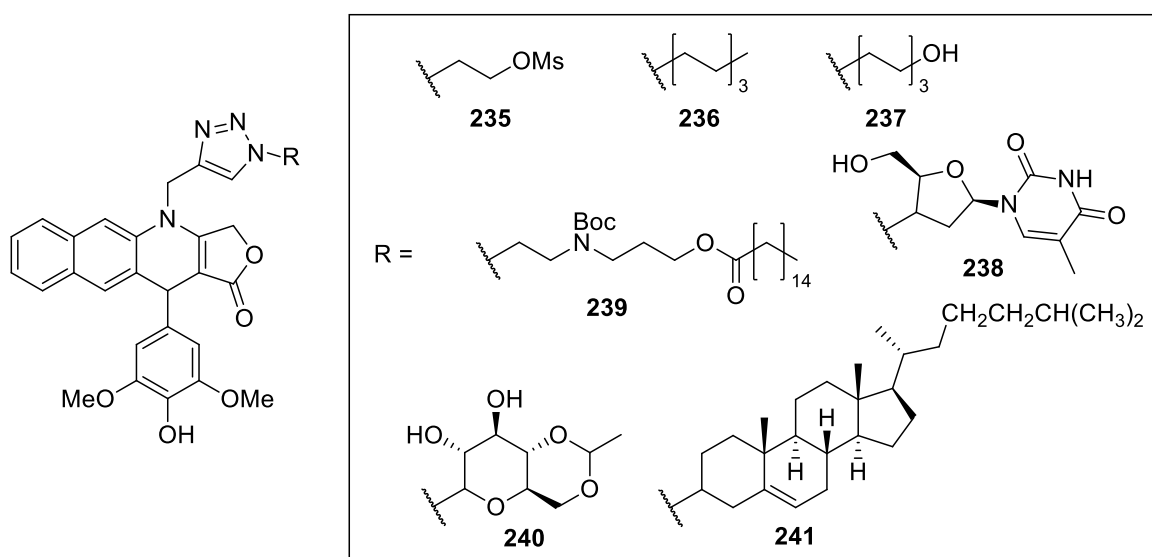
Figure 96: 2nd generation library of novel analogues.

Since the 3,5-dibromo-4-hydroxyphenyl analogues proved to have very good anticancer activity against the WHCO1 oesophageal cancer cell line, the deacylated analogue of compound **229**, compound **250** (Figure 97) will also be synthesized and tested for its antiproliferative activity.

177: IC$_{50}$ = 2.70 μM

229: R = Ac; IC$_{50}$ = 13.9 μM
250: R = H; IC$_{50}$ = ?
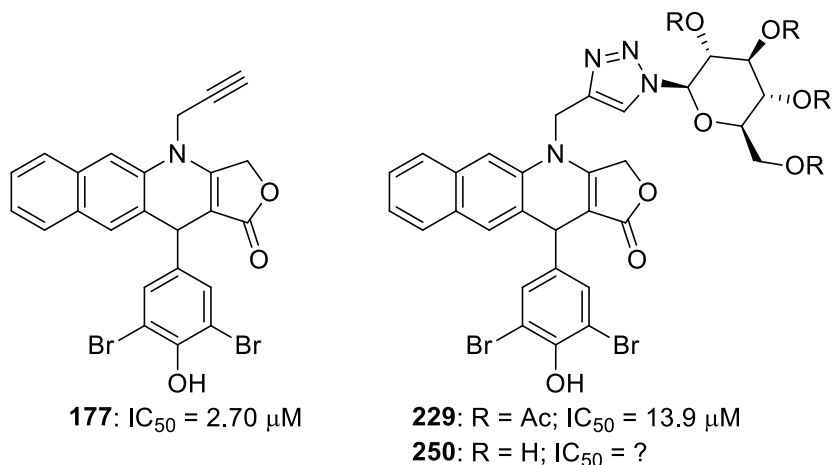
Figure 97: Compound **250** to be synthesized, based on the good anticancer activity of its two precursors, compounds **177** and **229**.

Most of our active analogues were those that retained the 4-hydroxy group on the pendent E-ring. These would thus serve as good candidates to investigate in terms of prodrug applications. Etopophos (**55c**) has been widely used as the water-soluble prodrug of etoposide (**55a**) and based on this, new probes have been investigating the use of new enzymatically cleavable groups.

55c

251: R = OMe
252: R = Br
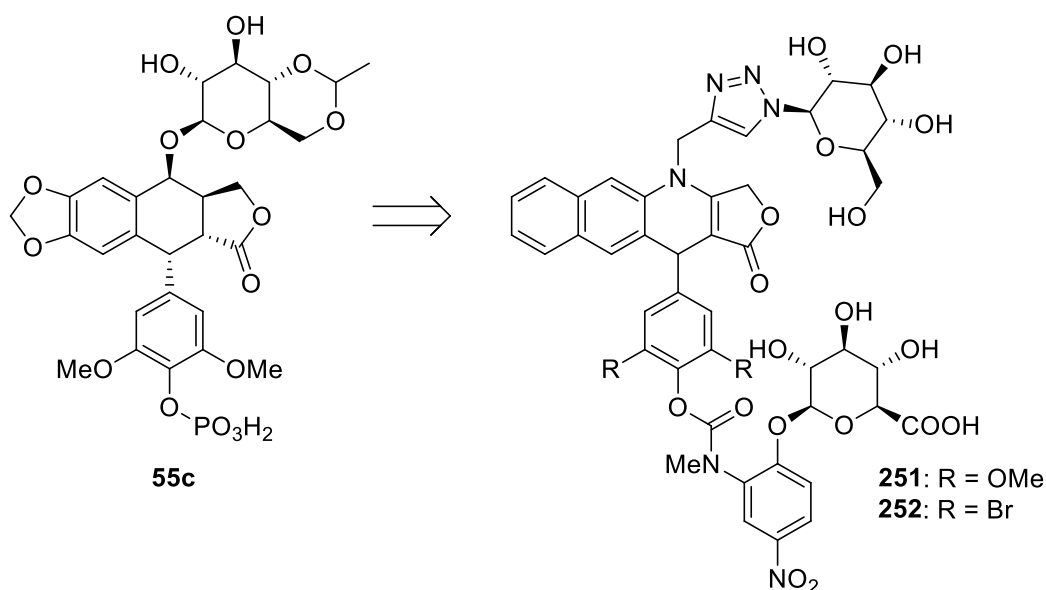
Figure 98: Etopophos (**55c**) and proposed glucuronide derivatives.

One such group, is the glucuronide group as reported by Schmidt and Monneret.[176] This group was found to increase the water-solubility of etoposide (**55a**) and underwent selective cleavage in tumour cells by means of an enzyme, β-glucuronidase. Schmidt and Monneret reported an IC_{50} value of 50.2 μM for the glucuronide derivative of etoposide against the leukemia cell line, L1210. Once the glucuronide group was cleaved by β-glucuronidase, the IC_{50} value of etoposide was retained against this cell line (0.93 μM) and the researchers remarked on the detoxifying effect of this prodrug group. They also reported that this prodrug group is stable at a pH of 7.2 in the absence of β-glucuronidase.[176] Investigating the effect of the glucuronide group (compounds **251** and **252**) on an active compound such as compound **231** or a compound yet to be synthesized, compound **250**, would seem to be a valuable endeavour.

As was shown by Magedov and co-workers, the *R*-isomers of 4-azapodophyllotoxins are up to four orders of magnitude more active than the *S*-isomers (this was discussed earlier in Section 2.1, *Natural Products in Chemistry*).[29] Therefore, it would be beneficial to investigate the difference in activity between the *R*- and *S*-isomers of our most active novel analogues (Figure 99).

R-**180**: R_1 = NO_2
R-**183**: R_1 = F
R-**186**: R_1 = H

R-**231**: R_2 = H
R-**232**: R_2 = CH_3
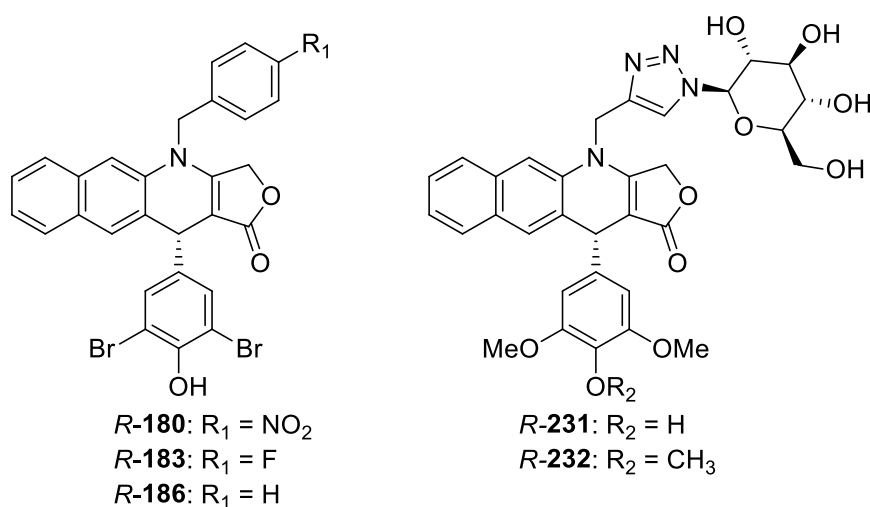
Figure 99: *R*-isomers of some of our most active analogues.

This separation could be achieved through the use of chiral high pressure liquid chromatography (HPLC), as was reported by Magedov and co-workers when they reported the great difference in activity between the *R*- and *S*-isomers (this exampled was discussed in the chapter *Natural Products in Chemistry* (Section 2.1).[29] However, as these MCRs produce racemates, this will lead to the generation of the unwanted *S*-isomer as well and an asymmetric approach would have to be considered. As the multicomponent reaction to generate the 4-azapodophyllotoxins discussed in this dissertation is derived from the

Hantzsch 1,4-dihydropyridine synthesis, it is necessary to consider the literature with regards to asymmetric variations of this method. Dondoni and co-workers investigated the use of chiral glycoconjugates in MCRs so as to determine whether the chirality of one of the starting materials would influence the diastereoselectivity of the reaction.[177] The chirality of the enamine **253** (Scheme 58) had very little effect on the diastereoselectivity of the product, compound **254**, as the desired diastereomer was isolated in a poor diastereomer excess of 20%.
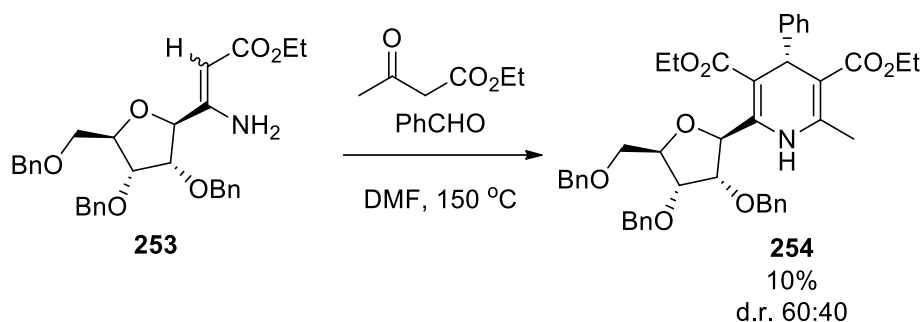
Scheme 57: MCR reported by Dondoni and co-workers.[177]

It does therefore seem that a catalyst that introduces chirality would be needed and work by Gong and co-workers does suggest that the addition of a chiral phosphonic acid could deliver a 1,4-dihydropyridine scaffold with a specific chirality in the C4 position.[178]
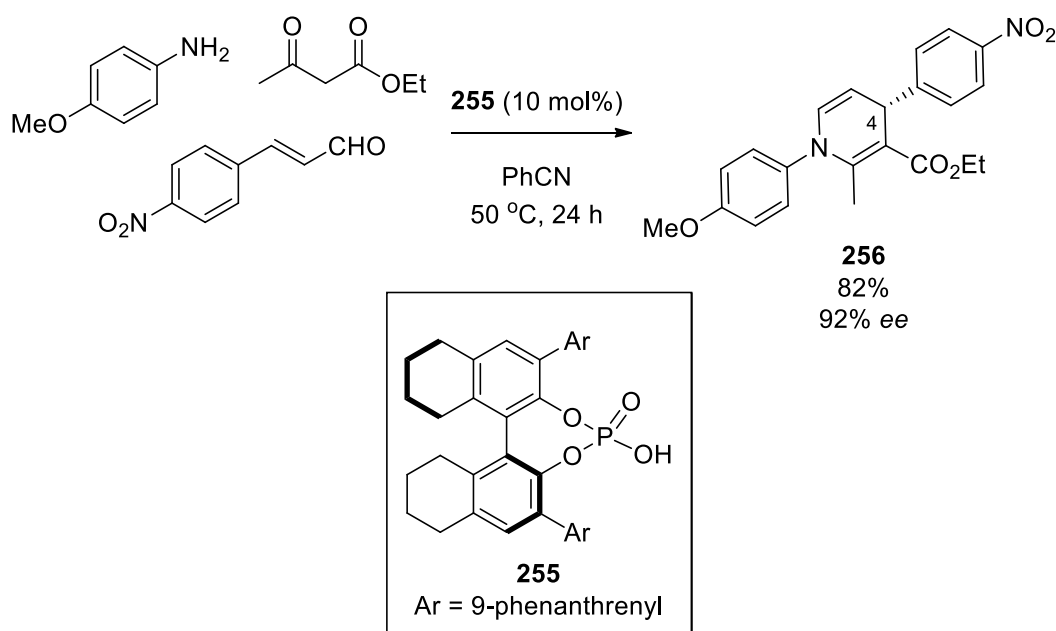
Scheme 58: Enantioselective synthesis of compound **256** reported by Gong and co-workers.[178]

167

The study investigated the use of BINOL-derived phosphonic acids, such as compound **255**, to afford products in fair to good enantiomeric excess (*ee*). A representative example is shown in Scheme 59, where compound **256** was synthesized in a good yield of 82% with an *ee* of 92%.

If this strategy could be employed in the synthesis of 4-azapodophyllotoxin analogues so as to more reliably produce the *R*-isomer, compounds with greater activity could potentially be produced.

In terms of insights gained during this study, there are also interesting variations of the AB-ring system to be explored. The strong intercalatory interactions of the linear fused-polyphenyl ring motifs with the guanine base of the DNA strand in the active pockets. The work by Lee and co-workers served as the main inspiration for this line of enquiry, as their novel phenazine podophyllotoxin analogues were not only found to be very active, but retained activity against etoposide resistant cancer cell lines such as KB/7d. Thus, novel compounds such as compounds **257a-c**, **258a-c** and **259a-c** (Figure 100) could be interesting compounds to investigate.

180: R = NO$_2$ IC$_{50}$ = 15.33 μM
183: R = F   IC$_{50}$ = 22.43 μM
186: R = H   IC$_{50}$ = 20.94 μM

257a-c: X$_1$ = CH, X$_2$ = H
258a-c: X$_1$ = N, X$_2$ = H
259a-c: X1 = N, X$_2$ = Cl
a: R$_1$ = NO$_2$; **b**: R$_1$ = F; **c**: R$_1$ = H
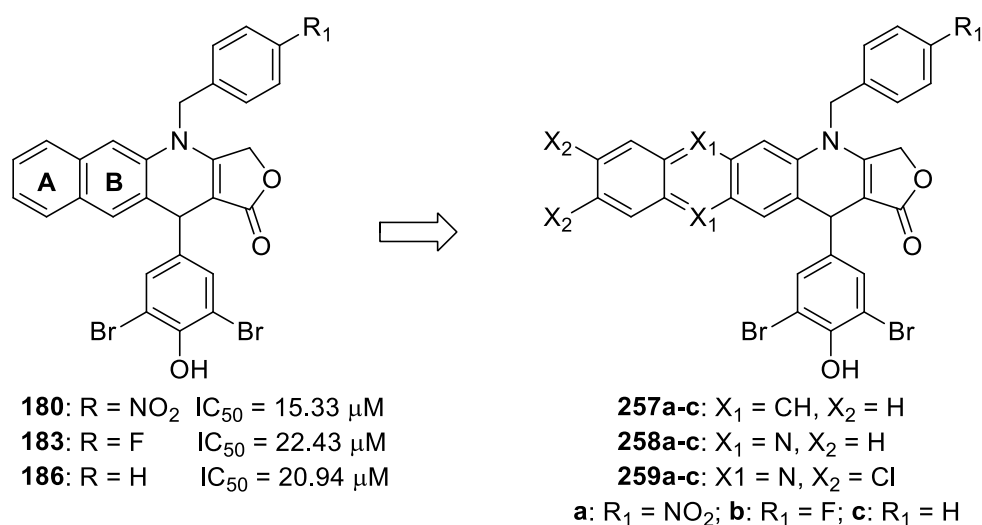
Figure 100: Proposed novel analogues based on active compounds **180**, **183** and **186**.

Finally, the exploration of compounds such as compound **173** (Figure 101) still hold merit, as the non-functionalized analogues (compound **97e**, Figure 101) reported by Magedov and co-workers had very promising biological activity profiles.[29] As the *N*-functionalized α-naphthylamines proved difficult to introduce to the 4-azapodophyllotoxin scaffold through a MCR approach, but α-naphthylamine (**131**) could be used to give compounds such as compound **97e**.
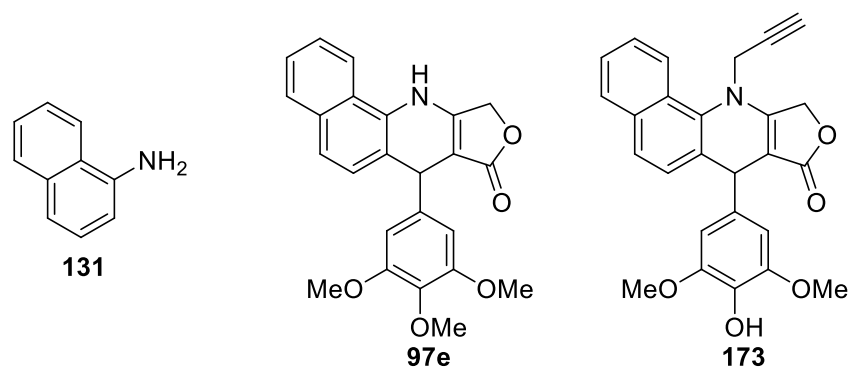
Figure 101: α-Naphthylamine (**131**) and representative analogues, compounds **97e** and **173**.

A possible strategy would therefore be the use of a scaffold such as compound **97e** as a starting point for functionalization and introducing the different groups to the 4*N*-position after the synthesis of the main scaffold by means of a MCR (Scheme 60).
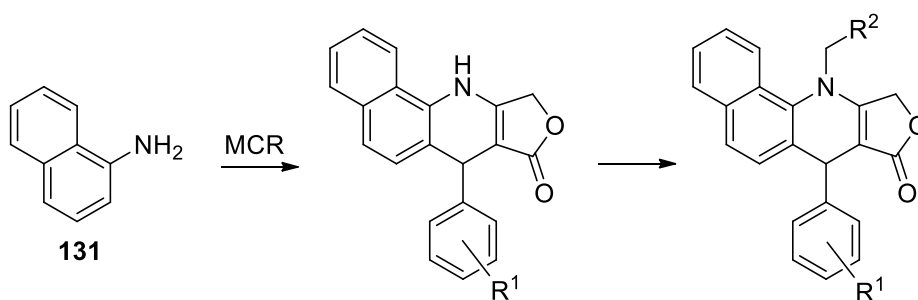
Scheme 59: Simplified scheme to generate the α-naphthylamine-based 4*N*-functionalized 4-azapodophyllotoxin analogues.

This would involve overcoming the low yields of synthesizing analogues such as compound **97e** and then optimizing the functionalization of the 4*N*-position.

9.1 Supporting Information

9.1.1 General information regarding experimental procedures

1.   Chemicals and solvents

The chemicals used in this study were purchased from Sigma Aldrich, Alfa Aesar and Merck, or otherwise obtained from the chemical stores of the De Beers Chemical building. When the compounds obtained from the De Beers chemical stores were not of sufficient purity, these compounds were purified using procedures described in Purification of Laboratory Chemicals.[179] Common laboratory solvents used for the work up of reactions such as ethyl acetate, CH_2Cl_2 and hexane were distilled open to the atmosphere before use and were used for TLC plate separation and column chromatography. In experiments that required the use of dry solvents, these solvents were distilled under inert conditions over a suitable drying agents: CH_2Cl_2 and acetonitrile over calcium hydride, toluene and tetrahydrofuran (THF) over sodium (benzophenone as indicator for the THF still). These solvents were stored over 4 Å molecular sieves upon distillation.

2.   Laboratory equipment and consumables

For reactions that required conventional heating, magnetic heater stirrers with temperature probes were used along with silicon oil baths. Solvents were removed *in vacuo* through the use of Büchi RII Rotovapor rotary evaporators with Büchi V-700 Vacuum Pumps, equipped with V-850 Vacuum controllers, and in preparation for analysis by nuclear magnetic resonance spectroscopy, compounds were dried using Edwards H-5 High Vacuum Pumps, capable of sustaining a vacuum of 0.08 mmHg. Upon cleaning, glassware items were placed in an oven maintained at a temperature of 70 °C. Synthesised compounds were stored in Bosch refrigerators and freezers, kept at 2 °C and -22 °C, respectively.

Machery-Nagel ALUGRAM® Xtra SIL G UV254 aluminium sheets were used for thin layer chromatography (TLC) analyses and a 254 nm UV light used for visualization. Various stains were used for the permanent development of TLC plates, including ninhydrin, potassium permanganate, cerium ammonium molybdate and *p*-anisaldehyde and iodine on silica. Purification was done by means of column chromatography, either by gravity separation or by Combiflash® (Model R_f 150 by Teledyne ISCO). Merck silica gel (particle size range of 0.063-0.200 mm with 60 Å pores) was used for both methods.

3.   Analysis equipment

NMR spectra were recorded on the instruments of the Central Analytical Facility (CAF) of Stellenbosch University. A 300 MHz Varian VNMRS spectrometer and a 400 MHz Varian Unity

Inova spectrometer were used for the recording of ^{1}H NMR spectra (75 MHz and 101 MHz on these two instruments respectively for ^{13}C NMR spectra).

9.2 Synthetic Procedures

The peaks of the first compound in every series will be fully assigned as representative of the members of the given series. Where compounds corresponded to literature reported values, the corresponding reference will be given.

9.2.1 General Procedure for the synthesis of *N*-propargyl naphthylamine analogues

The synthesis of the *N*-propargyl arylamines followed the same general procedure:

Propargyl bromide (80% in toluene)(1.1 eq.) was slowly added to a strirring solution of arylamine (1 eq.) and K_2CO_3 (anh.)(1 eq.) in DMF (20 mL) and stirred for 48 hours. The reaction mixture was diluted with water (dist.)(30 mL) and extracted with EtOAc (3 x 20 mL). The combined organic layers were subsequently washed with water (2 x 30 mL), isolated and dried over $MgSO_4$. The solvent was removed *in vacuo* and the resulting crude was purified by column chromatography.

The analytical data for the individual compounds are reported below:
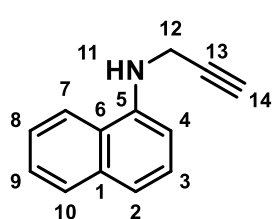
N-(prop-2-yn-1-yl)naphthalen-1-amine (*N*-propargyl-α-naphthylamine).

Orange solid (799 mg, 63% yield).

Melting Point: 71 -73 °C

NMR (300 MHz, CDCl₃) δ 7.90 – 7.76 (m, 2H, H7 & H10), 7.55 – 7.30 (m, 4H, H2, H3, H8 & H9), 6.75 (d, *J* = 6.3 Hz, 1H, H4), 4.13 (d, *J* = 2.0 Hz, 2H, H12), 2.31 (t, *J* = 2.0 Hz, 1H, H14)

¹³C NMR (75 MHz, CDCl₃) δ 142.1 (C5), 134.2 (C1), 128.7 (C10), 126.3 (C3), 125.9 (C9), 125.0 (C8), 123.8 (C7), 119.9 (C6), 118.8 (C2), 105.5 (C4), 80.9 (C13), 71.7 (C14), 33.9 (C12).

HRMS: calcd for $C_{13}H_{12}N^+$ [M + H]⁺, 182.0970 – found 182.0967.
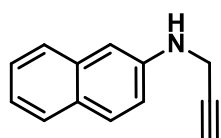
N-(prop-2-yn-1-yl)naphthalen-2-amine (**N-propargyl-β-naphthylamine)**.

Yellow oil (381 mg, 30% yield).

NMR (300 MHz, CDCl$_3$) δ 7.94 – 7.72 (m, 3H), 7.52 (ddd, J = 8.2, 6.9, 1.3 Hz, 1H), 7.48 – 7.32 (m, 1H), 7.19 – 6.91 (m, 2H), 4.05 (d, J = 2.2 Hz, 3H), 2.35 (t, J = 1.9 Hz, 1H).

^{13}C NMR (75 MHz, CDCl$_3$) δ 145.9, 136.3, 130.4, 129.5, 129.4, 129.3, 127.7, 124.0, 119.4, 107.1, 82.4, 72.9, 35.0.

HRMS: calcd for $C_{13}H_{12}N^+$ [M + H]$^+$, 182.0970 – found 182.0965.
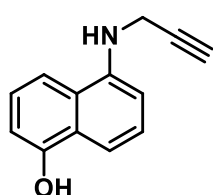
5-(prop-2-yn-1-ylamino)naphthalen-1-ol.

Dark purple solid (929 mg, 75% yield).

NMR (300 MHz, CDCl$_3$) δ 9.10 (d, J = 8.5 Hz, 1H), 8.88 – 8.79 (m, 2H), 8.70 (dd, J = 9.0, 6.9 Hz, 1H), 8.22 (dd, J = 15.1, 7.5 Hz, 2H), 5.55 (d, J = 2.4 Hz, 2H), 3.73 (t, J = 2.4 Hz, 1H).

^{13}C NMR (75 MHz, CDCl$_3$) δ 152.1, 142.1, 125.8, 125.3, 125.2, 112.7, 112.1, 109.2, 106.3, 80.9, 71.8, 34.0.

HRMS: calcd for $C_{13}H_{12}NO^+$ [M + H]$^+$, 198.0919 – found 198.0912.
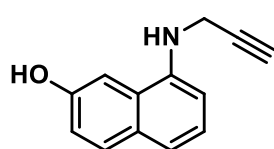
8-(Prop-2-yn-1-ylamino)naphthalen-2-ol.

Dark brown solid (40 mg, 3% yield).

NMR (300 MHz, CDCl$_3$) δ 7.68 (d, J = 8.8 Hz, 1H), 7.47 (dd, J = 10.1, 5.2 Hz, 2H), 7.28 – 7.16 (m, 2H), 7.04 (dd, J = 8.8, 2.6 Hz, 1H), 5.15 (s, 1H), 4.00 (d, J = 2.4 Hz, 2H), 2.23 (t, J = 2.3 Hz, 1H).

^{13}C NMR (75 MHz, CDCl$_3$) δ 154.0, 130.7, 125.0, 123.2, 118.8, 117.9, 105.6, 79.5, 73.5, 42.4.

HRMS: calcd for $C_{13}H_{12}NO^+$ [M + H]$^+$, 198.0919 – found 198.0925.
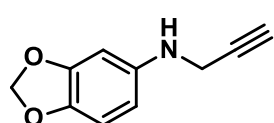
N-(Prop-2-yn-1-yl)benzo[d][1,3]dioxol-5-amine.

Yellow Oil (309.6 mg, 48% yield).

NMR (300 MHz, CDCl$_3$) δ 6.69 (d, J = 8.3 Hz, 1H), 6.32 (d, J = 2.2 Hz, 1H), 6.13 (d, J = 8.3 Hz, 1H), 5.86 (s, 2H), 3.86 (d, J = 2.2 Hz, 2H), 2.28 – 2.17 (m, 1H).

¹³C NMR (75 MHz, CDCl₃) δ 148.6, 142.7, 140.8, 108.8, 105.7, 101.0, 97.1, 81.4, 71.7, 34.8.

HRMS: calcd for $C_{10}H_{10}NO_2^+$ [M + H]⁺, 176.0712 – found 176.0709.
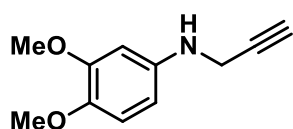
3,4-Dimethoxy-*N*-(prop-2-yn-1-yl)aniline.

Light brown oil (265.2 mg, 21% yield).

NMR (300 MHz, CDCl₃) δ 6.76 (d, *J* = 8.5 Hz, 1H), 6.31 (d, *J* = 2.4 Hz, 1H), 6.23 (dd, *J* = 8.5, 2.3 Hz, 1H), 3.88 (d, *J* = 2.2 Hz, 2H), 3.83 (s, 3H), 3.80 (s, 3H), 2.21 (t, *J* = 2.2 Hz, 1H).

¹³C NMR (75 MHz, CDCl₃) δ 150.1, 142.6, 141.8, 113.1, 104.7, 100.0, 81.5, 71.5, 56.8, 56.0, 34.7.

HRMS: calcd for $C_{11}H_{14}NO_2^+$ [M + H]⁺, 192.1025 – found 192.1032.

9.2.2 General Procedure for the synthesis of *N*-benzyl naphthylamine analogues

The various *N*-benzyl naphthylamine analogues were synthesized according to the following general procedure:

The benzaldehyde (1.05 eq) was added to a stirring solution of ZnBr (anh.)(1.1 eq) in acetonitrile (15 mL). Once all the solid had dissolved, naphthylamine (1 eq.) was added. The reaction was monitored by thin layer chromatography and upon consumption of naphthylamine, boric acid (1.1 eq.) and sodium borohydride (20 eq.) was added to the reaction mixture and the reaction stirred for 4 hours. The reaction mixture was then diluted with water (dist.)(15 mL) and saturated NaHCO₃ solution (15 mL). The mixture was then extracted with DCM (3 x 15 mL) and the organic layers combined. The combined organic layers were combined, dried over MgSO₄ (anh.) and concentrated *in vacuo*. The product was then purified by column chromatography.

The analytical data for the individual compounds are reported below:
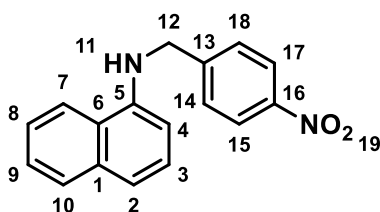
N-(4-nitrobenzyl)naphthalen-1-amine.

Dark orange solid (321 mg, 91% yield)

Melting Point: 108 – 116 ⁰C

NMR (300 MHz, CDCl₃) δ 8.15 – 8.08 (m, 2H, H15 & H17), 8.05 (dq, *J* = 6.8, 3.2 Hz, 1H, N-H11), 7.79 – 7.72 (m, 1H, H2), 7.58 – 7.52 (m, 2H, H14 & H18), 7.48 – 7.41 (m, 2H, H8 & H9), 7.22 – 7.13 (m, 2H, H7 & H10), 6.32 (dd, *J* = 6.3, 2.3 Hz, 1H, H4), 5.93 (t, *J* = 5.6 Hz, 1H, H3), 4.61 (d, *J* = 5.6 Hz, 2H, H12).

¹³C NMR (75 MHz, CDCl₃) δ 152.7 (C16), 151.7 (C13), 147.6 (C5), 139.1 (C1), 133.2 (C10), 132.5 (C14), 131.7 (C18), 131.3 (C4), 130.6 (C9), 129.4 (C8), 128.6 (C15), 127.9 (C17), 125.6 (C7), 122.1 (C6), 109.3 (C2), 52.0 (C12).

HRMS: calcd for $C_{17}H_{15}N_2O_2^+$ [M + H]⁺, 279.1134 – found 279.1132.
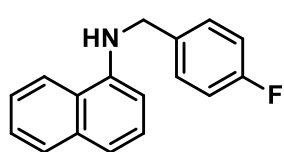
N-(4-fluorobenzyl)naphthalen-1-amine.

Thick red oil (469 mg, 89% yield).

NMR (300 MHz, CDCl₃) δ 7.84 (d, *J* = 7.6 Hz, 2H), 7.57 − 7.27 (m, 6H), 7.09 (t, *J* = 8.6 Hz, 2H), 6.63 (d, *J* = 7.2 Hz, 1H), 4.69 (s, 1H), 4.48 (s, 2H).

¹³C NMR (75 MHz, CDCl₃) δ 163.9, 160.6, 143.1, 134.9, 134.4, 129.3, 128.9, 126.7, 125.9, 125.0, 123.5, 120.0, 118.0, 115.8, 115.5, 104.9, 48.0.

HRMS: calcd for $C_{17}H_{15}NF^+$ [M + H]⁺, 252.1189 – found 252.1188.
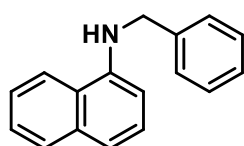
N-(benzyl)naphthalen-1-amine.

Light orange oil (686 mg, 42% yield)

NMR (300 MHz, CDCl₃) δ 7.87 − 7.79 (m, 2H), 7.51 − 7.43 (m, 4H), 7.43 − 7.26 (m, 5H), 6.65 (d, *J* = 7.4 Hz, 1H), 4.71 (s, 1H), 4.52 (s, 2H).

¹³C NMR (75 MHz, CDCl₃) δ 143.4, 139.2, 134.4, 128.9, 127.9, 127.5, 126.7, 125.9, 124.9, 123.5, 120.0, 117.8, 104.9, 48.8.

HRMS: calcd for $C_{17}H_{16}N^+$ [M + H]⁺, 234.1283 – found 234.1274.
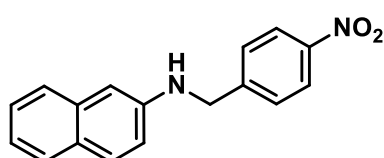
N-(4-nitrobenzyl)naphthalen-2-amine.

Dark yellow oil (778 mg, 90% yield).

174

NMR (300 MHz, CDCl₃) δ 8.19 (d, J = 8.7 Hz, 2H), 7.68 (dd, J = 8.2, 5.9 Hz, 2H), 7.55 (dd, J = 8.3, 4.4 Hz, 3H), 7.36 (ddd, J = 8.2, 6.9, 1.2 Hz, 1H), 7.26 – 7.19 (m, 1H), 6.94 (dd, J = 8.8, 2.4 Hz, 1H), 6.70 (s, 1H), 4.57 (s, 2H), 4.39 (s, 1H).

¹³C NMR (75 MHz, CDCl₃) δ 147.3, 146.1, 144.9, 134.3, 128.1, 127.1, 126.7, 125.5, 125.0, 122.9, 121.1, 117.4, 103.3, 46.3.

HRMS: calcd for $C_{17}H_{15}N_2O_2^+$ [M + H]⁺, 279.1134 – found 279.1125.
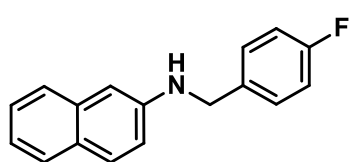
N-(4-fluorobenzyl)naphthalen-2-amine.

Light pink oil (438 mg, 83% yield).

NMR (300 MHz, CDCl₃) δ 7.71 – 7.56 (m, 3H), 7.41 – 7.35 (m, 2H), 7.22 (ddd, J = 8.1, 6.9, 1.2 Hz, 1H), 7.05 (ddd, J = 9.5, 5.8, 2.5 Hz, 2H), 6.92 (dd, J = 8.8, 2.4 Hz, 1H), 6.82 (d, J = 2.3 Hz, 1H), 4.41 (s, 2H), 4.17 (s, 1H).

¹³C NMR (75 MHz, CDCl₃) δ 163.9, 160.6, 145.7, 135.4, 134.8, 129.4, 129.0, 127.8, 126.5, 126.1, 122.3, 117.9, 115.8, 115.5, 104.9, 47.8.

HRMS: calcd for $C_{17}H_{15}NF^+$ [M + H]⁺, 252.1189 – found 252.1187.
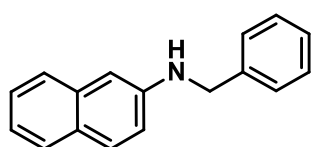
N-(benzyl)naphthalen-2-amine.

Yellow oil (883.4 mg, 54% yield).

NMR (300 MHz, CDCl₃) δ 7.73 – 7.60 (m, 3H), 7.47 – 7.29 (m, 6H), 7.26 – 7.18 (m, 1H), 6.93 (dt, J = 6.3, 3.2 Hz, 1H), 6.86 (t, J = 4.9 Hz, 1H), 4.46 (s, 2H), 4.19 (s, 1H).

¹³C NMR (75 MHz, CDCl₃) δ 145.9, 139.3, 135.3, 235.7, 126.0, 132.3, 129.3, 132.3, 128.1, 132.3, 126.6, 122.2, 118.0, 104.8, 48.5.

HRMS: calcd for $C_{17}H_{16}N^+$ [M + H]⁺, 234.1283 – found 234.1276.

9.2.3 Synthesis of azides
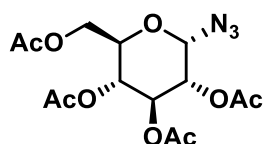
(2*R*,3*R*,4*S*,5*R*,6*S*)-2-(acetoxymethyl)-6-azidotetrahydro-2*H*-pyran-3,4,5-triyl triacetate (2,3,4,6-tetra-O-acetyl-α-D-glucopyranosyl azide).

D-glucose in (500 mg, 2.78 mmol) in DCM (10 mL) was added to a stirring solution of acetic anhydride (1.63 mL, 17.2 mmol) in pyridine (15 mL) at 0 °C. After 24 hours, the starting material was consumed according to analysis by TLC and the reaction was quenched with methanol (10 mL) and water (dist.) was added (20 mL). The solid was collected by vacuum filtration and dissolved in DCM (20 mL). The reaction mixture was cooled on ice bath and hydrobromic acid (50% in acetic acid (glacial) (v/v)) (10 mL) was slowly added. The reaction was then allowed to warm to room temperature and stirred for 8 hours, before it was quenched with a saturated solution of sodium bicarbonate (30 mL). The reaction mixture was extracted with DCM (3 x 30 mL) and concentrated *in vacuo*. The product was redissolved in MeCN (30 mL) and sodium azide (181 mg, 2.78 mmol) was added. The reaction mixture was stirred for 3 hours at room temperature and then quenched with a saturated solution of sodium bicarbonate (30 mL). The product was extracted with DCM (3 x 30 mL), dried over $MgSO_4$ (anh.) and concentrated *in vacuo*. Recrystallization from methanol afforded the desired product as a white solid (996 mg, 88% yield).[136]

NMR (300 MHz, CDCl₃) δ 5.23 (dd, J = 9.4, 9.4 Hz, 1H), 5.10 (dd, J = 9.8, 9. Hz, 1H), 4.94 (dd, J = 15.9, 6.5 Hz, 1H), 4.65 (d, J = 8.8 Hz, 1H), 4.28 (dd, J = 12.5, 4.8 Hz, 1H), 4.17 (dd, J = 12.5, 2.4 Hz, 1H), 3.79 (ddd, J = 9.9, 4.7, 2.4 Hz, 1H), 2.10 (s, 3H), 2.07 (s, 3H), 2.03 (s, 3H), 2.01 (s, 3H).
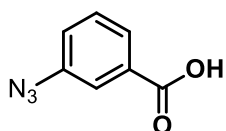
3-Azidobenzoic Acid.

3-Aminobenzoic acid (250 mg, 1.82 mmol) and *p*-toluenesulfonic acid (2.83 g, 16.4 mmol) were added to a stirring solution of water (dist.)(40 mL). Once all solids have dissolved, sodium Nitrite (1.13 g, 16.4 mmol) was added and the reaction mixture stirred for another 45 minutes. Sodium azide (190 mg, 2.92 mmol) was then added and the mixture stirred for another 20 minutes. The reaction mixture was then diluted with water (dist.)(40 mL) and extracted with DCM (3 X 20 mL). The combined organic layers were dried over $MgSO_4$ (anh.) and concentrated *in vacuo* to give the product as a light yellow solid (247 mg, 83% yield).[139]

NMR (300 MHz, CDCl₃): δ 8.09 (d, *J* = 8.0 Hz, 1H), 7.98 (s, 1H), 7.72 (t, *J* = 7.9 Hz, 1H), 7.50 (dd, *J* = 8.0, 2.4 Hz, 1H).

¹³C NMR (75 MHz, CDCl₃): δ 168.3, 141.0, 132.9, 130.3, 126.6, 123.8, 120.5.

IR (ATR, cm⁻¹): 2824, 2548, 2127, 1684, 1584, 1451, 1415, 1302, 1260, 930, 892, 750, 697, 672, 562

HRMS: calcd for $C_7H_4N_3O_2^+$ [M + H]⁺, 162.0304 – found 162.0309.
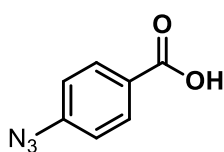
4-Azidobenzoic acid

4-Aminobenzoic acid (250 mg, 1.82 mmol) and *p*-toluenesulfonic acid (2.83 g, 16.4 mmol) were added to a stirring solution of water (dist.)(40 mL). Once all solids have dissolved, sodium Nitrite (1.13 g, 16.4 mmol) was added and the reaction mixture stirred for another 45 minutes. Sodium azide (190 mg, 2.92 mmol) was then added and the mixture stirred for another 20 minutes. The reaction mixture was then diluted with water (dist.)(40 mL) and extracted with DCM (3 X 20 mL). The combined organic layers were dried over $MgSO_4$ (anh.) and concentrated *in vacuo* to give the product as a light yellow solid (228 mg, 77% yield).[139]

^{1}H NMR (300 MHz, CD$_3$OD): δ 7.78 (d, *J* = 8.6 Hz, 2H), 6.83 (d, *J* = 8.6 Hz, 2H).

^{13}C NMR (75 MHz, CD$_3$OD): δ 168.6, 145.2, 132.0, 127.6, 119.2.

IR (ATR, cm^{-1}): 2810, 2541, 2403, 2099, 1674, 1600, 1426, 1281, 1175, 1118, 934, 860, 764, 690, 555.

HRMS: calcd for $C_7H_4N_3O_2^+$ [M + H]$^+$, 162.0304 – found 162.0303.
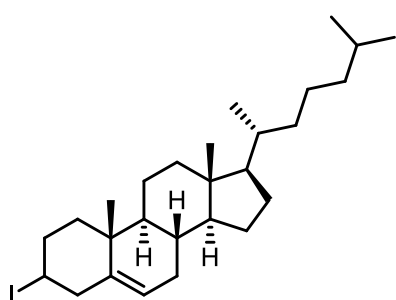
(8*S*,9*S*,10*R*,13*R*,14*S*,17*R*)-3-iodo-10,13-dimethyl-17-((*R*)-6-methylheptan-2-yl)-2,3,4,7,8,9,10,11,12,13,14,15,16,17-tetradecahydro-1*H*-cyclopenta[*a*]phenanthrene (Cholesteryl Iodide).

To a stirring solution of sodium iodide (982 mg, 6.55 mmol) in acetone (20 mL, was added cholesteryl chloroformate (0.25 g, 0.55 mmol) and diethyl ether (3 mL). The solution was stirred at room temperature for 72 hours. The reaction was then condensed *in vacuo* and distilled water (30 mL) was added. The solid was collected under vacuum filtration and then recrystallized from acetone to give a white solid (148 mg, 54% yield).

Melting Point: 107 – 109 °C.

NMR (300 MHz, CDCl$_3$) : δ 5.44 – 5.18 (m, 1H), 4.05 (tt, *J* = 12.6, 4.5 Hz, 1H), 3.03 – 2.87 (m, 1H), 2.68 (ddd, *J* = 13.5, 4.5, 2.2 Hz, 1H), 2.36 – 2.13 (m, 2H), 2.10 – 1.93 (m, 2H), 1.91 – 1.79 (m, 1H), 1.74 (dt, *J* = 13.3, 3.3 Hz, 1H), 1.64 – 0.95 (m, 23H), 0.92 (d, *J* = 6.4 Hz, 3H), 0.87 (dd, *J* = 6.6, 1.7 Hz, 6H), 0.68 (s, 3H).
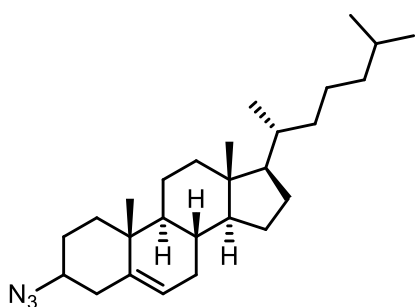
(8*S*,9*S*,10*R*,13*R*,14*S*,17*R*)-3-azido-10,13-dimethyl-17-((*R*)-6-methylheptan-2-yl)-2,3,4,7,8,9,10,11,12,13,14,15,16,17-tetradecahydro-1*H*-cyclopenta[*a*]phenanthrene (Cholesteryl Azide).

Cholesteryl Iodide (87 mg, 0.18 mmol) was added to a stirring solution of DMSO (5 mL) and sodium azide (23 mg, 0. 35 mmol) was added. The reaction was stirred at room temperature for 6 hours. The reaction mixture was then diluted with water (dist.)(40 mL) and the resulting white precipitate was filtered off and dried under high vacuum to give a white crystalline solid (64 mg, 89% yield).

IR (ATR, cm^{-1}) 2932, 2868, 2849, 2129, 1726, 1467, 1230, 995, 979, 752.

2-Azidoethyl methanesulfonate.

Sodium Azide (1.8 g, 28 mmol) was added to a stirring solution of 2-bromoethanol (2.0 mL, 28 mmol) in THF (15 mL) and stirred for 12 hours. Methanesulfonyl chloride (2.4 mL, 31 mmol) and triethylamine (4.4 mL, 31 mmol) were then added to the reaction mixture and stirred for another 6 hours. The orange precipitate that formed was filtered off and the mother liquor was concentrated *in vacuo*. The resulting crude product was purified by column chromatography to give a colourless liquid (4.3 g, 93% yield).

NMR (300 MHz, CDCl$_3$) : δ 4.28 (t, *J* = 4.9 Hz, 2H), 3.56 (t, *J* = 4.9 Hz, 2H).

IR (ATR, cm^{-1}): 2139, 1348, 1284, 1165, 1058.
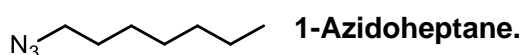
1-Azidoheptane.

Sodium azide (413 mg, 6.36 mmol) and 1-bromoheptane (0.500 mL, 3.18 mmol) were added to a stirring solution of DMF (10 mL) and heated to 75 °C. The reaction mixture was stirred overnight and then diluted with water. The resulting mixture was extracted with DCM (2 x 15 mL), the organic layer was isolated and dried over MgSO$_4$ (anh.). The organic layer was then condensed *in vacuo* to give a clear liquid (142 mg, 32% yield).

^{1}H NMR (400 MHz, CDCl$_3$) δ 3.24 (t, J = 7.0 Hz, 2H), 2.96 – 2.85 (m, 2H), 1.63 – 1.53 (m, 2H), 1.41 – 1.19 (m, 6H), 0.88 (dd, J = 8.8, 5.0 Hz, 3H).

IR (ATR, cm^{-1}): 2957, 2928, 2858, 2090, 1458, 1259.
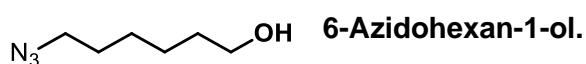
6-Azidohexan-1-ol.

Sodium azide (268 mg, 4.12 mmol) and 6-bromohexan-1-ol (0.500 mL, 3.45 mmol) were added to a stirring solution of THF (10 mL) and stirred for 12 hours. The reaction mixture was diluted with water and extracted with diethyl ether (2 x 10 mL). The organic layer was isolated,

dried over MgSO$_4$ (anh.) and then concentrated *in vacuo* to give a colourless liquid (531 mg, 99% yield).

IR (ATR, cm^{-1}): 2139, 1350, 1264, 1166, 1056.

9.2.4 Multicomponent Reactions: General procedure for the synthesis under conventional heating

The multicomponent reactions under conventional heating followed the following general procedure:

Naphthylamine (1 eq.), benzaldehyde (1 eq.) and tetronic acid (1 eq.) were added to a stirring solution of ethanol and 4-chloroaniline (20 mol%). The mixture was then stirred at reflux for 96 hours. The reaction mixture was then cooled on ice and the resulting solid was collected by vacuum filtration.

The analytical data for the individual compounds are reported below:
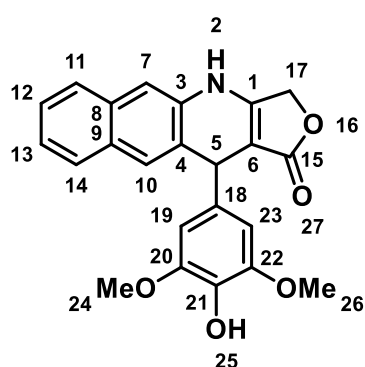
11-(4-Hydroxy-3,5-dimethoxyphenyl)-4,11-dihydrobenzo[*g*]furo[3,4-*b*]quinolin-1(3*H*)-one.

Orange powder (42 mg, 38% yield).

Melting Point: > 250 °C

NMR (300 MHz, DMSO-d$_6$): δ 10.22 (s, 1H, N-H2), 8.13 (s, 1H, H25), 8.01 – 7.84 (m, 2H, H11 & H14), 7.84 – 7.19 (m, 3H, H10, H12 & H13), 6.43 (s, 2H, H19 & H23), 5.58 (s, 1H, H5), 4.93 (q, J = 15.7 Hz, 2H, H17), 3.59 (s, 3H, H24), 3.34 (s, 3H, H26).

^{13}C NMR (75 MHz, DMSO-d$_6$): δ 172.6 (C15), 157.3 (C1), 148.2 (C20 & C22), 136.7 (C18), 135.4 (C21), 134.6 (C8), 132.4 (C9), 131.0 (C10), 129.3 (C14), 127.2 (C4), 124.2 (C11), 123.8 (C13), 118.0 (C12), 115.2 (C7), 105.9 (C19 & C23), 97.8 (C6), 65.3 (C17), 56.4 (C5), 37.2 (C24 & C26).

IR (ATR, cm^{-1}): 3481, 3260, 3113, 3061, 2991, 2950, 2932, 2883, 2834, 1708, 1644, 1610, 1586, 1533, 1514, 1455, 1425, 1403, 1357, 1329, 1294, 1273, 1255, 1241, 1226, 1195, 1811, 1152, 1127, 1106, 1078, 1030, 1020.
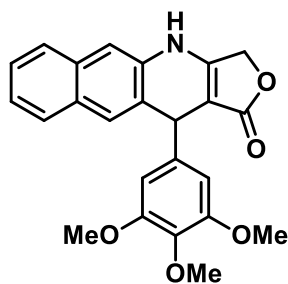
11-(3,4,5-Trimethoxyphenyl)-4,11-dihydrobenzo[*g*]furo[3,4-*b*]quinolin-1(3*H*)-one.

Light brown powder (36.3 mg, 31% yield).

Melting Point: 222 – 231 °C

NMR (300 MHz, DMSO-d₆): δ 10.28 (s, 1H), 7.86 (m, 3H), 7.49 – 7.24 (m, 3H), 6.47 (d, J = 19.6 Hz, 2H), 5.65 (s, 1H), 4.95 (q, J = 15.8 Hz, 2H), 3.59 (m, 6H), 3.35 (s, 3H).

¹³C NMR (75 MHz, DMSO-d₆): δ 172.5, 157.6, 153.0, 142.0, 136.3, 135.4, 132.3, 131.0, 129.4, 128.8, 127.3, 124.3, 123.7, 118.0, 114.9, 105.5, 97.5, 65.4, 60.3, 56.2, 37.4.

IR (ATR, cm⁻¹): 3276, 3105, 3050, 2990, 2942, 2838, 1751, 1671, 1619, 1594, 1581, 1525, 1507, 1464, 1451, 1425, 1397, 1373, 1338, 1325, 1270, 1236, 1207, 1236, 1207, 1150, 1140, 1121,
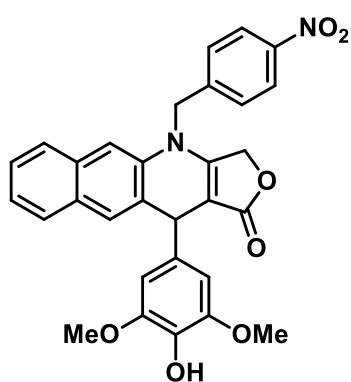
11-(4-Hydroxy-3,5-dimethoxyphenyl)-4-(4-nitrobenzyl)-4,11-dihydrobenzo[*g*]furo[3,4-*b*]quinolin-1(3*H*)-one.

Yellow-brown powder (50.4 mg, 52% yield).

Melting Point: 194 – 198 °C

¹H NMR (300 MHz, DMSO-d₆) δ 8.18 (d, J = 7.1 Hz, 4H), 7.95 (d, J = 8.3 Hz, 2H), 7.87 – 7.78 (m, 2H), 7.70 – 7.58 (m, 4H), 7.49 – 7.31 (m, 4H), 6.42 (s, 2H), 5.71 (s, 1H), 5.19 (m, 4H), , 4.43 (bs, 1H), 3.58 (s, 6H).

¹³C NMR (75 MHz, DMSO-d₆): δ 172.0, 158.2, 148.7, 147.8, 147.0, 146.4, 146.0, 144.8, 135.8, 135.3, 134.9, 134.2, 131.7, 130.4, 128.9, 128.5, 128.2, 127.8, 127.4, 127.0, 126.6, 126.0, 125.4, 124.5, 124.0, 123.3, 121.3, 118.1, 117.7, 115.2, 114.9, 105.4, 103.0, 98.8, 65.4, 62.8, 55.9, 48.8, 45.9, 36.6.

HRMS: calcd for C₃₀H₂₅N₂O₇⁺ [M + H]⁺, 525.1662 – found 525.1659.
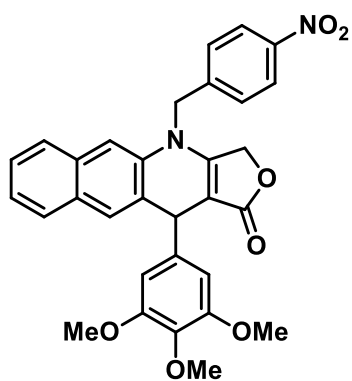
11-(3,4,5-Trimethoxyphenyl)-4-(4-nitrobenzyl)-4,11-dihydrobenzo[*g*]furo[3,4-*b*]quinolin-1(3*H*)-one.

Light brown powder (48 mg, 61% yield).

Melting Point: 224 – 227 °C

^{1}H NMR (300 MHz, DMSO-d$_6$) δ 8.21 (d, J = 7. Hz, 4H), 7.92 (d, J = 8.1 Hz, 2H), 7.95 – 7.81 (m, 2H), 7.70 – 7.62 (m, 4H), 7.51 – 7.36 (m, 4H), 6.49 (s, 2H), 5.79 (s, 1H), 5.22 (m, 4H), 3.59 (s, 6H), 3.35 (s, 3H).

^{13}C NMR (75 MHz, DMSO-d$_6$): δ 172.4, 158.9, 147.7, 146.9, 145.2, 144.8, 135.8, 132.1, 128.5, 127.8, 126.0, 125.4, 124.5, 124.0, 121.7, 118.6, 117.8, 115.6, 115.4, 105.5, 103.4, 98.9, 65.3, 60.3, 56.5, 56.1, 37.3.

IR (ATR, cm^{-1}): 1751, 1660, 1595, 1519, 1496, 1459, 1414, 1341, 1297, 1280, 1255, 1219, 1182, 1126, 1103, 1036, 1014, 999, 971, 925, 917, 858, 837, 817, 807, 792, 776, 768, 742, 684, 650, 423.

HRMS: calcd for C$_{31}$H$_{27}$N$_2$O$_7^+$ [M + H]$^+$, 539.1818 – found 539.1804.
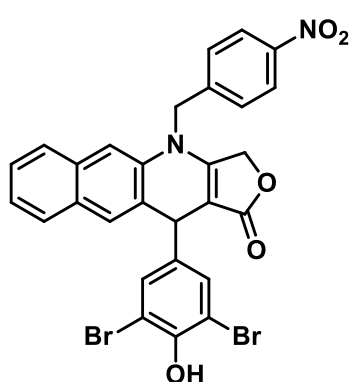
11-(3,5-Dibromo-4-hydroxyphenyl)-4-(4-nitrobenzyl)-4,11-dihydrobenzo[*g*]furo[3,4-*b*]quinolin-1(3*H*)-one.

Brown powder (62 mg, 53% yield).

Melting Point: Sample degrades above 160 °C

^{1}H NMR (300 MHz, DMSO-d$_6$): δ 8.22 (d, J = 8.8 Hz, 2H), 7.96 – 7.80 (m, 3H), 7.64 (d, J = 8.8 Hz, 2H), 7.50 – 7.33 (m, 3H), 7.28 (s, 2H), 5.81 (s, 1H), 5.42 – 5.25 (m, 4H), 4.43 (bs, 1H).

^{13}C NMR (75 MHz, DMSO-d$_6$): δ 171.8, 149.2, 146.9, 144.6, 139.6, 135.3, 131.2, 130.9 , 130.5, 129.3, 128.3, 127.8, 127.4, 124.7, 124.0, 123.5, 116.8, 116.1, 115.1, 112.0, 65.6, 62.8, 48.8, 35.2.

IR (ATR, cm^{-1}): 3187, 2863, 1732, 1619, 1594, 1492, 1407, 1388, 1282.

HRMS: calcd for C$_{28}$H$_{19}$N$_2$O$_5$Br$_2^+$ [M + H]$^+$, 620.9661 – found 620.9641.
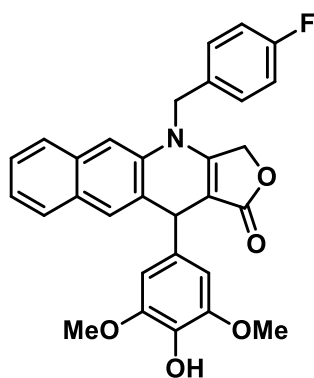
11-(4-Hydroxy-3,5-dimethoxyphenyl)-4-(4-fluorobenzyl)-4,11-dihydrobenzo[*g*]furo[3,4-*b*]quinolin-1(3*H*)-one.

Light brown powder (112.6 mg, 76% yield).

Melting Point: 209 – 213 °C

NMR (300 MHz, DMSO-d$_6$) δ 8.16 (s, 1H), 7.94 (d, *J* = 8.3 Hz, 1H), 7.89 – 7.78 (m, 2H), 7.52 – 7.31 (m, 5H), 7.18 (t, *J* = 8.8 Hz, 2H), 6.40 (s, 2H), 5.69 (s, 1H), 5.27 – 4.96 (m, 4H), 3.57 (s, 5H), 3.32 (s, 3H)

^{13}C NMR (75 MHz, DMSO-d$_6$) δ 172.1, 161.50 (d, J = 243.5 Hz), 158.3, 147.8, 135.9, 135.4, 134.1, 132.8, 131.6, 130.3, 128.6, 128.5, 128.1, 126.9, 124.4, 123.7, 117.7, 115.8 115.5, 115.1, 105.3, 98.4, 65.4, 55.9, 48.5, 36.6.

IR (ATR, cm^{-1}): 3309, 1726, 1592, 1510, 1426, 1384, 1230, 1141, 1089.

HRMS: calcd for C$_{30}$H$_{25}$NO$_5$F$^+$ [M + H]$^+$, 498.1711 – found 498.1714.
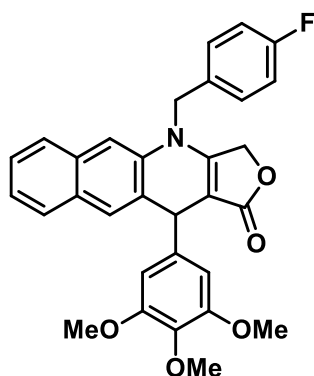
11-(3,4,5-Trimethoxyphenyl)-4-(4-fluorobenzyl)-4,11-dihydrobenzo[*g*]furo[3,4-*b*]quinolin-1(3*H*)-one.

White powder (119.3 mg, 78% yield).

Melting Point: 170 – 175 °C

^{1}H NMR (300 MHz, DMSO-d$_6$): δ 7.95 (d, J = 8.4 Hz, 1H), 7.83 (m, 2H), 7.52 – 7.32 (m, 5H), 7.18 (t, J = 8.8 Hz, 2H), 6.46 (s, 2H), 5.76 (s, 1H), 5.29 – 4.95 (m, 4H), 3.58 (s, 6H), 3.56 (s, 3H).

^{13}C NMR (75 MHz, DMSO-d$_6$): δ 172.0, 161.5 (d, J = 243.7 Hz) 158.6, 152.7, 141.2, 135.8, 135.4, 132.8, 131.6, 130.4, 129.2, 128.4, 128.1, 127.1, 124.5, 123.6, 117.3, 115.8, 115.5, 115.1, 104.9, 98.1, 65.5, 59.8, 55.7, 48.6, 36.9.

IR (ATR, cm^{-1}): 1733, 1620, 1510, 1447, 1319, 1256, 1085.

HRMS: calcd for C$_{31}$H$_{27}$NO$_5$F$^+$ [M + H]$^+$, 518.1865 – found 518.1870.
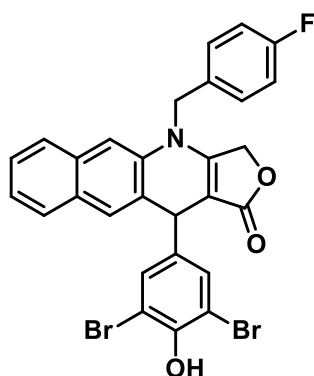
11-(3,5-Dibromo-4-hydroxyphenyl)-4-(4-fluorobenzyl)-4,11-dihydrobenzo[*g*]furo[3,4-*b*]quinolin-1(3*H*)-one.

Light pink powder (130.0 mg, 73% yield).

Melting Point: 219 – 223 °C

^{1}H NMR (300 MHz, DMSO-d$_6$): 7.92 – 7.81 (m, 3H), 7.54 – 7.34 (m, 5H), 7.27 (s, 2H), 7.20 (t, *J* = 8.8 Hz, 2H), 5.78 (s, 1H), 5.13 (m, 4H).

^{13}C NMR (75 MHz, DMSO-d$_6$): δ 171.9, 161.50 (d, *J* = 243.5 Hz), 159.9, 158.8, 149.2, 139.8, 135.4, 132.6, 131.2, 130.9, 130.4, 129.2, 128.6, 128.3, 127.3, 124.7, 123.4, 116.9, 115.9, 115.5, 112.0, 97.8, 65.7, 48.5.

IR (ATR, cm^{-1}): 3117, 1725, 1661, 1510, 1257, 1172, 1091.

HRMS: calcd for $C_{28}H_{19}NO_3FBr_2^+$ [M + H]$^+$, 595.9637 – found 595.9641.
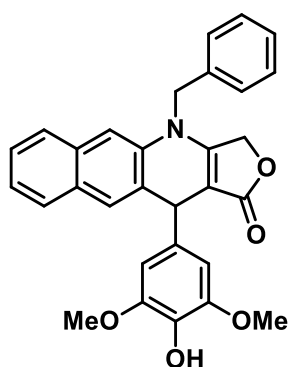
4-Benzyl-11-(4-hydroxy-3,5-dimethoxyphenyl)-4,11-dihydrobenzo[*g*]furo[3,4-*b*]quinolin-1(3*H*)-one.

Light brown powder (77 mg, 54% yield).

Melting Point: 199 – 206 °C

^{1}H NMR (300 MHz, DMSO-d$_6$): δ 7.95 (d, J = 8.3 Hz, 1H), 7.88 – 7.76 (m, 2H), 7.39 (m, 8H), 6.43 (s, 2H), 5.70 (s, 1H), 5.29 – 4.95 (m, 4H), 3.58 (s, 6H).

^{13}C NMR (75 MHz, DMSO-d$_6$): 172.1, 158.4, 147.8, 136.7, 136.0, 135.5, 134.1, 131.6, 130.3, 128.8, 128.1, 127.6, 126.9, 126.4, 124.3, 123.7, 117.6, 115.1, 105.3, 98.3, 65.4, 55.9, 49.2, 36.6.

IR (ATR, cm^{-1}): 3517, 1735, 1659, 1617, 1567, 1462, 1386, 1357, 1241, 1103, 1024.

HRMS: calcd for $C_{30}H_{26}NO_5^+$ [M + H]$^+$, 480.1809 – found 480.1805.
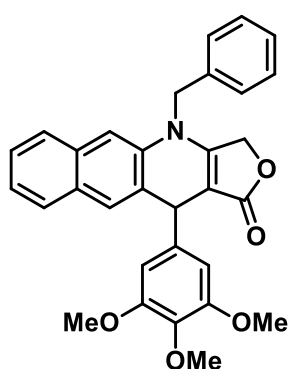
4-Benzyl-11-(3,4,5-trimethoxyphenyl)-4,11-dihydrobenzo[*g*]furo[3,4-*b*]quinolin-1(3*H*)-one.

Light brown powder (76 mg, 52% yield).

Melting Point: 175 – 181 °C

^{1}H NMR (300 MHz, DMSO-d$_6$): δ 7.96 (d, J = 8.4 Hz, 2H), 7.83 (m, 2H), 7.52 – 7.28 (m, 9H), 6.49 (s, 2H), 5.77 (s, 1H), 5.29 – 4.98 (m, 4H), 3.59 (s, 6H), 3.57 (s, 3H).

¹³C NMR (75 MHz, DMSO-d₆): δ 172.5, 159.1, 153.1, 141.7, 137.1, 136.3, 136.0, 132.0, 130.8, 129.3, 128.6, 128.1, 127.5, 126.9, 124.9, 124.0, 117.7, 115.6, 105.4, 98.4, 65.9, 60.3, 56.1, 49.7, 37.4.

IR (ATR, cm⁻¹): 2937, 1735, 1657, 1590, 1567, 1449, 1358, 1283, 1161, 1039.

HRMS: calcd for $C_{31}H_{28}NO_5^+$ [M + H]⁺, 494.1960 – found 494.1962.
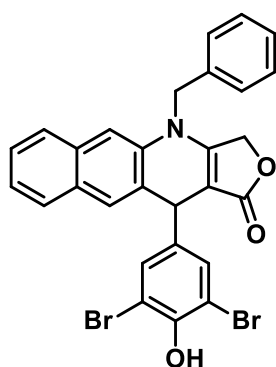
4-Benzyl-11-(3,5-dibromo-4-hydroxyphenyl)-4,11-dihydrobenzo[*g*]furo[3,4-*b*]quinolin-1(3*H*)-one.

Off-white powder (111 mg, 64% yield).

Melting Point: 168 – 172 °C

¹H NMR (300 MHz, DMSO-d₆): δ 7.90 (d, J = 8.5 Hz, 1H), 7.83 (m, 2H), 7.52 – 7.25 (m, 9H), 5.80 (s, 1H), 5.13 (m, 4H).

¹³C NMR (75 MHz, DMSO-d₆): δ 172.3, 159.4, 149.6, 140.3, 137.0, 136.0, 131.5, 130.9, 129.5, 128.7, 128.1, 127.7, 126.8, 125.1, 123.9, 117.2, 115.8, 112.5, 98.1, 66.1, 49.7.

IR (ATR, cm⁻¹): 3254, 1731, 1660, 1451, 1298, 1172, 1035.

HRMS: calcd for $C_{28}H_{20}NO_3Br_2^+$ [M + H]⁺, 575.9648 – found 575.9655.

9.2.5 Multicomponent Reactions: General procedure for the synthesis under Microwave Irradiation

The multicomponent reaction under microwave irradiation followed the same general procedure:

N-propargylnaphthyl-2-amine (1 eq.), benzaldehyde (1 eq.), tetronic acid (1 eq.) and ethylene glycol (8 mL) were added to a microwave vial and sealed. The reaction mixture was then heated and stirred at 110 °C under microwave irradiation for 35 minutes. The resulting solid was collected by vacuum filtration and the solid washed with cold ethanol. The solid was then dried under high vacuum.

The analytical data for the individual compounds are reported below:
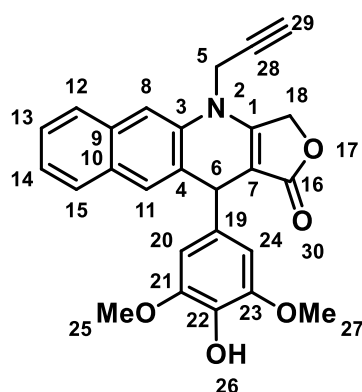
11-(4-Hydroxy-3,5-dimethoxyphenyl)-4-(prop-2-yn-1-yl)-4,11-dihydrobenzo[*g*]furo[3,4-*b*]quinolin-1(3*H*)-one.

Light orange solid (260.1 mg, 77% yield).

Melting Point: 219 – 227 °C

^{1}H NMR (300 MHz, DMSO-d$_6$) δ 8.00 (t, *J* = 8.1 Hz, 2H, H13 & H14), 7.89 (dd, *J* = 7.8, 1.5 Hz, 1H, H12), 7.71 (d, *J* = 9.2 Hz, 1H, H15), 7.48 – 7.36 (m, 2H, H8 & H11), 6.44 (s, 2H, H20 & H24), 5.61 (s, 1H, H6), 5.10 (dd, *J* = 65.7, 16.1 Hz, 2H, H18), 4.90 – 4.70 (m, 2H, H5), 3.58 (s, 6H, H25 & H27), 3.45 (t, *J* = 2.1 Hz, 1H, H29).

^{13}C NMR (75 MHz, DMSO-d$_6$) δ 171.8 (C16), 157.7 (C1), 147.8 (C21 & C23), 135.7 (C19), 134.8 (C22), 134.2 (C3), 131.5 (C15), 130.5 (C11), 128.6 (C9), 128.2 (C10), 126.9 (C4), 124.5 (C12), 123.6 (C14), 118.2 (C13), 115.0 (C8), 105.2 (C20 & C24), 99.8 (C7), 78.5 (C28), 75.9 (C29), 65.1 (C18), 56.0 (C6), 36.3, 35.8 (C25 & C27).

IR (ATR, cm^{-1}): 3245, 2999, 2941, 2114, 1728, 1654, 1617, 1595, 1382, 1232, 1135, 1036.

HRMS: calcd for C$_{26}$H$_{22}$NO$_5^+$ [M + H]$^+$, 428.1494 – found 428.1499.
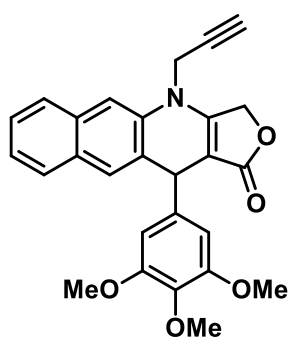
11-(3,4,5-Trimethoxyphenyl)-4-(prop-2-yn-1-yl)-4,11-dihydrobenzo[*g*]furo[3,4-*b*]quinolin-1(3*H*)-one.

Yellow solid (258.2 mg, 65% yield).

Melting Point: 221 – 230 °C

^{1}H NMR (300 MHz, DMSO-d$_{63}$) δ 8.07 – 7.97 (m, 2H), 7.90 (d, *J* = 7.8 Hz, 1H), 7.72 (d, *J* = 9.2 Hz, 1H), 7.51 – 7.35 (m, 2H), 6.50 (s, 2H), 5.67 (s, 1H), 5.11 (dd, *J* = 65.7, 16.1 Hz, 2H), 4.80 (m, 2H), 3.60 (s, 6H), 3.54 (s, 3H), 3.45 (t, *J* = 2.1 Hz, 1H).

^{13}C NMR (75 MHz, DMSO-d$_6$) δ 171.7, 158.0, 152.7, 141.0, 135.9, 134.9, 131.5, 130.5, 128.8, 128.2, 127.1, 124.6, 123.6, 117.9, 115.1, 104.8, 99.5, 78.4, 75.9, 65.2, 59.8, 55.8, 36.5, 35.8.

IR (ATR, cm^{-1}): 3254, 2969, 2830, 2118, 1729, 1653, 1619, 1504, 1467, 1353, 1230, 1124, 1005.

HRMS: calcd for C$_{27}$H$_{24}$NO$_5^+$ [M + H]$^+$, 442.1651 – found 442.1649.
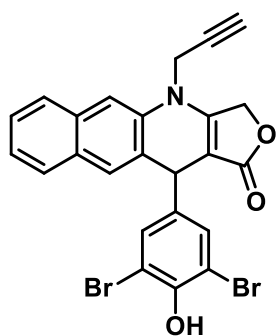
11-(3,5-Dibromo-4-hydroxyphenyl)-4-(prop-2-yn-1-yl)-4,11-dihydrobenzo[*g*]furo[3,4-*b*]quinolin-1(3*H*)-one.

Orange solid (174 mg, 60% yield).

Melting Point: 224 – 232 °C

^{1}H NMR (600 MHz, DMSO-d_6): δ 8.03 (d, J = 9.2 Hz, 1H), 7.92 (t, J = 9.0 Hz, 2H), 7.72 (d, J = 9.2 Hz, 1H), 7.47 (dd, J = 15.3, 1.3 Hz, 1H), 7.41 (dd, J = 14.8, 0.8 Hz, 1H), 7.31 (s, 2H), 5.73 (s, 1H), 5.12 (dd, J = 155.7, 16.0 Hz, 2H), 4.91 – 4.72 (m, 2H).

^{13}C NMR (151 MHz, DMSO-d_6): δ 172.0, 158.6, 149.6, 140.0, 135.5, 131.5, 131.1, 129.6, 128.8, 127.7, 125.2, 123.9, 117.3, 115.6, 112.4, 99.3, 78.6, 76.5, 65.7, 36.4, 35.5.

IR (ATR, cm^{-1}): 3270, 2122, 1727, 1655, 1616, 1466, 1438, 1357, 1264, 1026.

HRMS: calcd for $C_{24}H_{16}NO_3Br_2^+$ [M + H]$^+$, 525.9471 – found 525.9474.
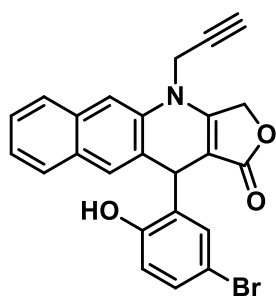
11-(5-Bromo-2-hydroxyphenyl)-4-(prop-2-yn-1-yl)-4,11-dihydrobenzo[*g*]furo[3,4-*b*]quinolin-1(3*H*)-one.

Yellow-orange solid (116 mg, 47% yield).

Melting Point: 224 – 227 °C

^{1}H NMR (300 MHz, DMSO-d_6): δ 8.11 (d, J = 8.4 Hz, 1H), 7.97 (d, J = 9.1 Hz, 1H), 7.92 – 7.85 (m, 1H), 7.70 (d, J = 9.2 Hz, 1H), 7.50 – 7.35 (m, 2H), 7.05 (dd, J = 8.6, 2.5 Hz, 1H), 6.91 (d, J = 2.5 Hz, 1H), 6.75 (d, J = 8.6 Hz, 1H), 5.97 (s, 1H), 5.34 – 4.95 (m, 3H), 4.92 – 4.74 (m, 2H), 3.44 (t, J = 2.1 Hz, 1H).

^{13}C NMR (75 MHz, DMSO-d_6): δ 171.8, 158.8, 152.4, 136.0, 135.3, 132.3, 132.0, 130.8, 130.5, 129.1, 128.8, 127.6, 125.1, 123.3, 119.6, 117.9, 115.7, 111.1, 100.2, 78.7, 76.5, 65.8, 36.3, 29.6.

IR (ATR, cm^{-1}): 3254, 1722, 1650, 1466, 1417, 1369, 1277, 1199, 1035.

HRMS: calcd for $C_{24}H_{17}NO_3Br^+$ [M + H]$^+$, 446.0381 – found 446.0385.

9.2.6 Click Chemistry: General Procedure

The click reactions followed the same general procedure, as described by Sharpless, Fokin and co-workers, only using DMSO instead of the *t*-BuOH/H$_2$O as solvent.[147]

186

The 4*N*-propargyl-4-azapodophyllotoxin analogue (1 eq.) and azide (1 eq.) were dissolved in DMSO, followed by the addition of Copper (II) acetate (10 mol%) and 1M sodium ascorbate. The reaction was then stirred at room temperature for 24-48 hours, monitoring the progress by TLC. Upon completion, the reaction mixture was diluted with water (dist.) and the precipitate collected under vacuum filtration and the washed with water (dist.) and cold ethanol.

The analytical data for the individual compounds are reported below:
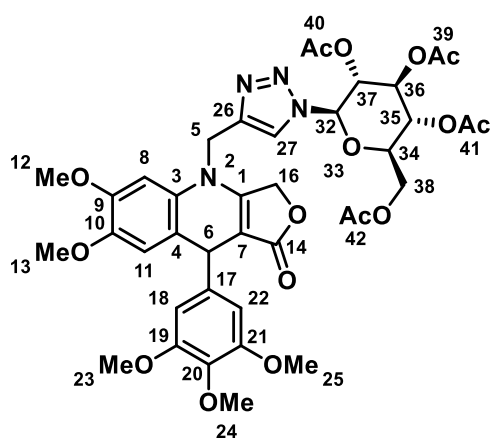
(2*R*,3*R*,4*S*,5*R*,6*R*)-2-(acetoxymethyl)-6-(4-((6,7-dimethoxy-1-oxo-9-(3,4,5-trimethoxyphenyl)-3,9-dihydrofuro[3,4-*b*]quinolin-4(1*H*)-yl)methyl)-1*H*-1,2,3-triazol-1-yl)tetrahydro-2*H*-pyran-3,4,5-triyl triacetate (226).

Dark yellow solid (98 mg, 95% yield).

Melting Point: Degrades above 160 ºC

¹H NMR (300 MHz, DMSO-d₆) δ 7.95 (s, 1H, H27), 6.68 (s, 1H, H8), 6.60 (s, 1H, H11), 6.22 (s, 2H, H18 & H22), 5.13 (d, J = 9.6 Hz, 1H, h38), 4.97 (dd, J = 17.8, 12.5 Hz, 2H, H16), 4.78 (t, J = 11.0 Hz, 1H, H32), 4.69 – 4.57 (m, 2H, H34 & H37), 4.48 (s, 1H, H6), 4.14 (t, J = 5.0 Hz, 1H, H36), 3.81 (s, 3H, H12), 3.60 (s, 3H, H13), 3.50 – 3.39 (m, 9H, H23, H24 & H25), 1.84 (s, 3H, H40), 1.83 (s, 3H, H39), 1.79 (s, 3H, H41), 1.75 (s, 3H, H42).

¹³C NMR (75 MHz, DMSO-d₆) δ 166.1 (C14), 151.2 (C19 & C20), 145.0 (C1), 140.6 (C9), 138.1 (C10), 134.1 (C17), 122.2 (C27), 110.1 (C11), 106.0 (C18 & C22), 96.7 (C8), 91.5 (C11), 89.9 (C32), 69.0 (C37), 65.7 (C16), 57.4 (C23 & C25), 51.6 (C24), 47.3 (C35), 47.1 (C34), 31.9 (C39, C40 & C41), 27.1 (C42).
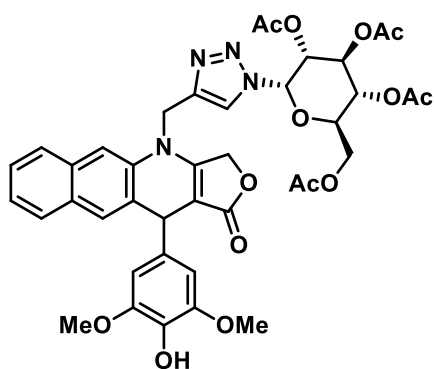
(2*R*,3*R*,4*S*,5*R*,6*S*)-2-(acetoxymethyl)-6-(4-((11-(4-hydroxy-3,5-dimethoxyphenyl)-1-oxobenzo[*g*]furo[3,4-*b*]quinolin-4(1*H*,3*H*,11*H*)-yl)methyl)-1*H*-1,2,3-triazol-1-yl)tetrahydro-2*H*-pyran-3,4,5-triyl triacetate (227).

Orange-brown powder (51.4 mg, 68% yield).

Melting Point: Degrades above 160 ºC

¹H NMR (300 MHz, DMSO-d₆) δ 8.14 (s, 1H), 8.00 (t, *J* = 7.9 Hz, 2H), 7.89 (d, *J* = 8.0 Hz, 1H), 7.70 (d, *J* = 9.2 Hz, 1H), 7.49 – 7.32 (m, 3H), 6.43 (d, *J* = 5.5 Hz, 2H), 5.60 (s, 1H), 5.32 (t, *J*

= 9.6 Hz, 1H), 5.17 (dd, *J* = 19.9, 12.5 Hz, 2H), 5.05 – 4.92 (m, 2H), 4.90 – 4.70 (m, 3H), 4.22 – 4.02 (m, 3H), 3.58 (s, 6H), 2.03 (m, 12H).

IR (ATR, cm⁻¹): 3246, 1753, 1730, 1655, 1567, 1287, 1234, 1136, 1058.

HRMS: calcd for $C_{40}H_{41}N_4O_{14}^+$ [M + H]⁺,801.2620 – found 801.2625.
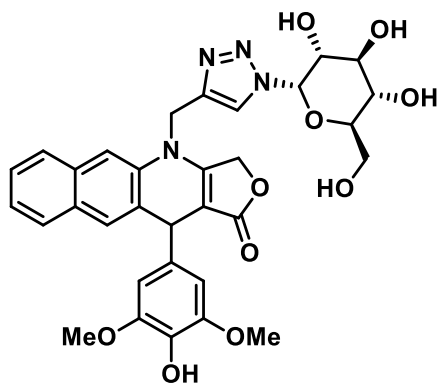
11-(4-Hydroxy-3,5-dimethoxyphenyl)-4-((1-((2*S*,3*R*,4*S*,5*S*,6*R*)-3,4,5-trihydroxy-6-(hydroxymethyl)tetrahydro-2*H*-pyran-2-yl)-1*H*-1,2,3-triazol-4-yl)methyl)-4,11-dihydrobenzo[*g*]furo[3,4-*b*]quinolin-1(3H)-one (231).

Orange powder (30.1 mg, 51% yield).

Melting Point: Degrades above 160 ºC

¹H NMR (300 MHz, DMSO-d₆) δ 8.00 (m, 2H), 7.92 – 7.78 (m, 2H), 7.65 (m, 2H), 7.62 (t, *J* = 9.3 Hz, 5H), 7.37 (m, 3H), 6.44 (m, 2H), 5.60 (s, 1H), 5.05 (m, 6H), 4.34 (m, 1H), 4.09 (m, 1H), 3.57 (s, 6H), 2.06 – 1.90 (m, 3H), 1.57 (d, J = 7.6 Hz, 1H).

¹³C NMR (75 MHz, DMSO-d₆) δ 172.3, 169.9, 168.8, 158.6, 158.2, 148.2, 143.6, 136.6, 136.2, 135.3, 134.6, 132.0, 130.9, 129.1, 128.6, 127.4, 124.9, 124.1, 118.6, 115.5, 105.6, 100.2, 78.9, 76.3, 73.8, 72.4, 71.0, 68.0, 65.6, 62.2 56.4.

IR (ATR, cm⁻¹): 3528, 3246, 2941, 1730, 1655, 1365, 1323, 1214, 1183, 1116, 1037.

HRMS: calcd for $C_{32}H_{33}N_4O_{10}^+$ [M + H]⁺,633.6867 – found 633.6865.
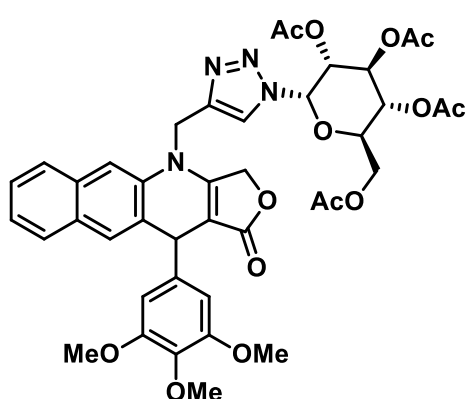
(2*R*,3*R*,4*S*,5*R*,6*S*)-2-(acetoxymethyl)-6-(4-((1-oxo-11-(3,4,5-trimethoxyphenyl)benzo[*g*]furo[3,4-*b*]quinolin-4(1*H*,3*H*,11*H*)-yl)methyl)-1*H*-1,2,3-triazol-1-yl)tetrahydro-2*H*-pyran-3,4,5-triyl triacetate (228).

Dark orange powder, 80% yield.

Melting Point: Degrades above 160 ºC

¹H NMR (300 MHz, DMSO-d₆): δ 8.57 (d, *J* = 16.4 Hz, 1H), 8.00 (m, 2H), 7.92 – 7.78 (m, 3H), 7.70 (m, 2H), 7.49 – 7.35 (m, 3H), 6.44 (s, 2H), 6.42 (d, *J* = 3.6 Hz, 2H), 5.57 (m, 1H), 5.24 – 5.16 (m, 3H), 4.99 (m, 1H), 4.23 – 4.02 (m, 2H), 3.58 (s, 6H), 3.55 (s, 3H), 2.06 – 1.90 (m, 12H).

^{13}C NMR (75 MHz, DMSO-d$_6$): δ 172.4, 170.5, 170.0, 169.7, 169.6, 158.8, 153.1, 143.5, 141.7, 136.2, 132.0, 130.8, 128.5, 127.4, 124.9, 124.0, 123.2, 118.1, 115.4, 114.9, 105.3, 98.8, 86.7, 84.3, 76.4, 73.8, 73.2, 72.2, 70.6, 68.2, 66.0, 62.1, 60.2, 56.2, 21.0, 20.8, 20.7, 20.1.

IR (ATR, cm^{-1}): 1747, 1732, 1660, 1592, 1233, 1211, 1123, 1086, 1058, 1037.

HRMS: calcd for $C_{41}H_{43}N_4O_{14}^+$ [M + H]$^+$, 815.2777 – found 815.2781.
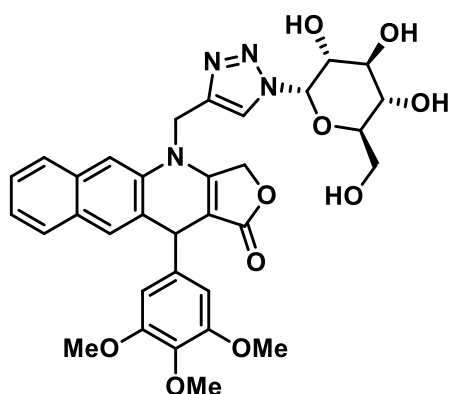
4-((1-((2S,3R,4S,5S,6R)-3,4,5-trihydroxy-6-(hydroxymethyl)tetrahydro-2H-pyran-2-yl)-1H-1,2,3-triazol-4-yl)methyl)-11-(3,4,5-trimethoxyphenyl)-4,11-dihydrobenzo[g]furo[3,4-b]quinolin-1(3H)-one (232).

Orange powder, 68% yield.

Melting Point: Degrades above 160 °C

^{1}H NMR (300 MHz, DMSO-d$_6$): δ 8.57 (d, J = 16.4 Hz, 1H), 8.00 (m, 2H), 7.92 – 7.78 (m, 3H), 7.70 (m, 2H), 7.49 – 7.35 (m, 3H), 6.44 (s, 2H), 6.42 (d, J = 3.6 Hz, 2H), 5.57 (m, 1H), 5.24 – 5.16 (m, 3H), 4.99 (m, 1H), 4.23 – 4.02 (m, 2H), 3.58 (s, 6H), 3.55 (s, 3H), 2.06 – 1.90 (m, 12H).

^{13}C NMR (75 MHz, DMSO-d$_6$): δ 172.1, 158.4, 153.1 153.0, 141.4, 136.3, 135.3, 131.9, 130.9, 129.2, 128.6, 127.5, 125.0, 123.9, 118.3, 115.5, 105.2, 99.9, 78.8, 76.3, 65.6, 60.2, 56.2.

IR (ATR, cm^{-1}): 3254, 2938, 2837, 1748, 1731, 1655, 1505, 1286, 1217, 1183, 1063, 1005.

HRMS: calcd for $C_{33}H_{35}N_4O_{10}^+$ [M + H]$^+$, 647.6941 – found 647.6945.
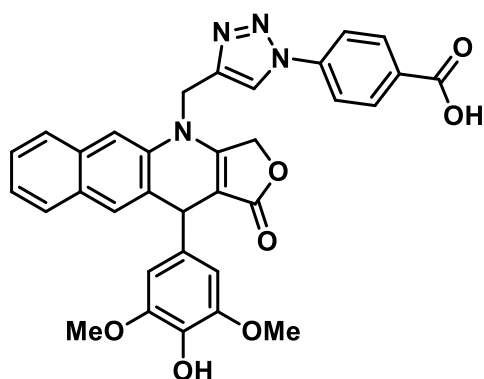
4-(4-((11-(4-Hydroxy-3,5-dimethoxyphenyl)-1-oxobenzo[g]furo[3,4-b]quinolin-4(1H,3H,11H)-yl)methyl)-1H-1,2,3-triazol-1-yl)benzoic acid.

Light orange powder, 58% yield.

Melting Point: 224 – 227 °C

^{1}H NMR (300 MHz, DMSO-d$_6$): δ 8.20 (d, J = 9.1 Hz, 2H) 8.13 (s, 1H) 8.05 – 7.96 (m, 2H), 7.93 – 7.80 (m, 2H), 7.72 (d, 5.8 Hz, 1H), 7.47 – 7.32 (m, 3H), 6.50 – 6.38 (m, 2H), 5.61 (s, 1H), 5.24 – 4.94 (m, 2H), 4.87 – 4.71 (m, 2H), 3.63 – 3.52 (s, 6H).

^{13}C NMR (75 MHz, DMSO-d$_6$): δ 172.2, 158.1, 148.2, 136.1, 135.3, 134.6, 131.9, 130.9, 129.1, 128.6, 127.4, 124.9, 124.1, 118.6, 115.5, 105.6, 100.2, 78.9, 76.3, 65.5, 56.4.

IR (ATR, cm^{-1}): 3238, 2999, 2978, 1730, 1619, 1518, 1254, 1232.

HRMS: calcd for $C_{33}H_{27}N_4O_7^+$ [M + H]$^+$, 591.1887 – found 591.1885.
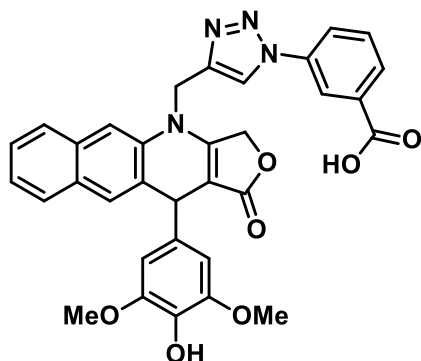
4-(4-((11-(4-Hydroxy-3,5-dimethoxyphenyl)-1-oxobenzo[*g*]furo[3,4-*b*]quinolin-3(1*H*,3*H*,11*H*)-yl)methyl)-1*H*-1,2,3-triazol-1-yl)benzoic acid.

Yellow-orange powder, 34% yield.

Melting Point: 211 – 219 $^{\circ}$C

^{1}H NMR (300 MHz, DMSO-d$_6$): δ 8.10 – 7.99 (m, 2H), 7.93 – 7.80 (m, 2H), 7.72 (d, 5.8 Hz, 1H), 7.47 – 7.32 (m, 3H), 6.50 – 6.38 (m, 2H), 5.61 (s, 1H), 5.24 – 4.94 (m, 2H), 4.87 – 4.71 (m, 2H), 3.63 – 3.52 (s, 6H).

^{13}C NMR (75 MHz, DMSO-d$_6$): δ 172.2, 158.1, 148.2, 136.1, 135.3, 134.6, 131.9, 130.9, 129.0, 128.6, 127.3, 124.9, 124.0, 118.6, 115.4, 105.6, 100.2, 78.9, 76.3, 65.5, 56.4.

IR (ATR, cm^{-1}): 3527, 3245, 2977, 2941, 1729, 1655, 1516, 1467, 1382, 1254, 1136.

HRMS: calcd for $C_{33}H_{25}N_4O_7^-$ [M - H]$^-$, 589.1719 – found 589.1721.

9.3 Biological Studies

9.3.1 Antiproliferative Activity

The antiproliferative activity of the novel *N*-functionalized 4-azapodophyllotoxins were determined by Dr Catherine Kaschula and co-workers against the oesophageal cancer cell line, WHCO1, derived from the squamous cell carcinomas collected from South African patients.[180] The cell viability assay was conducted by the following method, as received from Dr Kaschula.

Cell Viability Assay

The cells were cultured in Dulbecco's Modified Eagle medium (Gibco®, Life Technologies) supplemented with 10 % foetal bovine serum (HyClone™,GE Healthcare Life Sciences) and 100µg/mL penicillin and 100µg/mL streptomycin (Biochrom, Germany). Cells were incubated in a humidified 5 % CO$_2$/37°C incubator. All experiments were performed on logarithmically growing cells. A stock solution of 25 mM compound in DMSO was prepared and stored at -20 °C until use. Cells were seeded at a density of 2.5 x 10^3 cells per well in 90 µL in a 96-well

culture dish. The following day, 10 μL of the compound (0.5 - 50 μM) in DMSO (0.2% v/v) was added in triplicate to the cells and incubated for 48 h. Thereafter, 10 μL of 5mg/mL 3-(4,5-dimethylthiazol-2-yl)-2,5-diphenyltetrazolium bromide (MTT) (Sigma Aldrich) was added and incubated with the cells for 4 h. The resulting formazan crystals were solubilised into 100 μL sodium lauryl sulphate overnight at 37 ℃ and the resulting absorbance at 595 nm was measured using a Multiskan FC multi-well reader (Thermo Scientific). The data was analysed using GraphPad Prism 4 software fitted to a log(inhibitor) vs. response variable slope curve. Each IC50 determination was performed independently a minimum of three times to obtain the average and standard deviation.

9.3.2 *In Silico* **Molecular Modelling Studies**

The *in silico* molecular modelling studies were performed using the Schrödinger Suite version 2019-2, which included Maestro,[154] Glide[163] and Canvas.[160] Maestro and Glide were used to determine the docking scores as an indication of the individual molecules' fit into the active pocket.

Proteins were refined with the Protein Preparation Wizard.[181] The relevant crystal structure was imported from the *Import and Process* tab, the default settings used, and the structure preprocessed. The structure was then analyzed under the *Review and Modify* tab, deleting unwanted side chains and waters.[182] The structure was finally refined under the *Refine* tab, using the *Optimize* and *Interactive Optimizer* functions and then minimized with the OPLS 2005 force field.[181,183–185]

Ligands (compounds of interest in this study) were prepared with the *LigPrep* function. The compounds were imported as an .SDF file. With the OPLS 2005 force field, ligands were ionized to generate possible states that would exist at pH 7 ± 2 using Epik.[183] Ligands were also desalted and the relevant tautomers generated. Chiralities were varied for ligands where no chirality was specified. No more than 32 poses per ligand were generated.

Finally, the prepared ligands were docked into the prepared protein structure using Glide.[163,164] A receptor grid was generated using the *Receptor Grid Generation* function. The ligand (colchicine for PDB ID: 1SA0,[153] podophyllotoxin for PDB ID: 1SA1,[153] etoposide for both PDB ID: 3QX3,[161] and PDB ID 5GWK)[162] was identified and the default scaling factor of 1.0 used. The newly generated grids were used along with the prepared ligands in the *Glide Docking* function. The ligands were docked with standard precision (SP) and flexible ligand sampling. *Sample Nitrogen Inversions, Sample Ring Conformations*, and *Add Epik State Penalties to Docking Score* were selected. Under the *Output* tab, *Pose Viewer File* and *Perform Post-Docking Minimization* (10 poses per ligand) were selected and the calculation was run.

10.1 References

(1)   NCI Dictionary of Cancer Terms https://www.cancer.gov/publications/dictionaries/cancer-terms/def/cancer (accessed Jul 3, 2018).

(2)   Noncommunicable diseases http://www.who.int/news-room/fact-sheets/detail/noncommunicable-diseases (accessed Jul 5, 2018).

(3)   Parkin, D. M.; Bray, F.; Ferlay, J.; Jemal, A. Cancer in Africa 2012. *Cancer Epidemiol. Biomarkers Prev.* **2014**, *23*, 953–966.

(4)   Parkin, D. M.; Ferlay, J.; Hamdi-Cherif, M.; Sitas, F.; Whelan, S. L.; Thomas, J. O.; Wabinga, H., *IARC Sci. Publ.* **2003**, *153*.

(5)   Siegel, R. L.; Miller, K. D.; Jemal, A., *CA. Cancer J. Clin.* **2017**, *67*, 7–30.

(6)   Danaei, G.; Vander Hoorn, S.; Lopez, A. D.; Murray, C. J.; Ezzati, M., *Lancet* **2005**, *366*, 1784–1793.

(7)   Siegel, R. L.; Miller, K. D.; Jemal, A., *CA. Cancer J. Clin.* **2016**, *66*, 7–30.

(8)   Jemal, A.; Siegel, R.; Xu, J.; Ward, E., *CA. Cancer J. Clin.* **2010**, *60*, 277–300.

(9)   Jemal, A.; Siegel, R.; Ward, E.; Hao, Y.; Xu, J.; Thun, M. J., *CA. Cancer J. Clin.* **2009**, *59*, 225–249.

(10) Jemal, A.; Tiwari, R. C.; Murray, T.; Ghafoor, A.; Samuels, A.; Ward, E.; Feuer, E. J.; Thun, M. J., *CA. Cancer J. Clin.* **2004**, *54*, 8–29.

(11) Barnard, R. J., *Altern. Med.* **2004**, *1*, 233–239.

(12) Burkitt, D. P., *Lancet* **1969**, *2*, 1229–1231.

(13) Giovannucci, E., *J. Womens Heal.* **2003**, *12*, 173–182.

(14) Komninou, D.; Ayonate, A.; Richie, J. J.; Rigas, B., *Exp. Biol. Med.* **2003**, *228*, 396–405.

(15) Ziegler, R. G.; Mayne, S. T.; Swanson, C. A., *Cancer Cause Control* **1996**, *7*, 157–177.

(16) Alwens, W.; Jonas, W., *Acta Unio Int. contra Cancrum* **1938**, *3*, 103–108.

(17) Teleky, L., *Acta Unio Int. contra Cancrum1* **1938**, *3*, 253–260.

(18) Bosch, F. X.; Ribes, J.; Diaz, M.; Cleries, R., *Gastroenterology* **2004**, *127*, S5–S16.

(19) Bosch, F. X.; Ribes, J. The Epidemiology of Primary Liver Cancer: Global Epidemiology. In *Viruses and liver cancer, First Ed.*; Elsevier Science, 2002; pp 1–16.

(20) Stefan, D. C., *J. Glob. Oncol.* **2015**, *1*, 30–36.

(21) May, F. P.; Anandasabapathy, S., *Gastrointest. Endosc.* **2019**, *89*, 1238–1240.

(22) Irabor, D.; Adedeji, O. A., *Eur. J. Cancer Care (Engl).* **2009**, *18*, 110–115.

(23) Herbst, C.; Miot, J. K.; Moch, S. L.; Ruff, P., *J. Cancer Policy*, **2018**, *15*, 18–24.

(24) Torre, L. A.; Siegel, R. L.; Ward, E. M.; Jemal, A., *Cancer Epidemiol. Biomarkers Prev.* **2016**, *25*, 16–28.

(25) Gopal, S.; Wood, W. A.; Lee, S. J.; Shea, T. C.; Naresh, K. N.; Kazemba, P. N.; Casper, C.; Hesseling, P. B.; Mitsuyasu, R. T., *Blood* **2012**, *119* (22), 5078–5087.

(26) Bartel, S. B., *Am. J. Heal. Pharm.* **2007**, *94* (9), S8–S14.

(27) Smith, C. A., *J. Pharm. Soc. Wisconsin* **2002**, 17–22.

(28) Bebbington, M. W. P., *Chem. Soc. Rev.* **2017**, *46*, 5059–5109.

(29) Magedov, I. V; Frolova, L.; Manpadi, M.; Bhoga, U. D.; Tang, H.; Evdokimov, N. M.; George, O.; Georgiou, K. H.; Renner, S.; Getlik, M.; Kinnibrugh, T. L.; Fernandes, M. a; Van slambrouck, S.; Steelant, W. F. A; Shuster, C. B.; Rogelj, S.; van Otterlo, W. A L.; Kornienko, A., *J. Med. Chem.* **2011**, *54* (12), 4234–4246.

(30) Nicolaou, K. C.; Sorenson, E. J. *Classics in Total Synthesis*; Wiley: New York, **1996**.

(31) Nicolaou, K. C.; Snyder, S. A. *Classics in Total Synthesis II*; Wiley: New York, **2003**.

(32) Nicolaou, K. C.; Chen, J. S. *Classics in Total Synthesis III*; Wiley: New York, **2011**.

(33) Burke, M. D.; Schreiber, S. L., Angewandte. *Angew. Chemie - Int. Ed.* **2004**, *43*, 46–58.

(34) Wilson, R. M.; Danishefsky, S. J., *J. Org. Chem.* **2006**, *71*, 8329–8351.

(35) Chen, L.; Yang, S.; Jakoncic, J.; Zhang, J. J.; Huang, X. *Nature* **2010**, *464*, 1062–1066.

(36) Shinkre, B. A.; Raisch, K. P.; Fan, L.; Velu, S. E., *Bioorg. Med. Chem. Lett.* **2007**, *17*, 2890–2893.

(37) Davies-Coleman, M. T., *South African J. Chem.* **2010**, *63*, 105–113.

(38) Roberts, D.; Bros, M. A.; Joule, J. A.; Alvarez, M., *J. Org. Chem.* **1997**, *62*, 568–577.

(39) Botes, M. G.; van Otterlo, W. A. L.; Blackie, M. A. L.; Pelly, S. C. Stellenbosch

University, **2015**.

(40) Armstrong, R. W.; Combs, A. P.; Tempest, P. A.; Brown, S. D.; Keating, T. A., *Acc. Chem. Res.* **1996**, *29*, 123–131.

(41) Dömling, A.; Ugi, I., *Angew. Chemie - Int. Ed.* **2000**, *39*, 3168–3210.

(42) Slobbe, P.; Ruijter, E.; Orru, R. V. A., *Med. Chem. Commun.* **2012**, *3*, 1189.

(43) Laurent, A.; Gerhardt, C. F., *Ann. Chim. Phys.* **1838**, *66*, 181.

(44) Liu, Z.-Q., *Curr. Org. Synth.* **2015**, *12*, 20–60.

(45) Royer, D.; Wong, Y.-S.; Plé, S.; Chiaroni, A.; Diker, K.; Lévy, J., *Tetrahedron* **2008**, *64*, 9607–9618.

(46) Kumar, A.; Kumar, V.; Alegria, A. E.; Malhotra, S. V., *Eur. J. Pharm. Sci.* **2011**, *44*, 21–26.

(47) Newman, D. J.; Cragg, G. M., *J. Nat. Prod.* **2012**, *75*, 311–335.

(48) Gordaliza, M., *Clin. Transl. Oncol.* **2007**, *9*, 767–776.

(49) Imbert, T. F., *Biochimie* **1998**, *80*, 207–222.

(50) Sudo, K.; Konno, K.; Shigeta, S.; Yokota, T., *Antivir. Chem. Chemother.* **1998**, *9*, 263–267.

(51) Beutner, K. R. *Sexually Transmitted Diseases: Advances in Diagnosis and Treatment*; Elsner, P., Eichmann, A., Eds.; Karger: Basel, 1996.

(52) Berkowitz, D. B.; Maeng, J.; Dantzig, A. H.; Shepard, R. L.; Norman, B. H., *J. Am. Chem. Soc.* **1996**, *118*, 9426–9427.

(53) Takahashi, M.; Suzuki, N.; Ishikawa, T., *J. Org. Chem.* **2013**, *78*, 3250–3261.

(54) Magedov, I. V; Evdokimov, N. M.; Karki, M.; Peretti, A. S.; Lima, D. T.; Frolova, L. V; Reisenauer, M. R.; Romero, A. E.; Tongwa, P.; Fonari, A.; Altig, J.; Rogelj, S.; Antipin, M. Y.; Shuster, C. B.; Kornienko, A., *Chem. Commun. (Camb).* **2012**, *48*, 10416–10418.

(55) Wu, Y.; Zhao, J.; Chen, J.; Pan, C.; Li, L.; Zhang, H., *Org. Lett.* **2009**, *11*, 597–600.

(56) Hitotsuyanagi, Y.; Fukuyo, M.; Tsuda, K.; Kobayashi, M.; Ozeki, A.; Itokawa, H.; Takeya, K., *Bioorg. Med. Chem. Lett.* **2000**, *10*, 315–317.

(57) Hitotsuyanagi, Y.; Kobayashi, M.; Fukuyo, M.; Takeya, K.; Itokawa, H., *Tetrahedron Lett.* **1997**, *38*, 8295–8296.

(58)   Tratrat, C.; Giorgi-Renault, S.; Husson, H.-P., *Org. Lett.* **2002**, *4*, 3187–3189.

(59)   Semenova, M. N.; Kiselyov, A. S.; Tsyganov, D. V. Konyushkin, L. D.; Firgang, S. I.; Semenov, R. V.; Malyshev, O. R.; Raihstat, M. M.; Fuchs, F.; Stielow, A.; Lantow, M.; Philchenkov, A. A.; Zavelevich, M. P.; Zefirov, N. S.; Kuznetsov, S. A.; Semenov, V. V., *J. Med. Chem.* **2011**, *54*, 7138–7149.

(60)   Chernysheva, N. B.; Tsyganov, D. V.; Philchenkov, A. A.; Zavelevich, M. P.; Kiselyov, A. S.; Semenov, R. V.; Semenova, M. N.; Semenov, V. V., *Bioorg. Med. Chem. Lett.* **2012**, *22*, 2590–2593.

(61)   Frackenpohl, J.; Adelt, I.; Antonicek, H.; Arnold, C.; Behrmann, P.; Blaha, N.; Böhmer, J.; Gutbrod, O.; Hanke, R.; Hohmann, S.; Houtdreve, M. Van; Lösel, P.; Malsam, O.; Melchers, M.; Neufert, V.; Peschel, E.; Reckmann, U.; Schenke, T.; Thiesen, H.; Velten, R.; Vogelsang, K.; Weiss, H., *Bioorg. Med. Chem.* **2009**, *17*, 4160–4184.

(62)   Murlykina, M. V.; Sahkno, Y. I.; Desenko, S. M.; Konovalova, I. S.; Shishkin, O. V.; Sysoiev, D. A.; Kornet, M. N.; Chebanov, V. A., *Tetrahedron* **2010**, *69*, 9261–9269.

(63)   Tu, S.; Zhang, Y.; Zhang, J.; Jiang, B.; Jia, R.; Zhang, J.; S. Ji., *Synlett* **2006**, *17*, 2785–2790.

(64)   Katritzky, A. R.; Ostercamp, D. L.; T. I. Yousaf., *Tetrahedron* **1987**, *43*, 5171–5186.

(65)   Shi, F.; Ma, N.; Zhang, Y.; Zhang, G.; Jiang, B.; Tu, S. *Synth. Commun.* **2009**, *40*, 235–241.

(66)   Shi, F.; Tu, S.; Jiang, B.; Li, C.; Zhou, D.; Shao, Q.; Cao, L.; Wang, Q.; Zhou, J., *J. Heterocycl. Chem.* **2008**, *45*, 1103–1108.

(67)   Shi, F.; Zhang, G.; Zhang, Y.; Ma, N.; Jiang, B.; Tu, S., *J. Heterocycl. Chem.* **2009**, *46*, 965–970.

(68)   Shi, C.; Wang, J.; Chen, H.; Shi, D., *J. Comb. Chem.* **2010**, *12*, 430–434.

(69)   Shi, C.; Chen, H.; Shi, D., *J. Heterocycl. Chem.* **2012**, *49*, 125–129.

(70)   Jeedimalla, N.; Johns, J.; Roche, S. P. *Tetrahedron Lett.* **2013**, *54*, 5845–5848.

(71)   Magedov, I. V; Manpadi, M.; Slambrouck, S. Van; Steelant, W. F. a; Rozhkova, E.; Przheval'skii, N. M.; Rogelj, S.; Kornienko, A., *J. Med. Chem.* **2007**, *50*, 5183–5192.

(72)   Magedov, I. V; Manpadi, M.; Rozhkova, E.; Przheval'skii, N. M.; Rogelj, S.; Shors, S. T.; Steelant, W. F. a; Van slambrouck, S.; Kornienko, A., *Bioorg. Med. Chem. Lett.* **2007**, *17*, 1381–1385.

(73) Naeimi, H.; Rashid, Z.; Zarnani, A. H.; Ghahremanzadeh, R, Ionic Liquid. **2013**, *2013*.

(74) Wang, X.; Hao, W.; Tu, S.; Zhang, X.; Cao, X.; Yan, S.; Wu, S.; Han, Z.; Shi, F. *J. Heterocycl. Chem.* **2009**, *46*, 742–747.

(75) Kozlov, N. G.; Bondarev, S. L.; Kadutskii, A. P.; Basalaeva, L. I.; Pashkovskii, F. S., *Russ. J. Org. Chem.* **2008**, *44*, 1031–1037.

(76) Shestopalov, A. M.; Litvinov, Y. M.; Rodinovskaya, L. A.; Malyshev, O. R.; Semenova, M. N.; Semenov, V. V., *ACS Comb. Sci.* **2012**, *14*, 484–490.

(77) Kumar, A.; Alegria, A. E., *J. Heterocycl. Chem.* **2010**, *47*, 1275–1282.

(78) Kamal, A.; Suresh, P.; Mallareddy, A.; Kumar, B. A.; Reddy, P. V.; Raju, P.; Tamboli, J. R.; Shaik, T. B.; Jain, N.; Kalivendi, S. V., *Bioorg. Med. Chem.* **2011**, *19*, 2349–2358.

(79) Shi, F.; Zeng, X.-N.; Zhang, G.; Ma, N.; Jiang, B.; Tu, S., *Bioorg. Med. Chem. Lett.* **2011**, *21*, 7119–7123.

(80) Labruère, R.; Gautier, B.; Testud, M.; Seguin, J.; Lenoir, C.; Desbène-Finck, S.; Helissey, P.; Garbay, C.; Chabot, G. G.; Vidal, M.; Giorgi-Renault, S. *ChemMedChem* **2010**, *5*, 2016–2025.

(81) Magedov, I. V.; Kornienko, A., *Chem. Heterocycl. Compd.* **2012**, *48*, 33–38.

(82) Li, J. J. *Name Reactions in Heterocyclic Chemistry II*; Corey, E. J., Ed.; John Wiley & Sons, Inc., 2011.

(83) Shi, C.; Wang, J.; Chen, H.; Shi, D., *J. Comb. Chem.* **2010**, *12*, 430–434.

(84) Kusari, S.; Zühlke, S.; Spiteller, M., *Phytochem. Anal.* **2011**, *22*, 128–143.

(85) Kumar, A.; Kumar, V.; Alegria, A. E.; Malhotra, S. V., *Eur. J. Pharm. Sci.* **2011**, *44*, 21–26.

(86) Graaff, C. de; Ruijter, E.; Orru, R. V. A., *Chem. Soc. Rev.* **2012**, *41*, 3969–4010.

(87) Kamal, A.; Srinivasa Reddy, T.; Polepalli, S.; Paidakula, S.; Srinivasulu, V.; Ganga Reddy, V.; Jain, N.; Shankaraiah, N., *Bioorganic Med. Chem. Lett.* **2014**, *24*, 3356–3360.

(88) Magedov, I. V; Luchetti, G.; Evdokimov, N. M.; Manpadi, M.; Steelant, W. F. A; Van Slambrouck, S.; Tongwa, P.; Antipin, M. Y.; Kornienko, A. *Bioorg. Med. Chem. Lett.* **2008**, *18*, 1392–1396.

(89) Kandil, S.; Wymant, J. M.; Kariuki, B. M.; Jones, A. T.; Mcguigan, C.; Westwell, A. D.,

Eur. J. Med. Chem. **2016**, *110*, 311–325.

(90)   Kamal, A.; Reddy, T. S.; Polepalli, S.; Paidakula, S.; Srinivasulu, V.; Reddy, V. G.; Jain, N.; Shankaraiah, N., *Bioorg. Med. Chem. Lett.* **2014**, *24*, 3356–3360.

(91)   Yang, X.; Zhang, C.; Wu, L., *RSC Adv.* **2015**, *5*, 18945–18951.

(92)   Wongwanakul, R.; Vardhanabhuti, N.; Siripong, P.; Jianmongkol, S., *Fitoterapia* **2013**, *89*, 80–85.

(93)   Chang, C.-Z.; Wu, S.-C.; Kwan, A.-L.; Lin, C.-L. *World Neurosurg.* **2016**, *86*, 349–360.

(94)   Chaisit, T.; Siripong, P.; Jianmongkol, S., *Eur. J. Pharmacol.* **2017**, *795*, 50–57.

(95)   Chang, P.; Aillerie, A.; Kosmala, M.; Pellegrini, S.; Bousquet, T.; Bigan, M.; Pélinski, L., *New J. Chem.* **2015**, *39*, 8236–8239.

(96)   Pettit, G. R.; Searcy, J. D.; Tan, R.; Cragg, G. M.; Melody, N.; Knight, J. C., *J. Nat. Prod.* **2016**, *79*, 507–518.

(97)   Shareef, M. A.; Duscharla, D.; Ramasatyaveni, G.; Dhoke, N. R.; Das, A.; Ummanni, R.; Srivastava, A. K., *Eur. J. Med. Chem.* **2015**, *89*, 128–137.

(98)   Jeedimalla, N.; Flint, M.; Smith, L.; Haces, A.; Roche, P.; Minond, D., *Eur. J. Med. Chem.* **2015**, *106*, 167–179.

(99)   Hatti, I.; Sreenivasulu, R.; Singh Jadav, S.; Jayaprakash, V.; Kumar, C. G.; Raju, R. R., *Med. Chem. Res.* **2015**, *24*, 3305–3313.

(100) Vélez, C.; Zayas, B.; Kumar, A., *Open J. Med. Chem.* **2014**, *4*, 1–11.

(101) Kumar Ghosh, S.; Joshi, R.; Mukherjee, S.; Kumar, A.; Singh, A.; Concepcion-santana, M., *J. Photochem. Photobiol. A Chem.* **2017**, *349*, 49–62.

(102) Mukherjee, S.; Ganorkar, K.; Gupta, S.; Kumar, A.; Singh, A.; Kumar Ghosh, S., *J. Biomol. Struct. Dyn.* **2019**, *22*, 1–14.

(103) Mukherjee, S.; Ganorkar, K.; Kumar, A.; Sehra, N.; Kumar Ghosh, S., *Bioorg. Chem.* **2019**, *84*, 63–75.

(104) Andreoli, M.; Persico, M.; Kumar, A.; Orteca, N.; Kumar, V.; Pepe, A.; Mahalingam, S.; Alegria, A. E.; Petrella, L.; Sevciunaite, L.; Camperchioli, A.; Mariani, M.; Dato, A. Di; Novellino, E.; Scambia, G.; Malhotra, S. V; Ferlini, C.; Fattorusso, C., *J. Med. Chem.* **2014**, *57*, 7916–7932.

(105) De Donato, M.; Mariani, M.; Petrella, L.; Martinelli, E.; Zannoni, G. F.; Vellone, V.;

Ferrandina, G.; Shahabi, S.; Scambia, G.; Ferlini, C., *J. Cell Physiol.* **2012**, *227*, 1034–1041.

(106) Katsetos, C. D.; Draber, P., *Curr. Pharm. Des.* **2012**, *18*, 2778–2792.

(107) Michels, M.; Follmann, M.; Vakalopoulos, A.; Zimmermann, K.; Lobell, M.; Teusch, N.; Yuan, S. Bi- and Tricyclic Indazole-Substituted 1,4-Dihydropyridine Derivatives and Uses Thereof. US 8,759,341 B2, 2014.

(108) Chabot, G. G.; Giorgi-renault, S.; Desbene-Finck, S.; Helissey, P.; Labruere, R.; Testud, M.; Scherman, D. Water Soluble 4-Azapodophyllotoxin Analogs. WO 2015/107119 A1, 2015.

(109) Ahmed, K.; Paidakula, S.; Banala, A. K.; Adla, M.; Papagari, V.; Jaki, R. T. 4-Aza-2,3-Didehydropodophyllotoxin Compounds and Process for the Preparation Thereof. EP 2 649 078, 2016.

(110) Alam, M. A.; Naik, P. K. , *J. Mol. Graph. Model.* **2009**, *27*, 930–943.

(111) Cho, S. J.; Kashiwada, Y.; Bastow, K. F.; Cheng, Y.-C.; Lee, K.-H., *J. Med. Chem* **1996**, *39*, 1396–1402.

(112) MacDonald, T. L.; Lehnert, E. K.; Loper, J. T.; Chow, K. C.; Ross, W. E. Mechansim of Interaction of DNA Topoisomerase II with Chemotherapeutic Agents. In *DNA Topoisomerase in Cancer*; Potmesil, M., Kohn, K. W., Eds.; Oxford University Press: New York, 1991; pp 119–214.

(113) Hande, K. R. Clinical Oncology Update Etoposide : Four Decades of Development of a Topoisomerase II Inhibitor. **1998**, *34* (10), 1514–1521.

(114) Cheng, W.-H.; Cao, B.; Shang, H.; Niu, C.; Zhang, L.-M.; Zhang, Z.-H.; Tian, D.-L.; Zhang, S.; Chen, H.; Zou, Z.-M., *Eur. J. Med. Chem.* **2014**, *85*, 498–507.

(115) Chen, H.; Zuo, S.; Wang, X.; Tang, X.; Zhao, M.; Lu, Y.; Chen, L.; Liu, J.; Liu, Y.; Liu, D.; Zhang, S.; Li, T. *Eur. J. Med. Chem.* **2011**, *46* (9), 4709–4714.

(116) Reddy, P. B.; Agrawal, S. K.; Singh, S.; Bhat, B. A; Saxena, A. K.; Kumar, H. M. S.; Qazi, G. N., *Chem. Biodivers.* **2008**, *5*, 1792–1802.

(117) Byl, J. A. W.; Cline, S. D.; Utsugi, T.; Kobunai, T.; Yamada, Y.; Osheroff, N. *Biochemistry* **2001**, *40*, 712–718.

(118) Utsugi, T.; Shibata, J.; Sugimoto, Y.; Aoyagi, K.; Wierzba, K.; Kobunai, T.; Terada, T.; Oh-hara, T.; Tsuruo, T.; Yamada, Y., *Cancer Res.* **1996**, *56*, 2809–2814.

(119) Tron, G. C.; Pirali, T.; Billington, R. A.; Canonico, P. L.; Sorba, G.; Genazzani, A. A., *Med. Res. Rev.* **2008**, *28*, 278–308.

(120) Kamal, A.; Kumar, B. A.; Arifuddin, M., *Tetrahedron Lett.* **2003**, *44*, 8457–8459.

(121) Kamal, A.; Gayatri, N. L., *Tetrahedron Lett.* **1996**, *37*, 3359–3362.

(122) Zhang, Y. L.; Guo, X.; Cheng, Y. C.; Lee, K. H., *J. Med. Chem.* **1994**, *37*, 446–452.

(123) Zhang, Y. L.; Tropsha, A.; McPhail, A. T.; Lee, K. H. , *J. Med. Chem.* **1994**, *37*, 1460–1464.

(124) Majumdar, K. C.; Ganai, S. *Tetrahedron Lett.* **2013**, *54*, 6192–6195.

(125) Sakai, N.; Suzuki, H.; Hori, H.; Ogiwara, Y., *Tetrahedron Lett.* **2017**, *58*, 63–66.

(126) Greenwood, P. D. G.; Grenet, E.; Waser, J., *Chem. - A Eur. J.* **2019**, *25*, 3010–3013.

(127) Zhang, Z.; Zou, Y.; Deng, C., *RSC Adv.* **2017**, *7*, 14742–14751.

(128) Piras, S.; Carta, A.; Briguglio, I.; Corona, P.; Paglietti, G.; Luciani, R.; Costi, M. P.; Ferrari, S., *Eur. J. Med. Chem.* **2014**, *75*, 169–183.

(129) Wang, H.; Tang, L.; Tang, Y.; Yuan, Z., *Bioorg. Med. Chem.* **2014**, *22*, 6183–6192.

(130) Chang, H.; Shyu, K. G.; Lee, C. C.; Tsai, S. C.; Wang, B. W.; Lee, Y. H.; Lin, S., *Biochem. Biophys. Res. Commun.* **2003**, *302*, 95–100.

(131) Cho, B. T.; Kang, S. K., *Tetrahedron* **2005**, *61*, 5725–5734.

(132) Aida, T.; Kuboki, N.; Kato, K.; Uchikawa, W.; Matsuno, C.; Okamoto, S., *Tetrahedron Lett.* **2005**, *46*, 1667–1669.

(133) Wu, X.-F.; Neumann, H., *Adv. Synth. Catal.* **2012**, *354*, 3141–3160.

(134) Yang, H.; Cui, X.; Deng, Y.; Shi, F.; Yang, H.; Cui, X.; Deng, Y.; Shi, F., *Synth. Commun.* **2014**, *44*, 1314–1322.

(135) Jumde, V. R.; Gonsalvi, L.; Guerriero, A.; Peruzzini, M.; Taddei, M., *European J. Org. Chem.* **2015**, 1829–1833.

(136) Drillaud, N.; Banaszak-Léonard, E.; Pezron, I.; Len, C., *J. Org. Chem.* **2012**, *77*, 9553–9561.

(137) Takeda, T.; Sugiura, Y.; Hamada, C.; Fujii, R.; Suzuki, K.; Ogihara, Y.; Shibata, S., *Chem. Pharm. Bull.* **1981**, *29*, 3196–3201.

(138) Bohme, D.; Krieghoff, J.; Beck-Sickinger, A. G., *J. Med. Chem.* **2016**, *59*, 3409–3417.

(139) Kutonova, K. V., *Synthesis.* **2013**, *45*, 2706–2710.

(140) Zhu, W.; Ma, D., *Chem. Commun.* **2004**, 888–889.

(141) Fabre, B.; Pícha, J.; Vaněk, V.; Buděšínský, M.; Jiráček, J., *Molecules* **2015**, *20*, 19310–19329.

(142) Higa, C. M.; Tek, A. T.; Wojtecki, R. J.; Braslau, R. *J. Polym. Sci. Part A Polym. Chem.* **2018**, *56*, 2397–2411.

(143) Tahtaoui, C.; Parrot, I.; Klotz, P.; Guillier, F.; Galzi, J.; Hibert, M.; Ilien, B., *J. Med. Chem.* **2004**, *47*, 4300–4315.

(144) Kasper, J. J.; Hitro, J. E.; Fitzgerald, S. R.; Schnitter, J. M.; Rutowski, J. J.; Heck, J. A.; Steinbacher, J. L., *J. Org. Chem.* **2016**, *81*, 8095–8103.

(145) Kevill, D. N.; Weitl, F. L., *J. Org. Chem.* **1967**, *32*, 2633–2634.

(146) Kolb, H. C.; Finn, M. G.; Sharpless, K. B., *Angew. Chemie - Int. Ed.* **2001**, 2004–2021.

(147) Rostovtsev, V. V; Green, L. G.; Fokin, V. V; Sharpless, K. B. *Angew. Chemie - Int. Ed.* **2002**, *41*, 2596–2599.

(148) Wang, C.; Ikhlef, D.; Kahlal, S.; Saillard, J.-Y.; Astruc, D., *Coord. Chem. Rev.* **2016**, *316*, 1–20.

(149) Worrel, B. T.; Malik, J. A.; Fokin, V. V., *Science* **2013**, *340*, 457–460.

(150) Stoll, A.; Renz, J.; von Wartburg, A., *J. Am. Chem. Soc.* **1954**, *76*, 3103–3104.

(151) Stoll, A.; Renz, J.; von Wartburg, A., *Helv. Chim. Acta* **1954**, *37*, 1747–1762.

(152) Stoll, A.; von Wartburg, A.; Angliker, E.; Renz, J., *J. Am. Chem. Soc.* **1954**, *76*, 5004–5005.

(153) Ravelli, R. B.; Gigant, B.; Curmi, P. A.; Jourdain, I.; Lachkar, S.; Sobel, A.; Knossow, M., *Nature* **2004**, *428*, 198–202.

(154) Maestro. Schrödinger LLC: New York, NY 2019.

(155) Deweese, J. E.; Osheroff, N., *Nucleic Acids Res.* **2009**, *37*, 738–748.

(156) Lee, C. C.; Huang, T. S., *Pharm. Res.* **2001**, *18*, 846–851.

(157) Huang, T. S.; Lee, C.-C.; Chao, Y.; Shu, C.-H.; Chen, L.-T.; Chen, L.-L.; Chen, M.-H.; Yuan, C.-C.; Whang-Peng, J., *Pharmaceutical Res.* **1999**, *16*, 997–1002.

(158) Huang, T. S.; Shu, C. H.; Lee, C. C.; Chen, L. T.; Whang-Peng, J. *Apoptosis* **2000**, *5*,

79–85.

(159) Kaschula, C. H.; Hunter, R.; Stellenboom, N.; Caira, M. R.; Winks, S.; Ogunleye, T.; Richards, P.; Cotton, J.; Zilbeyaz, K.; Wang, Y.; Siyo, V.; Ngarande, E.; Parker, M. I., *Eur. J. Med. Chem.* **2012**, *50*, 236–254.

(160) Canvas. Schrödinger LLC: New York, NY 2019.

(161) Wu, C. C.; Li, T. K.; Farh, L.; Lin, L. Y.; Lin, T. S.; Yu, Y. J.; Yen, T. J.; Chiang, C. W.; Chan, N. L., *Science* **2011**, *333*, 459–462.

(162) Wang, Y. R.; Chen, S. F.; Wu, C. C.; Liao, Y. W.; Lin, T. S.; Liu, K. T.; Chen, Y. S.; Li, T. K.; Chien, T. C.; Chan, N. L., *Nucleic Acids Res.* **2017**, *45*, 10861–10871.

(163) Glide. Schrödinger LLC: New York, NY 2019.

(164) Friesner, R. A.; Banks, J. L.; Murphy, R. B.; Halgren, T. A.; Klicic, J. J.; Mainz, D. T.; Repasky, M. P.; Knoll, E. H.; Shaw, D. E.; Shelley, M.; Perry, J. K.; Francis, P.; Shenkin, P. S., *J. Med. Chem.* **2004**, *47*, 1739–1749.

(165) Helissey, P.; Giorgi-renault, S. **2008**, No. 6, 3642–3645.

(166) Laskowski, R. A.; Swindells, M. B. , *Chem. Inf. Model.* **2011**, *51*, 2778–2786.

(167) Silva Souza, E.; Zaramello, L.; Kuhnen, C. A.; da Silva Junkes, B.; Yunes, R. A.; Heinzen, V. E. F., *Int. J. Mol. Sci.* **2011**, *12*, 7250–7264.

(168) Ghose, A. K.; Viswanadhan, V. N.; Wendoloski, J. J., *J. Phys. Chem. A* **1998**, *102*, 3762–3772.

(169) Burden, D. A.; Osheroff, N., *Biochim. Biophys. Acta* **1998**, *1400*, 139–154.

(170) Bender, R. P.; Jablonksy, M. J.; Shadid, M.; Romaine, I.; Dunlap, N.; Anklin, C.; Graves, D. E.; Osheroff, N. , *Biochemistry* **2008**, *47*, 4501–4509.

(171) Wilcken, R.; Zimmermann, M. O.; Lange, A.; Joerger, A. C.; Boeckler, F. M., *J. Med. Chem.* **2013**, *56*, 1363–1388.

(172) Chin, C. F.; Tian, Q.; Setyawati, M. I.; Fang, W.; Tan, E. S. Q.; Leong, D. T.; Ang, W. H., *J. Med. Chem.* **2012**, *55*, 7571–7582.

(173) Frost, L.; Suryadevara, P.; Cannell, S. J.; Groundwater, P. W.; Hambleton, P. A.; Anderson, R. J., *Eur. J. Med. Chem.* **2016**, *109*, 206–215.

(174) Dohil, R.; Newbury, R. O.; Sellers, Z. M.; Deutsch, R.; Schneider, J. A., *J. Pediatr.* **2003**, *143*, 224–230.

(175) Bigorra Llosas, J.; Valls, R.; Raya, J.; Fabry, B.; De Regil-Hernandez, R.; Rodriguez-Bayon, A.; Sinisterra, J.-V. EP 2 184 286 A1. 08019325.3, 2010.

(176) Schmidt, F.; Monneret, C., *Bioorg. Med. Chem.* **2003**, *11*, 2277–2283.

(177) Dondoni, A.; Massi, A.; Minghini, E.; Bertolasi, V. *Helv. Chim. Acta* **2002**, *85*, 3331–3348.

(178) Jiang, J.; Yu, J.; Sun, X.-X.; Rao, Q.-Q.; Gong, L.-Z. *Angew. Chemie - Int. Ed.* **2008**, *47*, 2458–2462.

(179) Armarego, W. L. F.; Perrin, D. D. *Purification of Laboratory Chemicals*, Fourth Edi.; Reed Educational and Professional Publishing Ltd: London, England, 1996.

(180) Veale, R. B.; Thornley, A. L., *S. Afr. J. Sci.* **1989**, *85*, 375–379.

(181) Schrödinger Suite 2012 Protein Preparation Wizard. Schrödinger LLC: New York, NY 2012.

(182) Olsson, M. H. M.; Søndergard, C. R.; Rostowski, M.; Jensen, J. H., *J. Chem. Theory Comput.* **2011**, *7*, 525–537.

(183) Epik Version 2.3. Schrödinger LLC: New York, NY 2012.

(184) Impact Version 5.8. Schrödinger LLC: New York, NY 2012.

(185) Prime Version 3.1. Schrödinger LLC: New York, NY 2012.